



Project 034 Overall Integration and Coordination

University of Dayton

Project Lead Investigator

Joshua Heyne
Assistant Professor
Mechanical Engineering
University of Dayton
300 College Park
Dayton, OH 45458
937 229-5319
Jheyne1@udayton.edu

University Participants

University of Dayton

- P.I.(s): Joshua Heyne and Scott Stouffer
- FAA Award Number: 13-C-AJFE-UD (Amendment Nos. 9, 10, 13, 17, & 18)
- Period of Performance: September 18, 2015 to December 31, 2018
- Task(s):
 1. Overall NJFCP integration and coordination
 2. Chemical effects in Toroidal Jet Stirred Reactor
 3. Preferential vaporization effects on LBO of the Referee Rig
 4. Cross-experiment analysis
 5. Common format routine software and model development
 6. Spray modeling of Area 3 (GT P&W pressure atomizer)
 7. Cold ignition experiments in the Referee Rig of alternative fuel blends

Project Funding Level

Amendment No. 9: \$134,999.00 (September 18, 2015 to February 28, 2017)

Amendment No. 10: \$249,330.00 (July 7, 2016 to December 31, 2017)

Amendment No. 13: \$386,035.00 (August 30, 2016 to December 31, 2017)

Amendment No. 17: \$192,997.00 (August 3, 2017 to September 30, 2018)

Amendment No. 18: \$374,978.00 (December 7, 2017 to December 31, 2018)

Cost share is provided by GE Aviation (\$135,000.00), DLR Germany (\$3,113,564.00), United Technologies Research Center (\$150,000.00), ANSYS/FLUENT (\$175,000.00), and the University of Dayton (\$53,887.00) in form of in-kind research at GE Aviation, DLR Germany, and United Technologies, direct financial support at the University of Dayton, and reduced software license fees at ANSYS/FLUENT.

Investigation Team

- Joshua Heyne (University of Dayton) is the Project Lead Investigator for coordinating all NJFCP teams (both ASCENT and non-ASCENT efforts), Well-Stirred Reactor experiments, procuring additional geometrical configurations, and leading studies across experimental platforms within the NJFCP.
- Scott Stouffer (University of Dayton Research Institute) is the P.I. conducting ignition testing of NJFCP fuels in the Referee Rig.
- Alejandro Briones (University of Dayton Research Institute) is the P.I. responsible for leading the common format routine software development.
- Vaidya Sankaran (UTRC) is sub-contracted to conduct the spray modeling of the Area 3 pressure atomizing spray injector.





- Bob Olding (University of Dayton Research Institute) is part of the team managed by Alejandro Briones to develop the common format routine software. Mr. Olding's main task is on Scheme GUI/TUI programing for later use by OEM CFD teams.
- Mike Hanchak (University of Dayton Research Institute) is part of the team managed by Alejandro Briones to develop the common format routine software. Mr. Hanchak's main task is on CFD and combustion programing for later use by OEM CFD teams.
- Tyler Hendershott (University of Dayton Research Institute) is part of the team working on the ignition of conventional and alternative jet fuels in the Referee Rig.
- Jeffery Monfort (University of Dayton Research Institute) is part of the team working on the ignition of conventional and alternative jet fuels in the Referee Rig.
- Robert Stachler (University of Dayton) is a Ph.D. student conducting the Lean Blowout and emissions measurements in the Well-Stirred Reactor.
- Erin Peiffer (University of Dayton) is a Master's student linking experimental results across ASCENT and non-ASCENT teams.
- Sherri Alexander (University of Dayton) is an administrative assistant aiding in the compilation of meeting minutes and setting up teleconference times.
- Katherine Opacich (University of Dayton) is an undergraduate research assistant working to document NJFCP activities and analyze ignition data across NJFCP teams.
- Shane Kosir (University of Dayton) is an undergraduate research assistant working to analyze LBO data.
- Zhibin (Harrison) Yang (University of Dayton) is a graduate student research assistant working to develop physical surrogates
- Jen Colborn (University of Dayton) is an undergraduate research student assistant aiding in the testing of fuels on the Referee Rig.
- David Bell (University of Dayton) is a graduate student research assistant working to develop physical surrogates.

Project Overview

The NJFCP is composed of more than two dozen member institutions contributing information and data as diverse as expert advice from gas turbine Original Equipment Manufacturers (OEMs), federal agencies, other ASCENT universities and corroborating experiments at DLR Germany, NRC Canada and other international partners. The project is tasked to: coordinate and integrate among these diverse program stakeholders and academic Principle Investigators (PIs); cross-analyze results from other NJFCP areas; collect data for modeling and fuel comparison purposes in a Well-Stirred Reactor (WSR); conduct Large Eddy Simulations (LES) of sprays for the Area 3 High Sheer Rig; procure additional swirler geometries for the NJFCP Areas and Allied Partners while developing interface of NJFCP modeling capabilities with OEM requirements. Work under this program consists of, but is not limited to:

- conduct meetings with member institutions to facilitate the consistency of testing and modeling,
- coordinate timely completion of program milestones,
- document results and procedures,
- create documents critical for program process (e.g. fuel down selection criteria)
- solicit and incorporate program feedback from OEMs,
- report and present on behalf of the NJFCP at meetings and technical conferences,
- integrate the state-of-the-art combustion and spray models into user-defined-functions (UDFs),
- WSR testing of NJFCP Category A, Category C, and Surrogate fuels,
- LES of sprays for A2, C1, and C5 fuels using the Area 3 High Sheer Rig Pratt & Whitney swirler and air blast atomizer,
- facilitate travel for University of Cape Town student,
- advise the program Steering Committee.

Task 1- Integration and Coordination of NJFCP Teams

University of Dayton

Objective(s)

The objective of this task is to integrate and coordinate all ASCENT and non-ASCENT team efforts via facilitation of meetings, summarizing results, presenting results external to the NJFCP, communicating on a regular basis with the Steering Committee, and other related activities.





Research Approach

The NJFCP is integrated and coordinated via two main techniques: 1) the structural lumping of various teams into six Topic areas and 2) routine meetings and discussion both internal and external to individual Topic areas. The Topic areas are distinguished by the dominant physics associated with them (Topics I and IV), the culmination of all relevant combustion physics (Topics II, III, V), and wrapping all work into a singular OEM GUI package (Topic VI). These six Topic areas are:

- Topic I. Chemical Kinetics: Foundational to any combustion model is a chemical kinetic model and the validation data anchoring modeling predictions.
- Topic II. Lean Blow Out (LBO): This Topic covers data, screening, and validation at relevant conditions to statistically and theoretically anticipate fuel property effects on this Figure of Merit (FOM).
- Topic III. Ignition: Similar to the LBO topic, the focus here is experimental screening and validation data for statistical and theoretical predictions.
- Topic IV. Sprays: Historically, the dominant effect of fuel FOM behavior has been the spray character of the fuel relative to others. Experimentalists in this Topic area focus on measuring the fuel property effects on spray behavior. In analogy to Topic I, the spray behavior is not a FOM like Topic II and III, although it is critical to bound the physical property effects on combustion behavior relative to other processes, i.e. chemical kinetics.
- Topic V. Computational Fluid Dynamics (CFD) Modeling: Complementary to the empirical Topics II, III, and IV, the CFD Modeling Topic focuses on the theoretical prediction of measured data and facilitates the development of theoretical modeling approaches.
- Topic VI. User Defined Function (UDF) Development: Once the theoretical modeling approaches matured in Topic V are validated. UDFs are developed for OEM evaluation of fuel performance in proprietary rigs.

These topic area teams meet and coordinate on a regular basis. At minimum, NJFCP wide meetings are held monthly with Topic area meetings occurring typically every 2-3 weeks.

Milestone(s)

NJFCP Mid-Year Meeting 2018

Major Accomplishments

Invited NJFCP Related Presentations

- Colket, Heyne, Lee, "NJFCP Update: Properties and Modeling to FOM Predictions," JetScreen Meeting, Paris, FR, December 2018.
- Heyne, Colket, Lee, "An overview of ASCENT research efforts to improve our understanding of how fuel composition and characteristics determine performance," CAAFI Biennial General Meeting, December 2018.
- Heyne, J., Edwards, T., "What makes a Great Jet Fuel?," Keynote, Tri-Lateral US-Mexico-Canada Bio-Jet Workshop, Pacific Northwest National Laboratories, May 2018.
- Heyne, Colket, "Overview and Results from the National Jet Fuels Combustion Program," CAAFI SOAP-Jet Webinar, Jan. 2018.
- Med Colket, Sang Hee Won, Stephen, Dooley, Bill Pitz, Charlie Westbrook, Josh Heyne, Fred Dryer, Steve Zeppieri, "Surrogates for Practical Fuels: Historical Perspective, Palettes, Selection, Use and Modeling," 2018 MACCCR Meeting, Sandia National Laboratories, Livermore, CA, 2018.
- Colket, Heyne, "NJFCP Update," JET SCREEN Meeting, Rome, October 2017.

Publications

Peer-Reviewed Journal Publications

None

Published conference proceedings

Heyne, J., Peiffer, E., Colket, M., Moder, J., Edwards, J. T., Roquemore, W. M., Shaw, C., Li, C., Rumizen, M., and Gupta, M., "Year 3 of the National Jet Fuels Combustion Program: Practical and Scientific Impacts," 56th AIAA Aerospace Sciences Meeting, Kissimmee, FL: 2018, <https://doi.org/10.2514/6.2018-1667>

Stachler, R., Peiffer, E., Kosir, S., Heyne, J., and Stouffer, S., "A Study into the Chemical Timescale for a Toroidal Jet-Stirred Reactor (TJSR)," Central States Section of The Combustion Institute, Minneapolis: 2018, <https://doi.org/10.2514/6.2018-4914>





Bell, D. C., Heyne, J. S., Won, S. H., and Dryer, F. L., "The Impact of Preferential Vaporization on Lean Blowout in a Referee Combustor at Figure of Merit Conditions," ASME 2018 Power and Energy Conference, Lake Buena Vista: 2018, <https://doi.org/10.1115/POWER2018-7432>

Peiffer, E., Heyne, J.S., Colket, M., "Characteristic Timescales for Lean Blowout of Alternative Jet Fuels in Four Combustor Rigs," Joint Propulsion Conference, Cincinnati, OH: 2018, <https://doi.org/10.2514/6.2018-4914>

Outreach Efforts

Presentations at CRC Aviation Meeting, AIAA SciTech Meeting Paper and Presentation, ASCENT Spring and Fall presentations 2017, and DESS ASME conference.

Awards

None

Student Involvement

Erin Peiffer, Graduate Research Assistant, June 2017 - present.

Harrison, Graduate Research Assistant, August 2018 - present.

Katherine Opachich, Undergraduate Research Assistant, November 2017 – present.

Shane Kosir, Undergraduate Research Assistant, January 2018 – present.

Plans for Next Period

Continue to perform all relevant coordination and integration related tasks.

Overall NJFCP Summary Coordination

As it was reported previously^{1,2}, alternative jet fuels (AJFs) are identified as a means to mitigate climate change and pollution, potentially reduce costs and underlying volatility, and diversify the energy supply for national security. One of the key requirements of these new fuels is that they are “drop-in-ready,” i.e., require no augmentation of engine, air frame components or ground-based and aircraft on-board infrastructure. Historically, this requirement for new alternative fuels necessitates extensive testing ranging from fit-for-purpose to full-scale engine testing, resulting in high costs and longtime scales for certification. Thus, the National Jet Fuels Combustion Program (NJFCP) was initiated¹ to reduce and streamline this extensive testing process, with a sole focus on the combustion operability of these fuels, i.e., Lean Blowout (LBO) and Ignition at cold start and altitude relight conditions. Fuel certification of alternative fuels requires consideration of a broad range of other practical issues and will not be reviewed here. The last two years we reported an extensive description of the NJFCP structure, historical context, key contributors, programmatic shifts, and key technical findings^{1,2}. This year we are reporting on the results of the previous year from the perspective of key strategic technical findings as well as potential impacts in evaluating fuels via experiments and models.

The certification of an AJF largely focuses on three performance metrics, Figures of Merit (FOM), which largely bound a fuel’s use for safe flight operations: i) LBO, ii) cold start, and iii) altitude relight, see Figure 1 for pertinent operating conditions. The performance of a fuel for these FOM relative to conventional fuels establishes a minimum criteria for fuel approval. Following this logic, the NJFCP early in the program defined three conventional jet fuels to quantify an expected ‘best,’ ‘average,’ and ‘worst’ case performance of conventional jet fuels, referred to herein as ‘category A’ or ‘A’ fuels³. Correspondingly, a series of AJF-like blends are defined to bound and explore the potential effects of AJFs, referred to herein as ‘category C’ or ‘C’ test fuels³. The performance comparisons of these A and C fuels for various experiments, models, and conditions establish the basis of the NJFCP.

The certification of AJFs typically involves a range of testing of the fuels in laboratory experiments to full scale engines. The later tests in turn contribute largely to the significant costs of the certification process, with the NJFCP’s experimental platforms are a proof of concept that can reduce size and cost experiments while capturing the same effects as the larger, more costly full engine tests. Correspondingly, experimental platforms are paired in the NJFCP with a modeling complement. The experimental platforms and modeling complements are lumped into 6 major Working Groups which largely categorize the goals of the NJFCP to bound AJF FOM performance characteristics, and then create and deliver useful tools to the OEMs for AJF evaluation. These Working Groups are summarized below as well as a brief description of previous accomplishments:





- The *LBO Working Group* is focused on understanding the effects of fuel on the lean blowout limits in a combustor. Efforts include: a) screening category C fuels, NJFCP AJFs, with respect to the category A fuels, b) providing validation data to the CFD Working Group, and c) experimentally probing some more fundamental physical features of the results. Previous years of the NJFCP have reported combined statistical plots on LBO screening of A and C fuels. Here we report the most comprehensive statistical analysis of LBO behavior across 9 rigs in the NJFCP as well as referencing additional more fundamental physical effects of fuels effects on LBO.
- The *Ignition Working Group* is focused on fuel effects on ignition and altitude relight. It is similarly tasked with screening, providing validation data, and probing more fundamental physical effects of AJFs on FOM behavior. Previous years have resulted in screening for prevaporized fuels and Auxiliary Power Unit (APU) testing at Honeywell. Additionally, significant effort has been allocated to facility development to achieve the relevant low-pressure and low-temperature conditions in the lower right hand corner of Figure 1. These newly developed experimental capabilities are currently being utilized for screening with possibly additional validation data and probing of physical effects.
- The *Spray Working Group* is tasked with characterizing spray behavior at relevant conditions for the ignition and LBO conditions. These spray characterizations are used to determine the effect of spray on FOM performance, the effect of fuel properties on spray characterizations, and the validation of computational spray results. Over the last year, additional detailed phase Doppler particle anemometry (PDPA) measurements have been taken at LBO and cold ignition conditions. Moderate spray differences are observed at the LBO conditions, while initial results showing greater spray differences across the fuels are observed at chilled conditions.
- The *Computational Fluid Dynamics (CFD) Working Group* is currently focused on predicting the correct trends for the fuel sensitivity of lean blowout in the Area 6 referee rig. Large-Eddy reacting spray simulations begin at an experimentally-demonstrated stable flame condition near lean blowout (LBO). Approach to LBO in CFD simulations proceeds through a series of step reductions in fuel mass flow rate since the approach to lean blowout over tens of seconds in the experimental procedure is not practical for CFD large-eddy reacting spray simulations, even using thousands of processors. Lean blowout predictions have been completed, but the correct trend in the fuel sensitivity of LBO is still being pursued with a consistent set of boundary conditions and spray injection conditions. Initial CFD simulations for prevaporized forced ignition have also begun.
- The *Kinetics Working Group* is focused on understanding the effects of fuel chemistry on the FOMs. Major accomplishments over the past year include the development and demonstration of new capabilities for measurements on the evolution of species during fuel decomposition; new ignition delay data that show variability in the hot ignition region with DCN; refinement and documentation of the HyChem modeling approach; and exploration of alternate methods for reduction of chemical kinetic mechanisms.
- The *Common Format (CFR) Working Group* develops tools from academic research that Original Equipment Manufacturers (OEMs) can use to evaluate potential fuel effects in proprietary combustor configurations. In this way, OEMs can utilize the most recent research advances to evaluate fuel property effects in geometries not typically available in research institutions. During the past year of the NJFCP the CFR Working Group has developed and delivered a GUI which can tabulate Flamelet prolongation of the intrinsic low-dimensional manifold (FPI) and Flamelet progress variable (FPV).

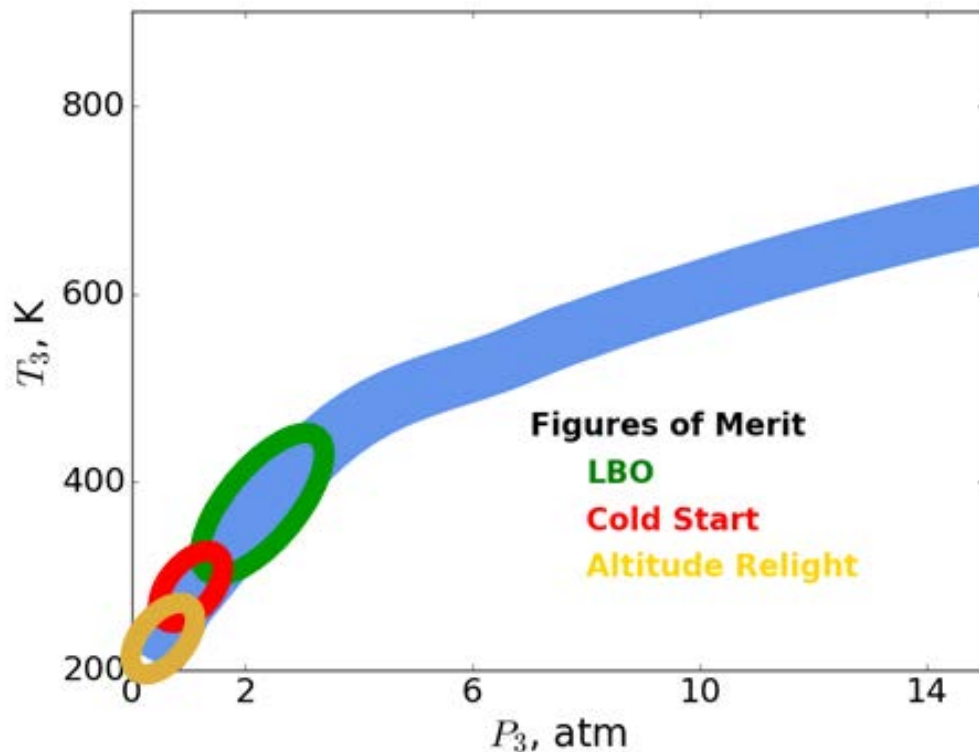


Figure 1. T_3 - P_3 conditions, which are the temperature and pressure at the inlet to the combustor, for measuring the Figure of Merit (FOM) behavior. Targeted Lean Blowout (LBO), Cold Start, and High Altitude Ignition conditions are given as 2-4 atm and 400-450 K, 1 atm and 255-350 K, and >0.25 atm and >230 K for each FOM respectively. Initial experimental capabilities allowed for experiments at LBO conditions vs. the other FOM.

Summary of Technical Results

Fuels

As described in previous papers^{1,3-5}, three conventional (petroleum-derived) fuels and various test fuels, with components from or representing molecules present in alternative fuels, have been identified to span the range of conventional and extreme alternative fuel combustion behavior. Brief descriptions and illustrations of key properties of these fuels are provided in Table 1 and Figure 2. In this way, the three conventional fuels are intended to exhibit ‘best,’ ‘average,’ and ‘worst’ case combustion behavior based on their relative aromatic content, flash point, and viscosity. Further, the various alternative test or ‘designed’ fuels represent a range of fuel properties and compositions expected from alternative fuel processes. Seven additional test fuels in three groups became available in 2017. The first group (C-7, C-8, C-9) were designed to explore new regions of composition/property space as shown in Table 1. Three other test fuels were originally developed by Haltermann for the Army Research Laboratory (ARL), and were designed to have relatively constant physical properties (such as viscosity, flash point, etc.) but widely varying derived cetane numbers (31, 45, 54) as shown in Table 2. These fuels are designed to be used to verify cetane number effects since the C-1 fuel has too many varying properties, other than low cetane. The last test fuel is a new “surrogate” fuel that is enabled by recent acquisition of “iso-dodecane”, which replaces iso-octane in the first two surrogates. iso-Octane significantly impacts flash point and initial boiling point, which can have uncertain effects on combustion behavior.



Table 1. NJFCP category A and C fuels targeted to be tested in as many rigs as possible. The Category A fuels represent the range of petroleum-derived fuels currently in use today. A-1 was recommended as the ‘best’ fuel with low flash point, viscosity, and aromatics, A-2 as the ‘nominal’ jet fuel, and A-3 as the ‘worst’ with high flash point, viscosity, and aromatics. The Category C fuels represent alternative jet fuels that have normal to extreme properties.

Fuel/Solvent Mixture	POSF Number	Composition, % volume	Description
A-1	10264	Petroleum JP-8 (w/high flash point and low viscosity and aromatics)	Low flash, viscosity, and aromatics
A-2	10325	Petroleum Jet A	Nominal jet fuel
A-3	10289	Petroleum JP-5	High flash, viscosity, and aromatics
C-1	11498, 12368, 12384	Gevo ATJ, Highly branched C12 and C16 paraffins	Low DCN, unusual boiling range
C-2	11813, 12223	16% <i>tri</i> -methylbenzene + 84% C14 <i>iso</i> -paraffins	Chemically-asymmetric boiling range
C-3	12341, 12363	64% A-3 + 36% farnesane	High viscosity fuel, at viscosity limit for jet fuel at -20°C
C-4	12344, 12489	60% C9-12 <i>iso</i> -paraffins, 40% C-1	Low DCN, conventional, wide boiling range
C-5	12345, 12713, 12789, 12816	73% C10 <i>iso</i> -paraffins, 17% <i>tri</i> -methylbenzene	Flat boiling range
C-6		High cycloalkane content	High cyclo-paraffins
C-7	12925	75% RP-2, 23% A-3, 2% decalin	High cyclo-alkanes
C-8	12923	Jet A + Exxon aromatic blend	High (maximum allowable) aromatics
C-9	12933	80% R-8 HEFA, 20% <i>n</i> -C12	High DCN

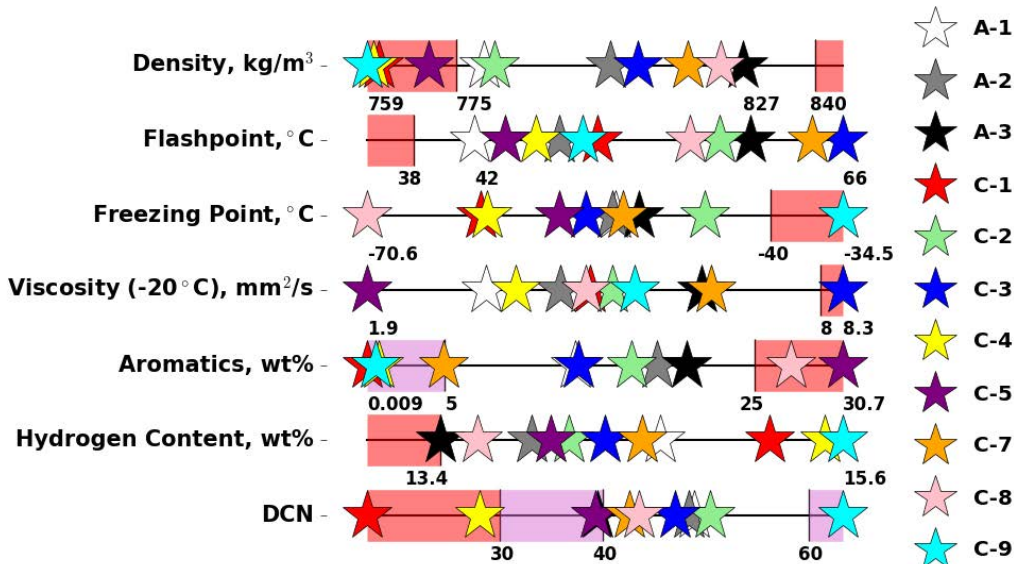


Figure 2. Category A and C range of fuel properties. Red regions represent established limits while purple areas represent proposed limits or areas to explore further. Category A fuels set the bounds of what is currently being used compared to the alternative jet fuel property ranges represented by the Category C fuels.



Table 2. Fuels blended to target specific fuel effects in experiments. These fuels were made to stress specific fuel characteristics at the key FOM. ‘F’ fuels are defined as blends of other NJFCP category ‘A’ and ‘C’ fuels. ‘S’ fuels are surrogate fuels blended to match certain combustion performance characteristics of A-2.

F-1	80/20 A-2/C-2	Blends
F-2	50/50 A-2/C-1	Blends
F-3	20/80 A-2/C-1	Blends
F-4	80/20 A-2/C-5	Blends
n-C12	n-C12	High DCN
n-C12/n-C16 mix	71.6% n-C12, 28.4% n-C16	High molecular weight blend
n-C12/M-xylene mix	75% n-C12, 25% m-xylene	Aromatic
n-C7	n-C7	High DCN, low molecular weight
n-C7/n-C12 mix	31.2% n-C7, 68.8% n-C12	Normal paraffin
n-C12/MCH mix	71.6% n-C12, 28.4% MCH	Cyclo-paraffin
n-C7/n-C16 mix	73.5% n-C7, 26.5% n-C16	Wide boiling range
Sasol (IPK)	~88% iso-alkanes, 12% cycloalkanes, 0.4% aromatic	Highly branched, low DCN
n-C12/i-C8 mix	69.1% n-C12, 30.9% i-C8	Branched paraffin
S-1	59.3/18.4/22.2 vol% n-dodecane/ iso-octane/ 1,3,5-tri-methylbenzene	Similar to A-2, lower density and average molecular weight
S-2	52.6/25.1/22.2 vol % n-hexadecane/ iso-octane/ 1,3,5-tri-methylbenzene	Similar to A-2, higher density and average molecular weight
S-3	34.3/17.4/26.7/21.5 vol% n-C12, n-hexadecane, PMH-iso-C10 (penta-methyl heptane), tri-methyl benzene	Similar to other surrogate fuels with less desirable initial boiling point and flash point properties
HTSI	53.7/17.6/28.8 vol% HRJ Camelina (POSF 10301), NORPAR 13 Solvent, Aromatics 100 (POSF12364)	High TSI, otherwise similar to A-2
Jet A – 55 CN	Nearly constant fuel properties with varying cetane numbers	High cetane (54)
Jet A 45 CN		Medium cetane (44)
Low Cetane Jet A 30 – 32		Low cetane (31)

In Figure 3 we report the total variation in category A and C fuels, and the correlation of properties amongst each other. The relative chemical composition and viscosity of the fuels varies the most across the category A and C fuels in terms of relative variation to A-2. Heats of combustion (both volumetric and mass), density, and surface tension vary the least across category A and C fuels. Perhaps a result of the jet fuel specifications, properties that are required to be within specific limits vary the least across category A and C fuels, while properties not specified in the specification vary the most with the exceptions of viscosity and aromatics.

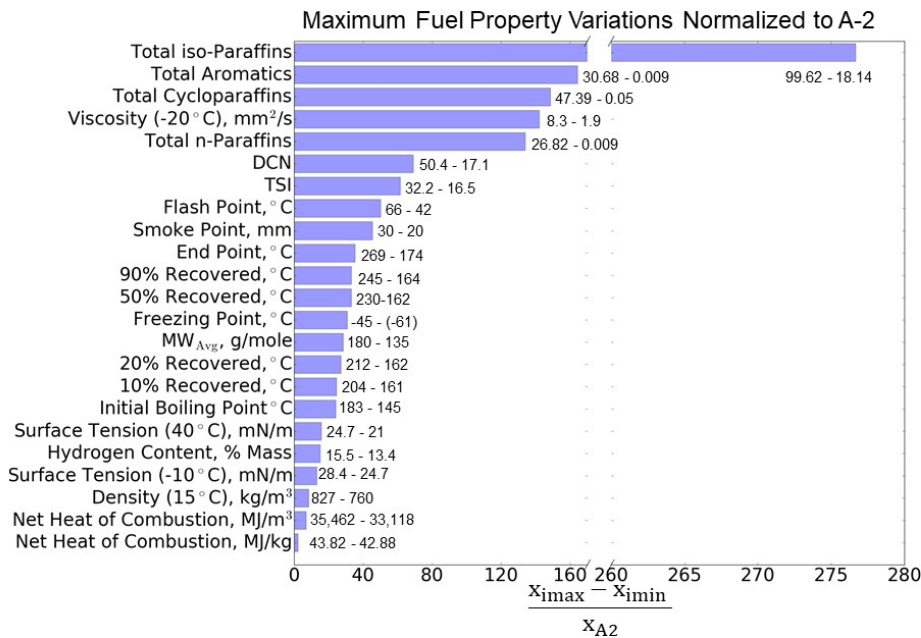


Figure 3. The maximum fuel property variations for Category A and C-1 through C-5 fuels. X_i represents a specific fuel property for a fuel while x_{A2} represents the fuel property for A-2. Chemical properties such as total *iso*-paraffins have the most relative variation while net heat of combustion for the fuels has the least. Knowing which properties vary the greatest can help when considering the bounds for new fuel blends to stress key combustion properties.

Properties are correlated across category A and C fuels via Pearson Correlation coefficients in Figure 4. Properties that are strongly positively/negatively correlated are represented with a large blue/red colored circle, with larger circles expressing more correlation and the absence of a circle expressing no correlation. These properties can be categorized correspondingly as volatility, physical properties, and chemical properties. The volatility properties relate to the distillate properties of the fuel which related to vaporization potential. The physical properties here refer to the viscosity, density, freeze point, average molecular weight, and surface tension. The physical properties most strongly impact the spray character and droplet breakup of a fuel. Finally, the chemical properties here refer to the chemical composition, DCN, H/C ratio, and the heat of combustion. In the subsequent random forest regression analysis, the cross correlation of properties can convolute interpretations of the regressions. Broadly, Figure 4 results show:

- all volatility-volatility properties (e.g. distillation fractions and flash point) are positively correlated;
- physical-volatility property correlations, with the minor exception of freezing point and initial distillation point, are positively correlated;
- the physical-physical properties of viscosity-molecular weight and surface tension-density are correlated;
- chemical-volatility and chemical-physical properties are largely uncorrelated except for DCN-freeze point and *n*-paraffins-freeze point; and
- several chemical-chemical properties are most strongly correlated with H/C ratio which is correlated with H_C , aromatics, and *iso*-paraffins respectively.

These correlations are important later in the paper while interpreting the Random Forest Regression plots which express the relative importance in predicting a FOM performance characteristic with a given fuel property.

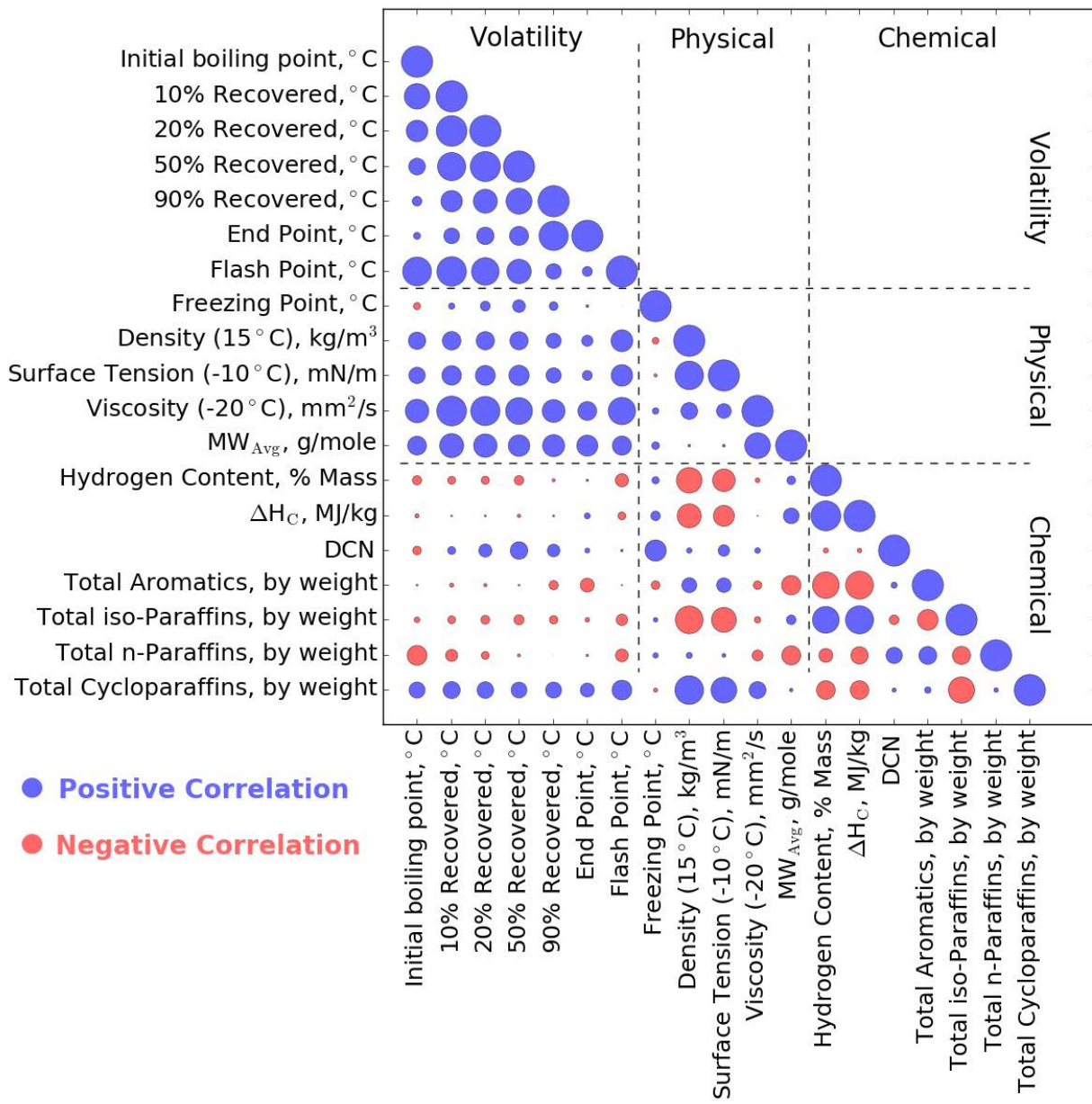


Figure 4. Pearson Correlation of Category A and C fuel properties. Marker size scales with the absolute Pearson Correlation between fuel properties, from zero to one. Positive correlations are marked in blue while negative correlations are marked in red. The properties are further broken down into volatility (distillate), physical, and chemical properties.

Lean Blowout (LBO)

LBO historically has been studied by Lefebvre and Mellor^{6,7}. Lefebvre compared the relative LBO limits of a fuel based on the relative properties of a fuel to JP-4⁶, which culminated in Eq. (1).



$$FAR_{LBO} = \left[\frac{A}{V_{pz}} \right] \left[\frac{\dot{m}_A}{P_3^{1/3} e^{(T_3/300)}} \right] \left[\frac{D_r^2}{\lambda_r H_r} \right] \quad (1)$$

(i) (ii) (iii)

Eq. (1) can be considered as three separate terms each nominally representing orthogonal effects that lead to LBO. The first term, (i), captures the relative effect that a combustor geometry can have on the relative LBO with A being an empirical fit and V_{pz} representing the primary combustion zone of the combustor. The second term, (ii), represents the effect that the mass flow rate (\dot{m}_A) which effects the fluid dynamics of the combustion chamber, the pressure in the combustion chamber (P_3), and the inlet temperature to the combustion chamber (T_3) which effects the chemical kinetic rates. The final term, (iii), represents the effect of fuel properties with D_r being the relative droplet size to JP-4, λ_r being the relative mass transfer coefficient of the fuel versus JP-4, and H_r being the relative heat of combustion as compared to JP-4. Combine these properties have been shown to reproduce experimental data fairly well for historical conventional fuels.

Work reported by Plee and Mellor focused on evaluating the relative time scales for various processes. The work of Burger⁸ more recently showed the relative effect of chemical and evaporative time scales with the chemical kinetic time scale of autoignition dominating the LBO stability limit at high loading parameters. Conversely, at low loading parameters the evaporative time scales dominated the stability limit. Similarly, last year we reported the stability limit for numerous NJFCP rigs at FOM conditions were dominated by the DCN, a property of a fuel's autoignition chemistry². Hence, analysis reported last year, and more so this year, focuses on fuel chemistry effects that are not incorporated into Eq (1). This equation was derived following results of historical conventional fuels which have much less chemical variations as compared to the variations we currently have in the NJFCP. The result of these previous studies can be illustrated phenomenologically as Figure 5.

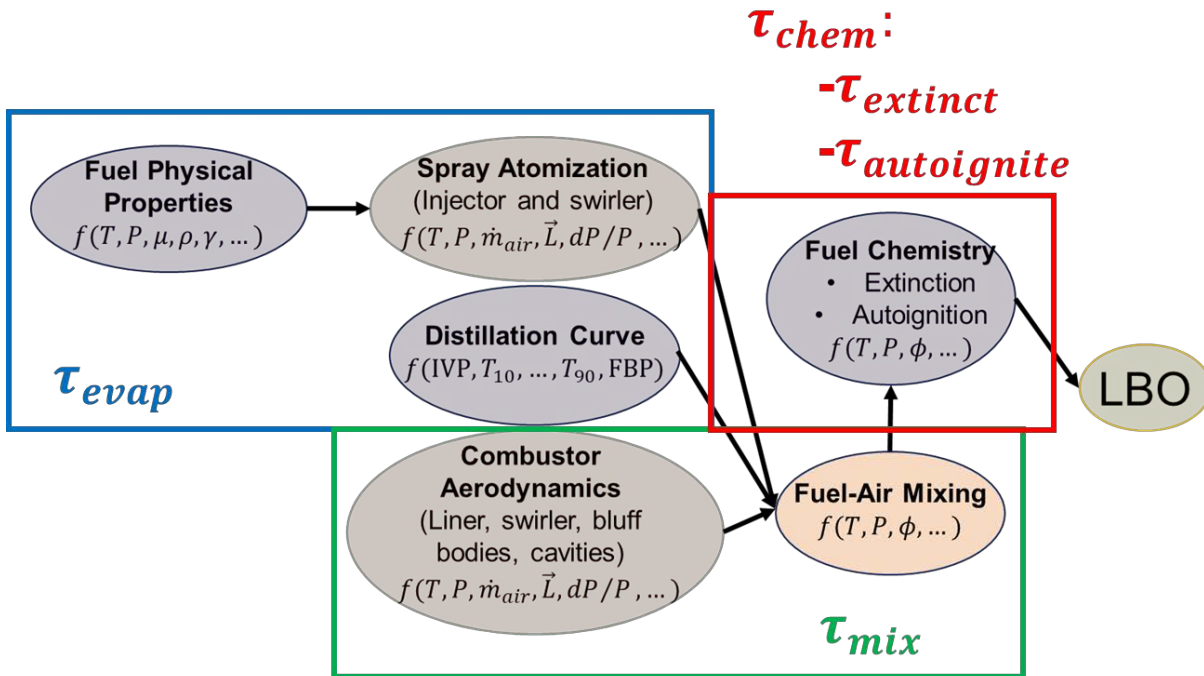


Figure 5. Phenomenological illustration of possible paths to LBO. Three generic time scales define stability with the limit determined by the longest time scale. The orange ovals are more associated with non-fuel property effects. The purple ovals are phenomena associated with fuel effects.



LBO thus scales with the inverse sum of each of the time scales boxed in Figure 5, see Eq. (2).

$$\phi_{LBO_i} \sim \left[\left(\frac{1}{\tau_{evap_i}} + \frac{1}{\tau_{mix_i}} + \frac{1}{\tau_{chem_i}} \right) \right]^{-1} \quad (2)$$

Here τ_{evap_i} is the time scale associated with fuel i 's droplets evaporating which is affected by thermodynamic, spray atomization and distillation curve properties of the combustor. The τ_{mix} time scale is the characteristic time to mix the fuel and air mixtures. This time scale is again dependent on thermodynamic parameters (T and P), geometries (\vec{L}), equivalence ratios (ϕ), and the pressure drop (dP/P) across the swirler and liner. Finally, the chemical time scale can be interpreted as at least two characteristic time scales: an autoignition ($\tau_{autoignite}$) and extinction ($\tau_{extinct}$) time scale, dependent on the fuel and the local equivalence ratio (ϕ). The autoignition time scale here refers to the time needed to raise the temperature locally from a temperature below the critical H+O₂ chain branching temperature to above it in the absence of sufficient heat or mass transfer to initiate or propagate a flame. Finally, it should also be noted that in reality there could be layered or nested timescales within each of these broadly defined time scales.

A brief description of the rigs to study such phenomena and results are detailed in other publications⁸⁻¹⁷, listed in Table 3 and Table 4, and test conditions are illustrated in Figure 6. Eight of the ten rigs in the NJFCP are able to determine LBO limit by reducing flowrates until combustor extinction. The other NJFCP rigs used to study LBO measure emissions as LBO is approached and measure incipient extinction – and not LBO – in the case of the NASA LDI rig and the Oregon State turbulent flame speed rig, respectively.

This year we report the culmination of data from 10 rigs associated with the NJFCP. Figure 7 reports LBO data as a Box and Whisker Plot for NJFCP fuels at conditions near those identified in Figure 1. Φ on the y-axis of the figure is the percent difference of a given fuel relative to the mean $\phi(LBO)$ of A-2, and is defined mathematically as:

$$\Phi = \frac{\phi(LBO_i) - \bar{\phi}(LBO_{A2})}{\bar{\phi}(LBO_{A2})} \quad (3)$$

where $\phi(LBO_i)$ is a single LBO event for fuel i and $\bar{\phi}(LBO_{A2})$ is the mean LBO ϕ for A-2. This normalization accounts for variations across rigs in dilution air and other combustor design characteristics. The symbols represent individual LBO observations, the whiskers of the plot represent the upper and lower 99.1% confidence intervals, the lower and upper limits of the shaded rectangles are the 25 and 75 percentiles respectively, data points outside the whiskers are outliers, and median is represented by the horizontal line in the rectangle for the percent difference relative to the nominal jet fuel (A-2). Values of $\Phi > 0$, for a given fuel, are LBO events with a $\phi(LBO_i)$ greater than the mean LBO ϕ of A-2. Thus, the stability of the fuel is worse than A-2. Inversely, $\Phi < 0$ is considered more stable LBO behavior as the fuel was able to stabilize in the rig at a lower equivalence ratio. This plot shows statistically the variation in the conventional (category A) fuels versus the observations with the alternative (category C) fuels. Statistically, only C-1 and C-4 are outside the LBO performance of all the category A fuels for the Referee Rig as the upper whiskers of the category A fuels do not overlap the lower whiskers of C-1 and C-4. Similarly, C-1 is observed to have distinguishable LBO performance for the GT rigs and the WSR. The Honeywell APU, however, does not exhibit this behavior with no category C fuels performing worse than the conventional fuels.

Analysis of these rigs suggests that the Derived Cetane Number (DCN) is the best predictor for combustor stability, see Figure 8. Eight of 9 rigs that measure LBO or the onset of it show strong correlations with DCN. Seven of the 8 rigs that can directly measure LBO also show this trend. In the case of several rigs, an $R^2 > 0.9$ is achieved by a simple one dimensional regression versus LBO. Further, Random Forest Analysis combining measured fuel properties with LBO data corroborates the dependency of LBO on DCN, see Figure 9. Additional Random Forest Analysis regressions are reported in the Task 4 Appendix. While to first order the LBO trends well with DCN, Random Forest Regressions show deviations across rigs and devices. Collectively, these results strongly corroborate our previous results and those more recently reported by Burger, and that the chemical time scale for autoignition is the limitation for combustor stability. More detailed studies have been performed at Georgia Tech to investigate the potential effect of autoignition⁹. This work focused on measuring the chemiluminescence in the rig near blow out. Movies of these diagnostics appear to show the approach to LBO being a two stage process, the first stage being the transition of a local signal to the absence of one, local extinction. Local extinction then begins to dominate the frame as fuel flow is sequentially reduced. During the progression of increasing local extinction, local autoignition appears in regions with no initial signal at earlier times. Thus,



the limit of the rig sustaining any combustion is when autoignition ceases to occur. The Georgia Tech team also reported that at a given ϕ above the LBO limit an indefinite series of autoignition-extinction events could be observed.

Additional regression parameters are observed to be important such as the relative atomizer and rig geometry as illustrated in Figure 9. These parameters and the subsequent Random Forest regressions in the Task 4 Appendix show that, while DCN is shown to be a common parameter determining the LBO limit, the regressions between two rigs can be drastically different. This is partially illustrated in Figure 10 which compares the slope of the lines in Figure 8 for various rigs. The most sensitive rig to LBO is the Sheffield rig, and the least sensitive rig to LBO is the prevaporized and premixed WSR.

Finally, the Honeywell rig, which showed no correlation between DCN and LBO, has shown to have different geometrical characteristics. The Honeywell rig has an Axillary Power Unit (APU) combustor geometry. Thus, the size is overall smaller than the other rigs which represent a more main engine size and configuration. The smaller size in turn means there is no swirler to generate a primary recirculation zone as in the Referee Rig, and the flow number of the nozzle is smaller than the corresponding Referee Rig. These features combine to make physical properties of the fuel drastically more important, see Figure 23 located in the Appendix to this section.

Table 3. Summary of LBO rigs and test conditions. LBO results for each rig are detailed in these papers⁸⁻¹⁸.

Rig Name	Geometry type (injector/swirler)	T _{air}	T _{fuel}	P	Institution
PA-GT	Pressure atomizer/ Pratt & Whitney Swirler	550, 450, 300 K	445- 460 K	3.4 atm	Georgia Tech
AA-GT	Air blast atomizer/ Pratt & Whitney Swirler	450 K	445- 460 K	3.4 atm	Georgia Tech
PA-HON	Pressure atomizer/ toroidal	324, 525, 557, 562, 394 K	288 K	1, 1.3, 1.4, 3.3, 5.7, 2 atm	Honeywell
PA-RR	Pressure atomizer/ High-Swirl (P03)	400 K	320 K	2 atm	AFRL/UDRI
PV-WSR	Prevaporized/ toroidal	450 K	450 K	1 atm	AFRL/UDRI
LDI-NASA	Lean Direct Injection/ swirl stabilized	575, 645, 730, 830 K		6.8, 10.9, 17 atm	NASA
AA-SH	Airblast atomizer/ swirler stabilized/Rolls-Royce Tay Combustor	323, 373, 423 K		1 atm	Sheffield
PA-OSU	Pressure atomizer/ swirl stabilized	470 K		1 atm	Oregon State
PA-CAM	Pressure in bluff-body/	340 K	300 K	1 atm	Cambridge
PA - UTRC	Pressure atomizer/ Pratt & Whitney Swirler	555, 494 K		8.64, 5.6 atm	UTRC
PA-DLR	Pressure atomizer/ swirl stabilized	323, 373 K		1 atm	DLR Germany

*Future analysis of GT data is only for the 450 K testing.





Table 4. LBO rigs and fuels tested. Bolded fuels were tested in the last year for Sheffield and Cambridge. Non-NJFCP fuels tested at UTRC and DLR Germany are listed in the table as well and included in some of the LBO results presented in this paper.

	A-1	A-2	A-3	C-1	C-2	C-3	C-4	C-5	F-1	F-2	F-3	F-4	S-1	S-2	nC12
GT	X	X	X	X	X	X	X	X	X	X	X		X	X	X
Honeywell	X	X	X	X	X			X							
Referee Rig	X	X	X	X	X	X	X	X	X	X	X	X	X	X	X
WSR		X	X	X			X	X							X
NASA		X		X		X									
Sheffield	X	X	X	X		X	X	X							
Oregon State		X		X					X						
Cambridge		X		X					X						
UTRC	Sasol IPK, F-76, L-210, JP-5, Jet-A, L-142, HRJ JP-5, Linpar 1416														
DLR	Crude-derived Jet A-1, Jet A-1 + 50% n-dodecane, FSJF (certification), FSJF (commercial), FSJF (commercial) + 1.5% HCPP, Experimental GTL kerosene, Synthetic paraffinic kerosene (SPK), Heavy naphtha refinery stream														

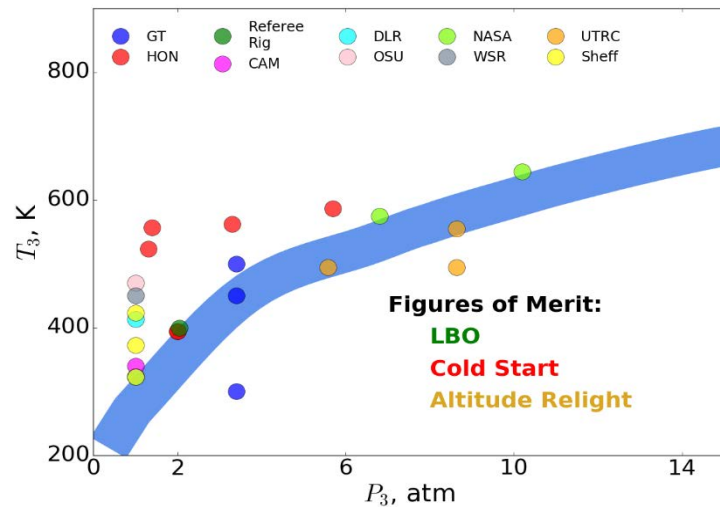


Figure 6. P_3 - T_3 figure displaying the rig conditions tested to measure LBO, one of the Figures of Merit (FOM), for Georgia Tech (GT), Honeywell (HON), Referee Rig, Cambridge (CAM), DLR Germany (DLR), Oregon State University (OSU), NASA, the Well-Stirred Reactor (WSR), United Technologies Research Center (UTRC), and the University of Sheffield (Sheff). LBO test conditions fall within 2-4 atm and 400-450 K for main engines. APU LBO conditions can vary as evident from the elevated T_3 s and lower P_3 s tested here.

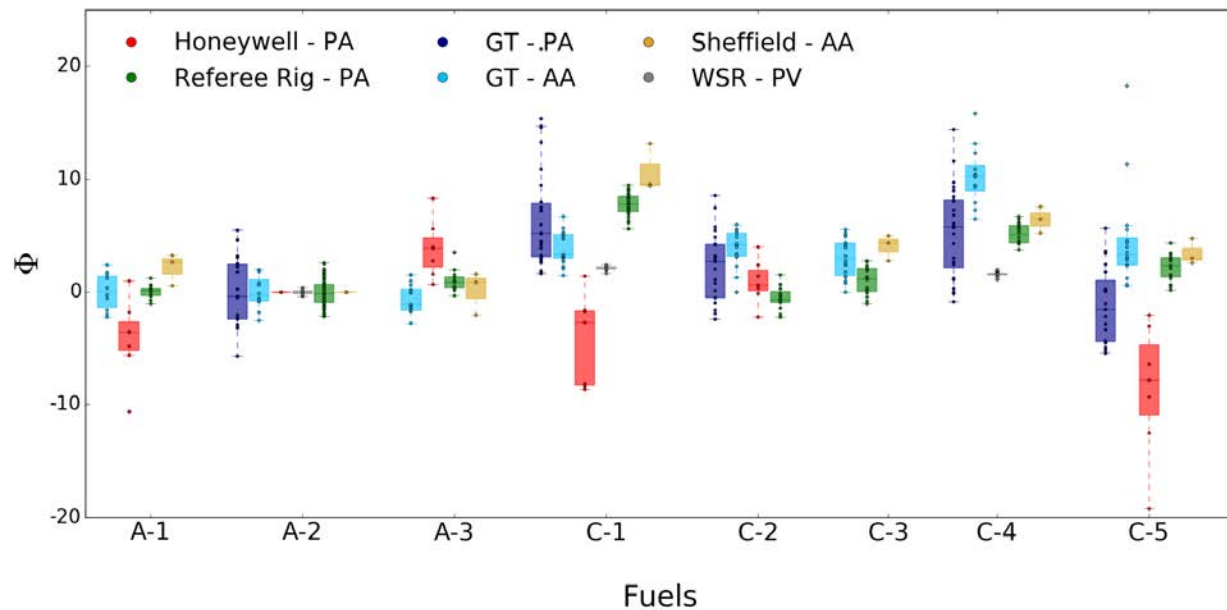


Figure 7. Box plot of LBO percent differences for NJFCP fuels across various rigs. PA (pressure atomized), AA (airblast atomized), PV (pre-vaporized), refers to the vaporizing mechanism used in the respective rigs. Honeywell, Referee Rig, GT (Georgia Tech), Sheffield (University if Sheffield), and WSR (Well-Stirred Reactor) refer to the respective institutions and/or rig at which the fuels where tested. The scatter for LBO percent difference can be observed for each rig for the category A and category C fuels where the circles represent individual data points and the box represents the lower and upper quartiles along with the median. Data that falls outside of the box and lines represents outliers. While C-1 and C-4 have the overall highest LBO equivalence ratio, variability among tests are still largely greater than the LBO differences observed among the fuels.

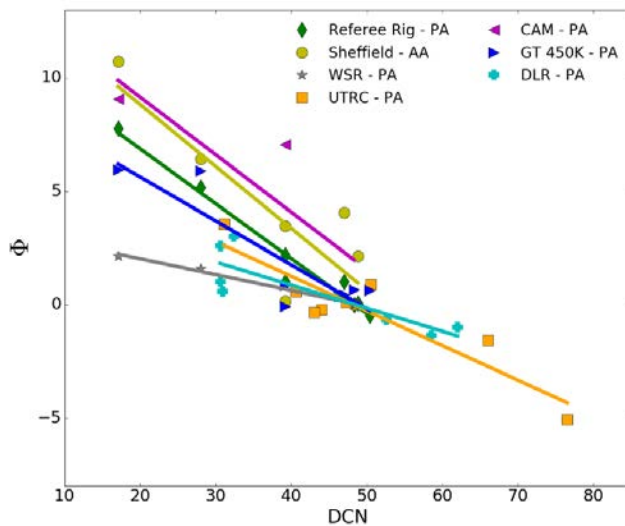


Figure 8. Relative LBO rig sensitivity to DCN. Currently, 7 of the 8 rigs that directly measure LBO show first order sensitivity to DCN. The Honeywell rig is the only one that is not stabilized with a swirler and has a low flow number injector. It does not show the sensitivity to DCN and is not plotted here.

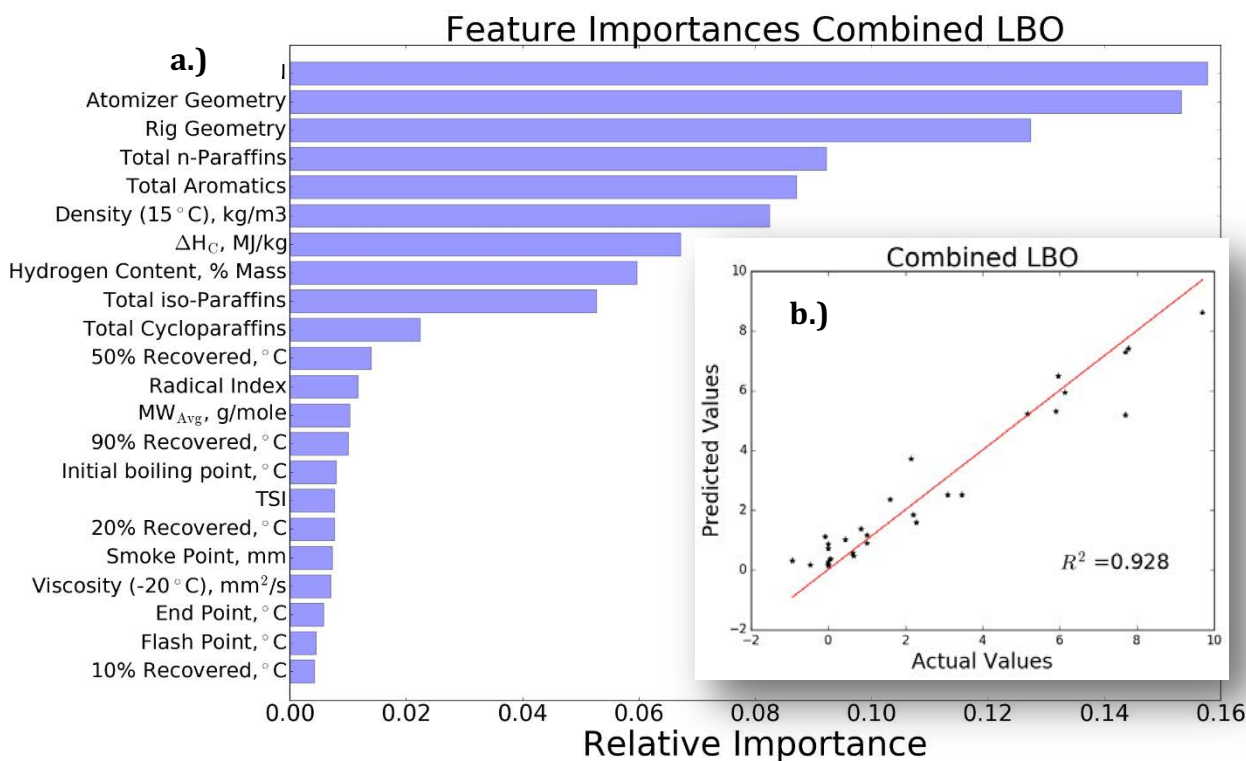


Figure 9. Random Forest regression feature importance and fit for combined LBO. a.) DCN is the most important factor in determining LBO when looking at the combined results from the Referee Rig, Georgia Tech, University of Sheffield, Oregon State and the Well-Stirred Reactor. b.) The predicted versus measured (actual) values for combined LBO for the five rigs included.

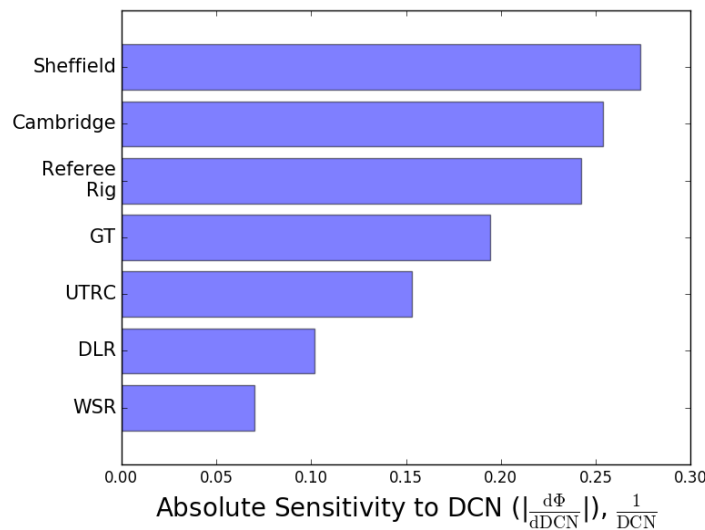


Figure 10. Absolute rig sensitivity to DCN for LBO. Comparing sensitivities across rigs, Sheffield shows the highest sensitivity to DCN while the Well-Stirred Reactor (WSR) shows the least sensitivity.



Ignition

Ignition is a critical performance metric for alternative fuel certification as the consequences of an unsuccessful relight in flight could be catastrophic. Thus, similar to LBO, the ignition performance of an alternative fuel undergoing certification must be equivalent or, preferably, better than typical conventional fuels. Historically, the certification of previous alternative fuels and experience has yielded the criteria that a fuel must have a viscosity less than 12 cSt at -40 °F. This criteria is required to enable sufficient spray performance to ignite. Not only do these cold conditions deleteriously effect the spray character, they also can inhibit the ability of a fuel to form a combustible mixture with air as the vapor pressure of the fuel is lower at lower temperatures. Testing fuels at the appropriate conditions is essential to mapping laboratory performance to real engines and the certification process. Year 2 of the NJFCP has largely been devoted to capacity development for these cold air and fuel at sub-atmospheric conditions. Table 5 and Table 6 report conditions, brief descriptions of rigs, and fuels tested in rigs associated with the NJFCP. Nominally, rigs are designed with the intention of matching the FOM conditions in Figure 1. Data from the Referee Rig and Cambridge ignition studies are still in process and will not be reported here, although a recent paper details the Referee Rig progress on ignition¹⁹. Figure 11 reports the air temperatures and pressures of experiments on the T_3 - P_3 plot reported earlier. Figure 12 reports the fuel temperatures the individual rigs are capable of testing at. Here we present nominal ignition results and their analysis from 4 different rigs: 2 combustor rigs and 2 more fundamental configuration.

Combustor rig test comparisons at Honeywell (APU combustor)¹¹ and NRC Canada (TRS18 engine)²⁰ are reported in Figure 13. These rigs are compared on the basis of minimum equivalence ratios for ignition as Box and Whisker plots. Unlike the previous LBO plot which illustrated results at a given condition, these results are for multiple conditions, see Figure 11, and the normalization of Φ for each point is at similar conditions. Fuels with minimum equivalence ratios (Φ_s) greater than zero once again have deleterious performance characteristics relative to A-2. Category C fuels with lower whiskers above the highest whisker of category A fuels are statistically distinct. The Honeywell rig did not observe any category C fuels that performed worse than the worst category A fuel (A-3). However, the C-3 results from NRC Canada did produce worse ignition performance than any of the tested category A fuels. It should be noted that NRC Canada did not test A-3 which is considered the 'worst' conventional fuel in the NJFCP, and the C-3 fuel was not tested at Honeywell. Random Forest regressions of the NRC Canada and Honeywell data (Figure 14) suggest that the properties most effecting minimum ignition equivalence ratios are viscosity and volatility/distillate properties. C-3 is a blend containing 64% of A-3 and 36% farnesane, suggesting that the results between the two rigs are largely consistent.

Figure 15 reports relative ignition probabilities for several NJFCP fuels at a fixed equivalence ratio^{21,22} at atmospheric pressure and at air temperatures of 478 K and 300 K for the prevaporized and liquid spray tests, respectively. The prevaporized fuel temperatures were around 450 K while the liquid spray was injected at 295 K. The probabilities as reported here are the single spark ignition probabilities determined from multiple ignition attempts. Two types of experiments are reported with one experimental configuration being prevaporized and partially premixed, while the other configuration employed a liquid spray jet. The deleterious fuel effects in this plot are associated with negative values on the y-axis. Interpretations from the spray configuration are preliminary and may change upon further analysis. Interestingly, A-3 is observed to perform better than all the category A and C fuels for the spray experiments. The prevaporized and partially premixed ignition experiments (GT PV) in Figure 15 show little fuel effect influence.

Additional cold fuel and air experiments at or below one atmosphere are being analyzed for two Referee Rig type geometries at AFRL/UDRI and ARL/UIUC. Preliminary analysis of these data sets suggest general consistencies with the Honeywell and NRC Canada results. Spray quality and fuel volatility via viscosity and distillation curve, respectively, determine the relative ignitability of a fuel. The implications for the fuel certification process is that alternative fuels preferably exhibit lower viscosities and higher volatilities to ensure safe and functional operability during altitude relight and cold start.



Table 5. Summary of ignition rigs and conditions tested. Ignition results for each rig are detailed in these papers^{10,11,18-22}.

Rig Name	Rig Description	Ignition Source	T _{air}	T _{fuel}	P	Institution
NRC-CAN	Pressure atomizer in a small gas turbine engine (TRS-18)	Discharge	254 to 268 K	254 to 268 K	10-17 kft	NRC-CAN
Honeywell	Pressure Atomizer in APU	Discharge	230 to 317 K	236 and 288 K	0.2 to 1.1 atm	Honeywell
Cambridge	Partially Prevaporized flow Rig	Laser (YAG)	323 to 373 K		1 atm	Cambridge
GT – PV	Prevaporized fuel/air flow split from air coflow	Discharge	478 K	450 K	0.96 atm	Georgia Tech
Referee Rig	Pressure atomizer, high swirl	APU Igniter	394 and 233 K	322 and 233 K	2 atm	AFRL/UDRI
GT – Spray	Pressure atomizer injected into air coflow	Discharge	300 K	244 and 295 K	0.96 atm	Georgia Tech

Table 6. Ignition rigs and fuels tested. Bolded fuels for the Referee Rig and Georgia Tech Spray are new fuels tested since last year.

	A-2	A-1	A-3	C-1	C-2	C-3	C-4	C-5
NRC-CAN	X			X		X		X
Honeywell	X	X	X	X	X			X
Cambridge	X			X				
GT – PV	X	X	X	X	X	X	X	X
Referee Rig	X	X	X	X				
GT – Spray	X							

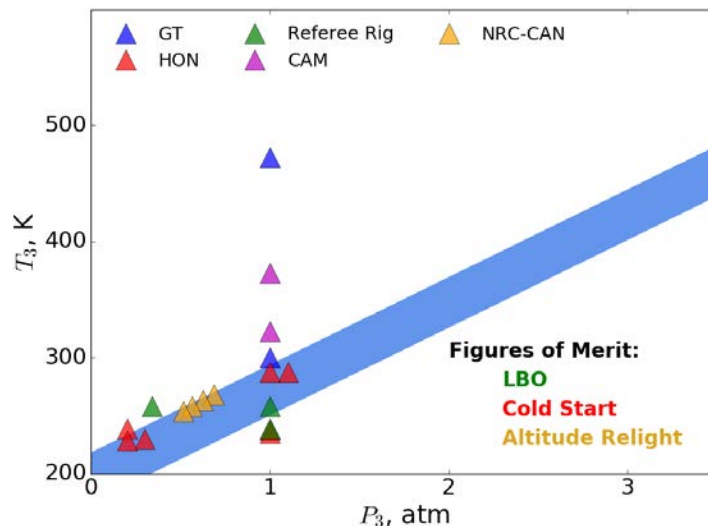


Figure 11. P₃-T₃ figure displaying the rig conditions tested to measure the Figures of Merit (FOM), specifically for the cold start ignition and altitude relight tests for Georgia Tech (GT), Honeywell (HON), Referee Rig, Cambridge (CAM), and NRC-Canada (NRC-CAN). Cold start and altitude relight conditions occur at 1 atm and 225-350 K, and >0.25 atm and >230 K, respectively.

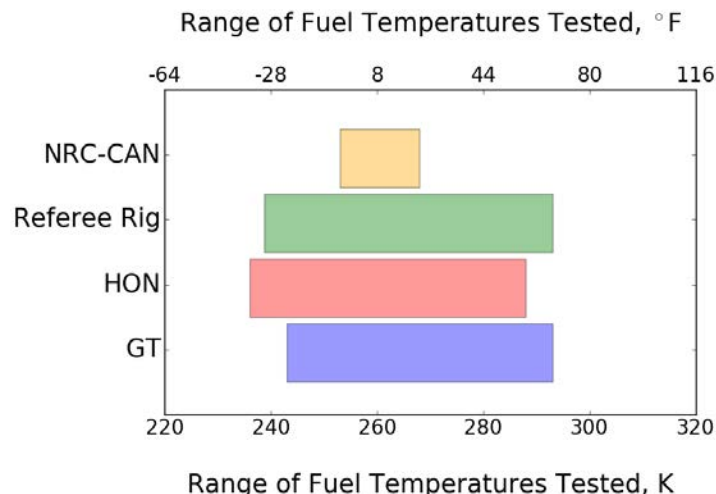


Figure 12. Range of fuel temperatures that were used in ignition testing from NRC Canada (NRC-CAN), Referee Rig, Honeywell (HON), and Georgia Tech (GT). Fuel temperatures heavily impact ignition performance as they change viscosity, surface tension, and density of the fuel making ignition more difficult at lower temperatures.

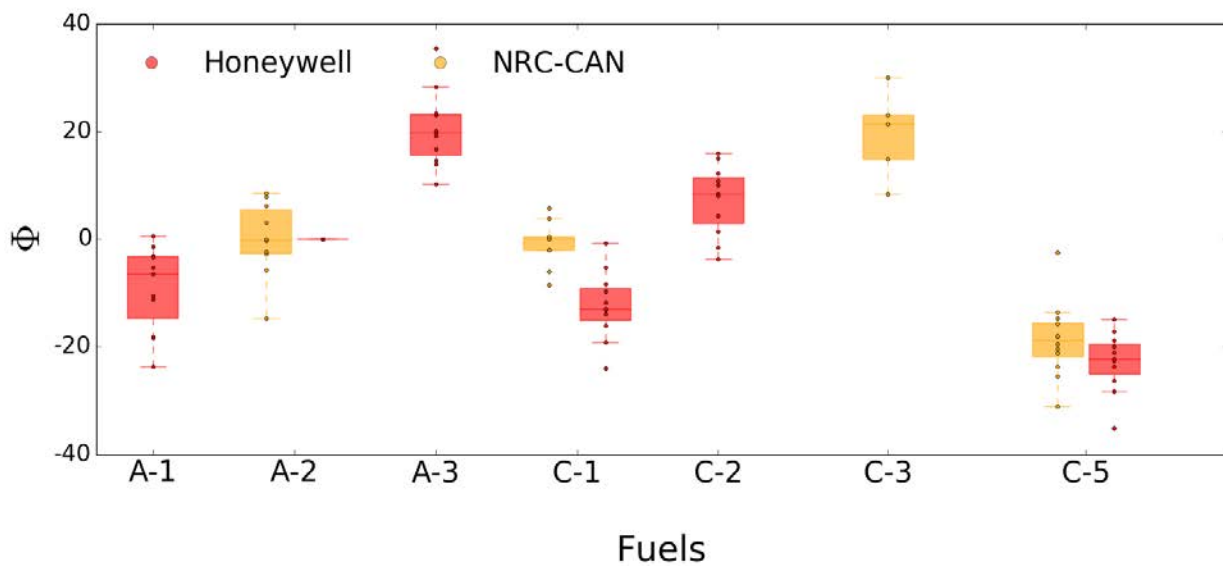


Figure 13. Honeywell and NRC Canada (NRC-CAN) ignition box plot of minimum normalized equivalence ratios for ignition. The circles represent individual data points while the box represents the median and lower and upper quartiles. Points that fall outside the box and line range are outliers. The Honeywell ignition data was collected at two different fuel temperatures (15°C and -37°C) at seven different inlet temperatures and pressures and was normalized to A-2 for each test condition. The NRC-Canada ignition data was collected at four different altitude conditions with a constant fuel temperature around -13°C and was normalized to A-2 for each altitude condition. Of the seven fuels tested, A-3 and C-3 performed the worst, while C-5 performed the best for both Honeywell and NRC-Canada.



Feature Importances Honeywell Ignition

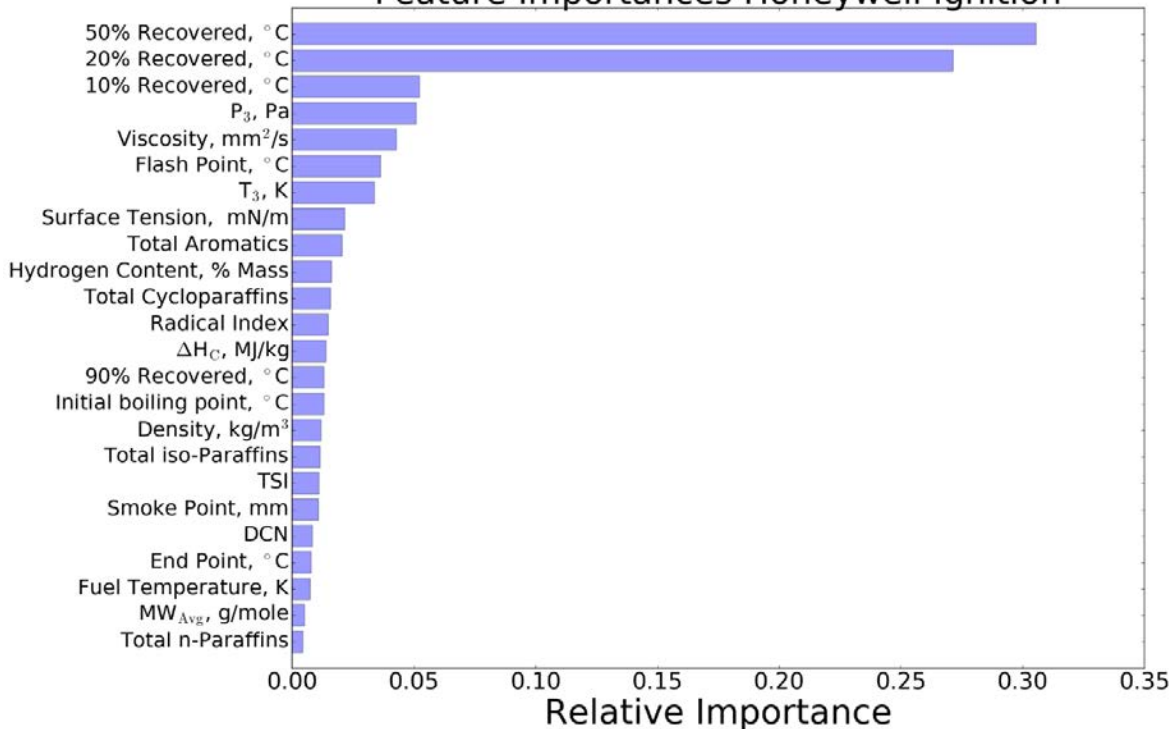


Figure 14. Random Forest regression feature importance and fit for minimum ignition FAR in a Honeywell APU. The physical properties, such as the distillation curve and viscosity, of the fuel dominate the relative ignition performance of a fuel in addition to the inlet pressure and temperature. The viscosity, surface tension, and density values used are based off of the temperature of the fuel tested. NOTE: Units have been intentionally renormalized such that these numbers are not relevant to actual operating limits.

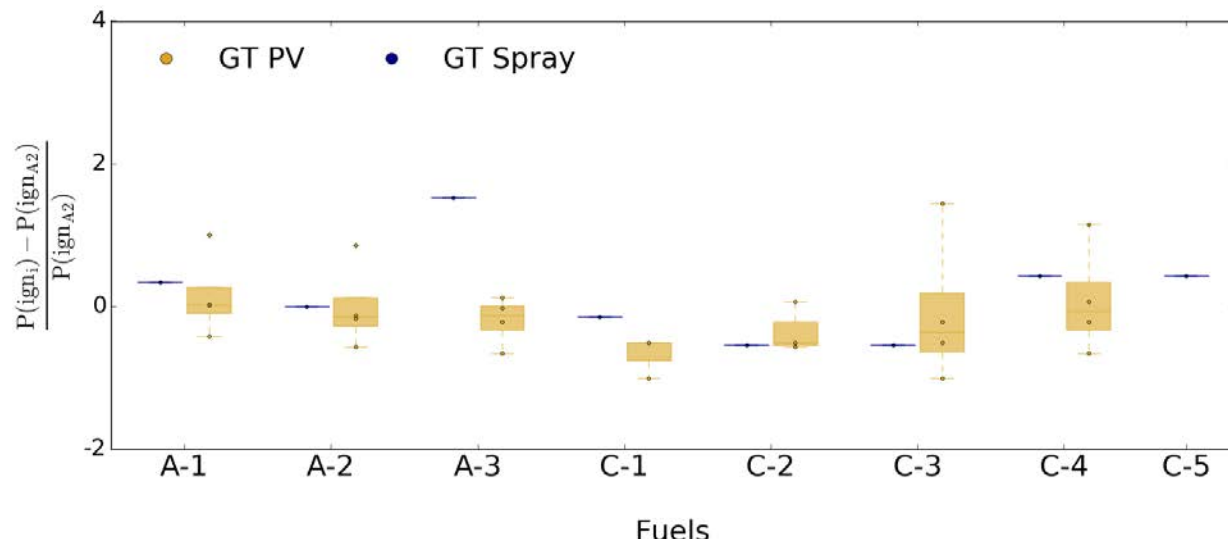


Figure 15. Georgia Tech Prevaporized (GT PV) and Georgia Tech Spray (GT Spray) ignition box plot of normalized probability of ignition. The circles represent individual data points while the box represents the median and low and upper quartiles. Points that fall outside of the box and line range are outliers. Instead of measuring ignition performance using minimum equivalence ratio to ignite, a fixed equivalence ratio for each test was used and the probability of ignition was measured. The Georgia Tech prevaporized ignition data included here was run at an equivalence ratio of 1.5-1.57 with an average test section temperature of 480 K and fuel vapor temperatures around 450 K. The Georgia Tech spray ignition data was run at an equivalence ratio of 0.55 with an air temperature of 300 K and fuel temperature of 295 K.

Computational Fluid Dynamics

Computational Fluid Dynamic (CFD) simulations of the combustion experiments conducted under this program were performed at several locations including Stanford University, Georgia Institute of Technology (GT), and United Technologies Research Center (UTRC). Current CFD simulations are focused on LBO predictions in the Area 6 referee rig for the NJFCP test fuels A-2, C-1 and C-5. Predictions of LBO fuel sensitivity were completed by Stanford using a Flamelet/progress-variable approach and spray injection based on Rosin-Rammler drop size distribution with secondary breakup included in the spray evolution²³; these simulations predicted the LBO fuel trend for A-2 versus C-5 in agreement with experiments, but predicted the opposite LBO fuel trend for A-2 versus C-1 compared to experiments. Since January 2017, the three CFD teams have agreed on a consistent set of spray injection conditions for A-2, C-1 and C-5 based on non-reacting spray measurements conducted at Purdue University and provided by the Spray Working Group. PDPA data measured at 25mm downstream of the injector cup exit is projected upstream into six concentric rings at a location 2mm from the fuel nozzle exit and the experimental drop size distribution is randomly sampled in each ring in the CFD simulations. Spray velocity magnitude and direction at several radial locations based on the PDPA data are also used in the spray injection conditions for the CFD simulations. No secondary spray breakup is used in current simulations of approach to LBO. PDPA measurements at the near LBO condition in the referee rig are available to compare with CFD simulations. Chemistry models for the A-2, C-1 and C-5 test fuels employed in the CFD simulations are the full HyChem models, reduced models based on HyChem, or a set one-step mechanisms tuned to match HyChem predicted laminar flame speeds over a range of equivalence ratios.

Approach to LBO simulations for the Area 6 referee rig begin at the experimental near LBO condition (an equivalence ratio $\phi=0.096$, or slightly higher if required to obtain a stable flame) for the A-2, C-1 and C-5 test fuels. Step reductions in fuel mass flow rate on the order of a 4% change in ϕ are performed after confirming that a stable flame exists at each new ϕ . Flame stability is evaluated in terms of time histories of integrated heat release rate (such as shown in Figure 16) and total evaporation rate oscillating about an essentially constant average value after an initial transient, as well as by inspection of contour plots of temperature and species concentration variables in cut planes through the center of the combustor



indicating a significant flame is still present in the combustor. All three teams have established stable flames at the near LBO condition using the new spray injection conditions. Improvements were seen in CFD predicted drop sizes and velocities compared to PDPA data at the near LBO condition using the new spray injection conditions. Simulations of approach to LBO are underway for the A-2 and C-1 test fuels. Also, while CFD work is currently focused on LBO predictions, initial simulations have begun on the forced ignition experiments in the Georgia Tech Prevaporized (GT PV) rig experiments²¹ which track the evolution of ignition kernels (but not the establishment of a stable flame).

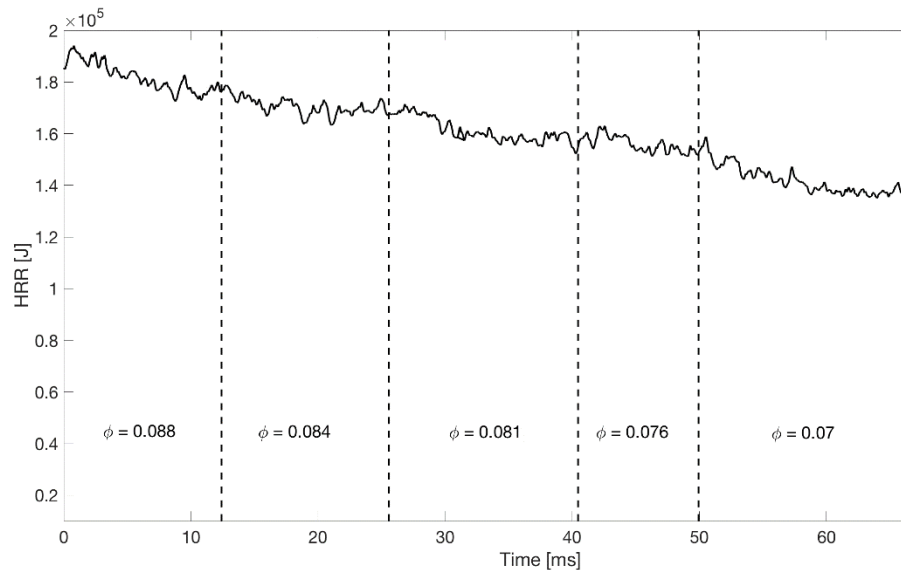


Figure 16. Time history of integrated heat release rate over entire CFD grid during approach to LBO simulations using step reductions in fuel mass flow rate for the A-2 fuel²⁴.

Common Format Routine

The performance evaluation of an alternative fuel has historically utilized OEM experimental hardware, which is costly. These tests are essential due to FOM dependency on rig geometries and otherwise proprietary information. And the proprietary information is critical to the proper comparison of an alternative jet fuel to conventional fuels. The CFD Working Group is iterating towards FOM evaluation methods using academic codes. Unfortunately, the CFD codes as written by the academic teams are not conducive to OEM usage. The codes maybe written in languages not standard in OEM workflows, and if they are, the formatting and communication between other engineering standard work by OEMs. A need is identified in the NJFCP to bridge this chasm between the latest CFD theory and codes and OEM standard work. For this reason, the Common Format Routine (CFR) Working Group was established to reformulate and package codes into software that can innately mesh with OEM modeling methods.

The current (CFD) evaluation of a jet fuel by the NJFCP involves many methods, models, and codes to represent essential chemistries, sprays, fluid dynamics, and other physics. Each of these physical models has its own impact on the evaluation of relative fuel performance. Year 2 of the NJFCP identified a critical need to develop a CFR for the development of two of these models: a flamelet prolongation of the intrinsic low-dimensional manifold (FPI) model, used for premixed combustion, and a flamelet progress variable (FPV) model, utilized for nonpremixed combustion²⁵. These models previously did not exist for OEM standard work and provided an opportunity for more robust fuel evaluation of OEM hardware by OEMs.

Figure 17 displays the results of four model predictions (lines) and experimental values (red symbols) for the Sandia D flame. Blue lines represent the CFR models developed as part of the NJFCP for $k-\epsilon$ and $k-\omega$ RANS simulations, and black lines are those of the default FLUENT capabilities. The CFR model reproduced experimental data as well or better than the default FLUENT code, particularly for the $k-\omega$ simulations.

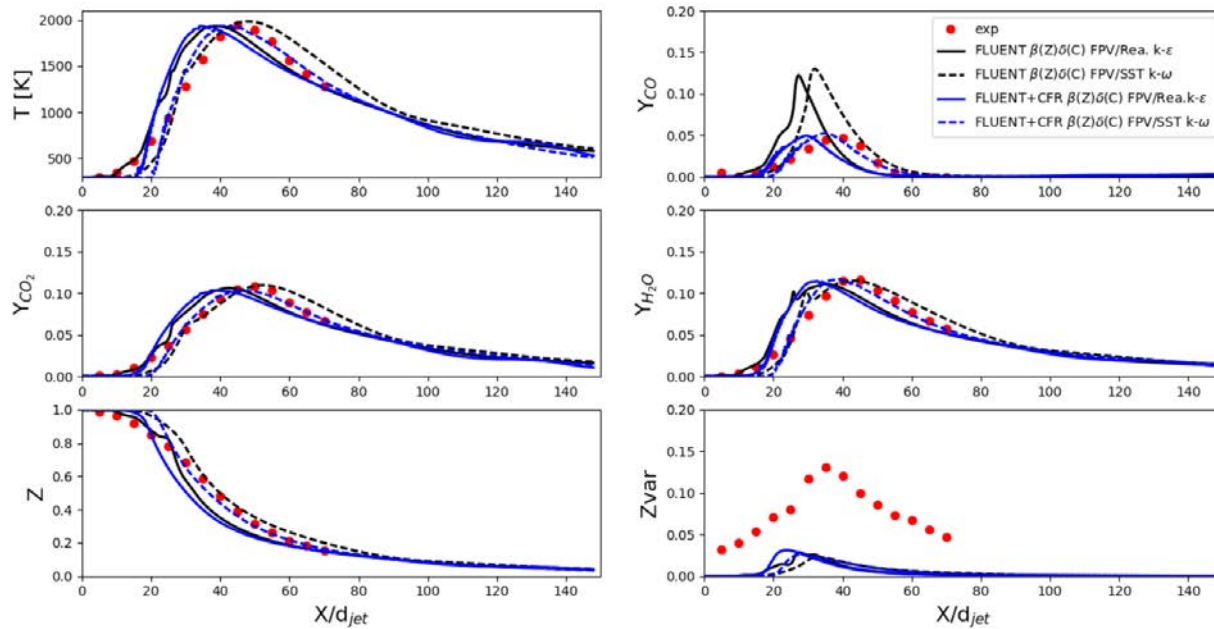


Figure 17. Centerline comparison between experiments and RANS simulations of the Sandia D turbulent flame. Reproduced from an anticipated publication²⁵.

In addition to model development, the CFR Working Group has packaged these codes into a Graphical User Interface (GUI) / Text-based User Interface (TUI) which removed the requirement that OEMs communicate with the software in a potentially non-native language.

Chemical Kinetics

Major accomplishments in the tracking of the chemical kinetics of fuels over the past year include:

1. Development of new capabilities for (nearly) simultaneous measurements for the evolution of species as a function of time in the shock tube
2. Collection of new speciation data, for more fuels, in the shock tube and in a new reactor facility
3. New ignition delay data showing variability in the hot ignition region with DCN
4. Refinement and documentation of the HyChem modeling approach, and
5. Exploration of alternate methods for mechanism reduction following strong pull from the CFD modeling teams for smaller, yet still reliable, mechanisms.

The next several paragraphs provide more details on the progress.

New optical diagnostic capabilities at Stanford have been developed this past year, using multiple infrared absorption lines that allow for the simultaneous determination of the evolution of olefinic species during pyrolysis of the parent fuel. In addition, infrared absorption characteristics of aromatic species have been explored to estimate the concentration of the aromatic species, specifically those of benzene and toluene. Along with the olefinic species and methane, the tracking of (limited) aromatics allows for the recovery of nearly 90% of the carbon contained in the pyrolytic products of the parent fuel molecules.

New shock tube data on the pyrolysis of the NJFCP fuels at Stanford have been collected. In addition, new pyrolytic data has been collected at AFRL by partially decomposing fuels under high temperature, high pressure conditions flowing through a long narrow reactor tube. Products at AFRL are being analyzed via an on-line FTIR. Similar to previous plots generated by Stanford showing a correlation between ethylene product yield and DCN, correlations were made for product species vs. the lean blow-off limit (LBO) as observed in the referee rig (described in the LBO section of this manuscript). Since LBO has been shown to correlate with DCN the AFRL results have similar trends to the Stanford results. The AFRL correlations, however, extend Stanford's results, since AFRL has found nearly all of the species data correlate with LBO (not



just ethylene) and that some species (e.g., isobutene and methane) are anti-correlated. This contrary dependence is consistent with the general understanding in chemical kinetics regarding the relative ease of combustion of ethylene and other straight chain olefins vs. slower combustion rates for methane and isobutene.

In addition to the speciation data under pyrolytic conditions, Stanford has also measured ignition delay times (IDT) above 1100K in the ‘hot ignition regime’ for a series of fuels with varying DCN values, ranging from about 17 to 55. Previously, it had been well established that IDT vary with DCN in the negative temperature coefficient region, typically lower than 1000 K. But the newly obtained results clearly show a consistent trend of increasing IDT with decreasing DCN above 1200 K.

The HyChem modeling approach for simulating the combustion kinetics of real fuels has been reviewed and is being documented in two companion articles to be submitted for publication^{26,27}. The first article reviews the theory behind the model construction. The second applies the method to several ‘real’ fuels that are approved for application. The model is based on the experimental data on pyrolytic products and then validated against the ignition delay, flame speed, and flame extinction data. Once this documentation is complete, the method will be re-applied to the Category C fuels.

Reduction methods of the chemical kinetic models have been successfully developed and applied by the University of Connecticut to the NJFCP fuels to reduce the reaction models down to about 35 species. While this reduction is a significant achievement with minimal loss of fidelity in replicating kinetic predictions, there is a desire to reduce further the models to facilitate detailed simulations using computational fluid dynamics (CFD). Pre-processed Flamelet solutions can be used to capture the characteristics of the detailed mechanisms, but does not guarantee accurate simulation of the interaction of the turbulence and the chemistry near limit behavior at flame extinction or re-ignition. The University of Connecticut, together with Georgia Institute of Technology, are now exploring Chemical Explosive Mode Analysis (CEMA) to see whether smaller reduced mechanisms can be developed using a few critical chemical targets.

Sprays

The spray performance of a jet fuel can enable or debilitate stable combustion near LBO, and prohibit the ability of a fuel to ignite with this performance nominally decreasing with decreasing temperature or low fuel flow rate, such as at reduced combustor pressures. Spray performance of a jet fuel is characterized by droplet size, droplet size distribution as a probability distribution function (PDF), and spray location. Sprays with large/small Sauter Mean Diameters (SMDs), which is the diameter (d) of a droplet with the same surface to volume ratio of the spray, are considered deleterious/advantageous for combustor performance. The PDF of a droplet distribution describes the relative distribution of the droplets in a spray, as the SMD only describes nominal distributions. PDFs with large/small deviations can be considered deleterious/advantageous because large deviations in the PDF leads to a disproportionate fraction of liquid volume/mass existing in the largest spray droplets which could lead to incomplete combustion. The final spray metric discussed here, spray location, can refer to a spray cone angle or other metric that describes where the maximum flux of fuel volume/mass exists in a spray. Here we report some combine spray results from various teams associated with the NJFCP and how the various fuel properties effect the aforementioned spray performance metrics.

Spray work in the NJFCP has involved the support of 4 rigs, only three rigs^{28-30,23} are discussed at present with the fourth being UTRC, which studied the performance of a different fuel injector. A brief description of the rigs, diagnostics, and test conditions are reported in Table 8. All spray data presented here used the same nozzle and swirler as reported in the LBO studies for the Referee Rig. Corresponding documentation of the fuels tested in the rigs are presented in Table 7. The tested conditions are also plotted on the T_3 - P_3 plot, Figure 18. Temperatures and pressures above ambient conditions are targeting LBO conditions, while experiments are sub ambient temperatures and pressures are aimed to inform ignition phenomena. Similar to the ignition studies, Year 4 of the program will focus on spray performance at sub ambient temperatures and pressures.

Figure 19 presents a Bar and Whisker plot for the Purdue and Referee Rig using PDPA data at LBO conditions. The Purdue data was collected under non-reacting conditions. The data presented from the Referee Rig is under a stable burning condition just above the LBO limit. SMD values with a significant spread suggest that the fuel SMD varies significantly versus various radial and axial locations. Values greater/less than the maximum/minimum category A fuels are associated with poorer/better spray performance as larger SMDs are associated with longer τ_{evap} time scales for LBO. The SMDs for each of the fuels in the Purdue rig are statistically similar, and the SMDs for A-2 and C-1 are also similar. A-2, C-1, and C-5 SMDs in the Referee Rig are shown to be greater than the SMDs in the Purdue rig for these PDPA measurements, which is likely due to the evaporation of smaller droplets relative to the larger droplets. The favorable vaporization of the small





droplets then could bias the SMD to larger droplets which evaporate on longer time scales and require additional energy/heat transfer to evaporate. Interestingly, C-5 in the Referee Rig is observed to have significantly higher SMDs relative to the C-5 fuel in the Purdue rig. This observation is likely explained by the much lower final boiling point of C-5 relative to the A-2 and C-1. C-5 has been reported to have a very flat and relatively low boiling point (174 °C for C-5 versus 263/269 °C for C-1/A-2) which implies a significantly increased vaporization potential for C-5³.

Figure 20 is a Box and Whiskers plot for chilled conditions at NRC Canada and Purdue for various NJFCP fuels, all under non-reacting conditions. It is important to note that the diagnostics at NRC Canada are different than the diagnostics used at Purdue. Purdue used a PDPA system while NRC Canada used a Malvern system. PDPA measurements are reported at specific locations, and Malvern measurements are reported as line of sight. The Purdue results for A-2, A-3, and C-3 are shown to deviate very little relative to the fuels tested implying very little viscosity effects. The relative ordering of the NRC Canada category A fuels is consistent with prior expectations as SMD_{A1} is less than SMD_{A2} and SMD_{A2} is observed to be less than the SMD_{A3} . The nominally smaller SMDs of C-1 relative to A-1 is consistent with the preliminary ignition work at cold conditions for the Referee Rig, which shows slightly better ignition behavior for C-1 vs. A-2.

Chilled versus heated SMD results are reported in Figure 21. The SMD of A-2 is observed to increase significantly between the heated and chilled conditions, and the relative SMD across fuels is not observed to deviate significantly. These results suggest that the relative ignition differences between fuels is not due to their relative droplet sizes when comparing SMD. There could, however, be additional spray performance characteristics that explain the observed ignitability differences, or the experimental temperatures and pressures were not sufficiently low enough to measure SMD differences here. Figure 22 reports PDF confidence intervals of 25%, 50%, and 75% as well as SMD for one chilled plane and 3 heated LBO planes. The 25% confidence interval determines the limit where 25% of the measured droplets are smaller, and 75% of droplets are larger. Interestingly, the SMD values are all larger than the 75% confidence interval. The SMD is thus biased by perhaps only a small number of relatively large droplets. These larger droplets in turn contain substantially more mass than a smaller droplet. The relative impact of these confidence intervals will be an ongoing area of investigation as the NJFCP proceeds into Year 4 as the pointed impact of sprays on FOM performance is yet to be determined.

Table 7. Rig descriptions and test conditions for spray. Spray results for the individual rigs can be found in these papers^{28-30,23,31}.

Rig Name	Description	T _{air}	T _{fuel}	P	ΔP/P	P _{pilot}	Institution
Purdue	PDPA	280 and 394 K	240 and 322 K	15 and 30 psia	2,3,4,6 %	25,35,45, 50,75 psi	NRC-CAN
Referee Rig	Pressure atomizer/ 2D PDA	394 K	236 and 288 K	30 psia	3%		AFRL/UDRI
NRC-CAN	Malvern	295 K		14.7 psia	2,4,6 %	25, 50, 75 psid	NRC-CAN

Table 8. Rigs and fuels tested for spray.

	A-1	A-2	A-3	C-1	C-2	C-3	C-4	C-5	C-7	C-8	C-9
Purdue		X	X	X		X		X	X	X	X
Referee Rig		X		X				X			
NRC-CAN	X	X	X	X			X				

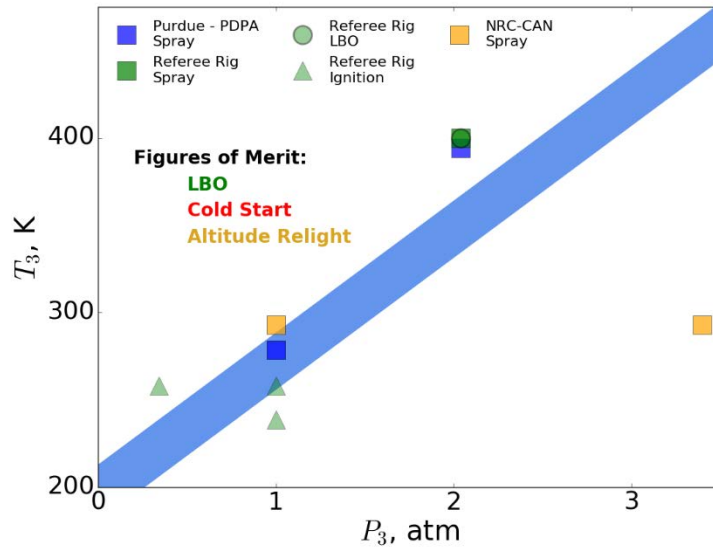


Figure 18. P_3 - T_3 figure displaying the rig conditions tested to measure the Figures of Merit (FOM), specifically for the spray tests for Purdue, Referee Rig, and NRC-Canada (NRC). Referee Rig LBO and Ignition test conditions are included on this plot for reference. LBO, cold start, and altitude relight conditions occur at 2-4 atm and 400-450 K, 1 atm and 225-350 K, and >0.25 atm and >230 K, respectively.

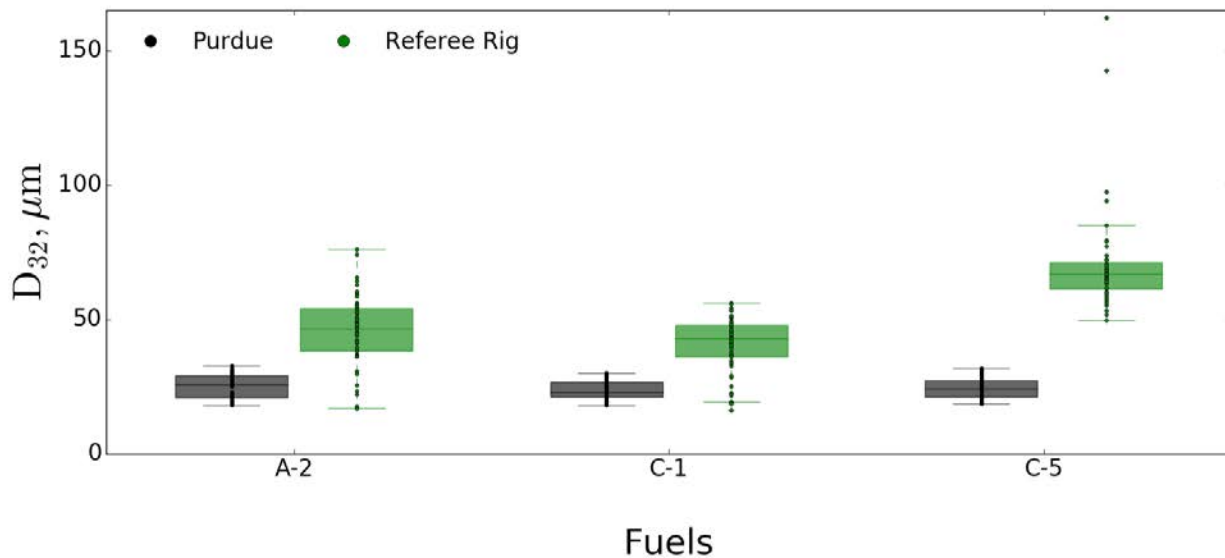
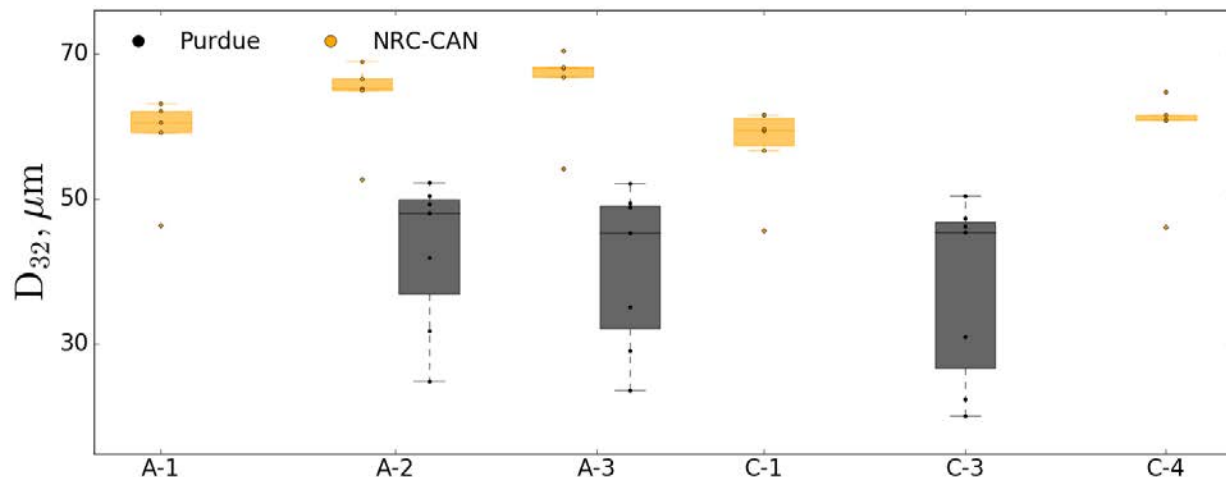
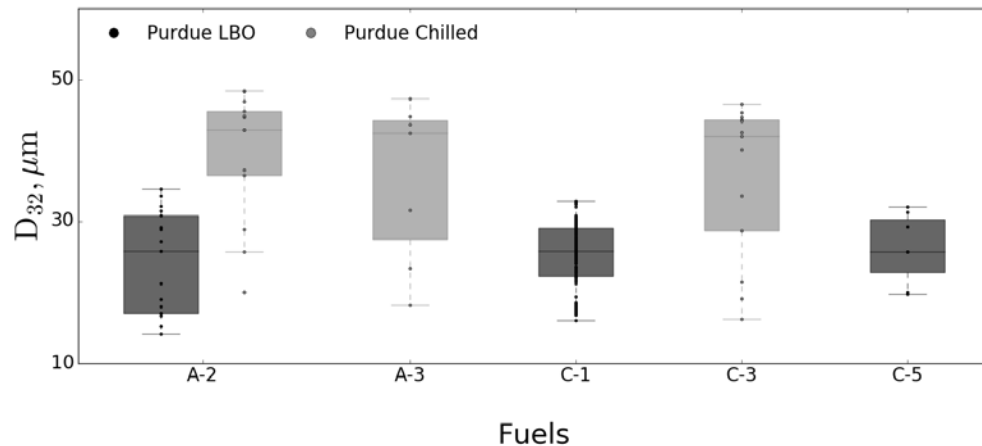


Figure 19. Spray box plot comparison of SMD (D_{32}) for Referee Rig and Purdue PDPA LBO test conditions. Data was taken at the 10 mm and 12.7 mm plane for the Referee Rig and Purdue PDPA, respectively. Radial locations span from -30 mm to 30 mm with a pressure drop of 3% and 25 psi pilot for Purdue. Each SMD point was normalized to A-2. Fuel C-5 is observed to have the largest SMD at this plane for the range of radial locations.



Fuels

Figure 20. Spray box plot comparison of SMD (D_{32}) for NRC Canada (NRC-CAN) and Purdue PDPA for cold start test conditions using Malvern and PDPA measurement methods respectively. Data was taken at the 1 inch plane with radial locations from 0 mm to 30 mm. The pressure drop was 2% with a pilot pressure of 25 psi, all normalized to A-2. Purdue's fuel temperature was chilled to 238 K while NRC Canada's fuel was 292 K. A-1, C-1, and C-4 all had better SMDs relative to A-2 for NRC Canada while Purdue, at colder fuel temperatures had a large spread for C-3 and saw some improvement from A-2 for the A-3 fuel.



Fuels

Figure 21. Spray box plot comparison of SMD (D_{32}) for chilled and heated fuels using PDPA diagnostics at Purdue. These data are reported previously in Figure 19 and Figure 20. This plot compares the effect of decreased temperatures on SMD. The SMD of A-2 is observed to increase significantly as test temperatures are reduced.

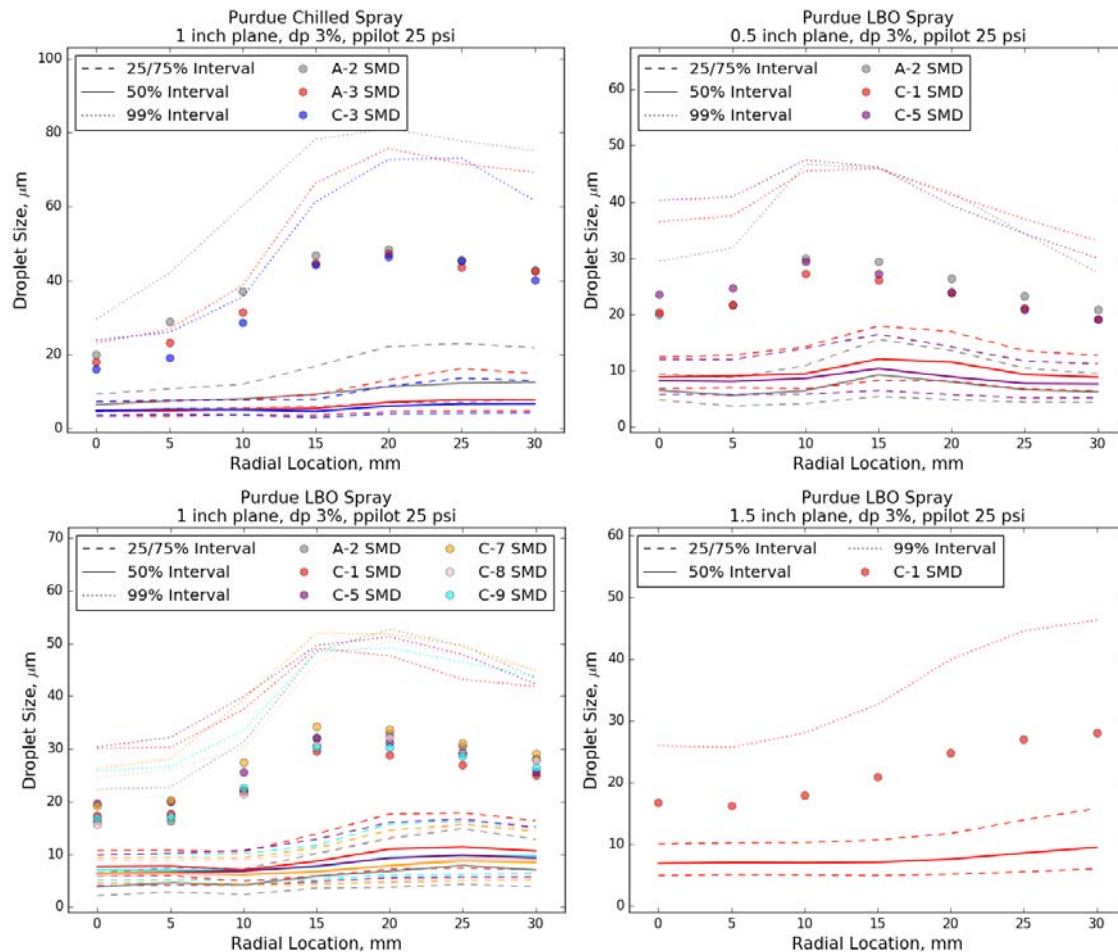


Figure 22. Confidence intervals for droplet size distribution and SMD for Purdue. All data taken with a pressure drop of 3% and pilot pressure of 25 psi. Top Left: Chilled spray at the 1 inch plane. A-2 has a larger droplet size distribution for all of the confidence intervals and SMD. Top Right: LBO spray at the 0.5 inch plane, droplet size peaks between the 10 and 15 mm radial location. Bottom Left: LBO spray at the 1 inch plane, droplet size peaks between the 15 and 20 mm radial location. Bottom Right: LBO spray at the 1.5 inch plane, droplet size peaks at the 30 mm radial location.

Summary and Conclusions

Year 3 of the NJFCP has been highlighted by multiple scientific and capacity developments. Significant gains have been made in combining the various LBO results from across the NJFCP and other rigs that have studied LBO. DCN has been shown to be a “least-common-denominator” predictor for combustion stability across 9 of the 10 rigs reported here. Other properties have been shown to have greater predictive fidelity for a given rig and conditions. Progress towards understanding the potential impact on ignition by AJFs has been accomplished by facility development and initial experimental data that suggests fuel spray and volatility characteristics determine AJF performance.

Additional gains have been made in the NJFCP in regards to models, kinetics rate measurements, and the development of these models for AJF evaluation by OEMs in OEM proprietary hardware. Various CFD models have been aligned, consistent boundary conditions and gridding where appropriate, to iterate towards predicting consistent and LBO predictions. The chemical kinetic modeling approach, HyChem, has submitted several publications detailing their modeling approach and results for several NJFCP fuels, which detailed laser diagnostic methods have been developed to balance carbon in shock tube experiments up to 85%. Finally, CFRs have been developed to enable OEM usage of the latest Flamelet modeling methods.



Year 4 of the NJFCP will entail experimental measurements that are yet to be determined to provide the maximum impact of the NJFCP and iterative improvements on current modeling paths. Some examples of identified experimental options are LBO and ignition studies with:

- additional geometries to access the relative impact on FOM performance by AJFs,
- different thermodynamic and loading parameters to access the relative importance of T3, P3, and τ_{mix} on FOM performance, and
- the use of additional fuels to stress test aforementioned hypotheses governing FOM behavior with respect to fuel properties.

These experimental directions will be determined in the coming weeks weighing the desires of Federal Sponsors and OEMs as to which test campaigns will yield the greatest impact on streamlining the certification process.

Milestone(s)

Presentation at the NJFCP Year-End Meeting. Contributing to the upcoming AIAA book.

Major Accomplishments

We have shown strong evidence that LBO is most strongly predicted by the chemical property DCN across four experimental platforms in the NJFCP. This could potentially aid in developing blending rules for fuels to proceed through the ASTM approval process.

Publications

Peer-reviewed Publications:

None

Conference Proceedings:

Peiffer, Erin, Heyne, Joshua, Colket, Meredith. 2018. "Characteristic Timescales for Lean Blowout of Alternative Jet Fuels." Joint Propulsion Conference. Cincinnati, Ohio: AIAA.

Joshua S. Heyne, Erin Peiffer, Meredith B. Colket, Aniel Jardines, Cecilia Shaw, Jeffrey P. Moder, William M. Roquemore, James T. Edwards, Chiping Li, Mark Rumizen, and Mohan Gupta. "Year 3 of the National Jet Fuels Combustion Program: Practical and Scientific Impacts of Alternative Jet Fuel Research", 2018 AIAA Aerospace Sciences Meeting, AIAA SciTech Forum, (AIAA 2018-1667)

Outreach Efforts

Oral presentations:

Peiffer, Erin, Heyne, Joshua. 2018. "Combustor Rig Sensitivity to Derived Cetane Number for Lean Blowout and Ignition Results from Year Three of the National Jet Fuels Combustion Program." Dayton-Cincinnati Aerospace Sciences Symposium. Dayton, Ohio: ASME.

Peiffer, Erin, Heyne, Joshua, Colket, Meredith. 2018. "Characteristic Timescales for Lean Blowout of Alternative Jet Fuels." Joint Propulsion Conference. Cincinnati, Ohio: AIAA.

Joshua S. Heyne, Erin Peiffer, Meredith B. Colket, Aniel Jardines, Cecilia Shaw, Jeffrey P. Moder, William M. Roquemore, James T. Edwards, Chiping Li, Mark Rumizen, and Mohan Gupta. "Year 3 of the National Jet Fuels Combustion Program: Practical and Scientific Impacts of Alternative Jet Fuel Research", 2018 AIAA Aerospace Sciences Meeting, AIAA SciTech Forum, (AIAA 2018-1667)

Awards

None

Student Involvement

Erin Peiffer, Graduate Research Assistant, June 2017 - present.

Jennifer Colborn, Undergraduate Research Assistant, August 2016 – August 2017, now at UDRI.
Katherine Opacich, Undergraduate Research Assistant, November – 2017 – present.





Plans for Next Period

We plan to continue our current research technique incorporating greater depth into our results and incorporating additional data into our work.

References

- 1 Colket, M. B., Heyne, J., Rumizen, M., Edwards, J. T., Gupta, M., Roquemore, W. M., Moder, J. P., Tishkoff, J. M., and Li, C., "An Overview of the National Jet Fuels Combustion Program," *54th AIAA Aerospace Sciences Meeting*, 2016, pp. 1-24.
- 2 Heyne, J. S., Colket, M. B., Gupta, M., Jardines, A., Moder, J. P., Edwards, J. T., Roquemore, M., Li, C., and Rumizen, M., "Year 2 of the National Jet Fuels Combustion Program: Towards a Streamlined Alternative Jet Fuels Certification Process," *55th AIAA Aerospace Sciences Meeting*, 2017, p. 145.
- 3 Edwards, J. T., "Reference Jet Fuels for Combustion Testing," *Submitted to the 55th AIAA Aerospace Sciences Meeting*, Grapevine: American Institute of Aeronautics and Astronautics, 2017.
- 4 Colket, M. B., Heyne, J. S., Rumizen, M., Edwards, J. T., Gupta, M., Roquemore, W. M., Moder, J. P., Tishkoff, J. M., and Li, C., "An Overview of the National Jet Fuels Combustion Program," *AIAA Journal*, Jan. 2017.
- 5 Edwards, T., Moses, C., and Dryer, F. L., "Evaluation of Combustion Performance of Alternative Aviation Fuels," *46th AIAA/ASME/SAE/ASEE Joint Propulsion Conference & Exhibit*, Nashville, TN: .
- 6 Lefebvre, A., and Ballal, D., *Gas Turbine Combustion Alternative Fuels and Emissions*, Boca Raton: Taylor and Francis Group, 2010.
- 7 Plee, S. L., and Mellor, A. M., "Characteristic time correlation for lean blowoff of bluff-body-stabilized flames," *Combustion and Flame*, vol. 35, 1979, pp. 61-80.
- 8 Burger, V., "The Influence of Fuel Properties on Threshold Combustion in Aviation Gas Turbine Engines," 2017.
- 9 Chtev, I., Rock, N., Ek, H., Smith, T., Emerson, B., Nobel, D. R., Seitzman, J., Lieuwen, T., Mayhew, E., Lee, T., Jiang, N., and Roy, S., "Simultaneous High Speed (5 kHz) Fuel-PLIE, OH-PLIF and Stereo PIV Imaging of Pressurized Swirl-Stabilized Flames using Liquid Fuels," *Submitted to the 55th AIAA Aerospace Sciences Meeting*, Grapevine: American Institute of Aeronautics and Astronautics, 2017.
- 10 Stouffer, S., Hendershott, T., Monfort, J. R., Diemer, J., Corporan, E., Wrzesinski, P., and Caswell, A. W., "Lean Blowout and Ignition Characteristics of Conventional and Surrogate Fuels Measured in a Swirl Stabilized Combustor," *55th AIAA Aerospace Sciences Meeting*, 2017, pp. 1-14.
- 11 Culbertson, B., and Williams, R., *ALTERNATIVE AVIATION FUELS FOR USE IN MILITARY APUS AND ENGINES VERSATILE AFFORDABLE ADVANCED TURBINE ENGINE (VAATE), PHASE II AND III*, AFRL-RQ-WP-TR-2017-0047: 2017.
- 12 Stachler, R. D., Heyne, J. S., Stouffer, S. D., Miller, J. D., and Roquemore, W. M., "Investigation of Combustion Emissions from Conventional and Alternative Aviation Fuels in a Well-Stirred Reactor," *Submitted to the 55th AIAA Aerospace Sciences Meeting*, Grapevine: American Institute of Aeronautics and Astronautics, 2017.
- 13 Podboy, D. P., Chang, C., and Moder, J. P., "Lean Blowout Fuel Sensitivity for a Lean Direction Injection Combustor," *55th AIAA Aerospace Sciences Meeting*, Grapevine, TX: American Institute of Aeronautics and Astronautics, 2017.
- 14 Khandelwal, B., and Ahmed, I., "Research Report on Lean Blowout Limit The University of Sheffield Department of Mechanical Engineering," 2017.
- 15 Jonathan, B., Nathan, S., Fillo, A., and David, B., "Effect of Sub-Atmospheric Pressures on the Turbulent Flame Speed of Jet Fuel," *Submitted to 56th AIAA Aerospace Sciences Meeting*, Kissimmee, FL: American Institute of Aeronautics and Astronautics, 2018.
- 16 Sidney, J. A. M., Allison, P. M., and Mastorakos, E., "The effect of fuel composition on swirling kerosene flames," *55th AIAA Aerospace Sciences Meeting*, Grapevine, TX: American Institute of Aeronautics and Astronautics, 2017.
- 17 Colket, M., Zeppieri, S., Dai, Z., and Hautman, D., "Fuel Research at UTRC," *In Multi-Agency Coordinating Council for Combustion Research 5th Annual Fuel Research Meeting*, 2012.
- 18 Allison, P. M., Sidney, J. A. M., and Mastorakos, E., "Forced Response of Kerosene Flames in a Bluff-body Stabilised Combustor," *55th AIAA Aerospace Sciences Meeting*, Grapevine, TX: American Institute of Aeronautics and Astronautics, 2017.
- 19 Hendershott, T. H., Stouffer, S. D., Monfort, J. R., Diemer, J., Corporan, E., Wrzesinski, P., and Caswell, A. W., "Ignition of Conventional and Alternative Fuel at Low Temperatures in a Sing-Cup Swirl-Stabilized Combustor," *56th AIAA Aerospace Sciences Meeting*, Kissimmee, FL: American Institute of Aeronautics and Astronautics, 2018.
- 20 Canteenwalla, P., and Chishty, W. A., "Investigation of Engine Performance at Altitude Using Selected Alternative Fuels for the National Jet Fuels Combustion Program," *55th AIAA Aerospace Sciences Meeting*, Grapevine, TX: American Institute of Aeronautics and Astronautics, 2017.
- 21 Sforzo, B., Wei, S., and Seitzman, J., "Non-premixed Ignition of Alternative Jet Fuels," *55th AIAA Aerospace Sciences*



- ²² Meeting, Grapevine, TX: American Institute of Aeronautics and Astronautics, 2017.
- Wei, S., Sforzo, B., and Seitzman, J., "Fuel Composition Effects on Forced Ignition of Liquid Fuel Sprays," *ASME/IGTI Turbo Expo: Power for Land, Sea and Air*.
- ²³ Corber, A., Rizk, N., and Chishty, W. A., "Experimental and Analytical Characterization of Alternative Aviation Fuel Sprays Under Realistic Operating Conditions," *ASME Turbo Expo*.
- ²⁴ Esclapez, L., Ma, P. C., Mayhew, E., Xu, R., Stouffer, S. D., Lee, T., Wang, H., and Ihme, M., "Large-Eddy Simulations of Fuel Effect on Gas Turbine Lean Blow-out," *55th AIAA Aerospace Sciences Meeting*, Grapevine, TX: American Institute of Aeronautics and Astronautics, 2017.
- ²⁵ Briones, A. M., Olding, R., Sykes, J. P., Rankin, B. A., McDevitt, K., and Heyne, J. S., "COMBUSTION MODELING SOFTWARE DEVELOPMENT, VERIFICATION AND VALIDATION," *Proceedings of the ASME Power and Energy Conference*, 2018.
- ²⁶ Wang, H., Xu, R., K. W., Bowman, C. T., Hanson, R. K., Davidson, D. F., Brezinsky, K., and Egolfopoulos, F. N., "A Physics-based approach to modeling real-fuel combustion chemistry - I. Evidence from experiments, and thermodynamic, chemical kinetic and statistical considerations," *Combustion and Flame*.
- ²⁷ Xu, R., Wang, K., Banerjee, S., Shao, J., Parise, T., Zhu, Y., Wang, S., Movaghari, A., Lee, D. J., Zhao, R., Han, X., Gao, Y., Lu, T., Brezinsky, K., Egolfopoulos, F. N., Davidson, D. F., Hanson, R. K., and Bowman, C. T., "A Physics-based approach to modeling real-fuel combustion chemistry - II. Reaction kinetic models of jet and rocket fuels," *Combustion and Flame*.
- ²⁸ Mayhew, E., Mitsingas, C., McGann, B., Hendershott, T. H., and Stouffer, S. D., "Spray Characteristics and Flame Structure of Jet A and Alternative Jet Fuels," *55th AIAA Aerospace Sciences Meeting*, American Institute of Aeronautics and Astronautics, 2017.
- ²⁹ Bokhart, A. J., Shin, D., Gejji, R., Buschhagen, T., Naik, S. V., Sojka, P. E., Gore, J. P., and Lucht, R. P., "Spray Measurements at Elevated Pressures and Temperatures Using Phase Doppler Anemometry," *Submitted to the 55th AIAA Aerospace Sciences Meeting*, Grapevine: American Institute of Aeronautics and Astronautics, 2017.
- ³⁰ Bokhart, A. J., Shin, D., Rodrigues, N., Sojka, P., Gore, J., and Lucht, R. P., "Spray Characteristics at Lean Blowout and Cold Start Conditions using Phase Doppler Anemometry," *56th AIAA Aerospace Sciences Meeting*, Kissimmee, FL: American Institute of Aeronautics and Astronautics, 2018.
- ³¹ Esclapez, L., Ma, P. C., Mayhew, E., Xu, R., Stouffer, S. D., Lee, T., Wang, H., and Ihme, M., "Large-Eddy Simulations of Fuel Effect on Gas Turbine Lean Blow-out," *Submitted to the 55th AIAA Aerospace Sciences Meeting*, Grapevine: American Institute of Aeronautics and Astronautics, 2017.
- ³² Hastie, Trevor, Tibshirani, Robert, Friedman, J., *The Elements of Statistical Learning The Elements of Statistical LearningData Mining, Inference, and Prediction*, Second Edition, 2009.



Appendix

Random Forest Regression Documentation for Individual Rig Results

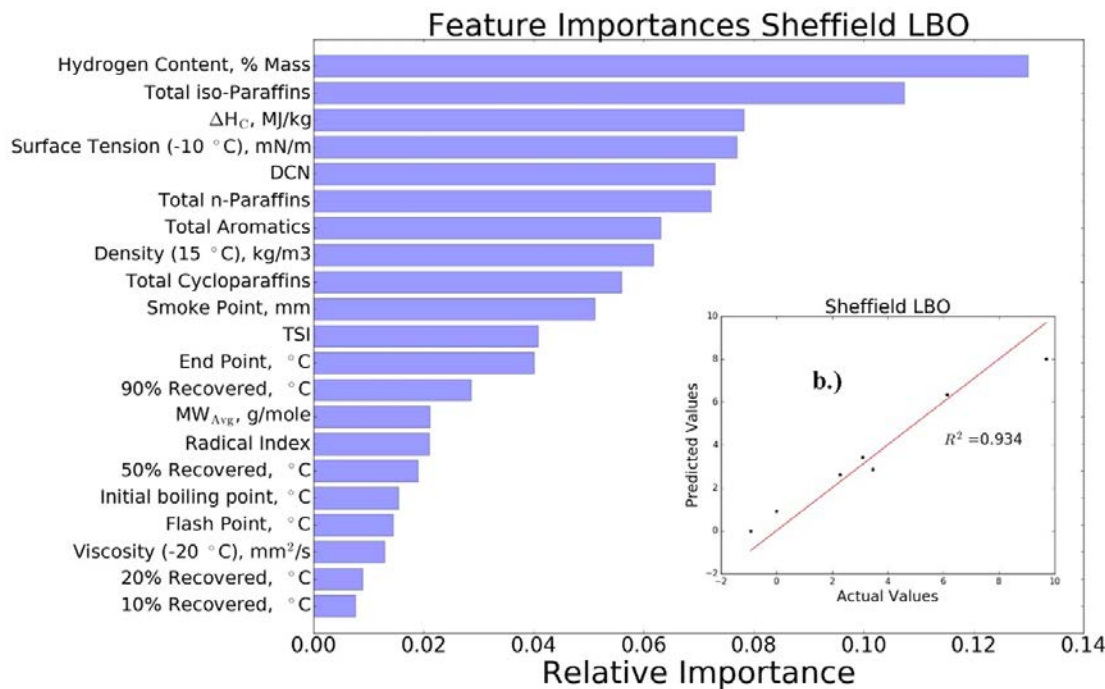


Figure 23. Random Forest regression feature importance and fit for Honeywell LBO. a.) Distillate properties and test conditions were the most important features in predicting LBO for the Honeywell rig, the one nonswirl stabilized rig in the program. Surface tension, density, and viscosity values are at the fuel temperatures. b.) the predicted versus measured (actual) values for Honeywell LBO. NOTE: Units have been intentionally renormalized such that these numbers are not relevant to actual operating limits.

Task 2- Chemical Effects in a Toroidal Jet Stirred Reactor

University of Dayton

Objective(s)

Measure the Lean Blowout (LBO) limit and emissions/speciation characteristics for NJFCP fuels within the program.

Research Approach

Introduction

Due to increasing global concern about climate change resulting from anthropocentric carbon emissions, the aviation sector has identified alternative jet fuels (AJFs) to have major potential for carbon mitigation. As alternative modes of transportation are seeking the usage of alternative fuel sources for the near and long term (e.g., fuel cells, batteries), power density is critical for the aviation sector resulting in hydrocarbon dependencies for years to come. Additionally, fuel costs for commercial airliners is large, accounting for roughly 27% of operating expenses with slight increases in the crude oil price resulting in millions of dollars of additional expenses [1,2]. Jet fuel made from alternative feedstocks has the opportunity to increase national security by reducing country dependence on foreign oil, reduce impacts of oil industry cost fluctuations, and create jobs. [1]. Use of bioderived jet fuels requires alternative pathways into the market as large capital cost paired with other economic and technological barriers exist in transition promising AJFs to market.



The National Jet Fuels Combustion Program (NJFCP) was created to streamline certification pathways of AJFs by minimizing the barrier of increased cost and testing in full scale combustor testing rigs [3]. Fuel properties to be studied against Combustor Figures of Merit (FOMs) include high altitude relight, cold start ignition, and lean blowout (LBO) [3,4]. Tests on these FOMs provide a scope of fuel performance among a variety of aviation gas turbine engine operating conditions.

LBO occurs when the flame extinguishes, which requires re-ignition of the given combustor cups or cans, during operation presenting potential safety concerns [3]. Chemical effects are shown to yield importance as lean flammability limits are being approached signifying the relevance of LBO as a FOM [3]. Target conditions for temperature and pressure, referenced to the inlet of the combustor, are 400-450 K and 2-4 atm., respectively [3]. Prior experiments with the Referee Rig and Toroidal Jet-Stirred Reactor (TJSR) have shown a first order correlation with derived cetane number (DCN) and LBO, assessed via equivalence ratio [3,5-7]. Identification of DCN, a metric seldom considered in initial fuel screening processes, illuminates the importance of fuel autoignition capabilities in these combustors near LBO.

Lefebvre, Mellor, and later Burger developed a phenomenological explanation of LBO behavior, relating it to the evaporation, chemical and mixing timescales shown in Equation 1 and Figure 1 [8-11]. Burger was able to integrate the use of non-conventional fuels into this timescale analysis to describe the competition between chemistry and evaporation in the fuels as it pertains to combustor performance. The time associated with fuel atomization and evaporation correlates to the evaporative timescale. Mixing timescales are primarily a function of combustor design, and effects of pressure, temperature, air flow rate, and recirculation within the device. Chemical timescales are influenced by the fuel, at the supplied temperature and pressure. The recent findings concerning LBO and DCN imply that the chemical timescales largely correspond to autoignition timescales. A common measure of autoignition timescales is ignition delay, which is indirectly how DCN is calculated per ASTM D6890, which will be leveraged in the subsequent analysis [12].

$$\phi(LBO) \sim \left(\frac{1}{\tau_{chem}} + \frac{1}{\tau_{evap}} + \frac{1}{\tau_{mix}} \right)^{-1} \quad (1)$$

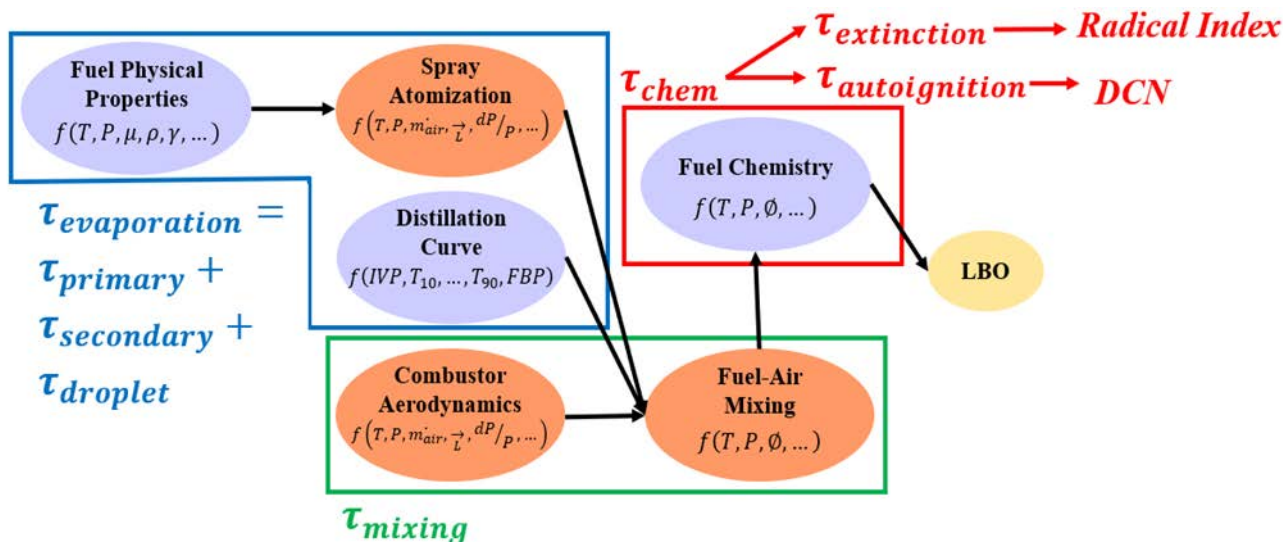


Figure 1. Relevant timescales driving LBO performance and the parameters influencing those associated timescales. Purple circles correspond to the fuel effects whereas orange circles are influenced by the combustor design.

A previous random forest regression analysis for the TJSR LBO data, including physical and chemical properties commonly measured for jet fuel performance, suggests radical index is a key predictor for LBO. Radical index (RI), a value used to measure the role of kinetics in extinction strain rate for counterflow diffusion flames, could effectively describe the effects of extinction within the TJSR [13]. Both DCN and RI are metrics that can lead to the fundamental timescales associated with autoignition and extinction, respectively. The relevant pathways to understand the competition between these timescales as they relate to the chemical timescale are shown below:



$$\tau_{extinction} \rightarrow Radical\ Index \rightarrow Extinction\ Strain\ Rate\ (a_e)$$

$$\tau_{autoignition} \rightarrow DCN \rightarrow Ignition\ Delay$$

The TJSR, an applied combustion device, has been previously used to investigate soot inception, emissions, and lean/rich blowout stability limits while operating in the well-stirred regime [14–20]. This well-stirred regime allows for reduced order physics to a 0-D system, synonymous to a perfectly-stirred reactor (PSR) with modeling efforts, where concentration, temperature, and flow fields are homogeneous with space and steady state. Minimal gradient effects exist near the wall of the TJSR, but temperature and species concentrations have yielded near constant profiles in prior experiments [15]. Using a premixed, prevaporized fuel-air mixture allows for assessment of fuels on a gas phase basis allowing for isolation of exclusively the chemical effects, as opposed to other combustion devices which study LBO in a multiphase environment where physical and chemical effects are coupled represented, in addition, by the evaporative timescale. Atomized fuel and air near the primary recirculation zone has been modeled previously as a PSR or an array of PSRs due to the 0-D nature in space and time with the reduced conservation equations associated to them. Development and implementation of a device operating near a well-stirred regime allows for the observation of chemistry effects of alternative fuels to be studied in an environment similar to that of typical gas turbine combustors, where a device to assess performance in this regime does not exist. The TJSR uses multiple jets injecting premixed, prevaporized fuel and air into the 250-mL reactor volume at temperatures and pressures near 458 K and 1 atm, respectively, and bulk fluid residence times of around 6-7 ms. LBO performance vs fuel type was assessed at high temperatures using fused silica (Rescor 750) reactor hemispheres with an Inconel jet-ring manifold and an absence of dilution. Experimental conditions for the TJSR are relatively similar to that of typical gas turbine combustors [3,18]. The influence of the chemical timescale will be discussed relative to the competition of extinction timescales and autoignition timescales.

Methods/ Experimental

TJSR Information and Instrumentation

LBO testing was performed in the TJSR where lean, premixed, prevaporized fuel and air enter the reactor via jets located on the outer diameter of the toroid. Fuel is vaporized and mixed with air upstream of the reactor, where it is then exhausted through exhaust ports located within the center of the toroid. Diagrams and additional reactor information are in Stachler, et. al., 2017 [7].

Four diagnostic ports are located within the bottom hemisphere of the TJSR. A linear tracking, bare, type B thermocouple (0.2 mm diameter, platinum – 6% rhodium, platinum – 30% rhodium) surrounded by alumina was used to measure the temperature within the reactor. Measurements were assessed approximately 0.25" from the bottom of the reactor and were not corrected for radiation and other heat losses. A custom igniter which was located flush with the reactor wall. Pressure fluctuations within the TJSR were measured using a high speed 0-5 psid pressure transducer, and it was found that pressure fluctuations were limited to +/- 5.5 kPa. Exhaust gas samples were extracted within the reactor using a 1.4 mm OD oil-cooled (420 K) probe. Measurements were taken as the probe rested approximately 5 mm from the lower wall of the toroid, situated 90 degrees relative to the thermocouple.

Fuels Tested

Various fuel/solvent mixtures were used for assessment of LBO in the TJSR that span a wide range of chemical and physical properties. These fuels are shown in Table 1, where additional fuel property information can be found in Edwards, 2017 [4]. DCN, a chemical property of fuels which is measured using ASTM D6890, varied from 17 to 74, outside of the 40 to 60 range that current aviation fuels exhibit [5,12]. RI values were estimated for A-2, C-1, and C-4 using previously published results, whereas the radical indices of the 1-3 species mixtures (nC12, S-1, and J-1) were calculated using the sum of mole fractions of the fuel multiplied by their respective radical index value [13].

A-2 is the nominal jet fuel, containing average values in flash point, viscosity, and aromatic content among the Jet-A fuels. C-1 and C-4 fuels have lower DCN values than that of conventional jet fuels and have an unusual and broad boiling range, respectively [3,4]. S-1, a surrogate fuel, was formulated to stress key combustion properties including DCN, molecular weight, H/C ratio, and threshold sooting index while emulating Jet-A fuel performance in prevaporized fuel-air environments [4,21]. The single species *n*-dodecane is a common fuel surrogate utilized for the contribution of n-alkanes in petroleum derived jet fuels [7,21]. Lastly, J-1, which has a similar DCN to C-1, was designed to stress the importance of RI to gain understanding of the kinetic influence in the progress to LBO. This 2-species fuel mixture contains a high mole fraction of aromatics to effectively lower RI without the presence of any *iso*-paraffins.





Table 1. Fuels tested within the TJSR for LBO testing. Additional fuel properties for A-2, C-1, C-4, and S-1 are in Edwards, 2017 [4]. Other 1-3 component fuel / solvent mixtures values were estimated using traditional blending methods [22,23].

Fuel / Solvent Mixture Nomenclature	Composition (% vol)	Fuel / Solvent Mixture Chemical Composition C_mH_n	Derived Cetane Number (DCN)	Radical Index (RI)
nC12	<i>n</i> -dodecane	$C_{12}H_{26}$	74.0	1.000
A-2	Petroleum Jet A	$C_{11.4}H_{22.1}$	48.3	0.750
S-1	59.3% <i>n</i> -dodecane, 18.4% <i>iso</i> -octane, 22.2% 1,3,5- <i>tri</i> -methylbenzene	$C_{10.3}H_{20.1}$	50.4	0.745
C-4	60% C9-12 <i>iso</i> -paraffins, 40% C-1	$C_{11.4}H_{24.8}$	28.0	0.720
C-1	Highly branched C12 & C16 paraffins	$C_{12.6}H_{27.2}$	19.08	0.700
J-1	75.5% 1,3,5- <i>tri</i> -methylbenzene, 24.5% <i>n</i> -dodecane	$C_{9.5}H_{14.3}$	17.01	0.466

Operating Conditions and Procedure

Liquid fuel is delivered using two syringe pumps (Teledyne Isco 500 D), where the fuel passes a swirler and heat exchanger to elevate the temperature to 473 K prior to being introduced in the vaporizer. Uncertainty in the liquid flow measurement with calibration is estimated to be +/- 1.4%, where the piston flow meter accuracy is +/- 0.5%. The heated fuel is introduced with 10-20% of the air flow in the beginning of the vaporizer via an air-swirled atomizer and air at 400 K. The remainder of air is introduced coaxially throughout the length of the vaporizer at 489 K. The air lines are filtered, monitored, and controlled upstream of the vaporizer using mass flow controllers (Brooks Instruments 5851i and 5853). Uncertainty for the mass flow controllers is +/- 1.5% FSO. PID-controlled electric heaters were used to establish consistent temperatures in the heated fuel and air streams. Total air flow rate was held constant at around 600 g/min, adjusting fuel flow rate to attain the desired equivalence ratio. The constant air flow rates establish a near constant residence time and constant turbulence intensities.

Measurements of pressure, temperature, and fuel and air mass flow rates were monitored and controlled via LABVIEW software. Calculations for other relevant parameters (equivalence ratio, bulk residence time, mass flow) were performed in real time with this software as well. Global residence time for the experiment was around 6-7 ms and varied slightly with temperature differences and reduction in overall mass flow due to fuel flow rate [15]. Inlet temperatures were held constant around 458K and were measured prior the fuel-air mixture to the jet ring manifold.

Initial operation of the TJSR uses a gaseous fuel (ethylene) to allow the initial warmup of the reactor and jet ring to avoid condensation of low volatility fuels in the small passages of the jet ring. Once operational temperatures are established, and the reactor is thermally stable, fuel usage was transitioned to the liquid fuel. Thermal conditions are stabilized again before LBO testing. The ethylene was controlled using a series of pressure regulators and a mass flow controller (MKS Instruments M100B).

Each LBO test was initiated at an equivalence ratio (ϕ) of 0.48, where temperatures within the reactor were below the maximum allowable temperature for the fused silica reactor. Equivalence ratios were reduced by reducing fuel flow rate until LBO. This limiting condition occurs when the heat loss becomes large enough to where combustion becomes unstable and is not sustained. A change in operating noise and a sharp decrease in reactor temperature correspond to LBO [15]. The





fuel flow rate was automated to decrease at approximately 0.05 mL/min ($\phi \sim 0.001$) every 4 seconds to LBO conditions to minimize hysteresis effects of the LBO values, e.g. hotter temperatures sustaining LBO to leaner conditions. Automation of decreasing fuel flow rate is similar to the methodology presented for the Referee Rig and their subsequent LBO testing [6]. This ramp rate for fuel flow provides for use of a singular fuel pump throughout the duration of the LBO test and minimizes transitional effects between operation of the two syringe pumps. To minimize fuel contamination between LBO testing of different fuels and dead volume associated with the syringe pumps, the pumps were flushed out with the new fuel approximately 4 times prior to the liquid fuel being introduced for testing. Also, as the WSR was approaching stable thermal conditions, the fuel lines experienced proper flushing of previous fuel to minimize contamination. Once LBO occurs, reignition of the fuel and air mixture occurs, where thermal equilibrium is achieved at $\phi = 0.48$ and LBO process begins again. Thirteen (13) LBO points were taken for all fuels except nC12. Only five LBO points were taken for nC12.

Computational Methods

Ignition delay estimations were calculated using Cantera and a constant volume ideal gas reactor [24]. Initial temperatures and pressures of 700-1500 K and 1 atm, respectively, were selected to emulate the TJSR experimental conditions. Simulations stepped through time using internal stepping to minimize gradients and increase computational efficiency. A 965-species model from Dooley, et. al. was employed as the mechanism in this work as it consisted of models for the species components in the fuels tested [25]. The time at which OH concentration reached a maximum was interpreted in this work is the ignition delay time.

Perfectly stirred reactor (PSR) modeling with Cantera was also explored using an ideal gas reactor, introducing mass flow aligning with the experimental conditions at a volume of 250 mL and a bulk residence time of 7.1 ms. Mass fractions of the fuel-air mixture and temperature were extracted at steady state conditions and at equivalence ratios at LBO. Equilibrium temperatures were also calculated using the experimental conditions ($T=458K$, $P=1atm$, $\phi=\phi_{LBO}$).

Results and Discussion

Lean blowout was measured using six fuels in the TJSR, which span a wide DCN range, to investigate the first-order dependence on DCN in a premixed, prevaporized configuration. Fuel flow rate was lowered, lowering the reactor temperature, until a large drop (> 20 K) in temperature occurred, at LBO. Figure 2 illuminates this trend as the different fuels blowout at different equivalence ratios, as shown in the larger symbols. Points beyond LBO are included to illustrate the rapid decrease in temperature that occurs once LBO is experienced

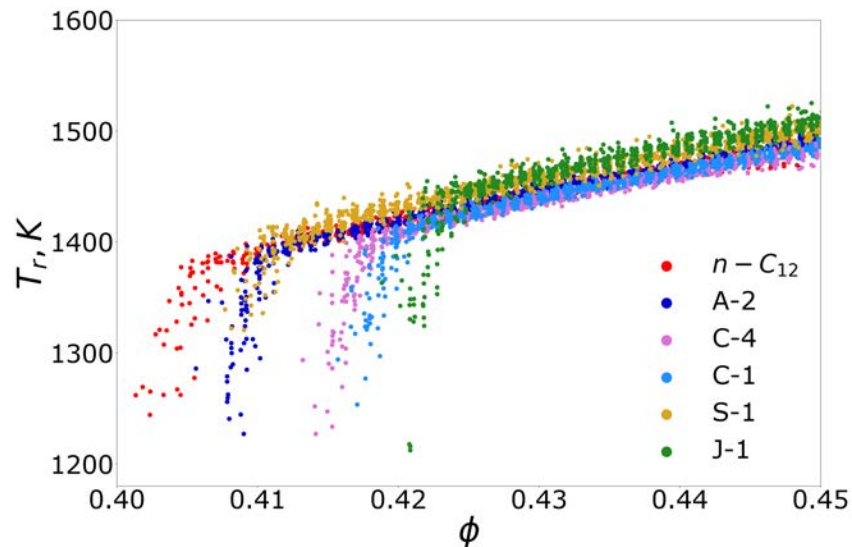


Figure 2. Reactor Temperature (K) as a function of ϕ in the TJSR. TJSR experimental conditions: $P \approx 1$ atm, $T_0 = 458$ K, $\tau = 6-7$ ms.

The LBO values were then normalized relative to the LBO values of A-2, where a random forest regression analysis was utilized. This analysis, shown in Figure 3, provides a method to assess the relative important factors from the ranging physical and chemical properties among the different fuels and fuel mixtures. DCN and RI are among the top feature



importances of the data set. Normalized fuel property regression results yield the same top feature importances, but to a lesser degree than the results shown in Figure 3. Chemical properties, like iso-paraffins and n-paraffins, correlate with the next important factors, being DCN and RI. The importance of DCN and RI are both fuel property values that can influence the timescales of autoignition and extinction within the TJSR.

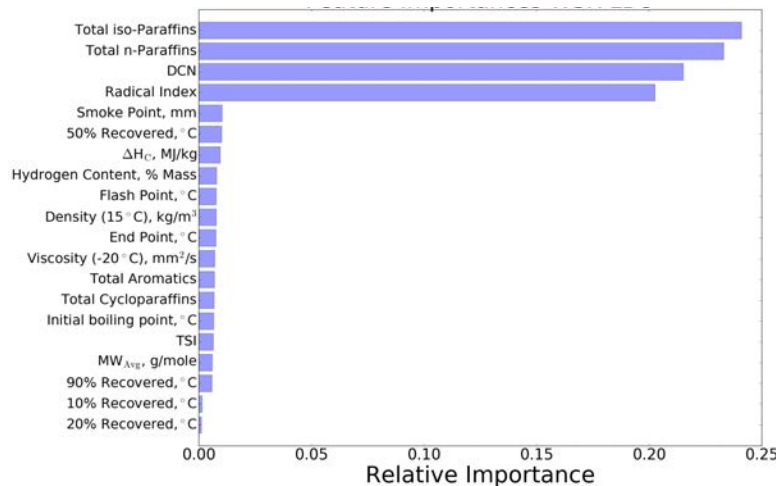


Figure 3. Relative feature importances using random forest regression analysis on the TJSR LBO data.

Figure 4 illuminates a first order correlation to LBO recorded using the TJSR. Although the LBO values are narrow with ~4% between max and min values, the statistical uncertainty with the testing performed still show a relative performance difference among the fuels and contains a moderate R^2 value. LBO for A-2 and S-1 yield consistent results in a premixed, prevaporized fuel-air environment, as with other experiments [6,21]. C-1 also exhibited an extended stability limit compared to J-1, although the fuels had similar DCN values (17.1 v. 19.08). It is also shown that the highest radical index value - 1 for nC₁₂ - has the most resistance to LBO. Moderate radical index fuels span the gap between DCN and RI, which have associated timescales corresponding to autoignition and extinction, respectively, within the chemical timescale category.

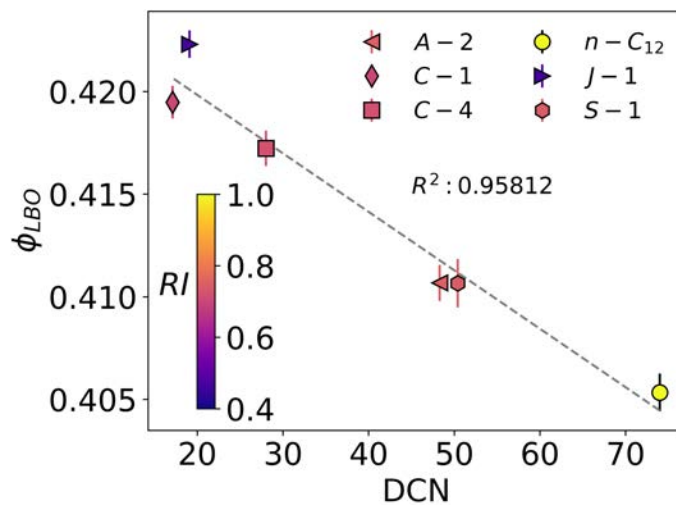


Figure 4. ϕ_{LBO} as a function of DCN in a TJSR. TJSR experimental conditions: P=~1atm, T_o=458K, τ = 6-7 ms. Error bars correspond to 1σ of the statistical uncertainty between measured LBO. RI values are included in figure as colors, indicated via the color bar. Gray dotted lines correspond to the line of best fit, with the given R^2 value provided in the figure.



Radical index aids in estimation of extinction strain rate values and toward an extinction timescale. Extinction strain rate values were calculated using the equation provided in Figure 5 from S.H. Won, et. al., 2012 [13], which is shown below for brevity. Fuel concentration represented by [Fuel] was estimated given the equivalence ratio at LBO. ΔH_c corresponds to the heat of combustion of the given fuel, where MW_{fuel} and $MW_{nitrogen}$ correspond to the molecular weights of the fuel and nitrogen, respectively.

$$a_e \left[\frac{1}{s} \right] = 230 RI [Fuel] \Delta H_c \left(\frac{MW_{fuel}}{MW_{nitrogen}} \right)^{-\frac{1}{2}} - 54 \quad (2)$$

Previous counterflow diffusion flame efforts were made to study the kinetic effect of extinction strain rate for varying fuel species and components. A correlation was established, collapsing the experimental and simulated data on a line. This was accomplished via RI and transport weighted enthalpy [13]. Values of RI, fuel used, and equivalence ratio allowed for relative comparison amongst the fuels and their LBO values. Figure 5 displays LBO as a function of the calculated extinction strain rate. Fuels with large n-alkane content show increased extinction had high strain rate values whereas the lower DCN fuels had smaller strain rate values. Surrogate mixtures with large amounts of aromatics tend to have lower extinction strain rates as the radical indices are smaller than that of the other components. A linear trend of increased strain rate to decreased LBO is additionally seen in the figure with a lower R^2 value than that of Figure 4. Inverses of strain rate yields values in the 1.5-2 ms range. However, it is not determined if an inverse of the strain rate, with a unit of time, is adequate as the higher extinction strain rate values result in lower time values.

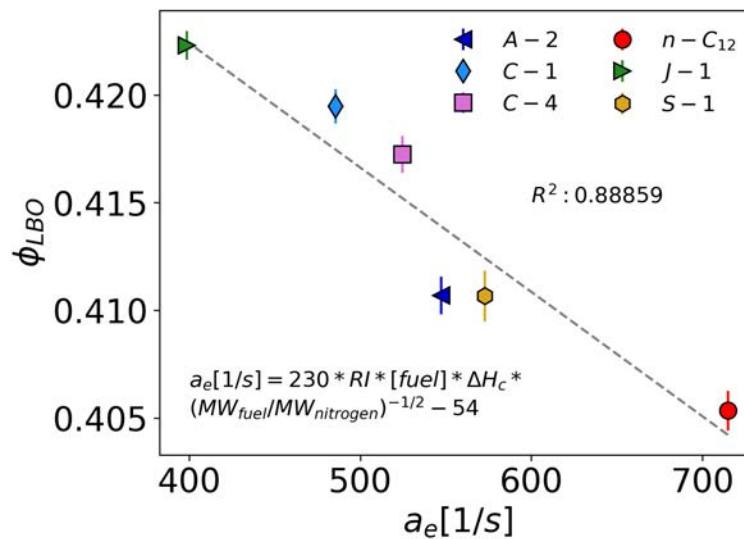


Figure 5. ϕ_{LBO} as a function of extinction strain rate (a_e) in a TJSR. TJSR experimental conditions: $P \sim 1$ atm, $T_0 = 458K$, $\tau = 6-7$ ms. Error bars correspond to 1σ of the statistical uncertainty between measured LBO. Gray dotted lines correspond to the line of best fit, with the given R^2 value provided in the figure.

Correlations with DCN and the TJSR indicate autoignition as an important characteristic when approaching LBO conditions. Ignition delay allows for investigation in the effect of autoignition and comparison of those timescales relative to other timescales that may exist. In Figure 6, ignition delay was estimated via simulation with Cantera using *n*-dodecane and *iso*-octane, the latter of which is utilized in this effort because the DCN value is very similar to that of C-1[26]. Because of this assumption, the experimental temperature in the plot where *iso*-octane is located is the temperature at which LBO occurred for C-1. To illuminate the effects of recirculation of burned exhaust products to fresh reactants, burned mass fractions of products, expressed as a percentage, were incorporated into the lines provided in the figures. The remaining percentage was multiplied by the respective mass fractions of fresh reactants at the given equivalence ratio. Burned mass fractions were extracted using a PSR simulation at the given LBO value. Figure 6 displays ignition delay for different percentages of burned products incorporated within the overall mixture. A green line on both figures indicates the bulk residence time. Toward the reactor temperature limits, ignition delay is roughly two orders of magnitude less than that of the bulk residence time, but



drastically approaches the bulk residence time around ~ 1111 K. Even among the two fuels presented in the figure, these small differences between *n*-dodecane and *iso*-octane impact the ability to autoignite in adequate time for a given gas turbine combustor.

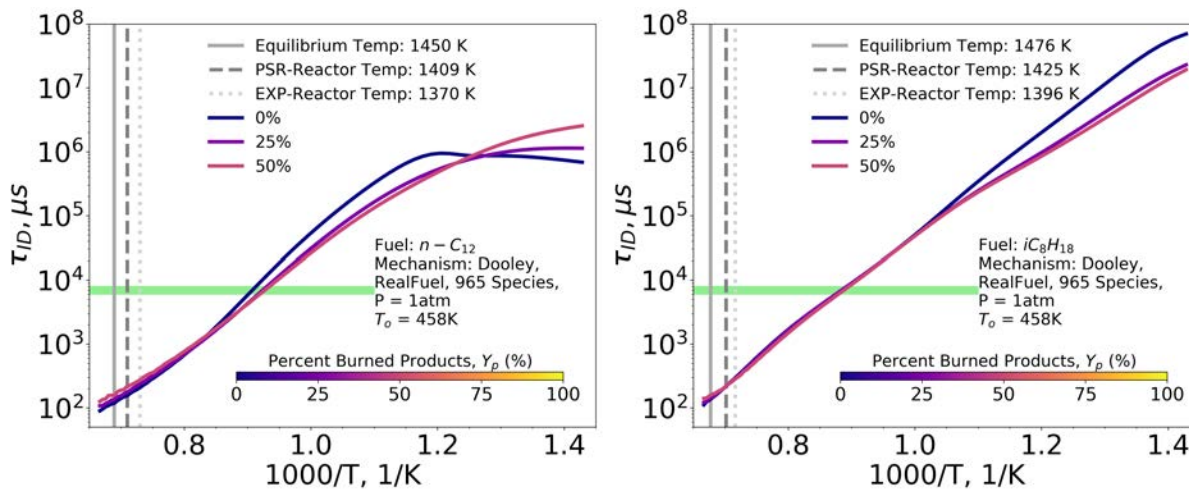


Figure 6. Ignition delay plots for *n*-dodecane and *iso*-octane for various mass percentages of burned products introduced in initial conditions. Equilibrium, PSR, and experimental temperatures are plotted in gray with the values provided in the legend. The experimental temperature for C-1 was assumed as the experimental value for *iso*-octane. The green bar on the plot signifies the order of magnitude of the bulk residence time relative to the other ignition delay times estimated from the simulation.

Conclusions

Lean blowout (LBO), a common combustor performance metric to assess alternative fuels, was assessed in a toroidal jet-stirred reactor (TJSR) with a variety of fuels spanning derived cetane numbers (DCN). This device operates in a premixed, prevaporized environment, under relevant gas turbine combustor conditions, where other combustor devices offer limited insight into experiments near perfectly stirred reactor environments. Key findings of this work include:

- LBO contains a first-order effect with DCN, which is additionally elucidated in other practical and applied combustor experiments.
- Radical index was identified as a feature importance in predicting LBO in this experimental configuration, emphasizing extinction timescales as a driving factor for LBO in a TJSR, which can be investigated using extinction strain rate.
- A competition between autoignition and extinction timescales exists on the approach to LBO, and this affects the overall chemical timescale as it relates to the bulk residence time of the reactor.

References

- [1] Alternative Aviation Fuels: Overview of Challenges, Opportunities, and Next Steps, US DOE, 2016.
- [2] W-C. Wang, L. Tao, J. Markham, Y. Zhang, E. Tan, L. Batan, E. Warner, M. Biddy. Review of Biojet Fuel Conversion Technologies, Report No TP-5100-66291, NREL, 2016.
- [3] M. Colket, J. Heyne, M. Rumizen, M. Gupta, T. Edwards, W.M. Roquemore, G. Andac, R. Boehm, J. Lovett, R. Williams, J. Condevaux, D. Turner, N. Rizk, J. Tishkoff, C. Li, J. Moder, D. Friend, V. Sankaran, AIAA J. 55 (2017) 1087-1104.
- [4] J.T. Edwards, Reference Jet Fuels for Combustion Testing. 55th AIAA Aerosp. Sci. Meet., AIAA, 2017.
- [5] J. Heyne, E. Peiffer, M. Colket, J. Moder, J.T. Edwards, W.M. Roquemore, C. Shaw, C. Li, M. Rumizen, M. Gupta, Year 3 of the National Jet Fuels Combustion Program: Practical and Scientific Impacts, 2018 AIAA Aerosp. Sci. Meet., AIAA, 2018.
- [6] S. Stouffer, T. Hendershott, J. Monfort, J. Diemer, E. Corporan, P. Wrzesinski, A. Caswell, Lean Blowout and Ignition Characteristics of Conventional and Surrogate Fuels Measured in a Swirl Stabilized Combustor, 55th AIAA Aerosp. Sci. Meet., AIAA, 2017.
- [7] R.D. Stachler, J.S. Heyne, S. Stouffer, J.D. Miller, W.M. Roquemore, Investigation of Combustion Emissions from Conventional and Alternative Aviation Fuels in a Well-Stirred Reactor, 55th AIAA Aerosp. Sci. Meet., AIAA, 2017.



- [8] A.H. Lefebvre, D.R. Ballal. Gas Turbine Combustion: Alternative Fuels and Emissions. 3rd ed. CRC Press, Boca Raton, FL, USA, 2010.
- [9] A.H. Lefebvre, Int. J. Heat Fluid Flow 107 (1985) 24-37.
- [10] S.L. Plee, A.M. Mellor, Combust. Flame. 31 (1979) 61-80.
- [11] V. Burger, The Influence of Fuel Properties on Threshold Combustion in Aviation Gas Turbine Engines. 2017.
- [12] A Standard Test Method for Determination of Ignition Delay and Derived Cetane Number (DCN) of Diesel Fuel Oils by Combustion in a Constant Volume Chamber, D6890-16e1, ASTM Int., 2016.
- [13] S.H. Won, S. Dooley, F.L. Dryer, Y. Ju, Combust. Flame 159 (2012) 541-551.
- [14] S.D. Stouffer, D.R. Ballal, J. Zelina, D.T. Shouse, R.D. Hancock, H.C. Mongia. Development and Combustion Performance of High Pressure WSR and TAPS Combustor. 43rd AIAA Aerosp. Sci. Meet. Exhib., AIAA, 2005.
- [15] S. Stouffer, R. Pawlik, G. Justinger, J. Heyne, J. Zelina, D. Ballal, Combustion Performance and Emissions Characteristics for a Well Stirred Reactor for Low Volatility Hydrocarbon Fuels. 43rd AIAA/ASME/SAE/ASEE Jt. Propuls. Conf. Exhib., AIAA, 2007.
- [16] D. Blunck, J. Cain, R.C. Striebich, S.Z. Vijlee, S.D. Stouffer, W.M. Roquemore, Fuel-rich Combustion Products from a Well-Stirred Reactor Operated using Traditional and Alternative Fuels. Cent. States Combust. Meet., The Combustion Institute, 2012.
- [17] S.Z. Vijlee, Effects of Fuel Composition on Combustion Stability and NOX Emissions for Traditional and Alternative Jet Fuels. University of Washington, 2014.
- [18] J. Zelina, D.R. Ballal, J. Eng. Gas Turbines Power 119 (1997) 70-75.
- [19] A. Briones, B. Sekar, J. Zelina, R. Pawlik, S. Stouffer, Numerical Modeling of Combustion Performance for a Well-Stirred Reactor for Aviation Hydrocarbon Fuels, 44th AIAA/ASME/SAE/ASEE Jt. Propuls. Conf. Exhib., AIAA, 2008.
- [20] J.E. Nenniger, A. Kridiotis, J. Chomiak, J.P. Longwell JP, A.F. Sarofim, Proc. Comb. Inst. 20 (1984) 473-479.
- [21] S.H. Won, F.M. Haas, S. Dooley, T. Edwards, F.L. Dryer, Combust. Flame 183 (2017) 39-49.
- [22] S. McAllister, J-Y. Chen, A.C. Fernandez-Pello, Fundamentals of Combustion Processes. Springer New York, New York, NY, 2011.
- [23] B.E. Poling, J.M. Prausnitz, J.P. O'Connell, The Properties of Gases & Liquids. vol. 1. 5th ed. The McGraw-Hill Companies, Inc., 2001.
- [24] D.G. Goodwin, H.K. Moffat, R.L. Speth, Cantera: An Object-oriented Software Toolkit for Chemical Kinetics, Thermodynamics, and Transport Processes, 2017.
- [25] S. Dooley, F. Dryer, S.H. Won, T. Farouk, Reduced Kinetic Models for the Combustion of Jet Propulsion Fuels, 51st AIAA Aerosp. Sci. Meet. Incl. New Horizons Forum Aerosp. Expo, AIAA, 2013.
- [26] J. Yanowitz, M.A. Ratcliff, R.L. McCormick, J.D. Taylor, M.J. Murphy. Compendium of Experimental Cetane Numbers, Report No. TP-5400-67585, NREL, 2017.

Milestone(s)

- Measured LBO, a Figure of Merit in the NJFCP, for four fuels. Results are consistent with the more complicated Area 6 Referee Rig. LBO trends with both DCN and Radical Index, chemical properties that correspond to autoignition and extinction phenomena, respectively.
- Emissions were additionally recorded, and trends for a surrogate fuel, S-1, are similar to that of A-2, a conventional jet fuel.

Major Accomplishments

Reporting LBO equivalence ratios for four NJFCP fuels.

Publications

Peer-reviewed Publications

None. (One publication is in preparation.)

Conference Proceedings

Stachler, R., Peiffer, E., Kosir, S., Heyne, J., and Stouffer, S., "A Study into the Chemical Timescale for a Toroidal Jet-Stirred Reactor (TJSR)," Central States Section of The Combustion Institute, Minneapolis: 2018, <https://doi.org/10.2514/6.2018-4914>

Outreach Efforts

Conference presentations





Stachler, R., Peiffer, E., Kosir, S., Heyne, J., and Stouffer, S., "A Study into the Chemical Timescale for a Toroidal Jet-Stirred Reactor (TJSR)," Central States Section of The Combustion Institute, Minneapolis: 2018, <https://doi.org/10.2514/6.2018-4914>

Awards

Outstanding Research Award - Mechanical Engineering - Robert Stachler, Ph.D. student (Awarded at University of Dayton April 2018)

Student Involvement

Robert Stachler, Ph.D. student, leads this effort.

Plans for Next Period

Finalize the publication in progress and for Robert Stachler to finish his PhD.

Task 3- Preferential Vaporization Effects on LBO in the Referee Rig

University of Dayton

Objective(s)

Explain Lean blowout (LBO) results from the Referee Rig, including NJFCP and non-NJFCP fuels. Some of these fuels exhibited non-monotonic behavior at LBO.

Research Approach

The certification process for non-conventional jet fuels historically has required significant time and financial resources, as full-scale engine tests for multiple engine geometries have been used in the past to evaluate fuel effects. (These large-scale tests then jeopardize the plausibility of a new fuel's implementation.) Not only does this restrict the development and deployment of biotechnological research and results, but also it fosters a non-sustainable, longer term dependence on fossil fuels which are contributing to climate change. Jet fuel certification rightfully errs to the side of caution as system failure in flight will likely result in catastrophic results. For non-conventional fuels this caution is amplified, as these fuels often contain unique molecular compositions resulting in different chemical and physical properties from conventional fuel sources. Thus, paramount to the decarbonization of aviation transportation and the certification of alternative jet fuels is the mapping of unique chemical and physical properties to the fit-for-purpose performance and safety criteria for conventional fuels.

The National Jet Fuels Combustion Program (NJFCP) was formulated with the mission of reducing the costs and time of the jet fuel certification process [1,2]. The NJFCP's method for accomplishing this task is to map the performance of extreme alternative fuel properties to three so called Figures of Merit: cold start ignition, altitude relight, and lean blowout (LBO). These areas were selected because of their implications on safety and because of their sensitivity to fuel properties [2]. In the context of the NJFCP, significant progress has been made toward the evaluation of alternative fuel effects on LBO, with significant progress toward ignition sensitivity only occurring very recently [3]. The NJFCP tests a wide variety of fuels on multiple different experimental rigs with different geometries to evaluate Figure of Merit performance in diverse geometries [4].

A keystone of the experimental NJFCP work is the development of a combustor rig capable of capturing fuel sensitivity typical of a swirl stabilized rich-quench-lean geometry with effusion cooling. This combustor rig, in theory, would be able to capture fuel effects in an aircraft main engine by screening the fuel, which would either reduce or eliminate subsequent and costly large-scale tests. The motivation to develop this rig has led to the development of the Referee Rig at AFRL/UDRI. Previous LBO work reported on the Referee Rig has shown that fuels with conventional fuel properties exhibit an LBO first order dependency on the fuel DCN. That is, fuels with a higher DCN exhibited greater stability limits than fuels with a lower DCN. These results, and detailed measurements reported by Chtev et al.[5], suggest that the LBO limit of a fuel in a swirl stabilized rig is limited to first order by the ability of a fuel to autoignite, which has only very recently been suggested [2,4,6,7].

Fundamentally, LBO behavior will scale with evaporative, mixing, and chemical time scales. Both fuel properties and combustor design will have impacts on the significance of each of these relative time scales with LBO being limited by the longest relative time scale. A phenomenological description of LBO, based on these time scales, was developed by Mellor,





where he hypothesized LBO will occur when combustion efficiency drops below a certain threshold [8,9]. The time scale behavior described is shown in Equation 1.

$$\eta_c = f \left((\text{air flow rate})^{-1} \left(\frac{1}{\tau_{evap}} + \frac{1}{\tau_{mix}} + \frac{1}{\tau_{chem}} \right)^{-1} \right) \quad (1)$$

The evaporative time scales will be determined by droplet spray and atomization behavior as well as by the volatility of the fuel. The mixing timescales will primarily be driven by combustor fluid dynamic properties. In turbulent combustion, mixing will be dominated by convection; combustor flow behavior will determine mixing time scales. The correlation found between LBO and DCN in the Referee Rig suggests the chemical time scales are at least in part determined by autoignition time scales as indicated by DCN. As DCN is a property describing a fuel's propensity to autoignite, the chemical time scales could be effectively ignition delay times. Regardless, the chemical timescales will also be a function of temperature, pressure, and concentrations of the fuel and oxidizer. As the individual time scales increase in magnitude, the overall time scale of the process increases correspondingly. When the overall process exceeds the time available in the combustor, LBO will occur. Therefore, reducing any of these time scales will improve overall combustion stability.

Historically, fuel property effects on combustor performance have been studied by Lefebvre, Mellor, and more recently by Burger, whose work was initiated with altitude LBO experiments as part of the certification of a Fully-Synthetic-Jet-Fuel (FSJF) [7–11]. Lefebvre and Mellor's work focused on the variation of properties associated with conventional fuels and did not include as significant of variations of alternative fuel property effects as those within the NJFCP. Conventional fuels chemical properties do not vary significantly between fuels, obscuring the impact of chemical effects as they relate to LBO. Burger did consider the inclusion of non-conventional fuels in his work and leveraged Mellor's time scale analysis to explain the various trends in LBO data by the competing time scales for chemistry and evaporation. The inclusion of non-conventional fuels increased the range of chemical properties tested, highlighting the effects of the chemical time scales.

While much of the Referee Rig LBO data are consistent with the propensity of a fuel to autoignite, some of the data appear anomalous. This could be a result of second order effects from other time scales interfering with the autoignition correlation. Lefebvre and Mellor showed physical properties dominating fuel performance effects, and correspondingly their results have served as the primary fuel guidelines for certification. The identification of autoignition as a property of interest will also serve as important guidelines for new fuel certification. With added fuel property requirements, there will be more clarity on how future alternative fuels must be composed. New fuels will be able to be screened for certification/qualification using relatively inexpensive, small volume fuel property tests as opposed to expensive full-scale combustor tests.

The fuels tested for LBO on the Referee Rig are intentionally diverse in nature. With the goal to understand fuel effects on performance, fuels with diverse chemical and physical properties are utilized. Physical property variations will affect droplet atomization and vaporization, while chemical variations will affect combustion behavior. The fuels include conventional fuels, alternative fuels and fuel blends [12]. Real fuels used in applications generally contain many different species of diverse properties. Multi-species fuels vaporize differently from single species fuels [13–18]. Because future alternative fuels are expected to be multi-species in nature, understanding multi-species effects on combustion is of particular interest.

Here we propose three potential hypotheses explaining the previously reported anomalous Referee Rig LBO data by coupling droplet theory, distillation curve properties, and reactivity (via DCN). The possible explanations suggested here are: preferential vaporization (τ_{evap} and τ_{chem} coupling), extended droplet lifetimes (τ_{evap}), and local thermal quenching (τ_{evap} dilation via distillation and droplet time scale coupling). No single hypothesis is shown to explain all observed LBO behavior. Finally, fuel blends to test preferential vaporization are suggested for future work.

Methodology

Time Scale Approach to LBO Modeling

Similar to the previously reported work by Mellor and Burger, time scales can be assigned to the various competing phenomena and related to the three hypothesized criteria for deviation from DCN-LBO correlations. LBO thus can be interpreted to scale with the inverse sum of evaporative (τ_{evap}), chemical (τ_{chem}), and mixing (τ_{mix}) time scales.

$$\phi(LBO) \sim \left(\frac{1}{\tau_{chem}} + \frac{1}{\tau_{evap}} + \frac{1}{\tau_{mix}} \right)^{-1} \quad (2)$$





Evaporative times scales are associated with the relative spray and evaporation time scales of a fuel. Mixing time scales are associated with the fluid dynamic primary recirculation time scales. Chemical time scales are best characterized by an autoignition time scale. Nominally, one can interpret the time scales to be independent, as in the prevaporized premixed toroidal jet-stirred reactor which could be considered a two time scale device (chemical and mixing) [6]. Results from the toroid stirred reactor were found to be largely consistent with the Referee Rig results with greater agreement with subtle variations that are still being investigated.

The agreement between the Referee Rig and the toroidal jet stirred reactor suggest the chemical time scales are a function DCN and equivalence ratio, ϕ , and not heat of combustion as implied with Lefebvre's correlation. DCN is a measure of the fuels autoignition propensity; this is consistent with the observation of the simultaneous extinction and ignition events as blowout is approached [19]. Although DCN is a measure of autoignition in the negative temperature coefficient regime, DCN correlates accurately with ignition delays at high temperatures, which is the case in LBO [20]. From this, the significant chemical time scale could be proposed to be the ignition delay time. Regardless, the chemical time scale of significance can be described as,

$$\tau_{chem} = \tau_{chem}(DCN, \phi, T)$$

with the DCN being a function of the local (net species evolved/evaporated since droplet inception) or global (sum of total reactivity of the fuel).

Evaporation time scales can be interpreted as the algebraic sum of primary and secondary atomization (τ_{atom}) and droplet evaporation time ($\tau_{droplet}$) scales. Spray experiments on the same geometry and conditions as the Referee Rig have shown nominally similar Sauter Mean Diameters in the primary combustion region for fuels with significantly different fuel properties associated with primary and secondary atomization such as viscosity and surface tension[21]. These results imply similar primary and secondary atomization time scales.

$$\Rightarrow \tau_{atom} = \text{constant}$$

Droplet evaporation time scales ($\tau_{droplet}$) conventionally have been described by the d^2 -law for a droplet of SMD [22]. The d^2 -law assumes single species vaporization of a spherically symmetric, isolated droplet at steady state in a quiescent environment [23]. In the highly turbulent, multi-species vaporization of a spray, most of these assumptions are not met [24]; however the d^2 -law is still generally used as an indicator of relative droplet evaporation times [25].

Initial droplet size, d_0 , is a function of atomizer and physical properties of the fuel. Spray measurement experiments with the atomizer used in the Referee Rig have been made showing little variation in droplet distribution amongst fuels with variation amongst properties associated with spray quality [21].

The vaporization rate constant expression in the classic d^2 -law, K_v , is a function of thermal conductivity, specific heat, heat of vaporization, fuel density, heat of combustion, air inlet temperatures and droplet surface temperature. All of these properties except for droplet surface temperature are approximately constant across fuels [12]. Droplet surface temperature will change throughout the vaporization process and is analogous to distillation temperatures in combustion applications.

Two fuels which with extreme distillate properties were tested, C-3 and C-5. C-3 distills between 183-256 °C and C-5 distills between 156-173 °C[12,26], with $\tau_{droplet}(C5) < \tau_{droplet}(C3)$. Neither of these fuels performed abnormally according the LBO vs. DCN trend suggesting the absolute distillate temperatures didn't result in measurable differences. The surface temperature term in K_v does not have a significant impact on the overall value because the term is included as a temperature difference from the surrounding temperature; because the surrounding temperature is much greater than the vaporization temperatures, K_v is relatively insensitive to it. The coupling of the relatively constant droplet distribution and the relative vaporization rate constant suggest overall absolute evaporative time scales are either relatively constant or small as compared to the other timescales. And droplet time scales that followed the DCN-Law correlation follow the following relationship.





$$\begin{aligned} \tau_{droplet} \ll \tau_{mix} \text{ and/or } \tau_{chem} \\ \Rightarrow \forall \text{ fuels with } \tau_{droplet} < \tau_{droplet} (\text{C3}) \end{aligned}$$

In a swirl stabilized combustor like the Referee Rig, mixing is primarily driven by convection (as opposed to diffusion). Because all of the fuels were tested in the same geometry with the same conditions, it is assumed mixing time scales are constant across all fuels.

$$\tau_{mix} \cong \text{constant}$$

Given these results, the divergence in the DCN-Law suggest performance variation could be explained by the eclipsing of chemical time scales by droplet time scales or a coupling of the chemical and droplet timescales. In the latter case, the time scales cannot be viewed as independent characteristics, but rather co-dependent as they progress simultaneously. In these LBO results, chemical time scales are to first order DCN dependent with droplet time scales being described with a d^2 -law accounting for distillation properties. The two hypothesized explanations both examine how the fuel vaporization could impact the chemical time scales and thus affect the stability of the fuel. Both explanations will assume vaporization and combustion follow the batch distillation limit. Each of these theories describe the vaporization of the entire spray as the vaporization of a single droplet.

Fuels

The fuel data considered in this study have been reported previously [4,12,27] and are for fuels that have been widely tested at a number of experimental facilities within the NJFCP. This suite of fuels is composed of three conventional fuels (a ‘best,’ average, and worse case jet fuel), five alternative fuels with fuel properties near those of jet fuel specifications, four conventional-alternative fuel blends, 2 single species fuels, and 9 blends of pure components. Two of the blended pure component (S-1 and S-2) surrogates were designed to mimic the fully prevaporized chemical combustion property targets of A-2, but have significantly differing physical properties than A-2. A full list of all fuels and their properties can be found in Table 1 and are detailed further by Edwards [12].

The listed fuel properties can be related to relative time scale estimates for each fuel. The evaporative time scale is most closely related to the distillation curve of a fuel and the fuel’s effect on the spray/droplet character. High relative T_{10} , T_{50} , and T_{90} distillation properties are associated with lower vapor pressures, flash points, and increased heat transfer to the droplet surface to maintain a constant hydrocarbon vapor pressure. Higher relative viscosities, densities, and surface tensions are associated with poorer spray character as these properties inhibit atomization and mixing.

At the LBO conditions referenced here, negligible spray effects have been observed for fuels with varying properties associated with spray quality [21]. Thus, deviations in evaporative time scales are likely due to the relative distillation differences rather than spray effects based on these spray data. Additional support for this claim has been documented in reacting versus non-reacting spray data at AFRL/UDRI and Purdue respectively. These data show that for the non-reacting case very little variation is seen in the A-2 and C-5 fuels. However, very few small droplets were measured in the C-5 reacting case versus A-2 as C-5 has much lower distillation temperatures relative to A-2. The chemical time scales can be associated with the relative DCN of the fuels. A very wide range of DCNs for the fuels have been reported previously.

LBO Data Analyzed

Data used in this paper is reported in previously published literature, see [26,27]. Nominally, the LBO of a fuel is measured at a constant air mass flow rate (0.392 kg/sec), $\Delta P/P$ (3%), T (394/322 K air/fuel), and P (2 atm), with the LBO of a fuel being determined as the fuel mass flow rate limit in which extinction is global within the rig. The LBO conditions of these data are typical where LBO events at altitude occur. The LBO point as reported here is determined from multiple LBO events with uncertainties of the LBO point of approximately $\pm 1.5\%$ the reported value. LBO data from 23 fuels are used in the reported analysis, see a description of these fuel in Table 1. Three conventional fuels associated with ‘best’ (A-1), ‘average’ (A-2), and ‘worse’ (A-3) combustion properties are used to determine stability limits of conventional fuels. While, 20 additional alternative fuels, alternative-conventional fuel blends, and solvent blends are used to approximate the ‘best’ and ‘worse’ case alternative fuel behavior for LBO by significantly varying their associated properties [4]. Fuels distinguished with a ‘C’ are fuels studied extensively in the NJFCP.





Table 1. Fuels tested for LBO on the Referee Rig. The fuels have diverse chemical, physical and distillate properties. The 2/3 species blends are shown in bold.

Fuel/Solvent Mixture	Composition, % volume
A-1	Petroleum JP-8 (w/high flash point and low viscosity and aromatics)
A-2	Petroleum Jet A
A-3	Petroleum JP-5
C-1	Highly branched C12 and C16 paraffins
C-2	16% <i>tri</i> -methylbenzene + 84% C14 <i>iso</i> -paraffins
C-3	64% A-3 + 36% farnesane
C-4	60% C9-12 <i>iso</i> -paraffins, 40% C-1
C-5	73% C10 <i>iso</i> -paraffins, 17% <i>tri</i> -methylbenzene
F-1	80/20 A-2/C-2
F-2	50/50 A-2/C-1
F-3	20/80 A-2/C-1
F-4	80/20 A-2/C-5
<i>n</i> -C12	<i>n</i> -C12
<i>n</i>-C12/<i>n</i>-C16 mix	71.6% <i>n</i>-C12, 28.4% <i>n</i>-C16
<i>n</i>-C12/<i>m</i>-xylene mix	75% <i>n</i>-C12, 25% <i>m</i>-xylene
<i>n</i> -C7	<i>n</i> -C7
<i>n</i>-C7/<i>n</i>-C12 mix	31.2% <i>n</i>-C7, 68.8% <i>n</i>-C12
<i>n</i>-C12/MCH mix	71.6% <i>n</i>-C12, 28.4% MCH
<i>n</i>-C7/<i>n</i>-C16 mix	73.5% <i>n</i>-C7, 26.5% <i>n</i>-C16
Sasol (IPK)	~88% <i>iso</i> -alkanes, 12% cycloalkanes, 0.4% aromatic
<i>n</i>-C12/<i>i</i>-C8 mix	69.1% <i>n</i>-C12, 30.9% <i>i</i>-C8
S-1	59.3/18.4/22.2 <i>n</i>-dodecane/ <i>iso</i>-octane/ 1,3,5-<i>tri</i>-methylbenzene
S-2	52.6/25.1/22.2 <i>n</i>-hexadecane/ <i>iso</i>-octane/ 1,3,5-<i>tri</i>-methylbenzene

LBO for these fuels are reported in Figure 1. The LBO points are plotted relative to the fuel's respective DCN. Blue symbols are fuels that do not include fuels composed of only 2/3 species, and the dashed line is a regression of $\phi(LBO)$ versus DCN for fuels excluding 2/3 species blends. All LBO measurements are found to be in agreement with the reported regression within their statistical uncertainty. Red symbols are fuels that are composed of only 2/3 species, and the solid black line is a DCN regression for all fuels plotted. Strong agreement between the non-2/3 species blends and the DCN was observed. There is a strong correlation of LBOs with DCN when the 2/3 species blends are excluded. Their correlation for all fuels is much weaker, especially in terms of correlative results for only the 2/3 species blends. Of particular note is the disparity of the S-2 fuel LBO (labeled with red text) from the strong correlation results, while the LBO data for A-2 lie very near the correlation. Recall that the S-2 mixture was derived by matching the fully pre-vaporized combustion property targets of A-2. Regression analysis, considering all fuel properties, continues to demonstrate that the DCN is still the leading order predictor for LBO behavior in the Referee Rig and 8 other rig geometries [4].

Fuels are distinguished by their apparent ability to stress the following three criteria:

- A lag in the relative mass evaporation rate of a droplet leading to local *thermal quenching*. Again, fuels with significant quantities of a light front distillate fraction and a heavy back distillate fraction, such as *n*-cetane, could



lead to lower mass evaporation rates after the light end of the droplet evaporates and before the heavy end of the droplet begins.

- The *relative lifetime of a droplet* (τ_{evap}) evaporating in the rig is substantially longer than other droplets. The longer droplet lifetime leads to incomplete combustion and, again, poorer stability limits at LBO. High concentrations of *n*-cetane, for example, could extend the lifetime of a droplet significantly, leading to lower combustion efficiencies that are associated with the onset of LBO [6].
- The ability of a droplet to have locally varying autoignition propensities as a function of evaporated droplet mass fraction, referred to as *preferential vaporization*. Fuels with non-reactive light components and highly reactive heavy components, such as S-2, could exhibit less stability as LBO is approached than a fuel of similar DCN but no evaporation-reactivity sensitivity [28].

Fuels composed of 2 or 3 components meet one or more of the above criteria and are distinguished as such in **Figure 1**. It should be additionally noted that all the 2 and 3 component blends investigated here exhibited poorer stability than their corresponding DCN would predict.

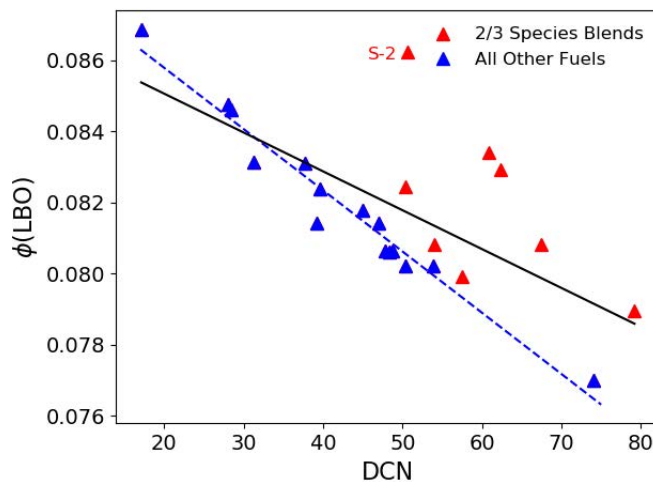


Figure 1. Experimental lean blowout as a function of DCN. The correlation is weak ($R^2=0.40$) until the 2 and 3 species blends are removed ($R^2=0.97$). The correlation with the 2 and 3 species blends removed represents the ‘DCN-law.’ ‘S-2’ is labeled as it represents the greatest deviation from the d^2 -law and is used as the representative fuel.

Results and Discussion

Thermal Quenching

The first explanation is the multi-species nature of the blends alone is causing the change in behavior. The explanation would support the theory of a ‘DCN trend’. Each species has a unique volatility. If the species have significantly different volatilities, the species could vaporize in multiple phases divided by a heating phase in between. This concept has been observed experimentally in a heptane/cetane mixture [29]. Conventional fuels have a wide array of species and therefore volatilities. The distribution of volatilities causes the vaporization and by extension the combustion to occur at a relatively constant rate. Figure 2 shows how fuels with conventional distillation curves, like Jet A (A-2), have relatively constant vaporization rates similar to the d^2 -law.

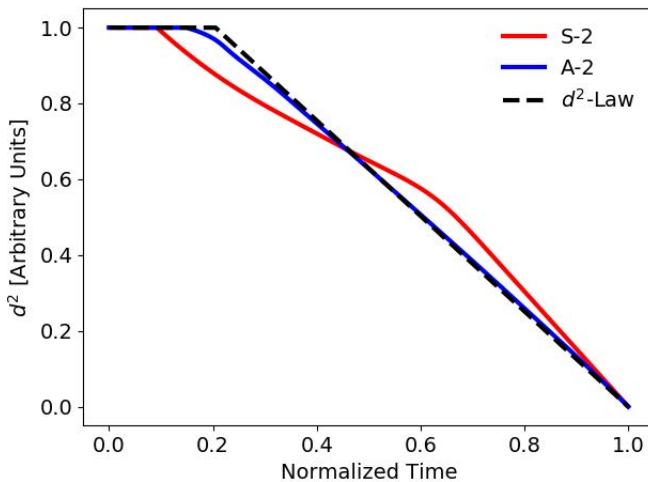


Figure 2. The relative normalized vaporization rates of a 3 species blend with bi-modal vaporization behavior, a conventional fuel, and the d^2 -law. Conventional fuels with many species have a constant volatility distribution which causes them to follow similar behavior to the d^2 -law.

It is unclear how multispecies blends would affect LBO behavior, however, there are multiple theories as to why this behavior could affect lean blowout. The first explanation is a concept called *thermal quenching*. Thermal quenching refers to the change in heat transfer behavior during the transition phase between the highly volatile and less volatile component. During the transition period, heat transfer continues to enter the droplet, but significantly less vapor is created per unit energy. Extinction and ignition phenomena are both highly temperature sensitive events. If at any point in the vaporization and combustion process extinction without reignition occurs, then blowout will occur. At each limit there is a balance of heat loss and energy generation which describes their limit. If during the transition phase, the heat entering into the droplet is viewed as heat loss, extinction and, correspondingly, lack of ignition could be described by the Semenov criterion. The Semenov criterion states that reactions will continue as long as heat generation exceeds heat losses. If heat generation is constant, then the increase in instantaneous heat losses could cause this limit to be reached.

Following the same assumption, during the transition phase the gaseous temperatures will decrease. Reduced gaseous temperatures will decrease flame speed which will lead to increased extinction probability. Simultaneously, reduction of the temperature of the vapor will have non-linear effects on ignition delay. If reignition is attempted at lower temperatures, it is highly unlikely it would occur and correspondingly no combustion would occur, signifying blowout.

The heat transfer into the droplet will be driven by the temperature of the flame and products. When these temperatures are high, increased amounts of heat are consequently lost to the walls and non-reacting air. If during the volatility transition this temperature decreases because of less mass combusting, the heat transfer into the droplet would decrease. Subsequently, a decrease in heat transfer would lead to further decrease in mass transfer, resulting in a negative feedback loop concluding with extinction.

Similar to thermal quenching, another theory is the volatility transition period has an effect on specifically mass transfer. During the transition, the reduction in mass vaporization rate would have an impact on instantaneous localized equivalence ratio. Chemical time scales will be significantly affected by reduced mass concentrations. Due to the turbulent environment, combustion occurs at fuel-to-air ratios other than stoichiometric. Because chemical time scales have been described as functions of equivalence ratio, potentially, the reduction in mass vaporization rate could have an impact on effective chemical time scales.

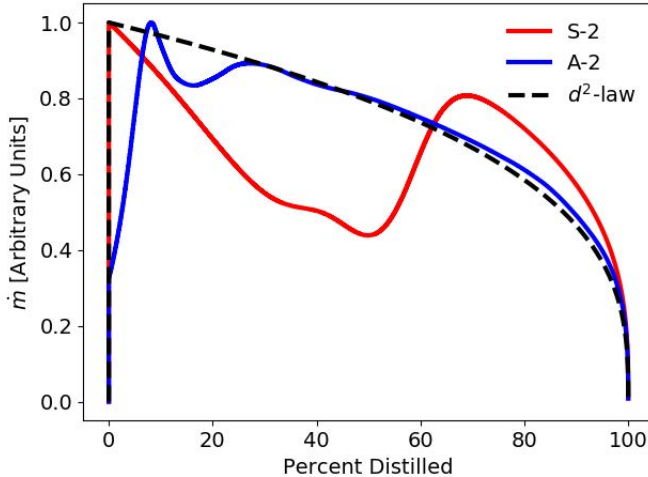


Figure 3. Mass vaporization/combustion rate as a function of volume combusted. Again, real fuels follow a similar trajectory to idealized fuels, but 2 and 3 species blends do not. Vaporization rates significantly slow down during the transition period.

During blowout testing, it was qualitatively observed that while testing S-2, unburned liquid particles were escaping the combustor [30]. This did not occur for other fuels. This supports the theory that the discontinuous volatility distribution of 2 and 3 species blends is causing the issue. Each of the explanations proposed suggest there is difficulty in advancing past the transition period to the less volatile component. Other fuels tested with comparably high final boiling points didn't show this behavior.

To stress test this theory, more 2/3 species blends need to be tested. The blends should be constructed of species with highly different volatilities. Ideally the concentrations of each species are close to equal as possible; this would maximize the distinctness between the different phases of distillation and highlight the effects.

Relative Lifetime of Droplets

The second explanation for the unique behavior of some of the fuels is that the time scale of vaporization is lower for the blends. Three of the greatest outliers include nC_{16} as a blending component. This molecule is among the least volatile molecules typically found in jet fuel. Inherently this increases vaporization time to some degree. If the more volatile component vaporizes first, the remaining non-volatile nC_{16} will be left with less surface area for heat transfer into the droplet, enhancing the effect of the high distillation temperatures. This is strongly influenced by the observation of liquid fuel escaping the combustor for the tests of the fuel S-2 [30]. This effect does not explain all of the outliers but could contribute to moving these points closer to the DCN trend line.

Preferential Vaporization

The third explanation of the unique behavior of the 2 and 3 species blends is preferential vaporization. Each of the 2 and 3 species blends tested were a blend of a more reactive, less volatile species with a less reactive volatile species. Preferential vaporization suggests that the species concentrations vaporizing as a function of time changes which, by extension, impacts combustion behavior. Preferential vaporization has been shown to occur in droplet vaporization [13,29]. Preferential vaporization has been shown to have an effect in both ignition and extinction experiments [31,32]. If this behavior is occurring in the Referee Rig, the bulk DCN may not be the chemical property of significance, but rather some intermediate DCN partially through the distillation process.

The more volatile species will be the first to vaporize. Once vaporized they will be present throughout the process either in the form their original molecule, intermediate species, or products with their corresponding heat. The species with the most time in vapor form have the most potential to impact combustion. If preferential vaporization is the behavior driving the



performance deviation between the 2 and 3 species blends from the DCN-law, then it would be possible to have a fuel that outperforms the DCN-law.

To validate a preferential vaporization model, the instantaneous property, in this case DCN, needs to be numerically estimated throughout the distillation process. Because of the variety of fuels tested to be compared, three different approximations are used: 1) a constant DCN throughout the distillation process, 2) a linear by volume blending rule of DCN and 3) a Quantitative Structure-Property Relation (QSPR) regression approximation. A constant DCN was approximated throughout the distillation process for fuels that were never blended before testing. This approximation is used for the conventional fuels. Although it is possible these fuels have variation in properties throughout the distillation process, these variations are approximated as negligible because of the relatively normal distribution of the different species types throughout the molecular weight (MW) distribution [12]. A linear by volume blending rule, in conjunction with an approximated blend distillation method, is used to approximate fuels which are blends of fuels with known properties [33,34]. QSPR regression combined with the Antoine Equation and vapor-liquid equilibrium is used to estimate DCN throughout the distillation of the fuels with known species and concentrations [28]. The methods used for each fuel is shown in Table 2

Table 2. The method used to estimate DCN as a function of percent distilled for each fuel. * =Methyl-cyclohexane could not be used in QSPR because it does not yet include cyclo-paraffin behavior.

Constant DCN	Linear by Volume	QSPR Regression
A-1, A-2, A-3, Sasol IPK	C-2, C-3, C-4, C-5, A-2/C-1 blends, A-2/C-5 blend, nC ₁₂ /MCH*	C-1, nC ₁₂ , nC ₇ , nC ₁₂ /M-Xylene, nC ₁₂ /iC ₈ , nC ₁₂ /nC ₁₆ , nC ₇ /nC ₁₂ , S-1, S-2

Using the methods described above, the DCNs throughout the distillation curve are calculated and power law regressions of LBO, as a function of the instantaneous DCN, are run to identify the optimal predictive value. In Figure 4, the R²'s of the regressions of LBO, with the calculated instantaneous DCN as the only indicator, are shown. The ideal predictor is found to be the DCN through 34% of the distillation process with a corresponding R² of 0.824. This result suggests that for the Referee Rig the first 34% of the fuel to vaporize are the species which will drive when blowout will occur. For different combustor designs, the physical time scales would vary and would thus have a different ideal predictive indicator. The predicted LBO will follow the regression shown in equation 4.

$$\frac{\phi(LBO_i)}{\phi(LBO_{A2})} = \left(\frac{DCN34_i}{DCN34_{A2}} \right)^{-0.069} \quad (4)$$

This analysis shows DCN through 34% of the distillation process is a better indicator than the overall DCN of a fuel, however the current data only contains fuels with more reactive, 'second halves' of the distillation process. Although this parameter does not predict the overall combustion perfectly, the predicted results from the chemistry alone are unbiased. Figure 5 shows the absence of bias between predicted and experimental results. The resulting error could potentially be explained by other chemical and physical properties.

None of the fuels tested have 'beat' the limiting 'DCN trend.' To show preferential vaporization has an effect, it needs to be shown preferential vaporization can be leveraged to improve a fuels performance and not only make it perform worse. The goal is to produce a fuel that will land in below the DCN-law line. If the partially vaporized DCN value appropriately captures the chemical-physical interaction in describing lean blowout, then designing a fuel to beat this trend should be possible.

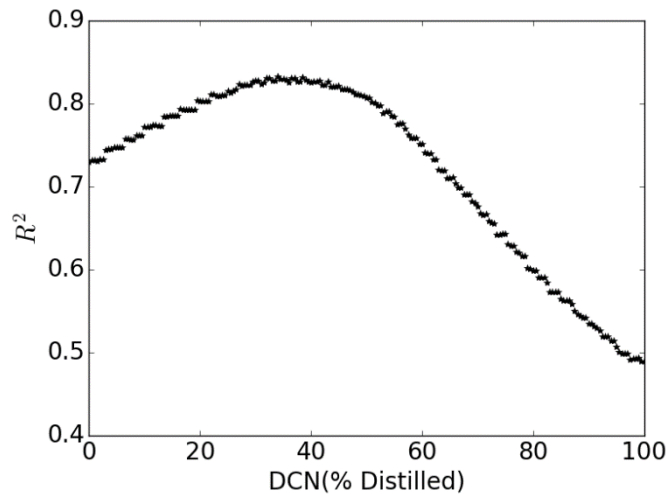


Figure 4. The R^2 of LBO vs instantaneous DCN, where DCN is a function of percent distilled. This result shows the optimal predictor of LBO for this experiment is the DCN at 34% distilled ($R^2 = 0.824$).

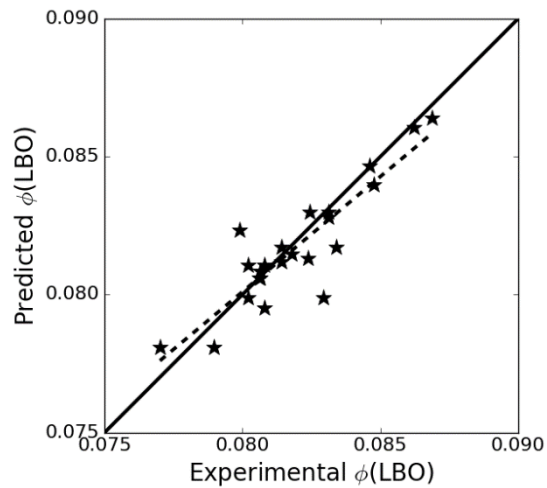


Figure 5. Predicted $\phi(LBO)$ vs. Experimental $\phi(LBO)$ for fuels reported in Table 1. The error associated with a prediction using Equation 4 is the distance from the solid line ($R^2=0.824$). The dashed line is a fit showing that there is consistency between experimental and predicted values.

Proposed Fuels

A fuel that will land below the DCN-law line needs to have a higher DCN at 34% vaporized than its overall DCN. To accomplish this, a fuel with high DCN and low molecular weight (MW), which corresponds with lower volatility, needs to be blended with a fuel with low DCN and high MW. Normal paraffins have the highest DCN among the different general molecular structures. Unfortunately, the normal paraffins with the highest DCN are the molecules with the highest MW. A range of *n*-paraffins are considered for use as the high DCN, low MW component in the blend. Low DCN, high MW fuels include large aromatics and large highly branched *iso*-paraffins. Highly branched *iso*-paraffins are preferred as the primary blending component because high concentrations of aromatics could have unforeseen effects as they less mimic previously tested fuels.



Fuel availability constraints lead us to a fuel which has already been tested, C-1. C-1 is a mix of almost exclusively *iso*-paraffins ranging from 5 to 20 carbons. It is heavily weighted towards highly branched *iso*-dodecane and *iso*-cetane [12]. For the purposes of this research, C-1 is approximated to be exclusively 80% by mole *iso*-dodecane and 20% by mole *iso*-cetane. *iso*-Cetane would be a near perfect candidate for the less reactive blending component due to its high MW and low DCN. In conventional jet fuels, there are very few molecules larger than 16 carbons, thus *iso*-cetane represents the upper bound for MW. *iso*-Cetane blends are considered as they represent an upper bound for maximizing preferential vaporization behavior.

The final fuel blend is selected as the blend that produces the highest difference between predicted LBOs by the DCN trend and the new 34% vaporized DCN regression in equation [2] (Figure 6). *n*-Paraffins between 7 carbons and 10 carbons are considered and blended with both C-1 and *iso*-cetane. Figure 7 shows the potential fuel blends and their respective differences between their predicted LBOs. The C-1 blended with *n*-heptane (*n*C₇) is the best option among C-1 blends offering a predicted difference of about 0.0022 in equivalence ratio at blowout with concentrations of 21% *n*C₇ and 79% C-1 by moles. The blend showing the greatest improvement with *iso*-cetane occurs similarly with *n*-octane (*n*C₈) and *n*-nonane (*n*C₉) offering a difference of about 0.0026 in equivalence ratio at blowout from the DCN-law line. This difference is achieved with 17% *n*C₈ and 83% *iso*-cetane as well as with 17% *n*C₉ and 83% *iso*-cetane.

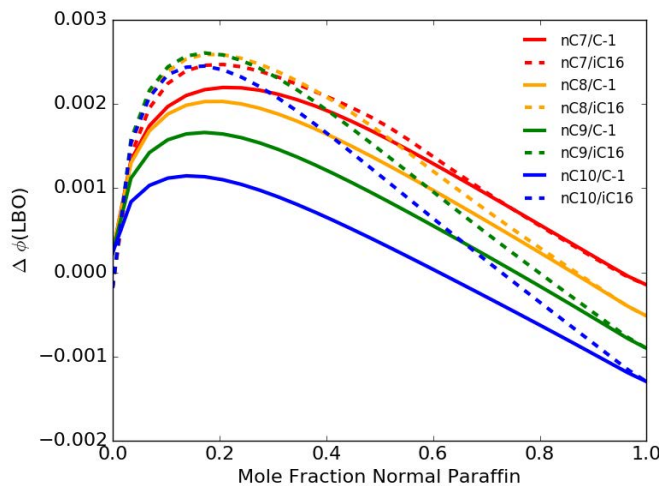


Figure 6. The difference between LBO predictions using DCN vs DCN through 34% of distillation. The difference is plotted for different blending ratios of *n*-paraffins mixed with C1 and Distilled C1. The peaks represent the ideal blending ratio for each blending combination.

The new blends as they are expected to perform are shown in Figure 8. Both the points for the generated fuels are in the target region, but not to the degree of the surrogates on the opposite side of the line. This is caused by physical limitations in the chemistry as low molecular weight species cannot have as high of DCN's as large molecular weight fuels. Each of the blends is shown as to their performance relative to the DCN trend line. Unfortunately, the predicted improvement below the DCN-law line is very close to the bounds of experimental error.

Both of the explanations for the outlier experimental results described above could be tested with one fuel. A 2-species blend fuel designed to test preferential vaporization would illuminate the impact of both effects if they are present. If the proposed fuels perform significantly worse than the DCN law line, then it would suggest it is not a chemical effect but rather a characteristic of 2 species blends. If the proposed fuels perform better than the DCN trend line, then it would be further evidence of preferential vaporization and its corresponding impact on chemistry, having an effect.

The Referee Rig, similar to other gas turbine combustors, requires a minimum amount of aromatics present in fuel to facilitate o-ring swelling. A large aromatic in relatively low concentrations can be added to the fuel and it should not significantly affect performance.



In theory, the effect of both of the described phenomenon would be enhanced in a low-pressure experiment. At lower pressures, individual species vaporize more ordinarily. Figure 8 shows the preferential distillation DCN values of S-2 at three different pressures. At 20 atm, the nC₁₆ has higher relative partial vapor pressures resulting in higher molar concentrations to vaporize early in the process. This causes the partially distilled DCN to be higher at lower volumes distilled. At low pressures, a local minimum can be seen around 45% distilled. This is caused by the vaporization of the 1,3,5 TMB. At each of the pressures the final ~30% distilled is all nC₁₆ vaporizing, resulting in similar paths.

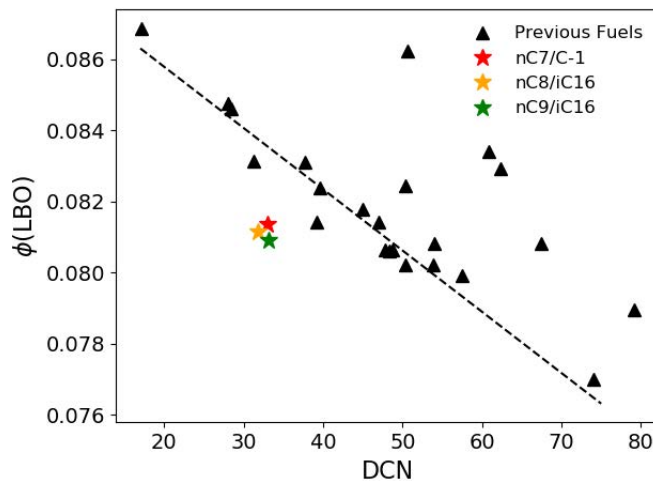


Figure 7. Shows the predicted LBO using preferential vaporization of the newly generated fuels. The new fuels would land below the current limiting bound.

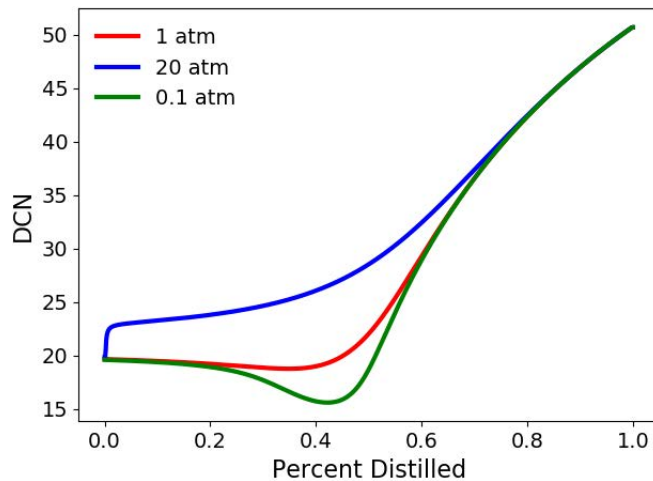


Figure 8. The DCN as a function of percent distilled of S-2 at various pressures. At high pressures, the species vaporize less ordinarily. At 0.1 atm the decrease in DCN seen is the vaporization of 1,3,5 TMB. To maximize preferential distillation behavior, a low-pressure experiment is preferred.

It should be noted, tests at different pressures will significantly affect boiling points and correspondingly vaporization rates. This could have unanticipated impact on the overall behavior near lean blowout.



Conclusions

The time scales of evaporative, chemical, and chemical-evaporative have been discussed and developed into several hypothesis to explain LBO events anomalous to the previously reported DCN trend. This time scale analysis has been applied to LBO data reported on the Referee Rig at AFRL/UDRI. These analyses suggest that no single time scale analysis or coupling is sufficient to explain all the observation in the Referee Rig. Numerical analysis suggests that one developed hypothesis, preferential vaporization, has the possibility to explain much of the observed discrepancies versus the DCN trend. Additionally, fuel blend and compositions to test this hypothesis have been suggested to confirm or discredit this hypothesis (21% by mole *n*-heptane and 79% Gevo ATJ (C-1)). Finally, additional work is needed to explore in greater depth the quantitative effects of the other two hypothesis listed and discussed (thermal quenching and relative lifetime of a droplet).

References

- [1] Colket, M. B., Heyne, J., Rumizen, M., Edwards, J. T., Gupta, M., Roquemore, W. M., Moder, J. P., Tishkoff, J. M., and Li, C., 2016, "An Overview of the National Jet Fuels Combustion Program," *54th AIAA Aerospace Sciences Meeting*, (Jan), pp. 1-24.
- [2] Heyne, J. S., Colket, M. B., Gupta, M., Jardines, A., Moder, J. P., Edwards, J. T., Roquemore, M., Li, C., and Rumizen, M., 2017, "Year 2 of the National Jet Fuels Combustion Program: Towards a Streamlined Alternative Jet Fuels Certification Process," *55th AIAA Aerospace Sciences Meeting*, p. 145.
- [3] Hendershott, T. H., Stouffer, S. D., Monfort, J. R., Diemer, J., Corporan, E., Wrzesinski, P., and Caswell, A. W., 2018, "Ignition of Conventional and Alternative Fuel at Low Temperatures in a Single-Cup Swirl-Stabilized Combustor," *56th AIAA Aerospace Sciences Meeting*, American Institute of Aeronautics and Astronautics, Kissimmee, FL.
- [4] Heyne, J. S., Peiffer, E., Colket, M., Shaw, C., Jardines, A., Moder, J., Edwards, J. T., Roquemore, W. M., Li, C., Rumizen, M., and Gupta, M., 2018, "Year 3 of the National Jet Fuels CombustionProgram: PRactical and Scientific Impacts of Alternative Jet Fuel Research," *56th AIAA Aerospace Sciences Meeting*.
- [5] Chtev, I., Rock, N., Ek, H., Smith, T., Emerson, B., Nobel, D. R., Seitzman, J., Lieuwen, T., Mayhew, E., Lee, T., Jiang, N., and Roy, S., 2017, "Simultaneous High Speed (5 kHz) Fuel-PLIE, OH-PLIF and Stereo PIV Imaging of Pressurized Swirl-Stabilized Flames Using Liquid Fuels," *Submitted to the 55th AIAA Aerospace Sciences Meeting*, American Institute of Aeronautics and Astronautics, Grapevine.
- [6] Stachler, R. D., Heyne, J. S., Stouffer, S. D., Miller, J. D., and Roquemore, W. M., 2017, "Investigation of Combustion Emissions from Conventional and Alternative Aviation Fuels in a Well-Stirred Reactor," *Submitted to the 55th AIAA Aerospace Sciences Meeting*, Grapevine, TX.
- [7] Burger, V., 2017, "The Influence of Fuel Properties on Threshold Combustion in Aviation Gas Turbine Engines," (Feb).
- [8] Plee, S. L., and Mellor, A. M., 1979, "Characteristic Time Correlation for Lean Blowoff of Bluff-Body-Stabilized Flames," *Combust. Flame*, **35**(C), pp. 61-80.
- [9] Mellor, A. M., 1980, "Semi-Empirical Correlations for Gas Turbine Emissions, Ignition, and Flame Stabilization," *Prog. Energy Combust. Sci.*, **6**(4), pp. 347-358.
- [10] Lefebvre, A. H., and Ballal, D. R., 2010, "Gas Turbine Combustion," Book, **Third Edit**.
- [11] Lefebvre, A. H., *Influence of Fuel Properties on Gas Turbine Combustion Performance*, West Lafayette, IN.
- [12] Edwards, J. T., 2017, "Reference Jet Fuels for Combustion Testing," *Submitted to the 55th AIAA Aerospace Sciences Meeting*, American Institute of Aeronautics and Astronautics, Grapevine.
- [13] Law, C. K., Prakesh, S., and Sirignano, W. A., 1981, "Theory of Transient Multicomponent Droplet Vaporization in a Convective Field," *Symp. Combust.*, **18**(1), pp. 1365-1374.
- [14] Yang, S., Ra, Y., and Reitz, R. D., 2010, "A Vaporization Model for Realistic Multi-Component Fuels," *Proceedings of the 22nd Annual Conference on on Liquid Atomization and Spray Systems*.
- [15] Sirignano, W. A., 1983, "Fuel Droplet Vaporization and Spray Combustion Theory," *Prog. Energy Combust. Sci.*, **9**(4), pp. 291-322.
- [16] Clercq, P. Le, and Dou, N., 2009, "Validation of a Multicomponent-Fuel Model for Spray Computations *," *47th AIAA Aerospace. Sci. Meet.*, (January), p. 2009.
- [17] Rauch, B., Le Clercq, P., Aigner, M., Rachner, M., Calabria, R., and Massoli, P., 2011, "Jet A-1 Fuel Spray Evaporation in a Turbulent Flow: Experimental Investigations and Validation of Numerical Models," *49th AIAA Aerospace Sciences Meeting*, Orlando, FL, pp. 1-13.
- [18] Liu, Y. C., Savas, A. J., and Avedisian, C. T., 2012, "Surrogate Fuel Development Based on Droplet Combustion : Comparison of Multi-Component Mixtures with an Aviation Fuel," *50th AIAA Aerospace Sciences Meeting Including the New Horizons Forum and Aerospace Exposition*, Nashville, TN, pp. 1-8.
- [19] Emerson, B., Lieuwen, T., and Juniper, M. P., 2017, "Local Stability Analysis and Eigenvalue Sensitivity of Reacting Bluff-Body Wakes," *J. Fluid Mech*, **788**, pp. 549-575.
- [20] Hanson, R. K., "Personal Communication," December 2017.



- [21] Bokhart, A. J., Shin, D., Rodrigues, N., Sojka, P., Gore, J., and Lucht, R. P., 2018, "Spray Characteristics at Lean Blowout and Cold Start Conditions Using Phase Doppler Anemometry," *56th AIAA Aerospace Sciences Meeting*, Kissimmee, FL.
- [22] Law, C. K., 2006, *Combustion Physics*, Cambridge University Press, New York.
- [23] Law, C. K., 1982, "Recent Advances in Droplet Vaporization and Combustion," *Prog. Energy Combust. Sci.*, **8**(3), pp. 171–201.
- [24] Marti, F., Martinez, O., Mazo, D., Garman, J., and Dunn-Rankin, D., 2017, "Evaporation of a Droplet Larger than the Kolmogorov Length Scale Immersed in a Relative Mean Flow," *Int. J. Multiph. Flow*, **88**, pp. 63–68.
- [25] Law, C. K., and Law, H. K., 1982, "A d2-Law for Multicomponent Droplet Vaporization and Combustion," *AIAA J.*, **20**(4), pp. 522–527.
- [26] Stouffer, S., Hendershott, T., Monfort, J. R., Diemer, J., Corporan, E., Wrzesinski, P., and Caswell, A. W., 2017, "Lean Blowout and Ignition Characteristics of Conventional and Surrogate Fuels Measured in a Swirl Stabilized Combustor," *55th AIAA Aerospace Sciences Meeting*, Grapevine, TX, pp. 1–14.
- [27] Corporan, E., Edwards, J. T., Stouffer, S., DeWitt, M., West, Z., Klingshirn, C., and Bruening, C., 2017, "Impacts of Fuel Properties on Combustor Performance, Operability and Emissions Characteristics," *55th AIAA Aerospace Sciences Meeting*, pp. 1–19.
- [28] Won, S. H., Haas, F. M., Dooley, S., Edwards, T., and Dryer, F. L., 2017, "Reconstruction of Chemical Structure of Real Fuel by Surrogate Formulation Based upon Combustion Property Targets," *Combust. Flame*, **183**, pp. 39–49.
- [29] Wang, C. H., Liu, X. Q., and Law, C. K., 1984, "Combustion and Microexplosion of Freely Falling Multicomponent Droplets," *Combust. Flame*, **56**(2), pp. 175–197.
- [30] Stouffer, S. D., "Personal Communication," Novemb. 2017.
- [31] Stagni, A., Esclapez, L., Govindaraju, P., Cuoci, A., Faravelli, T., and Ihme, M., 2017, "The Role of Preferential Evaporation on the Ignition of Multicomponent Fuels in a Homogeneous Spray/air Mixture," *Proc. Combust. Inst.*, **36**(2), pp. 2483–2491.
- [32] Yi, F., and Axelbaum, R. L., 2014, "Utilizing Preferential Vaporization to Enhance the Stability of Spray Combustion for High Water Content Fuels," *Combust. Flame*, **161**(8), pp. 2008–2014.
- [33] Bell, D., Heyne, J. S., Won, S. H., Dryer, F. L., Haas, F. M., and Dooley, S., 2017, "On the Development of General Surrogate Composition Calculations for Chemical and Physical Properties," *55th AIAA Aerospace Sciences Meeting*, American Institute of Aeronautics and Astronautics, Grapevine, TX.
- [34] Lefkowitz, J. A., and Haas, F. M., 2017, "Distillation-Resolved Evolution of Key Combustion Properties," *10th U.S. National Combustion Meeting*, College Park, Maryland.

Milestone(s)

- ASME Power Expo Convergence Publication

Major Accomplishments

- Explained the anomalous non-monotonic LBO behavior previously

Publications

Peer-reviewed Publications:

None

Conference Proceedings:

Bell DC, Heyne JS, Won S, Dryer FL. The Impact of Preferential Vaporization on Lean Blowout in a Referee Combustor at Figure of Merit Conditions. ASME. ASME Power Conference, Volume 1: *Fuels, Combustion, and Material Handling; Combustion Turbines Combined Cycles; Boilers and Heat Recovery Steam Generators; Virtual Plant and Cyber-Physical Systems; Plant Development and Construction; Renewable Energy Systems* ()V001T01A011. doi:10.1115/POWER2018-7432.

Outreach Efforts

Conference presentations:

Bell DC, Heyne JS, Won S, Dryer FL. The Impact of Preferential Vaporization on Lean Blowout in a Referee Combustor at Figure of Merit Conditions. ASME. ASME Power Conference, Volume 1: *Fuels, Combustion, and Material Handling; Combustion Turbines Combined Cycles; Boilers and Heat Recovery Steam Generators; Virtual Plant and Cyber-Physical Systems; Plant Development and Construction; Renewable Energy Systems* ()V001T01A011. doi:10.1115/POWER2018-7432.





Awards

David Bell, 2018 Young Engineer of the Year- ASME Dayton Section Award

Student Involvement

David Bell is lead for this project.

Plans for Next Period

Continue with additional LBO tests for the remaining NJFCP fuels (i.e., the remaining category A and C fuels as well as the fuel blends and surrogate blends). This paper will also proceed to publication once the foundational data for the analysis is published.

Task 4- Cross-Experiment Analysis

University of Dayton

Objective(s)

The objective of this task is to link low cost fundamental experiments to larger cost more complicated experiments internal to the NJFCP.

Research Approach

Methodology

The combustor rigs in the NJFCP aim to capture combustor variations found in actual gas turbine engines. In testing in the different combustors, rig sensitivity to fuel properties can be more fully realized. The Referee Rig, Georgia Tech, Sheffield, Cambridge, UTRC, and DLR rigs are all variations of traditional Rich-Quench-Lean combustors. The Honeywell rig is an Auxiliary Power Unit, a combustor that is used to start the main engines and provide emergency backup for electrical systems in the case of engine failure during flight. As such, this combustor is smaller than the other rigs in the program. The last rig in the program, the Well Stirred Reactor (WSR), is premixed and prevaporized. Although not currently used in gas turbine engines, the WSR is a useful research tool to evaluate the chemical fuel property effects on combustion. Table 1 provides a breakdown of the combustor rigs in the NJFCP including atomizer geometry and the operating conditions tested. An additional column, "Random Forest", was included to indicate the rigs that were used in the random forest regression results presented later.

The results discussed in this paper include conventional (Category A) and test (Category C) fuels, with the latter representing a large range of physical, volatile, and chemical properties. Category A fuels are conventional petroleum-derived fuels in use today that characterize the 'best' to 'worst' range of fuel properties while Category C fuels represent alternative jet fuels having extreme properties.

Figure 2 shows how the Category C fuel properties compare to the conventional Category A fuels. Notably, many of the Category C fuels fall outside the range of current experience, as depicted in the red regions on the plot, allowing for insight into how these fuels impact the key FOM.

Tables 2 and 3 provide a summary of the fuels tested and included in the results for this paper. In addition to the A and C fuels included in Table 2, there are F fuels which are blends of the A and C fuels, and there are the surrogate (S) fuels which were designed to stress specific fuel properties. Detailed properties of the Category A and C fuels are provided by Edwards¹³ and properties for other mixtures and blends were estimated using standard (linear) mixing rules. Radical indexes, a scaled determination of a fuels reactivity at strained extinction, for the A and C fuels were obtained from previously published literature¹⁴ while surrogate values were calculated by the summation of mole fractions multiplied by their corresponding radical index¹⁵.



Table 1. NJFCP combustor rig descriptions and LBO test conditions for each institution. The DCN Slope column records the LBO vs DCN slope representing rig sensitivity to DCN. Rig data used in future Random Forest results are indicated here.

Rig Name	Geometry type (injector/swirler)	Secondary air jets	T _{air} , K	T _{fuel} , K	P, atm	DCN Slope	Institution	Random Forest
PA-GT	Pressure atomizer/ Pratt & Whitney Swirler	No	550, 450, 300	445- 460	3.4	-0.194	Georgia Tech	
PA-HON	Pressure atomizer/ toroidal	No	324, 525, 557, 562, 394	288	1, 1.3, 1.4, 2, 3.3, 5.7	NA*	Honeywell	X
PA-RR	Pressure atomizer/ High-Swirl (P03)	Yes	239, 258, 400	239, 258, 320	2	-0.242	AFRL/ UDRI	X
PV-WSR	Prevaporized/ toroidal	No	450	450	1	-0.070	AFRL/UDRI	X
AA-SH	Airblast atomizer/ swirler stabilized/Rolls-Royce Tay Combustor	Yes	323, 373, 423		1	-0.273	Sheffield	X
PA-CAM	Pressure in bluff-body/	Yes	340	300	1	-0.254	Cambridge	
PA - UTRC	Pressure atomizer/ Pratt & Whitney Swirler	No	555, 494		8.64, 5.6	-0.153	UTRC	
PA-DLR	Pressure atomizer/ swirl stabilized	No	323, 373		1	-0.102	DLR Germany	

*HON data renormalized to protect proprietary rig information

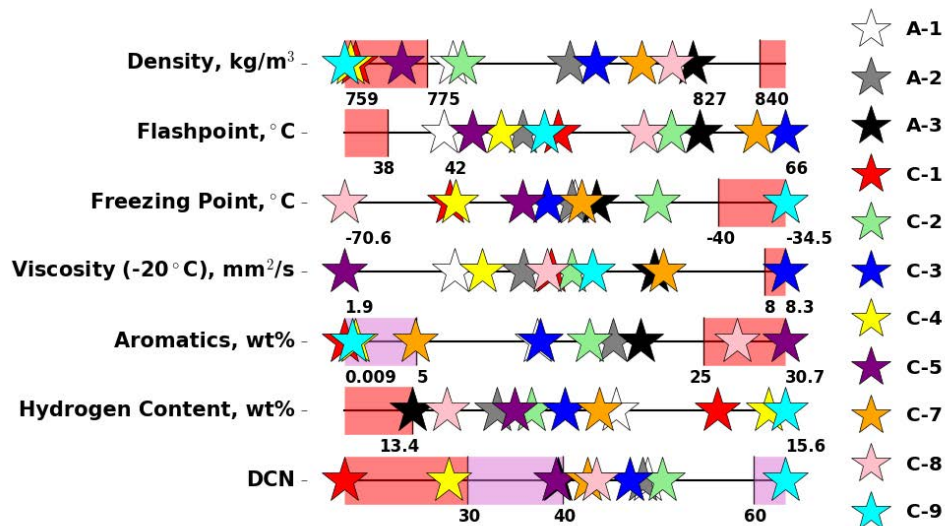


Figure 2. Category A and C range of fuel properties. The red regions represent current specification limits while the purple regions represent areas of interest to explore.

Table 2. NJFCP category A and C fuels representing petroleum-derived and alternative fuels, respectively. The F fuels are blends consisting of both the A and C fuels. The S fuels are surrogates that were designed to stress certain fuel properties.

Fuel/Solvent Mixture	POSF Number	Composition, % volume	Description
A-1	10264	Petroleum JP-8	Low flash, viscosity, and aromatics
A-2	10325	Petroleum Jet A	Nominal jet fuel
A-3	10289	Petroleum JP-5	High flash, viscosity, and aromatics
C-1	11498, 12368, 12384	Gevo ATJ, Highly branched C12 and C16 paraffins	Low DCN, unusual boiling range
C-2	11813, 12223	16% <i>tri</i> -methylbenzene + 84% C14 <i>iso</i> -paraffins	Chemically-asymmetric boiling range
C-3	12341, 12363	64% A-3 + 36% farnesane	High viscosity fuel, at viscosity limit for jet fuel at -20°C
C-4	12344, 12489	60% C9-12 <i>iso</i> -paraffins, 40% C-1	Low DCN, conventional, wide boiling range
C-5	12345, 12713, 12789, 12816	73% C10 <i>iso</i> -paraffins, 17% <i>tri</i> -methylbenzene	Flat boiling range
C-6		High cycloalkane content	High <i>cyclo</i> -paraffins
C-7	12925	75% RP-2, 23% A-3, 2% decalin	High <i>cyclo</i> -alkanes
C-8	12923	Jet A + Exxon aromatic blend	High (maximum allowable) aromatics
C-9	12933	80% R-8 HEFA, 20% <i>n</i> -C12	High DCN
F-1	NA	80/20 A-2/C-2	Blends
F-2	NA	50/50 A-2/C-1	Blends
F-3	NA	20/80 A-2/C-1	Blends
F-4	NA	80/20 A-2/C-5	Blends



J-1	NA	75.5% 1,3,5-tri-methylbenzene, 24.5% n-dodecane	Similar DCN to C-1 with low Radical Index
n-C12	NA	n-C12	High DCN
S-1	12765	59.3/18.4/22.2 vol% n-dodecane/ iso-octane/ 1,3,5-tri-methylbenzene	Similar to A-2, lower density and average molecular weight
S-2	12785	52.6/25.1/22.2 vol % n-hexadecane/ iso-octane/1,3,5-tri-methylbenzene	Similar to A-2, higher density and average molecular weight

Table 3. Fuels tested for LBO in each of the NJFCP rigs.

	A-1	A-2	A-3	C-1	C-2	C-3	C-4	C-5	F-1	F-2	F-3	F-4	S-1	S-2	nC12
GT	X	X	X	X	X	X	X	X	X	X	X		X	X	X
Honeywell	X	X	X	X	X			X							
Referee Rig	X	X	X	X	X	X	X	X	X	X	X	X	X	X	X
WSR		X	X	X			X								X
Sheffield	X	X	X	X		X	X	X							
Cambridge		X		X				X							
UTRC	Sasol IPK, F-76, L-210, JP-5, Jet-A, L-142, HRJ JP-5, Linpar 1416														
DLR	Crude-derived Jet A-1, Jet A-1 + 50% n-dodecane, FSJF (certification), FSJF (commercial), FSJF (commercial) + 1.5% HCPP, Experimental GTL kerosene, Synthetic paraffinic kerosene (SPK), Heavy naphtha refinery stream														

A methodological approach was taken to examine the observed differences in rig sensitivities, starting first with a statistical analysis of the LBO data from each rig using random forest regressions, as seen in Figure 4- Figure 7. Random forests, a machine learning technique, utilize a “forest” of decision trees to model complex sets of data without overfitting. A “forest” of regression trees, 500 in this case, is formed from the original data set by random sampling with replacement, also called bagging, which helps to de-correlate the trees and reduce bias. Each regression tree is then grown using Equation 2 where j is the splitting variable, s is the split point, R is the region, and c is the average y_i in the region. Trees are then modeled using Equation 3 where c_m is the average of $y_i/x_i \in R_m$.

$$\min_{j,s} \left[\min_{c_1} \sum_{x_i \in R_1(j,s)} (y_i - c_1)^2 + \min_{c_2} \sum_{x_i \in R_2(j,s)} (y_i - c_2)^2 \right] \quad (2)$$

$$f(x) = \sum_{m=1}^M c_m I(x \in R_m) \quad (3)$$

For the regression, an additional level of randomness is added by randomly selecting m variables from p total variables at each node. The random forest predictor is then calculated using Equation 4 where B is the number of trees, $\{T(x; \theta_b)\}_1^B$ is the actual trees in which θ_b describes the b^{th} tree in terms of split variables, cut points, and terminal-node values. In this case, the tree continues to grow until the number of samples left at a given node is two.

$$\hat{f}_{rf}^B(x) = \frac{1}{B} \sum_{b=1}^B T(x; \theta_b) \quad (4)$$



From the random forest predictor, features from the regression can be identified based on their importance to the model. These feature importance plots were used to understand the properties most impactful in LBO for each rig. For the LBO random forest regressions, the equivalence ratios (ϕ) at blowout for each fuel were normalized to A-2 to allow for equivalent comparison across rigs in combined regressions. This normalized phi value was used as the output of the regression while all other fuel characteristics, including volatile, physical, and chemical properties, along with test conditions (when relevant) were used as the predictors.

To better illuminate the importance of the characteristic timescales resulting in LBO, one fuel property was chosen to represent each of the timescales. The properties chosen in an attempt to maintain orthogonality, that is the variables (properties) are not correlated or covariate of each other. Twenty percent (20%) recovered, one measure of a fuel's volatility, was chosen to represent droplet evaporation. Viscosity was considered to represent the primary and secondary droplet breakup, but due to its high correlation with the distillate properties, density was chosen instead to characterize droplet break-up times.¹⁶ Although DCN and radical index are highly correlated for fuels with high aromatic or n-alkane content, fuels with high *iso*-alkane content, such as C-1, break this correlation as seen in Figure 3. Additionally, the J-1 fuel was designed to have a DCN similar to C-1 with a lower radical index to stress the difference in the two fuel properties as explore by Stachler, et. al.¹⁵ As such, DCN was used to represent the autoignition timescale while radical index was used to characterize the extinction timescale. Table 4 shows the breakdown of fuel property and corresponding timescale.

Results

The results presented here focus on individual rig regressions as it was found that combined regressions were limited by the geometrically known properties of each rig. Of the nine rigs mentioned, only four are discussed here to show the range of rig physical property effects, where the WSR and Honeywell APU rig represent the extreme ends, and the Referee Rig and Sheffield rig represent real main engine effects. For the combined regressions to capture more variability in the data adequately, more detailed rig descriptions are needed. While past combined random forest regression results showed DCN as being the most important feature, interestingly, individual rig regressions show a wide range of results with additional fuel properties and test conditions appearing to have significant influence. As shown in Figure 4 the individual regression for the Referee Rig, when considering only the timescale representative fuel properties, shows DCN, or the autoignition timescale, as being the dominating timescale followed by droplet evaporation and droplet breakup. The extinction timescale, represented by radical index, was the least important timescale for this rig. The WSR, as seen in Figure 5 shows both the autoignition and extinction strain rate chemical timescales as being the most important in determining LBO, supporting past reported results. In contrast, for example to the WSR regression, the random forest regression for Honeywell shows DCN and radical index as the least important fuel properties in determining LBO while volatile and physical properties dominate, as seen in Figure 6¹⁷. Honeywell was able to test for LBO at a variety of inlet temperature and pressures unlike the other rigs discussed here, and as expected, these inlet conditions were among the top features important in determining LBO. Lastly, Sheffield, in Figure 7, showed droplet breakup and the autoignition timescales to be of near equal importance in the progression to LBO followed by droplet evaporation and extinction. Interestingly, using only four fuel properties representative of the various timescales in the progression to LBO yielded R-squared values comparable to the random forest regressions in which all fuel properties were included.

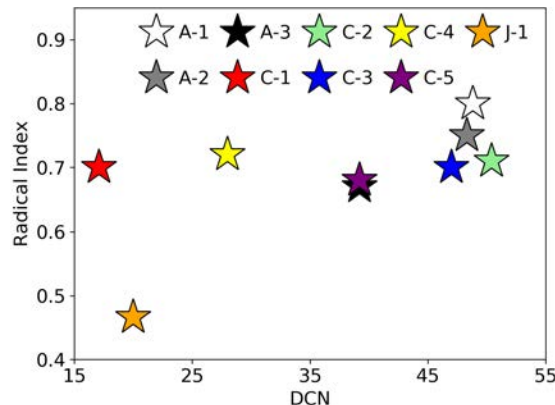


Figure 3. DCN versus Radical Index for the A and C fuels shows how high *iso*-octane fuels such as C-1 stress their correlation. The J-1 fuel was designed to further explore the importance of Radical Index relative to DCN.

Table 4. Fuel properties were chosen to characterize each of the different timescales on the progression to LBO to orthogonalize the random forest results.

Fuel Property	Timescale
DCN	Autoignition
20% Recovered	Droplet Evaporation
Density	Primary and Secondary Droplet Breakup
Radical index	Extinction

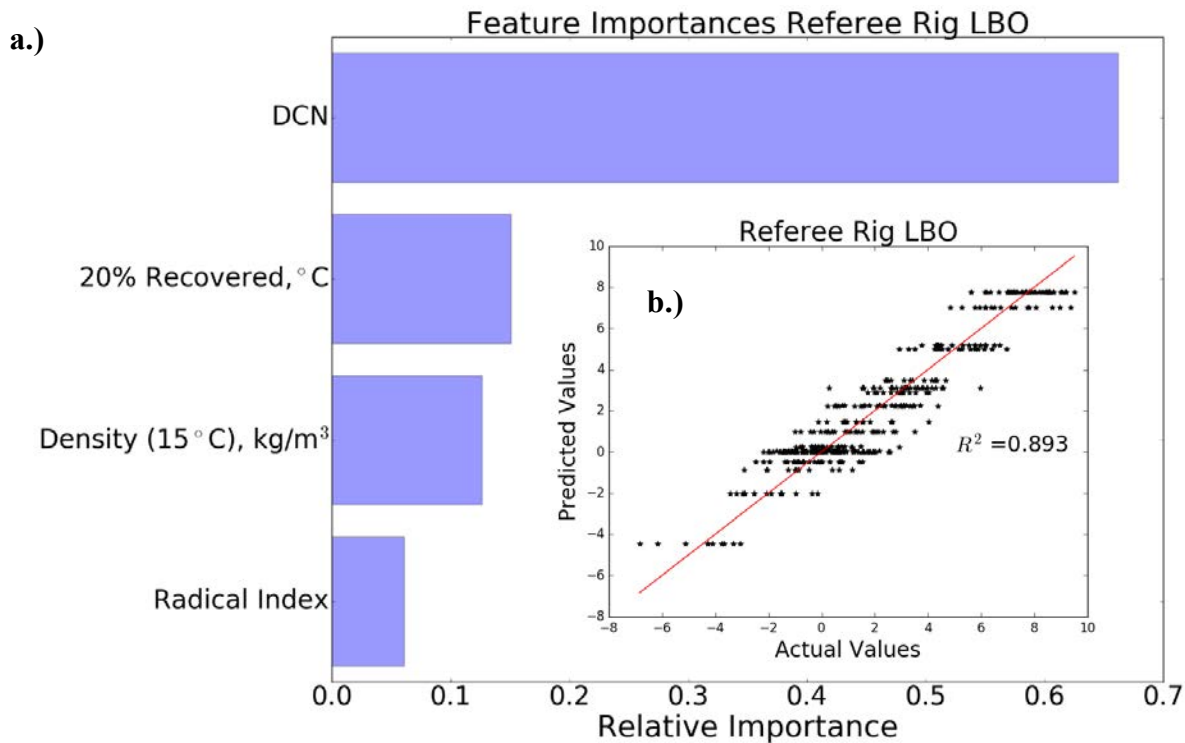


Figure 4. a.) Feature importances from the random forest regression for the Referee Rig show DCN as the most important fuel property representative of the autoignition timescale. b.) The predicted versus actual LBO data points are presented here.

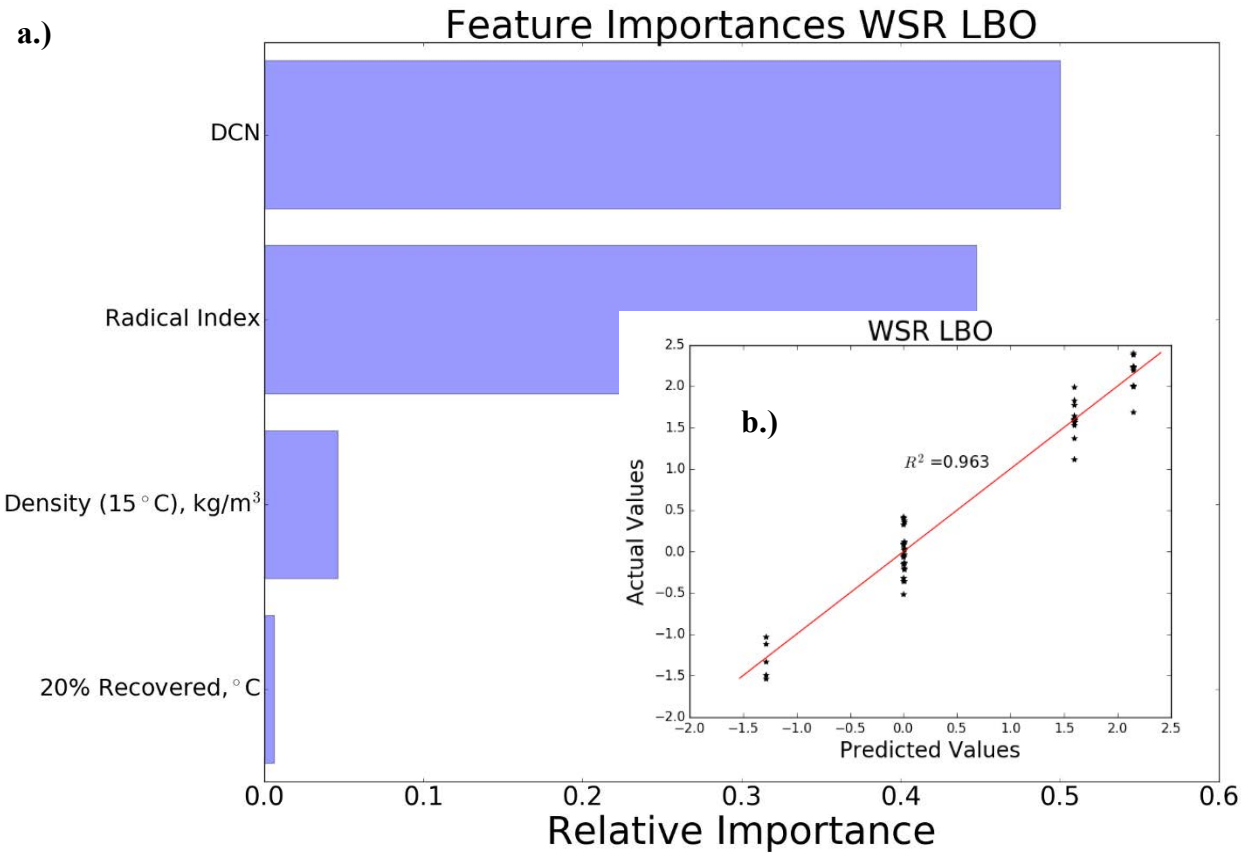


Figure 5. a.) Feature importances from the random forest regression for the Well-Stirred Reactor show the chemical timescales represented by DCN and radical index as being the most important features in determining LBO. Other properties such as distillate and physical properties show almost no statistical significance in the regression. b.) The predicted versus actual normalized LBO points are shown here.

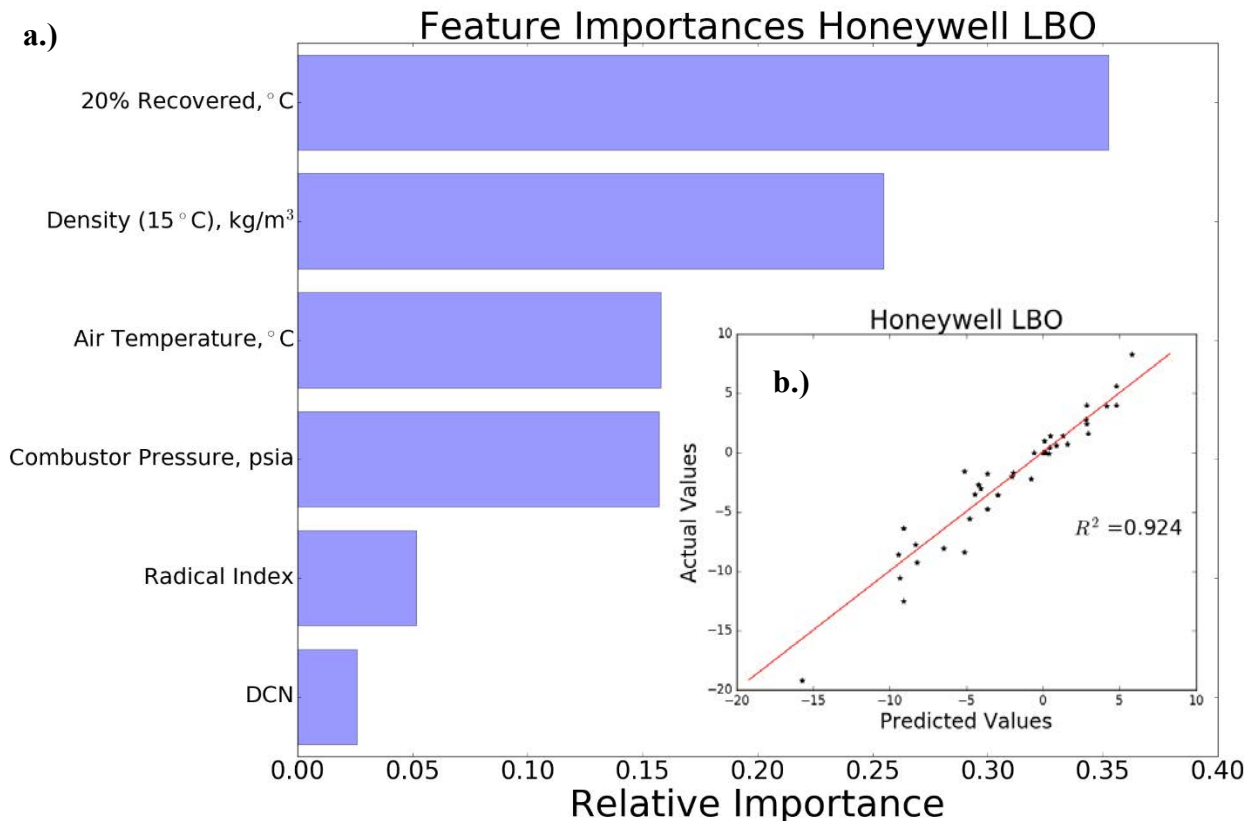


Figure 6. a.) Feature importances from the random forest regression for the Honeywell APU rig, the only rig in the NJFCP that does not show a dependency on DCN for predicting LBO. Distillate and density fuel properties, representative of droplet evaporation and breakup size, respectively, along with inlet temperature and pressure conditions were identified as the most import features for LBO for this rig. b.) Please note that the actual versus predicted values have been intentionally renormalized to protect proprietary information. Without the air temperature and combustor pressure parameters, the random forest regression only captures 61% of the variability in the data compared to the 92% presented here.



a.)

Feature Importances Sheffield LBO

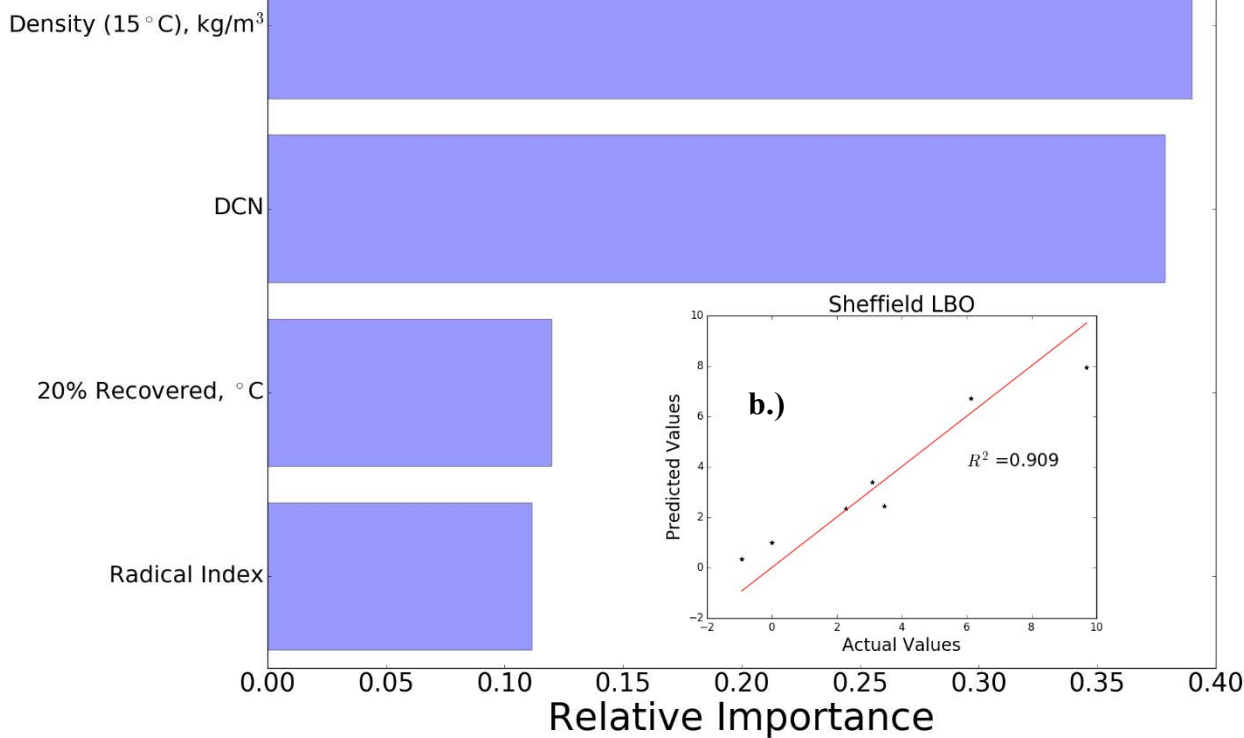


Figure 7. a.) Feature importances for the Sheffield rig show density, representative of droplet breakup, and DCN, representative of the autoignition timescale, as being of equal importance. b.) The predicted versus actual normalized LBO points are shown here.

Discussion

Although each rig expressed a different sensitivity to DCN, here we elaborate on a previously reported theory tying the observed sensitivity to experimental configuration of various rigs. Previously, a timescale analysis was suggested to account for preferential vaporization¹⁸, spray-chemical reactivity timescales⁴, and historical explanations of relative physical process times³. Figure 8 illustrates LBO as conceptual flow chart, beginning with fuel atomization and terminating with chemistry. LBO occurs when any of the six broad independent variables perturb the system sufficiently that chemical heat release effectively terminates. Three of these broad physical variables revolve around fuel properties, and three physical variables revolve around geometrical and flow rate variables. Purple ovals represent fuel properties that can perturb stable burning and coral ovals represent geometrical biases to the system. Fuel properties, purple ovals, are incorporated in the each of the previously reported random forest regressions. Geometrical variations across rigs, coral ovals, are only captured in combined random forest regressions, not reported here, through atomizer and rig geometry distinctions.

The six broad independent variable sets that can lead to LBO can additionally be described as three dependent times scales-referred to as evaporative, mixing, and chemical timescales. These timescales, therefore, are a combination of relevant fuel properties, geometrical biases, thermodynamic conditions, and rig flow rates. LBO occurs when a geometrically biased fuel property dependent timescale exceeds some other critical rig dependent timescale, such as primary recirculation or bulk rig residence times. Here the three dependent timescales are further explored and estimated to explain the relative fuel sensitivity differences across rigs.

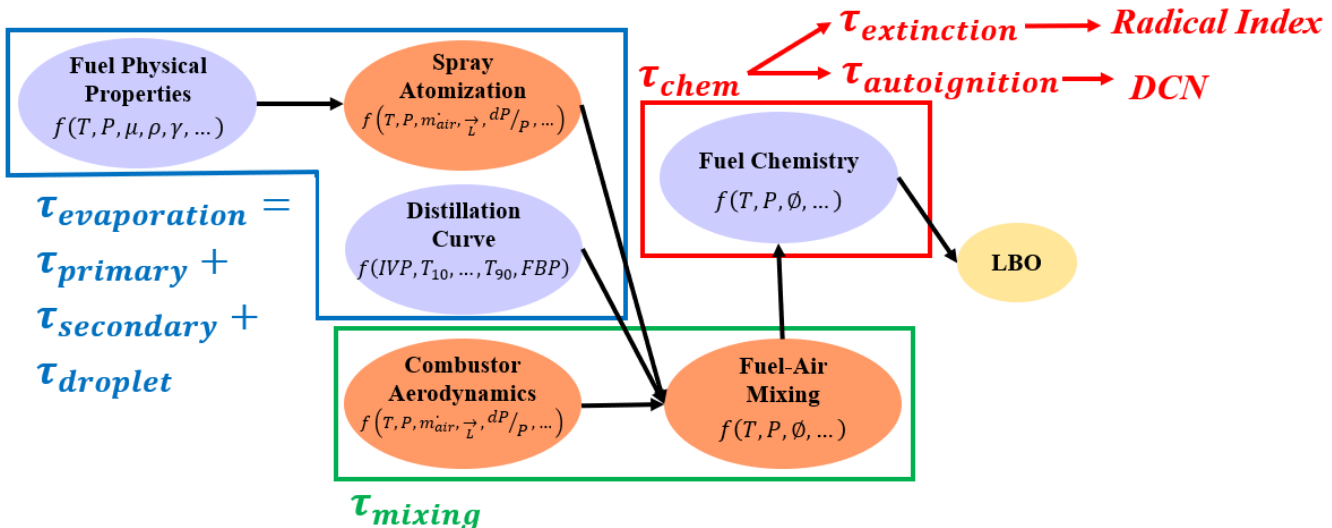


Figure 8. The pathways to LBO can be broken down into a conceptual flowchart. The purple ovals represent fuel properties while the orange ovals represent combustor characteristics. These pathways can be grouped to illustrate the evaporative, mixing, and chemical timescales that are factors in affecting blowout.

The evaporation timescale is a function of fuel physical properties, distillate properties, and atomizer characteristics for a given set of conditions. It can be approximated as the algebraic sum of primary atomization, secondary atomization, and droplet timescales. Primary and secondary atomization timescales increase with increasing fuel density, surface tension, and viscosity. Larger atomization timescales then result in larger droplets and longer evaporation times, and it should be noted that the atomization method has a significant effect on the primary and secondary atomization timescales. The droplet timescale of a fuel can be estimated with fuel volatility, as expressed through the distillation curve. Increases in the relative distillation temperatures of a fuel result in longer droplet timescales via larger characteristic heat capacities and lower vapor pressures. While all of the distillate properties are highly correlated, the 20% recovered temperature has been found to be the most influential in predicting LBO of the volatile properties for the rigs discussed here and thus was used in the earlier regressions.

The mixing timescale includes both combustor aerodynamics and fuel-air mixing, no fuel properties. Combustor aerodynamics is a function of combustor geometry (\vec{L}), temperature (T), pressure (P), mass flowrates of fuel and air (\dot{m}), relative pressure drop ($\frac{dP}{P}$), along with other combustor operating conditions. The combustor timescale for mixing is assumed to be constant for a given rig at a given set of conditions.

Finally, the chemical timescale is a function of the fuel chemical properties and, similar to perfectly stirred reactor (PSR) theory, can be described as two timescales. PSR theory predicts an extinction and ignition timescale. Similarly, extinction and autoignition timescales have been observed⁶ and speculated¹⁵ from various NJFCP rigs reported here. Autoignition timescales are estimated from the DCN of a fuel, and extinction timescales can be approximated using radical indexes and extinction strain rates¹⁵. The relative concentrations of aromatics, iso-paraffins, n-paraffins, and cyclo-paraffins result in a fuel's radical index and DCN, which are derived directly from a fuel's chemical reaction pathways, specific energy [MJ/kg], and diffusivity [molecular weight, gm/mol]. Interestingly, autoignition timescales can be derived from both zero dimensional simulations and measurements, but extinction timescales have been best approximated by one dimensional experiments.

Combined, these timescales can be used to illuminate dominate/controlling timescales/physics in each of the aforementioned rigs, which can be used to inform the ASTM alternative jet fuel evaluation and approval process. Figure 9 illustrates estimated (relative) timescale differences between the four rigs with the total time normalized to the same value. Evaporation timescale (blue) and chemical timescale (red) are estimated from the random forest regressions while the mixing timescale (green) is currently unquantified between the rigs (but is nearly constant for a rig across the fuels tested).



Collectively, the four rigs show chemical and evaporative dominated results as well as a rig with a competition between chemical and evaporative timescales.

Chemical timescales dominate for the Referee Rig and the WSR. The observed results for the WSR corroborate expectations, as the rig introduces prevaporized and premixed fuel into the reacting region. In the absence of any two phase flow in the reactor, the evaporative timescale influence is anticipated to be zero. Similarly, Stachler et al. have shown in more detail that extinction strain rates (via radical indexes) are likely the controlling timescale for extinction strain rates. From the above regressions and past results, the WSR has demonstrated a dependence on DCN for predicting LBO. Alternatively, it can be argued that pure extinction is playing a much larger and limiting role than in the other combustor designs with strong recirculation.

The swirler and wide nozzle spray angle of the Referee Rig are anticipated to be the root causes for chemical timescale dominance in the Referee Rig. It is hypothesized that the strong recirculation zone, caused by the swirler, of the Referee Rig relative to the Honeywell APU elevates the probability of a reignition event in the region of primary recirculation. Additionally, the wide spray angle of the Referee Rig causes wetting on the surface of the swirler⁷. This wetting in turn enables an additional mechanism for atomization and spray break-up. Combined, it is hypothesized that the swirler and wide spray angle diminish the sensitivity of LBO to evaporative timescales.

Evaporative timescales are observed to dominate in the Honeywell APU, with chemical-evaporative timescales appearing to be in equilibrium in the Sheffield rig. Honeywell, in complete contrast to the WSR, showed almost no dependence on the chemical properties encompassing the chemical timescale in the progression to LBO¹⁶. Instead the droplet breakup and evaporation are the dominating timescales. The Honeywell rig, in contrast to the WSR and Referee Rig, does not have a swirler, nor does it prevaporize or premix the fuel. Additionally, the Honeywell rig has a considerably smaller pressure atomizer. Pressure atomizers are known to be more sensitive to atomization properties relative to air blast atomizers, with smaller pressure atomizers known to be even more sensitive to physical properties than larger pressure atomizers. This analysis, again, is consistent with existing/historical conceptual understandings of fuel spray effects.

The Sheffield rig shows an even split between the droplet breakup and autoignition timescale on the progression to LBO. As the Sheffield rig utilizes an airblast atomizer in contrast to the other pressure and prevaporized rigs, the larger dependence on density and other droplet breakup properties is well explained, although further analysis is needed to explain the autoignition timescale importance. The evaporative timescale and extinction timescale were found to be of lesser significance on the progression to LBO.

Of the seven rigs, the three most sensitive to DCN have secondary air jets which act to strengthen the primary recirculation zone. This would help to explain past results showing the DLR rig⁴, a rig similar to the Referee Rig except without secondary air jets, having a much smaller sensitivity to DCN. This hypothesis could be confirmed through the acquisition of swirl numbers, a property than can be used to describe a combustors primary recirculation zone strength. Additionally, continued LBO tests with varying secondary air jet configurations/strengths could confirm this hypothesis as well.

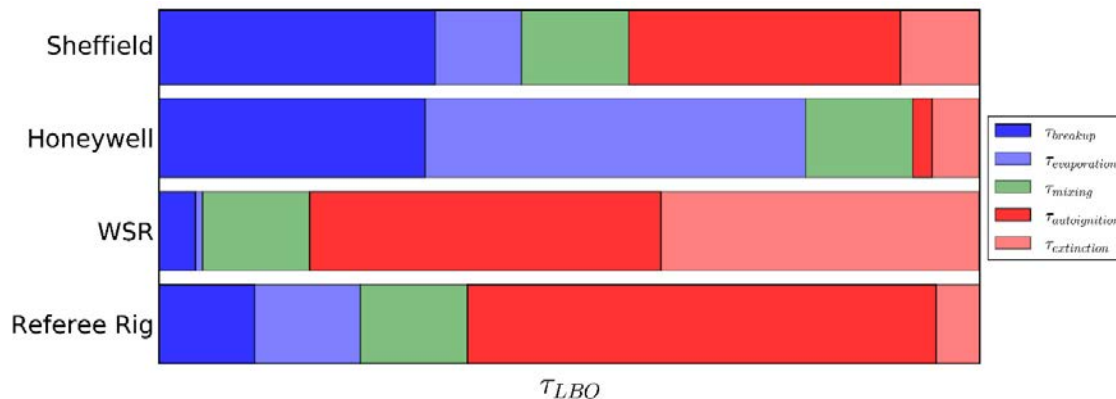


Figure 9. The LBO timescale, a summation of the evaporative (blue), mixing (green), and chemical (red) timescales, for the Referee Rig, Well-Stirred Reactor (WSR), and Honeywell based on feature importances from the random forest regressions. The mixing timescale was not captured in the regressions and thus the relative size of its timescale is unknown, represented here by two areas that suggest the true value could be larger or smaller than what is shown here.

Conclusion

The sensitivity of a combustor to fuel effects at LBO will remain a hurdle towards the certification of alternative jet fuel. This paper has sought to explain the differences in rig sensitivity at LBO for four down selected fuel properties. These down selected fuel properties are proposed to represent four fuel property dependent timescales near LBO. Random forest regressions with these four properties over four rigs were able to explain nearly 90% or better of all variance across all fuels considered. This analysis was extended to describe the relative timescales in each rig as LBO is approached.

Two rigs were shown to have chemical timescales dominate near LBO. Chemical timescales were dominate in the event of minimal spray importance via swirler recirculation, prevaporization, and rapid atomization as in the WSR and Referee Rig. The Honeywell APU, with its small pressure atomizer and lack of swirler, was shown to be dominated by evaporative timescales. The Sheffield rig was observed to have nearly equal evaporative and chemical timescale importance. Additional investigation into this rig is needed to fully explain the relative fuel effects in this rig. Future work will involve quantifying each timescale through modelling.

References

- [1] Friedrich, C., and Robertson, P. A., "Hybrid-Electric Propulsion for Aircraft," *Journal of Aircraft*, vol. 52, 2015, pp. 176-189.
- [2] Plee, S. L., and Mellor, A. M., "Characteristic time correlation for lean blowoff of bluff-body-stabilized flames," *Combustion and Flame*, vol. 35, 1979, pp. 61-80.
- [3] Mellor, A. M., "Semi-empirical correlations for gas turbine emissions, ignition, and flame stabilization," *Progress in Energy and Combustion Science*, vol. 6, 1980, pp. 347-358.
- [4] Burger, V., "The Influence of Fuel Properties on Threshold Combustion in Aviation Gas Turbine Engines," 2017.
- [5] Heyne, J., Peiffer, E., Colket, M., Moder, J., Edwards, J. T., Roquemore, W. M., Shaw, C., Li, C., Rumizen, M., and Gupta, M., "Year 3 of the National Jet Fuels Combustion Program: Practical and Scientific Impacts," *56th AIAA Aerospace Sciences Meeting*, Kissimmee, FL: 2018.
- [6] Chtev, I., Rock, N., Ek, H., Smith, T., Emerson, B., Nobel, D. R., Seitzman, J., Lieuwen, T., Mayhew, E., Lee, T., Jiang, N., and Roy, S., "Simultaneous High Speed (5 kHz) Fuel-PLIE, OH-PLIF and Stereo PIV Imaging of Pressurized Swirl-Stabilized Flames using Liquid Fuels," *Submitted to the 55th AIAA Aerospace Sciences Meeting*, Grapevine, TX: American Institute of Aeronautics and Astronautics, 2017.
- [7] Stouffer, S., Hendershott, T., Monfort, J. R., Diemer, J., Corporan, E., Wrzesinski, P., and Caswell, A. W., "Lean Blowout and Ignition Characteristics of Conventional and Surrogate Fuels Measured in a Swirl Stabilized Combustor," *55th AIAA Aerospace Sciences Meeting*, 2017, pp. 1-14.
- [8] Stachler, R. D., Heyne, J. S., Stouffer, S. D., Miller, J. D., and Roquemore, W. M., "Investigation of Combustion Emissions from Conventional and Alternative Aviation Fuels in a Well-Stirred Reactor," *Submitted to the 55th AIAA Aerospace Sciences Meeting*, 2017.



- Sciences Meeting*, Grapevine, TX: American Institute of Aeronautics and Astronautics, 2017.
- [9] Khandelwal, B., and Ahmed, I., "Research Report on Lean Blowout Limit The University of Sheffield Department of Mechanical Engineering," 2017.
- [10] Allison, P. M., Sidney, J. A. M., and Mastorakos, E., "Forced Response of Kerosene Flames in a Bluff-body Stabilised Combustor," *55th AIAA Aerospace Sciences Meeting*, Grapevine, TX: American Institute of Aeronautics and Astronautics, 2017.
- [11] Sidney, J. A. M., Allison, P. M., and Mastorakos, E., "The effect of fuel composition on swirling kerosene flames," *55th AIAA Aerospace Sciences Meeting*, Grapevine, TX: American Institute of Aeronautics and Astronautics, 2017.
- [12] Colket, M., Zeppieri, S., Dai, Z., and Hautman, D., "Fuel Research at UTRC," *In Multi-Agency Coordinating Council for Combustion Research 5th Annual Fuel Research Meeting*, 2012.
- [13] Edwards, T., "Reference Jet Fuels for Combustion Testing," *55th AIAA Aerospace Sciences Meeting*, Grapevine: American Institute of Aeronautics and Astronautics, 2017.
- [14] Won, S. H., Dooley, S., Dryer, F. L., and Ju, Y., "A radical index for the determination of the chemical kinetic contribution to diffusion flame extinction of large hydrocarbon fuels," *Combustion and Flame*, vol. 159, Feb. 2012, pp. 541–551.
- [15] Stachler, R., Peiffer, E., Kosir, S., Heyne, J., and Stouffer, S., "A Study into the Chemical Timescale for a Toroidal Jet-Stirred Reactor (TJSR)," *Central States Section of The Combustion Institute*, Minneapolis: 2018.
- [16] Heyne, J. S., Peiffer, E., Colket, M. B., Jardines, A., Shaw, C., Moder, J. P., Roquemore, W. M., Edwards, J. T., Li, C., Rumizen, M., and Gupta, M., "Year 3 of the National Jet Fuels Combustion Program: Practical and Scientific Impacts of Alternative Jet Fuel Research," *2018 AIAA Aerospace Sciences Meeting*, Reston, Virginia: American Institute of Aeronautics and Astronautics, 2018.
- [17] Culbertson, B., and Williams, R., *ALTERNATIVE AVIATION FUELS FOR USE IN MILITARY APUS AND ENGINES VERSATILE AFFORDABLE ADVANCED TURBINE ENGINE (VAATE), PHASE II AND III*, AFRL-RQ-WP-TR-2017-0047: 2017.
- [18] Bell, D. C., Heyne, J. S., Won, S. H., and Dryer, F. L., "The Impact of Preferential Vaporization on Lean Blowout in a Referee Combustor at Figure of Merit Conditions," *ASME 2018 Power and Energy Conference*, Lake Buena Vista: 2018.

Task 5- Common Format Routine Software Development

University of Dayton Research Institute

Objective(s)

We aim to develop a software package in which the OEMs can utilize the state of the art models being developed by the other NJFCP modeling teams.

Research Approach

This work is motivated for the imperative necessity of expediting combustor rig evaluation process for ASTM D4054 through improved combustion modeling capabilities. This fuel certification entails three main figures of merit, lean blowout, ignition, and cold relight. Current fuel certification requires expensive and time-consuming experimental testing in gas turbine engines. State-of-the-art combustion models that could expedite this process are not readily available for original engine manufacturers (OEMs). The main objective of this work is to bridge the gap between state-of-the-art academic combustion models and industrial software. The second aspect of this project is to speed up the academic codes for reaching industrial grade software category. The third aspect of this project involves verification and validation of this common format routine (CFR) software.

Modeling and simulation of complex fuels in gas turbine combustors is not trivial. Gas turbine combustors are intricate devices with characteristic length scales varying from the sub-millimeter laminar flamelet thickness to the large centimeter-size dilution holes. Therefore, the mesh resolution for gas turbines combustors is in the order of millions to even hundreds of million cells. The time scales associated with combustion and turbulence in the combustor vary from microseconds for the Kolmogorov turbulent length scales and species reaction rates to milliseconds associated with the flow through-time of the combustor. The time steps and mesh requirements for modeling and simulating a combustor are nearly prohibitive. In order to mitigate some of the challenges associated with modeling and simulation of gas turbine combustors, the lower-dimensional manifold combustion (LDMC) models decouple the chemistry and chemistry-turbulence interaction from the complex turbulence computational fluid dynamics (CFD) calculations. The chemistry is computed *a priori* from one-dimensional stagnation flow equations and/or equilibrium calculation. The chemistry-turbulence interaction is computed by presuming probability density functions (PDFs). Transport equations for the moments of the





mixture fraction (Z) and progress variable (C) are solved in the physical space. These values are then used to interpolate and to extract the thermo-chemical and transport information of the pre-tabulated table.

Commercial software such as Fluent [1,2] and Star-CCM+ already have built-in LDMC models. However, there are always limitations in terms of implementation. For instance, Fluent [1,2] pre-tabulates the table in a mixture fraction space directly. Hence, it does not solve for the one-dimensional equations. On the other hand, the CFR software presented in this paper uses a modified Cantera 2.3 [1] package. The CFR pre-tabulates chemical-turbulence interaction in the one-dimensional physical space. This allows the user to vary the transport coefficient formulation and investigated such effects on numerical predictions. Another difference between Fluent [1,2] and the CFR is that the latter can compute the three branches of the combustion phenomenon. The CFR is also more flexible because molecular properties are directly interpolated from the table. Fluent [1,2] does not offer this capability. However, other commercial software package such as Chemkin [1] offers flamelet calculations that include the three branches of combustion. This software is very robust, but does not offer the turbulence-chemistry convolution capability needed for computing turbulent flames. To the best of our knowledge there is no standalone software that offers the capability of performing turbulence-chemistry convolution of a flamelet library. In addition, the CFR software is designed in a manner that more modules and capability can be easily annexed providing more flexibility to the user.

The purpose of this paper are to document the development of the CFR as well as to prove that such software has been verified and validated. Subsequently, the software is introduced. Important definitions are illustrated and discussed. The verification and validation tests are then presented.

Common Format Routine (CFR) Software

In short, the CFR software can be sub-divided into two components, the pretabulator and the flamelet-based software, which is illustrated in Appendix Figure 1. The pretabulator is capable of tabulating thermo-chemical and transport data for laminar and turbulent flames. The pretabulator is based on a modified version of Cantera 2.3 [3]. Cantera is written in C++ and Python wrappers/codes were developed in order to include new capabilities in Cantera. This Python codes also interact with a C# GUI. This can currently tabulate flamelet prolongation of the intrinsic low-dimensional manifold (FPI) and flamelet progress variable (FPV). The flamelet-based software can attach the pretabulated turbulence-chemistry interaction table to a CFD code. In this case the flamelet-based software was attached to Fluent [1,2]. The flamelet-based software machinery can perform bilinear, trilinear and tetralinear interpolation of this thermochemical table. This software is written in C and its GUI is written using C#. Now detailed description of the software is provided next.

A. Mixture Fraction Definition

Mixture fraction is a conserved scalar. This means that mixture fraction cannot be created or destroyed. Because atomic elements and enthalpy cannot be created or destroyed, mixture fractions is typically defined in this context. Here the mixture fraction is defined in terms of atomic elements and any combination of atomic elements is valid. However, the atomic composition needs to be chosen so that mixture fraction varies between zero and unity.

$$Z = \sum_{i=1}^{N_{atomic\ selection}} \sum_{n=1}^{N_{species}} \frac{MW_i}{MW_n} Y_n \quad (1)$$

The user selection of the mixture fraction definition is given by Appendix Figure 2.

B. Progress Variable Definition

The progress variable provides quantitative information of the combustion efficiency. The latter is equal to zero when the flame blows out and combustion efficiency is zero. The maximum value of the progress variable is a real number less than unity. The progress variable is defined in terms of species mass fractions. The equation below indicates that the mixture fraction is the summation of species mass fractions. Typically in the literature CO and CO₂ are selected to indicate the level of completeness of the combustion process. In addition, CO, CO₂, H₂ and H₂O are also chosen species to indicate the combustion efficiency (or completeness of the combustion process).

$$C = \sum_{n=1}^{N_{species\ selected}} Y_n \quad (2)$$

The user selection of the mixture fraction definition is given by Appendix Figure 3.



C. Progress Parameter Definition

For premixed and diffusion flamelets, the progress variable defined by Eq. (2) varies in the spatial direction. For a premixed flamelet C increases monotonically from the unburned reactants from zero to a maximum value downstream the flame front. For diffusion flamelets the behavior is non-monotonic and the maximum value of C occurs near stoichiometry and then its value decreases to zero towards the reactant inlets. Therefore, the progress variable definition is a function of mixture fraction, i.e. $C = C(Z)$. Thereby, the progress parameter Λ is defined as a bijective, unique identifier that can be used to sort each flamelet. This definition is given below.

$$\Lambda = f(C, Z) \quad (3)$$

This definition is particularly useful for modeling diffusion flamelets and has been implemented in the current software. In the CFR this conversion can be enable or disable.

D. Convolved Thermochemical and Transport Variables

Once state relationships have been computed between thermochemical and transport properties and the lower dimensional manifold variables (i.e., Z and ϕ) these quantities need to be convoluted for the turbulence-chemistry interaction using the equation below. The probability density functions (PDF) in this equation reads as “the probability density function of Z as a function of \tilde{Z} and $\tilde{Z}^{\prime 2}$.” Then, all thermochemical and transport properties (ϕ) such as density (ρ), molecular weight (MW), temperature (T), specific heat capacity (c_p), dynamic viscosity (μ), thermal conductivity (k), species mass fractions (Y_i) and species reaction rates (ω_i) are a function of the transported lower-dimensional manifold variables ($\tilde{Z}, \tilde{Z}^{\prime 2}, \tilde{\Lambda}$ and $\tilde{\Lambda}^{\prime 2}$).

$$\tilde{\phi}(\tilde{Z}, \tilde{Z}^{\prime 2}, \tilde{\Lambda}, \tilde{\Lambda}^{\prime 2}) = \int_0^1 \int_0^1 \phi(Z, \frac{\Lambda}{\Lambda_{max}}) PDF(Z; \tilde{Z}, \tilde{Z}^{\prime 2}) PDF(\frac{\Lambda}{\Lambda_{max}}; \tilde{\Lambda}, \tilde{\Lambda}^{\prime 2}) dZ d\Lambda \quad (4)$$

Importantly to note is that the above equation, the progress parameter requires normalization before integration.

E. Lower Dimensional Manifold Transported Variables For Laminar Flows

Equations (5) and (6) are mixture fraction (Z) and progress variable (C) transported equations. When solving for laminar flows convolutions such as that represented by (4) are not necessary. Both equations here contain a transient, a convective and a diffusive term. However, the progress variable in addition contains a source term $\dot{\Omega}_C$.

$$\frac{\partial(\rho Z)}{\partial t} + \frac{\partial(\rho Z u_j)}{\partial x_j} = \frac{\partial}{\partial x_j} \left(\frac{\lambda}{c_p} \frac{\partial Z}{\partial x_j} \right) \quad (5)$$

$$\frac{\partial(\rho C)}{\partial t} + \frac{\partial(\rho C u_j)}{\partial x_j} = \frac{\partial}{\partial x_j} \left(\frac{\lambda}{c_p} \frac{\partial C}{\partial x_j} \right) + \dot{\Omega}_C \quad (6)$$

The source term ($\dot{\Omega}_C$) is computed as follows,

$$\dot{\Omega}_C = \sum_{i=1}^{N_{species\ selected}} \dot{\Omega}_i \quad (7)$$

Hence, the definition of Eq. (7) has to be consistent with the definition of Eq. (2). Then, all thermochemical and transport properties such as density (ρ), molecular weight (MW), temperature (T), specific heat capacity (c_p), dynamic viscosity (μ), thermal conductivity (k), species mass fractions (Y_i) and species reaction rates (ω_i) are a function of the transported lower-dimensional manifold variables. The progress parameter can be obtained via Eq. (3).

F. Lower Dimensional Manifold Transported Variables For Turbulent Flows

The transport equations for the lower-dimensional manifold variables (i.e., mixture fraction (\tilde{Z}), mixture fraction variance ($\tilde{Z}^{\prime 2}$), and progress variable (\tilde{C}) are illustrated by equations (8)-(10) in tensor notation (and in conservative form) in the context of either the unsteady Reynolds-Averaged Navier Stokes (URANS) or Large-eddy simulation (LES) turbulence model formulations. For the former formulation the dependent variable represents the Favre-weighted time-averaged variable whereas for the latter the dependent variable represents the Favre-weighted filtered variable. Equations (8) through (10), respectively, correspond to the mixture fraction (\tilde{Z}), mixture fraction variance ($\tilde{Z}^{\prime 2}$), and progress variable (\tilde{C}).





1. Transport Equations

The transported equations of the lower-dimensional manifold variables contain at least three terms, transient, convection and diffusion. The mixture fraction variance in addition contains a destruction and production of \widetilde{Z}^2 represented by the last two terms of Eq. (9), respectively. The progress variable transport equation also contains a source term represented by the last term of Eq. (10).

$$\frac{\partial(\bar{\rho}\bar{z})}{\partial t} + \frac{\partial(\bar{\rho}\bar{z}\bar{u}_j)}{\partial x_j} = \frac{\partial}{\partial x_j} \left(\left(\frac{\lambda}{c_p} + D_t \right) \frac{\partial \bar{z}}{\partial x_j} \right) \quad (8)$$

$$\frac{\partial(\bar{\rho}\widetilde{Z}^2)}{\partial t} + \frac{\partial(\bar{\rho}\widetilde{Z}^2\bar{u}_j)}{\partial x_j} = \frac{\partial}{\partial x_j} \left(\left(\frac{\lambda}{c_p} + D_t \right) \frac{\partial \widetilde{Z}^2}{\partial x_j} \right) - \bar{\rho}\widetilde{\chi}_Z \quad (9)$$

$$+ 2\bar{\rho}D_t \left(\frac{\partial \bar{z}}{\partial x_j} \right)^2 \\ \frac{\partial(\bar{\rho}\mathcal{C})}{\partial t} + \frac{\partial(\bar{\rho}\mathcal{C}\bar{u}_j)}{\partial x_j} = \frac{\partial}{\partial x_j} \left(\left(\frac{\lambda}{c_p} + D_t \right) \frac{\partial \mathcal{C}}{\partial x_j} \right) + \bar{\rho}\bar{\omega}_C \quad (10)$$

2. Closure Models

For RANS, SAS, DES and LES models the scalar dissipation rate associated with the progress variable (C) is as computed as follows [5].

$$\widetilde{\chi}_C = \gamma_C \frac{\widetilde{Z}^2}{\widetilde{C}^2} \widetilde{\chi}_Z \quad (11)$$

The closure models for the RANS-based lower-dimensional manifold transported variable equations are given by the following equations [5].

$$D_t = \frac{\mu_t}{Sc_t} \quad (12)$$

$$\widetilde{\chi}_Z = 2.0 \frac{\varepsilon}{k} \widetilde{Z}^2 \quad (13)$$

The turbulent Schmidt number (Sc_t) is a constant that is typically chosen to be equal to 0.9. The closure models for the LES-based lower-dimensional manifold transported variable equations are given by the following equations [5].

$$D_t = C_\phi \Delta^2 |S| \quad (14)$$

$$\widetilde{\chi}_Z = 2.0 \frac{\mu_t}{Sc_t} \frac{1}{\Delta^2} \widetilde{Z}^2 \quad (15)$$

The constant C_ϕ is typically chosen to be equal to 0.4.

G. Low-Dimensional Manifold Combustion Models

The flamelet prolongation of ILDM (FPI) and the flamelet/progress variable (FPV) model utilize the one-dimensional stagnation flow equations for computing freely-propagating premixed flames and counterflow diffusion flames, respectively. The freely-propagating premixed flamelets of the FPI model are computed in the physical space and each flamelet is converted to the progress variable space (C) using Eq. (2). In turn, each premixed flamelet correspond to a mixture fraction (Z), which is directly related to an equivalence ratio. On the other hand, FPV model invokes the calculation of multiple diffusion flames. Each flame is computed in the physical space as well. The physical space can be converted to a mixture fraction state relationship (Z) following Eq. (1). Each flamelet correspond to a progress parameter (Λ). Therefore, calculations of multiple premixed and diffusion flamelets lead to a tabulation of thermochemical and transport properties as a function of mixture fraction (Z) and progress variable (C).





1. Transport Equations

The one-dimensional stagnation flow equations are presented above from Eqs. (16)-(21). In ascending order these equations represent the continuity, radial momentum, pressure curvature or strain rate eigenvalue, energy, species and a one-point or two-point dummy differential equation. The equations on the left of the table represent the original equations in Cantera 2.3 [3] for which the pressure curvature is the eigenvalue. The equations on the right represent the optional equations in a modified Cantera 2.3 in which strain rate (a) replaces the pressure curvature as the eigenvalue. The species

Table 1. Original and modified Cantera governing equations.

Equation	Cantera	Modified Cantera	
Continuity	$\frac{\partial \rho u}{\partial z} + 2\rho V = 0, V = \frac{v}{r}$	$\frac{\partial \rho u}{\partial z} + a\rho V = 0, V = \frac{v}{v_e}$	(16)
Radial Momentum	$\rho u \frac{\partial v}{\partial z} + \rho V^2 = -\Xi + \frac{\partial}{\partial z} \left(\mu \frac{\partial V}{\partial z} \right)$	$\rho u \frac{\partial v}{\partial z} = \frac{\partial}{\partial z} \left(\mu \frac{\partial V}{\partial z} \right) + \Xi (\rho_F - \rho V^2)$	(17)
Pressure Curvature/Strain Rate	$\frac{d\Xi}{dz} = 0, \Xi = \frac{1}{r} \frac{dp}{dr}$	$\frac{d\Xi}{dz} = 0, \Xi = a$	(18)
Energy	$\rho u c_p \frac{\partial T}{\partial z} = \frac{\partial}{\partial z} \left(\lambda \frac{\partial T}{\partial z} \right) - \sum_k j_k c_{p,k} \frac{\partial T}{\partial z} - \sum_k h_k W_k \dot{\omega}_k$		(19)
Species	$\rho u \frac{\partial Y_k}{\partial z} = -\frac{\partial j_k}{\partial z} + W_k \dot{\omega}_k$		(20)
One- or Two-point Control	$\frac{du_o}{dz} = 0$		(21)

and temperature equations are not modified. However, an additional dummy Eq. () was added to the governing equations for when the flame control methods are activated.

2. Flamelet Prolongation of ILDM (FPI)

The FPI model computes premixed flamelets for each mixture fraction (Z). When the calculations do not converge because either the flamelets have exceeded the flammability limits or because the maximum temperature of the flamelet is higher than that of equilibrium, equilibrium calculations replace the freely-propagating premixed flamelets. The transport equations for the freely-propagating flamelets are given by Eqs. (22) – (26). The boundary conditions associated with the freely-propagating flamelets are shown in Table 2.

Table 2. Premixed flame boundary conditions.

Equation	Fuel Inlet	Oxidizer Inlet	
Continuity	-----	$\rho u = (\rho u)_o$	(22)
Radial Momentum	$V = V_F$	$V = V_O$	(23)
Pressure Curvature/Strain Rate	$\rho u = (\rho u)_F$	-----	(24)
Energy	$T = T_F$	$T = T_O$	(25)
Species	$\rho u Y_k + \rho Y_k V_k = (\rho u Y_k)_F$	$\rho u Y_k + \rho Y_k V_k = (\rho u Y_k)_O$	(26)

Table 3. Nonpremixed flamelet boundary conditions.

Equation	Inlet B.C.	Internal B.C.	Outflow B.C.	
Continuity	-----	$T_{j=specified} = T_{fixed,specified}$	-----	(27)
Radial Momentum	$V = V_0$	-----	$\frac{dV}{dz} = 0$	(28)
Pressure Curvature/Strain Rate	$\Xi = 0$	-----	-----	(29)
Energy	$T = T_0$	-----	$\frac{dT}{dz} = 0$	(30)
Species	$\rho u Y_k + \rho Y_k V_k = (\rho u Y_k)_0$	-----	$\frac{dY_k}{dz} = 0$	(31)

3. Flamelet Progress/Variable

The FPV model computes diffusion flamelets for each progress parameter (Λ) along the S-curve. Multiple diffusion flamelets are necessary to build a table of thermochemical and transport properties. The first flamelet is computed at $\Lambda_{max}|Z$ and



then the strain rate is increased by either increasing the inlet velocities, reducing the distance between the opposing jets, or by either the one-point or two point continuation. The computation of diffusion flamelets as a function of strain rates leads to the calculation of the S-curve containing two stable branches (strong and weak) and one unstable (middle) branch. Special continuations techniques are needed to compute the S-curve associated with the diffusion flamelets. This will be discussed in subsequent chapters. The boundary conditions associated with the counterflow flamelets are shown in Table 3.

H. Continuation Methods

Continuation techniques are now presented, zero-order, scaling rules, arc-length, and one- and two-point continuation techniques are presented. The zero-order continuation technique is used for FPI, whereas hybrid continuation techniques of zero-order, scaling rules, some features of arc-length continuation, and one- and two-point continuation techniques are used for the FPV model. The arc-length continuation technique was, however, fully utilized for perfectly-stirred reactors (PSRs) in order to progressively attain the now-used continuation technique for the FPV model. The arc-length continuation for PSR is only available in Python scripts and not through the GUI.

1. Zero Order Continuation

Zero-order continuation techniques can be applied to any flamelets. This technique only supposes that the previous solution is the initial solution to the current solution. This can be represented as $x^* = x_0$, where x refer to a vector solution with M grids points times N equations. This continuation methods can be applied to both FPI and FPV methods. For the former this is the only method available for continuation. For the latter the number of zero-order continuation can be selected from the Flame Control tab as illustrated in the Task 5 Appendix, Figure 4.

2. Scaling Rules

The scaling rules are ideal for computing the upper branch of S-curve. The scale factor proposed by Fiala and Sattelmayer [2] are suitable for the FPV model. These scaling factors are $u \sim a^{-1/2}$, $V \sim a$, $\dot{m} \sim a^{1/2}$, and $\Lambda \sim a^2$. The strain factor, which is the ratio of two sequential flame strain rates, can be entered by the user as illustrated in Appendix Figure 4.

3. Arc-Length Continuation

The system of nonlinear ODEs is represented by $F(x) = 0$. The solution is given by the vector x . The results of these equations depend on the parameter λ . The extended solution is represented by $F(x(\lambda), \lambda) = 0$. The arc-length continuation [3] is a predictor-corrector continuation technique.

1. Predictor:

One such predictor is the forward Euler predictor given by:

$$x^* = x_0 + \frac{dx}{ds} ds \quad (32)$$

The gradient dx/dF can be either a tangent or a secant gradient. Here the former is used. The predicted solution x^* is the initial guess for computing the new flame. The solution vector x that lies on the path depends on the parameter λ and this, in turn, depends on arclength s .

2. Corrector:

The plane equation parameterized as a function of arclength, s , needs to correct the initial guess x^* .

$$N(x(\lambda(s)), \lambda(s)) \equiv \left\| \frac{\partial x}{\partial s} \right\|_2^2 + \left(\frac{\partial \lambda}{\partial s} \right)^2 - 1 = 0 \quad (33)$$

Now the augmented systems of equations is given by:





$$\begin{vmatrix} \mathbf{F}(\mathbf{x}(\lambda(s)), \lambda(s)) \\ N(\mathbf{x}(\lambda(s)), \lambda(s)) \end{vmatrix} = \begin{vmatrix} 0 \\ 0 \end{vmatrix} \quad (34)$$

This new vector can also be written as $G(F(y), N(y)) = 0$. The augmented solution vector is given by $y = (\mathbf{x}(\lambda(s)), \lambda(s))$. The Jacobian matrix for the augmented system is represented by the following equation.

$$J = \begin{vmatrix} \frac{\partial F}{\partial x} & \frac{\partial F}{\partial \lambda} \\ \frac{\partial N}{\partial x} & \frac{\partial N}{\partial \lambda} \end{vmatrix} \quad (35)$$

The partial derivative of the plane equations needs to be determined from the plane equation:

$$N(\mathbf{x}(\lambda(s)), \lambda(s)) \equiv \left\| \frac{\partial \mathbf{x}}{\partial s} \right\| dx + \frac{\partial \lambda}{\partial s} d\lambda - ds = 0 \quad (36)$$

$$\frac{\partial N}{\partial x} = \left\| \frac{\partial \mathbf{x}}{\partial s} \right\|^T \quad (37)$$

$$\frac{\partial N}{\partial \lambda} = \frac{\partial \lambda}{\partial s} \quad (38)$$

After substituting the equations above into the Jacobian, the augmented Jacobian is now given by:

$$J = \begin{vmatrix} \frac{\partial F}{\partial x} & \frac{\partial F}{\partial \lambda} \\ \left\| \frac{\partial \mathbf{x}}{\partial s} \right\|^T & \frac{\partial \lambda}{\partial s} \end{vmatrix} \quad (39)$$

The augmented Jacobian and the residual equations are used in a Newton-Raphson type solver. The previous k solution is used to compute the new solution k+1.

$$\mathbf{y}_{k+1} = \mathbf{y}_k - J^{-1} \mathbf{G} \quad (40)$$

The Newton-Raphson solver proceeds in this way. It computes the new change in the solution vector, $\Delta \mathbf{y}_k$. This change is added to the solution vector of the previous iteration. Note that k=0 the values of $\mathbf{y}_0[0:N_{eqs}-2]$ are equal to the values of \mathbf{x}^* .

$$J \Delta \mathbf{y}_k = -\mathbf{G} \quad (41)$$

$$\mathbf{y}_{k+1} = \mathbf{y}_k + \Delta \mathbf{y}_k \quad (42)$$

$$if \Delta \mathbf{y}_k < \varepsilon \rightarrow \mathbf{y}_n = \mathbf{y}_{k+1} \quad (43)$$

3. Step-size Control:

The user specifies an initial step size ds that is very large at first and the simulation proceeds. Near the turning points (bifurcations) the step size needs to become smaller in order to resolve the curve and avoid divergence of the Newton solver. Once the solution has passed the turning point the step size ds needs to increase again towards the other turning point. This is accomplished using the following step size control method.

$$\delta = N_{opt}/i_{Newton} \quad (44)$$

$$if \delta < 0.5 \rightarrow \delta = 0.5 \quad (45)$$

$$if \delta > 2.0 \rightarrow \delta = 2.0 \quad (46)$$

$$ds = \delta \cdot ds \quad (47)$$



This step size control technique works by allowing the user to specify the optimum number of Newton iterations, N_{opt} . If the number of Newton iterations i_{Newton} is below or above the N_{opt} the step size will increase or decrease, respectively. The multiplication factor δ is bounded between 0.5 and 2.0 in order to avoid very small step size or very large step sizes that would either get the simulation stagnant or diverging. The step size control can be accessed through the Flame Control tab.

Some verification calculations are shown in Figure 1 through Figure 3 with numerical results available in the literature. There is nearly perfect match between previously computed S-curve for perfectly-stirred reactors (PSRs) and those computed here. This demonstrates that homotopic calculations and step size control are appropriately programmed for later used in the FPV tabulation procedure.

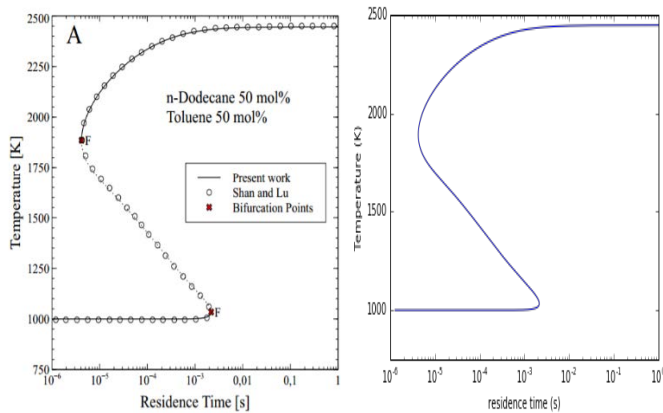


Figure 1. Comparison between Acampora and Marra [7] and in-house arc-length continuation for perfectly-stirred reactor (PSR). The inlet mass flow rate is the independent variable. Both temperature and residence time are output of the PSR. Reprinted from Computers and Chemical Engineering, 85, Acampora, L., Marra, F.S., A general study of counterflow diffusion flames at subcritical and supercritical conditions: Oxygen/hydrogen mixtures, with Permission from Elsevier



4. Flame Control Methods: One- and Two-Point

When the zero-order continuation and the scaling rules fail a flame control can be used to continue the bifurcation path of the S-curve. In the CFR this is automatically activated. The one- and two-point boundary conditions are based on the work of Nishioka et al. [8]. The boundary conditions for the pressure curvature or strain rate eigenvalue (Eq. (24)) is removed and replaced with an internal boundary condition (Eq. (48)) for the one-point continuation method. For the two-point continuation method the continuity equation boundary condition (Eq. (22)) is removed and a new internal boundary condition is added (Eq. (49)). For the one-point control method the oxidizer flux is specified as well as a fixed temperature on the fuel side. For the two-point control method neither the fuel nor the oxidizer flux are specified, but instead two fixed temperature location for the consecutive flamelet calculation at each side of the stagnation plane are prescribed.

Figure 4 shows the calculation of the S-curve for a more practical fuel used in gas turbine combustors.

Table 4. One- and two-point control boundary conditions.

Equation	Fuel Inlet	Internal B.C.	Internal B.C.	Oxid Inlet	
Pressure Curvature/Strain Rate	-----	$T(j_{F,specified}) = T_{F,specified}$	-----	-----	(48)
Two-Point Control	-----	-----	$T(j_{O,specified}) = T_{O,specified}$	-----	(49)

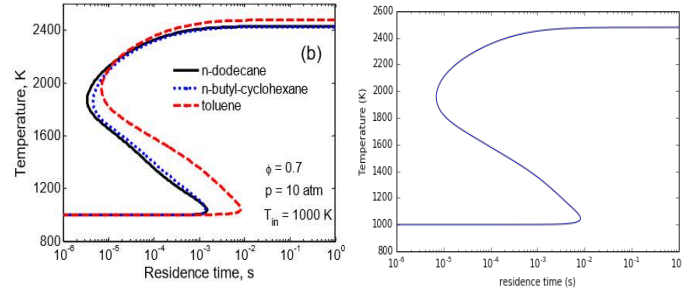


Figure 2. Comparison between Shan and Lu [1] and in-house arc-length continuation for perfectly-stirred reactor (PSR) burning Toluene. The inlet mixture temperature is the independent variable.

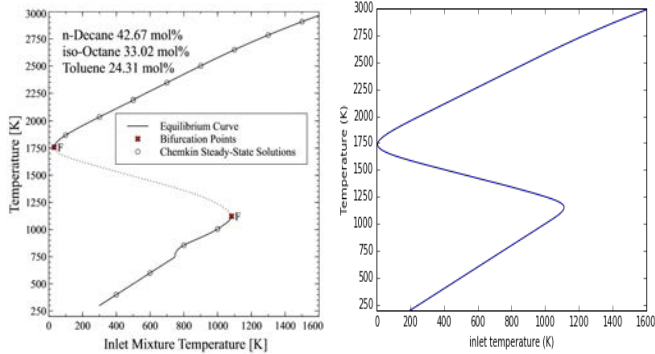


Figure 3. Comparison between Acampora and Marra [8] and in-house arc-length continuation for perfectly-stirred reactor (PSR). The inlet mixture temperature is the independent variable. Reprinted from Computers and Chemical Engineering, 85, Acampora, L., Marra, F.S., A general study of counterflow diffusion flames at subcritical and supercritical conditions: Oxygen/hydrogen mixtures, with Permission from Elsevier.



Figure 5 clearly shows that upper and middle branches can be successfully calculated with the CFR at low and high pressure conditions. Figure 5 illustrates the effect of transport model on the S-curve. There is a slight change on the S-curve for hydrogen-oxygen combustion. This is important because it suggests that the inexpensive unity Lewis number computation is sufficient for PSR without having to invoke more computationally-expensive calculations such as mixture-averaged diffusivity. Figure 7 demonstrates that effect of varying the detailed chemistry. The same fuel-air composition is used with two different chemistry sets, but there is substantial change in the extinction strain rate.

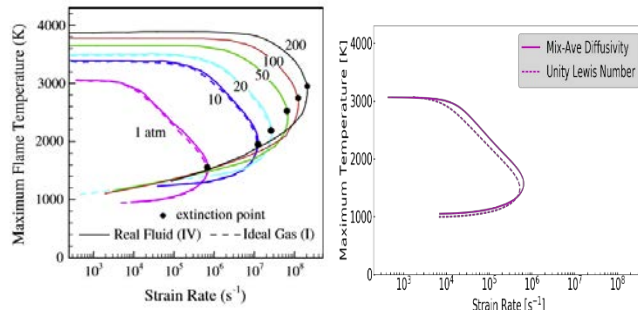


Figure 4. Comparison between mixture-averaged diffusivity and unity Lewis number. The mechanism used here is that of Burke et al. [13] Reprinted from Combustion and Flame, 161, Huo, H., Wang, X., Yang, V., A general study of counterflow diffusion flames at subcritical and supercritical conditions: Oxygen/hydrogen mixtures, with Permission from Elsevier.

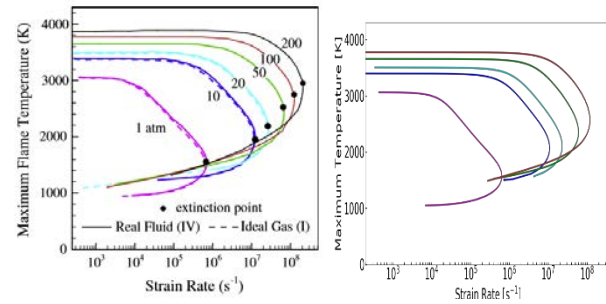


Figure 5. Comparison of strain rate vs. maximum flame temperature between Wang et al. [11] (left) and the in-house model (right). Wang et al. uses Li et al. [12] mechanism, whereas the in-house model uses Burke et al. [13] Reprinted from Combustion and Flame, 161, Huo, H., Wang, X., Yang, V., A general study of counterflow diffusion flames at subcritical and supercritical conditions: Oxygen/hydrogen mixtures, with Permission from Elsevier.

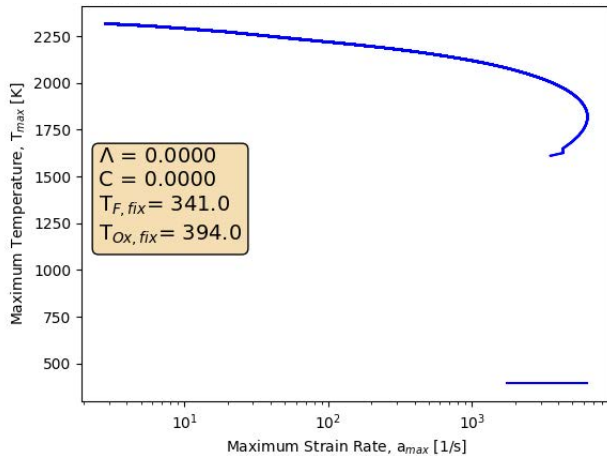


Figure 6. POSF10325-air diffusion flame s-curve.

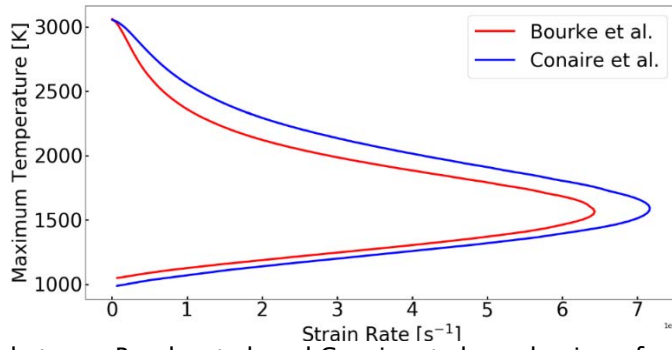


Figure 7. Comparison between Bourke et al. and Conaire et al. mechanisms for the H₂-O₂ flame at 1 atm and inlet temperatures of 300K.

I. Probability Density Functions

Here the Dirac-delta and Beta probability density functions (PDFs) are discussed here. These PDFs could be applied to either the lower-dimensional manifold variables. However, it has been proven that the Beta PDF is more suitable for mixture fraction (Z), whereas Dirac-delta or Beta PDF can be used for progress parameter (Λ).

1. Dirac Delta

The Dirac-delta probability density function is given by the equation below. Dirac-delta could be used for the progress parameter. Hence the x in the equation can be substituted by Λ .

$$\delta(x - x_0) = \begin{cases} 0, & x \neq x_0 \\ 1, & x = x_0 \end{cases} \quad (50)$$



2. Beta

The Beta probability density function is given by the equations below. The probability density function is appropriate for the mixture fraction (Z). Hence, the x in the equation can be substituted for the Z. This PDF could also be utilized to model the progress parameter and the x below would be substituted by Λ .

$$\beta(x; \tilde{x}, \tilde{x}^2) = \frac{\Gamma(a+b)}{\Gamma(a)\Gamma(b)} x^{a-1} (1-x)^{b-1} \quad (51)$$

$$a = \frac{\tilde{x}(\tilde{x}-\tilde{x}^2-\tilde{x}^2)}{\tilde{x}^2} \quad (52)$$

$$b = \frac{(1-\tilde{x})(\tilde{x}-\tilde{x}^2-\tilde{x}^2)}{\tilde{x}^2} \quad (53)$$

The demonstration of these convolutions are shown in Figure 8. The images correspond to a convoluted methane-air diffusion flame. Dirac-delta PDF was used for the progress variable. Note that the effect of turbulence-chemistry interaction represented by the variance of the mixture fraction (in this case) is to weaken the flame by lowering the peak temperature from ~ 2050 K to ~ 1750 K. Similar the peak progress variable source term drops from ~ 500 to ~ 100 $\text{ks/m}^3\text{s}^{-1}$.

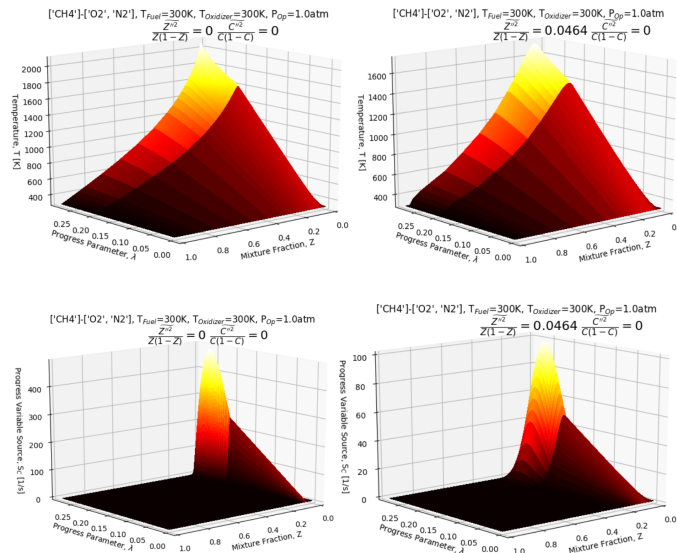


Figure 8. Sample images of a tabulated thermochemical transport tables for a CH_4 -air diffusion flame. The top and bottom images illustrate temperature and progress variable source, respectively. The left images show the tabulated variables when both mixture fraction and progress variables are zero. The right images show the tabulated variables when the mixture fraction variance is non-zero.

J. Verification Tests

There are several verification and validation tests. A canonical laminar triple flame was computed using FPI or FPV models. The Sandia D piloted flame was also simulated using RANS/FPV and LES/FPV model. Finally, a single cup combustor rig was simulated using the LES/FPV model.

A. Simulations of a Canonical Triple Flame

Here is the verification test for the laminar formulation for the FPI model. Figure 9 indicates that both calculations are very similar in terms of temperature and CO mass fraction contours. Subtle difference can be attributed to the fact that Wu et al. [9] used FlameMaster solver [10], which computes the flamelets in mixture fraction space directly.

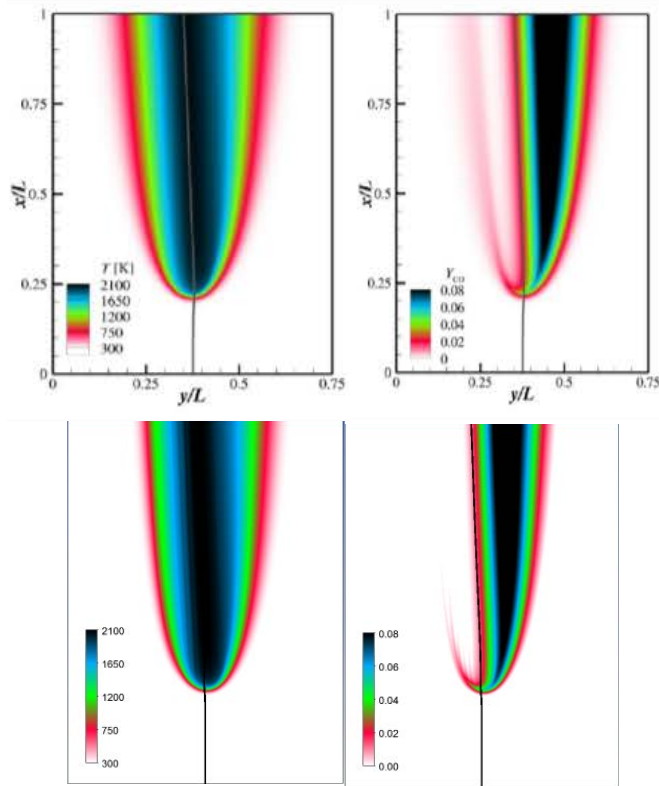


Figure 9. Comparison between (top) Wu et al. [15] and (bottom) CFR results of a laminar triple flame using FPI in terms of (left) temperature and (right) CO mass fractions.



B. Laminar Fpv Simulations For A Canonical Triple Flame

Here is the verification test for the laminar formulation for the FPV model. Figure 10 illustrates the verification step for computing the laminar version of the FPV combustion model of the CFR software.

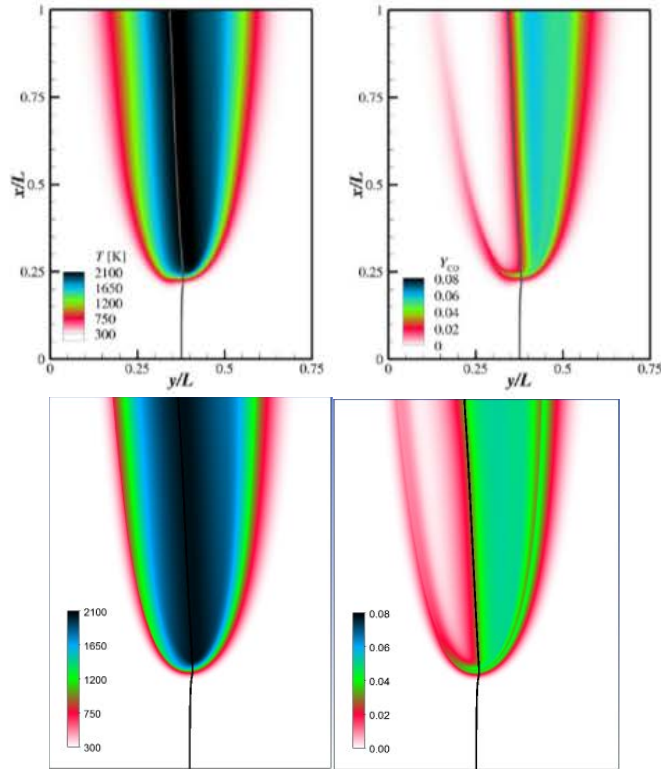


Figure 10. Comparison between (top) Wu et al. [15] and (bottom) CFR results of a laminar triple flame using FPV in terms of (left) temperature and (right) CO mass fractions.

C. Turbulent Simulations of Sandia D Flame

Here are the verification and validation tests for turbulent formulation of the FPV model. Figure 11 presents the experimental measurements against numerical predictions. Numerical simulations were performed only with Fluent [1,2] and with Fluent+CFR software. The k- ϵ and k- ω RANS version of FPV model were utilized. The Beta PDF is used for mixture fraction and Dirac-delta is used for progress variable. Generally, both the Fluent and Fluent+CFR results compared well with the experimental measurements in terms of temperature and species mass fractions. However, the Fluent+CFR outperforms the Fluent results, specifically, in terms of CO mass fraction. Both Fluent and Fluent+CFR results, nonetheless, underpredict the mixture fraction variance. In terms of RANS model, the k- ω better approximates the measurements.

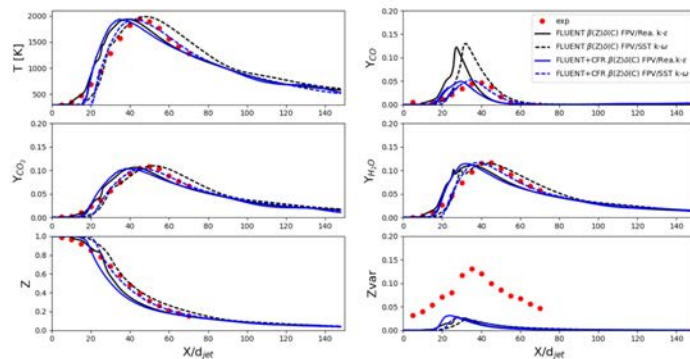


Figure 11. Centerline comparison between experiments and RANS simulations of the Sandia D turbulent flame.

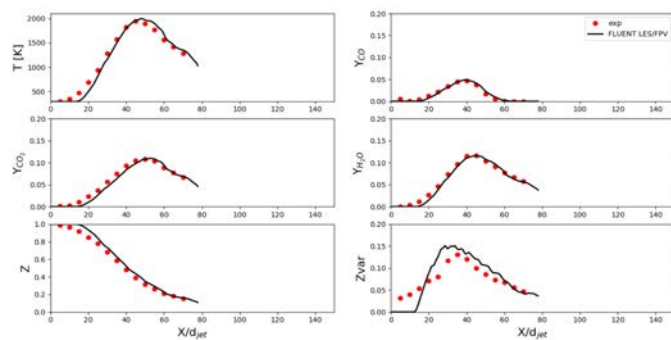


Figure 12. Centerline comparison between experiments and LES simulations of the Sandia D turbulent flame.

Conclusions

A common format routine (CFR) software for modeling combustion problems have been developed. This software is subdivided into a thermochemical transport property pretabulator software and a flamelet-based software. The former can be used to create flamelet prolongation of the ILDM (FPI) or flamelet/progress variable (FPV) tables for either laminar or turbulent flames. The pretabulator allows for turbulence-chemistry interaction through either Beta or Dirac-delta probability density function (PDF) of the independent variables. The flamelet-based software can read, search and interpolate the table to extract thermochemical and transport composition based on lower-dimensional manifold transport variables (i.e., mixture fraction, mixture fraction variance and progress parameter). The $k-\epsilon$ and $k-\omega$ RANS, SAS, DES and LES turbulence model were coupled with the flamelet-based combustion models. A multiphase spray model successfully couples with the gas phase by exchanging mass. The CFR software was positively compared against laminar and turbulent flames in canonical configurations as well as in more practical single-swirler combustor rig. The developed software is reliable for modeling and simulation of complex combustion phenomena.

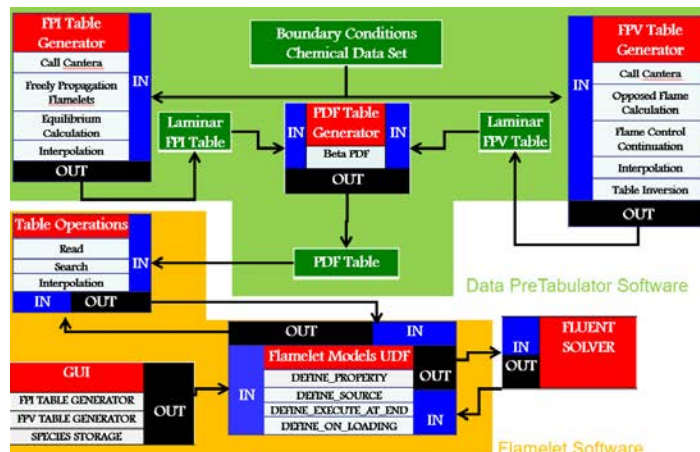
References

1. Ansys Inc., Fluent User's Guide, v18.0.
2. Ansys Inc., Fluent Theory Guide, v18.0.
3. Goodwin, D.G., Moffat, H.K., Speth, R.L., Cantera: An object - oriented software toolkit for chemical kinetics, thermodynamics, and transport properties," <http://www.cantera.org>, 2017, Version 2.3.0. doi:10.5281/zenodo.170284
4. ANSYS 18.0, Chemkin-Pro Theory Manual, ANSYS, Inc.: San Diego, 2017.
5. Ihme, M., Pitsch, H., "Prediction of extinction and reignition in nonpremixed turbulent flames using flamelet/progress variable model: 2. Application in LES of Sandia flames D and E," Combustion and Flame, 155, (1-2), pp. 90-107, 2008.
6. Fiala, T., Sattelmayer, T., "Nonpremixed Counterflow Flames: Scaling Rules for Batch Simulations," Journal of Combustion, 2014, 484372.
7. H. B. Keller, in Applications of bifurcation Theory, P. Rabinowitz, Ed. (Academic Press, New York, 1977).



8. Luigi Acampora and Francesco S. Marra, "Numerical Strategies for the Bifurcation Analysis of Perfectly Stirred Reactors with Detailed Combustion Mechanisms," *Computers and Chemical Engineering* 82 (2015) 273-282.
9. Ruiqin Shan, Tianfeng Lu, Effects of Surrogate Jet-Fuel Composition on Ignition and Extinction in High Temperature Applications, 8th U. S. National Combustion Meeting Organized by the Western States Section of the Combustion Institute and hosted by the University of Utah May 19-22, 2013.
10. Nishioka, M., Law, C., Takeno, T., "A flame controlling continuation method for generating S-curve responses with detailed chemistry," *Combust. Flame* 104 (3):328-342
11. Huo, H., Wang, X., Yang, V., "A general study of counterflow diffusion flames at subcritical and supercritical conditions: Oxygen/hydrogen mixtures," *Combustion and Flames*, 161, 2014.
12. J. Li, Z. Zhao, A. Kazakov, F.L. Dryer, "An updated comprehensive kinetic model of hydrogen combustion," *Int. J. Chem. Kinetics*, 36, 2004, 566-575.
13. Burke, M.P., Chaos, M., Ju, Y., Dryer, F.L., Klippenstein, S.J., "Comprehensive H₂/O₂ Kinetic Model for High-Pressure Combustion," *Int. J. Chem. Kinet.* (2011).
14. Connaire, M. O., Curran, H J., Simmie, J. M., Pitz, W. J. and Westbrook, C.K., "A Comprehensive Modeling Study of Hydrogen Oxidation", *International Journal of Chemical Kinetics*, 36:603-622, 2004.
15. Wu, H., See, Y.C., Wang, Q., and Ihme, M., "A Pareto-efficient combustion framework with submodel assignment for predicting complex flame configurations," 162(1), 2015, 4208-4230
16. Pitsch, H., FlameMaster v3.1, "A C++ computer program for 0D combustion and 1D laminar flame calculations," 1998.

TASK 5- APPENDIX



Appendix Figure 1. Schematic of the Common Format Routine (CFR) software. All the components with the green background correspond to the thermochemical and transport data pretabulator. All the components with the amber background corresponds to the flamelet-based software.



Mixture Fraction

Element	Composition
O	<input type="checkbox"/>
H	<input checked="" type="checkbox"/>
C	<input checked="" type="checkbox"/>
N	<input type="checkbox"/>
Ar	<input type="checkbox"/>

Num variance

Appendix Figure 2. PreTabulator software selection of user's mixture fraction definition is indicated within the magenta-line box.

Progress Variable

Species Name	Composition
H ₂	<input checked="" type="checkbox"/>
H	<input type="checkbox"/>
O	<input type="checkbox"/>
O ₂	<input type="checkbox"/>
OH	<input type="checkbox"/>

Skip number Delta Beta SMLD
 Num variance

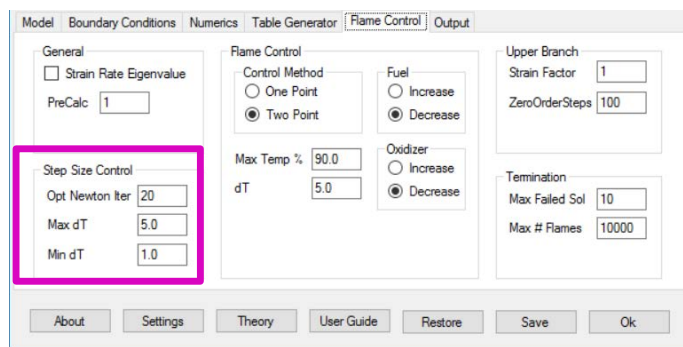
Appendix Figure 3. PreTabulator software selection of user's progress variable definition is indicated within the magenta-line box.

Model Boundary Conditions Numerics Table Generator Flame Control Output

General	Flame Control	User Define
<input type="checkbox"/> Strain Rate Eigenvalue	Control Method	Strain Factor <input type="text" value="1"/>
PreCalc <input type="text" value="1"/>	<input type="radio"/> One Point	ZeroOrderSteps <input type="text" value="100"/>
	<input checked="" type="radio"/> Two Point	
Step Size Control	Fuel	
Opt Newton Iter <input type="text" value="20"/>	<input type="radio"/> Increase	
Max dT <input type="text" value="5.0"/>	<input checked="" type="radio"/> Decrease	
Min dT <input type="text" value="1.0"/>	Oxidizer	
	<input type="radio"/> Increase	
	<input checked="" type="radio"/> Decrease	
	Max Temp % <input type="text" value="90.0"/>	Termination
	dT <input type="text" value="5.0"/>	Max Failed Sol <input type="text" value="10"/>
		Max # Flames <input type="text" value="10000"/>

About Settings Theory User Guide Restore Save Ok

Appendix Figure 4. PreTabulator software selection of zero order continuation steps and strain factor are indicated in the magenta boxes.



Appendix Figure 5. PreTabulator software selection of step size control is indicated in the magenta box.

Task 6- Spray Modeling of Area 3 Pressure Atomized Spray Injector

UTRC (Sub-contract)

Objective(s)

The objective of this task is to simulate the Area 3 High Sheer Rig pressure blast spray atomizer. Simulations of NJFCP experiments in the Area 3 High Sheer Rig will be done to explore the relative performance of simulations versus experiments and the relative spray and combustor character between the A-2, C-1, and C-5 fuels. These computational results will also illuminate the relative impact of a Pratt & Whitney swirl-injector geometry as compared to the other geometries in the program.

Research Approach

Research & Development Final Report 2018 Executive Summary

The objective of this effort is to develop, enhance and apply computational fluid dynamics-based models to simulate stable combustion and lean blowout behavior in a high shear rig combustor that was also experimentally studied at Georgia Institute of Technology. The goal is to understand if the models can predict the dependence of lean blowout (LBO) phenomena on fuel physical and chemical properties of the alternative jet fuels. A Large Eddy Simulation (LES) based modeling is employed to simulate the unsteady combustion phenomena for the stable and LBO conditions. Several sub-models for unsteady flow simulation, spray injection boundary conditions, spray evaporation models, wall heat flux boundary conditions and turbulent combustion models are required to correctly simulate the physical processes. Detailed description of the different submodels, along with validation or verification where possible, is presented as a part of this work. Simulation of lean blowout were performed upon completing the reacting LES for the two fuels at near blowout but stable conditions. To simulate lean blowout, fuel flow rate is reduced in discrete steps 6% (instantaneously instead of gradually) for three different values of fuel-flow rates. Each flow rate was held constant for 100 mill-seconds for the combustor to respond to the flow rate change and stabilize at the new condition. Overall, the two fuels show differences in evaporation rate and also commensurate differences in heat release rates. Both the simulation show reduction in heat release rate as the flow rate is reduced but C1 seems to be dropping faster relatively compared to A2. C1 fuels also shows increased evaporation rates compared to A2, however this leads to quick build of fuel vapor in a concentrated region and if the flow conditions in that region is not conducive in terms of residence time to complete the reaction, it contributes to even more accumulation of fuel vapor from the incomplete combustion. In the case of C1 fuel, this is hypothesized to be the mechanism for earlier flame blow out compared to the A2 fuel. Long combustor dimension coupled with very small time steps to resolve the flame structure, leads to excessive computational time at each flow rate for the combustion to reach a quasi-steady state. As a result, it was not possible to reduce the flow-rate all the way to the lean blowout value to demonstrate the lean blowout behavior. However the qualitative trend observed from the three simulate fuel flow rate conditions seems to indicate that the models employed in this study have the ability to discriminate between the different fuel physical properties and its impact on the lean blow out behavior.



Research in Support of FAA-ASCENT Program & National Jet Fuels Combustion Program LES of High Shear Rig Combustor – Area 3 support

Introduction

Fuel cost, availability and environmental impact are main concerns that drive the search and use of alternative fuels (petroleum and non-petroleum derived) in commercial and military aviation. By understanding and establishing the properties of fuel and their impact on engine (combustor) performance, it may be possible to broaden the fuel specification and, in turn, broaden the available choice of economical and eco-friendly fuels for aviation engines. However, the introduction of fuels from alternative sources presents potential risks to aircraft engine operability, emissions and durability and hence requires a comprehensive understanding of the fuel properties and their potential impact on the systems and their performance. For instance, flame blowouts can occur during transient events in the flight envelope during rapid throttle movements. For example, during flight decent when the fuel flow-rates are typically low, the combustor fuel-air ratio may approach lean flammability limits that may result in a flame-out. This is typically known as the Lean Blow Out (LBO) and has obvious safety implications. During such highly transient events, fuel property variations have a large effect on the combustion processes. Since the fuel flow rates are low, physical properties of the fuel can alter the fuel spray atomization and vaporization processes, leading to a strong effect on combustion. In addition, fuel chemistry effects are presumed to be strongest at lean conditions, where chemical reaction rates are lowest and can therefore be coupled with the combustor aerodynamic stabilization processes. For these reasons, LBO is considered one of the most important operability metrics for evaluating alternative fuel effects. Other combustor performance metrics such as ignition at ground (cold start) and altitude conditions, gaseous and particulate emissions, liner temperature, radiation and durability, pattern/profile factor and combustion efficiency are all linked intimately to different physical and chemical properties of the fuel such as viscosity, surface tension, heating values, specific heats, boiling point distribution, vapor pressure, Cetane number etc. In general, there is some understanding of the impact of physical fuel properties on selective combustion behavior. However, the collective impact due to all or multiple properties (chemical and physical) is not well understood. Because the next-generation of combustors will be operating closer to stability limits they are more likely to exhibit stronger fuel sensitivity which warrants research to better understand the potential impacts of the new fuels on engines.

One of the important objectives of this research program is to develop modeling tools for predicting the performance of gas turbine combustors when using future alternative fuels. The success would enable a significant reduction in cost and effort when qualifying new fuels for use in aircraft engines. Computational Fluid Dynamics (CFD) simulations of the High Shear Combustor are being performed to develop and assess the ability of models to capture the impact of fuel properties on Lean Blow Out phenomena.

Experimental Facility

The high shear rig combustor is a canonical representation of an aviation combustor which was experimentally characterized by the teams at Georgia Institute of Technology. This rig was designed with optical access to enable non-intrusive diagnostics and for visualization of the combustion. Data obtained include non-reacting and reacting PIV for the velocity fields at an equivalence ratio close to LBO where a stable flame configuration can be realized. PDPA measurements of the spray under non-reacting conditions close to the swirler/nozzle exit were also obtained in this configuration at UTRC. Temperature measurements at the combustor bulk-head were also obtained to characterize / quantify lean blowout phenomena.

Figure 1 shows the key components of this rig such as preconditioning air flow path, fuel supply, the optically accessible pressure vessel and liner and exhaust section. Compressed air at pressures up to 20 atm is heated to temperatures from 350 to 750 K. Following the heating process, a portion of the air is sent to the test section and the remainder is cooled to approximately 320 K in a heat exchanger. The secondary air flows around the liner and keeps the pressure vessel structure and windows cool. Hot combustion products mix with the cooling air downstream of the test section and exit through a water cooled exhaust. A choked orifice plug of variable size is installed at the exhaust exit to maintain elevated pressure in the combustion chamber. Air mass flow rates and the air temperature were measured upstream of the dump plane and its value was continuously recorded during measurements.



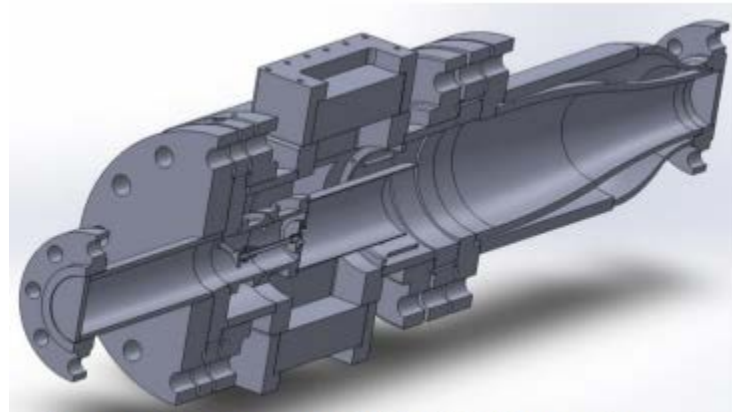


Figure 1. Geometrical model of the High Shear combustor rig

The combustor liner consists of a 30.5 cm long, 105 mm inner diameter quartz section. The front end of the combustor, called the bulkhead, is a stainless steel wall without secondary cooling passages. This bulkhead face contains four thermocouples situated flush with the surface for monitoring bulkhead temperature, a static pressure transducer, and an ignitor. The pressure vessel that houses the liner has optical access on all four sides and four quartz windows (Figure 1). The fuel nozzle uses a Pratt & Whitney proprietary swirler geometry, through which the pressurized preheated air passes through prior to entering the test section. The pressure atomizer is a commercially available McMaster-Carr misting nozzle (part number 3178K45) with a 0.51 mm orifice diameter and a flow number of 2.3.

Computational Models and Setup

The experimental setup of the high shear combustor rig was simulated using Large Eddy Simulations. Figure 2 shows a simple schematic diagram of the combustor. The simulation domain has an upstream plenum or air preconditioning flow path, from where the air enters the domain. Air mass flow rate is specified at the inflow boundary along with correct air temperature. This air passes through the swirler to enter into the combustor. A part of this air also flows on the outside of the combustor wall and enters the convergent section on the aft of the combustor to cool the hot gases that leave the cylindrical combustion chamber. Cooling air is specified at a surface near the exit of the combustion chamber using measured cooling mass flow that enters the convergent section.

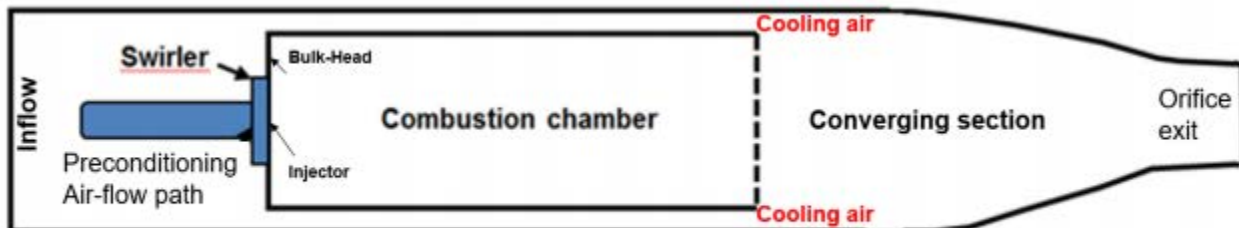


Figure 2. Schematic diagram of the High Shear combustor rig simulated using LES

The long computational domain is needed to setup the correct exit boundary conditions even though it makes the simulation run time longer to obtain statistically steady solutions. Measurements of the wall temperatures on the bulkhead and secondary flow path were used to setup isothermal boundary conditions on these boundaries to simulate the heat transfer that happens at these walls. Before we present the results from this work, a brief summary of the CFD models are being provided here. LES solver used for this work is the fully compressible finite-volume based code LESLIE. It is a block-structured solver that uses a predictor-corrector scheme which is 2nd accurate in time and employs 2nd/4th order accurate spatial integration schemes. More details of the submodels are provided in the Table 1. Computational domain was resolved with hexahedral cells with finest mesh of 0.1 mm near the swirler walls and a coarsest mesh of 3mm in some plenum locations. Fine meshes were used in the vicinity of the swirler in the front end of the combustor to resolve the



turbulent flow structures, swirling flow and the flame anchoring in this region. The combustor region is resolved with nearly uniform sized cells to avoid dissipation errors. The total mesh count is little over 6 million cells.

Table 1. A comprehensive list of all the sub-models used in the current study

	Sub-Models
Solver Name	LESLIE
Spray Flame Modeling Approach	Eulerian-Lagrangian (EL),
Governing Equations	Compressible multi-species Navier-Stokes with spray
Grid Type	Multi-block structured
Solver Type	Finite volume
Spatial Discretization	2 nd /4 th order MacCormack,
Time Integration	2 nd order explicit predictor-corrector 2 nd /4 th order explicit Runge-Kutta for spray equations
Boundary Conditions	Characteristic boundary conditions
Thermodynamics	Thermally perfect gas
Transport	Sutherland,
Chemical Kinetics	Finite-rate (reduced/skeletal/detailed)
Momentum Flux Closure	Boussinesq hypothesis, Constant coefficient k^{**} ,
Energy Flux Closure	Gradient diffusion hypothesis
Species Flux Closure	Gradient diffusion hypothesis
Reaction Rate Closure	Quasi-laminar (QL),
Dispersed Phase Physics	Polydisperse with Evaporation

Results and Discussion

Validation of non-reacting aerodynamic flow-fields

A series of step-by-step validation for the various sub-models used in this study was completed before performing the Lean Blowout simulations. As a first step, cold-flow validations were conducted to ensure the grids, boundary conditions and subgrid momentum closure models are adequate to simulate the non-reacting conditions.

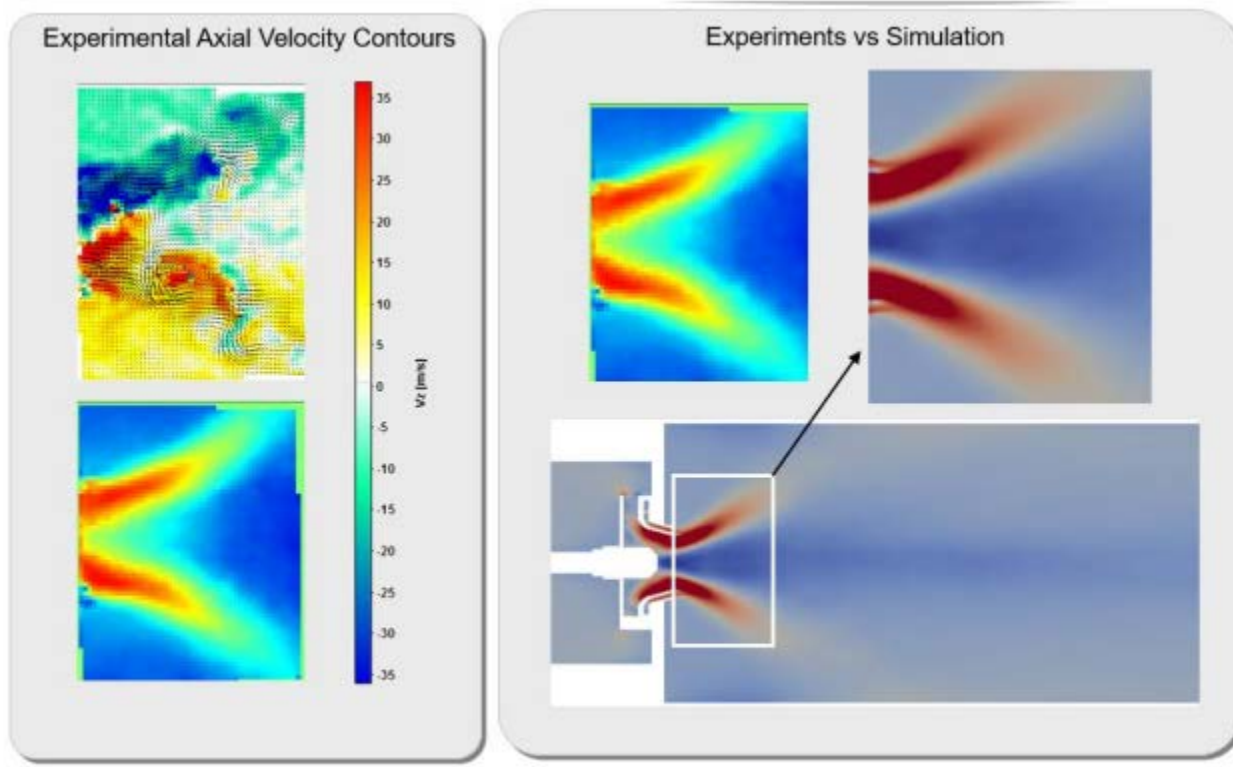


Figure 3. Time averaged contours of axial velocity from experiments (left panel) compared to simulations (right panel) from the central cross-sectional plane at non-reacting conditions in the High Shear Rig

Figure 3 shows the time-averaged contours of instantaneous and mean axial velocity obtained from PIV measurements on the left panel in the central cross-sectional plane of the combustor for non-reacting conditions. Flow through the radial and axial swirlers are clearly visible in this plot. As the flow enters the confining passages of the swirler from the preconditioning flow path, area reduction and continuity accelerates the flow significantly causing a high velocity annular jet to emanate out of the swirler. The tangential flow trajectory pushes the flow away from the center line of the swirler and hence a region of negative axial velocity or recirculation zones are created in the central sections of the combustor near the swirler exit. This recirculation region is intended for flame stabilization. Large velocity gradients near the swirler are also intended to help with better spray atomization. Overall, all the flow features are captured well in the simulation and are qualitatively in good agreement with the data. The spread angle, velocity magnitudes and the extent of the central recirculation regions were compared to be in good agreement with the measurements.

Figure 4 shows the time-averaged axial velocity field from the non-reacting experiments compared to non-reacting simulations in the high shear rig. Measurement data was obtained using stereo PIV. Overall there is a reasonable agreement even though some particular discrepancies can be noticed. Simulations are over predicting the shear layer width especially in the near-field of the swirler. This could be attributed to the subgrid momentum closure models and the grid resolution. The mesh resolution near the solid wall in the swirler passages is usually inadequate as it would be prohibitively expensive to resolve the fine scales in the turbulent boundary layer. It is typical to use some specialized wall models or hybrid RANS-LES models to account for the lack of resolution near the wall. However, in this study no such models have been used. On the other hand the measurements also report errors related to the inability of the stereo PIV technique to distinguish between the spray droplets and the PIV tracer particles. This can lead to systemic errors in the measurement data. Moreover, the measurements near the periphery of the optical windows have increased errors due to reflections and other issues related to light intensity. The swirling motion also causes flow perpendicular to the optical plane which also would introduce measurement errors. Considering all this, the overall qualitative and quantitative



agreement between the experiments and the simulation is reasonable to provide confidence in the mesh, subgrid momentum closure models and other boundary conditions used for nonreacting flow simulations.

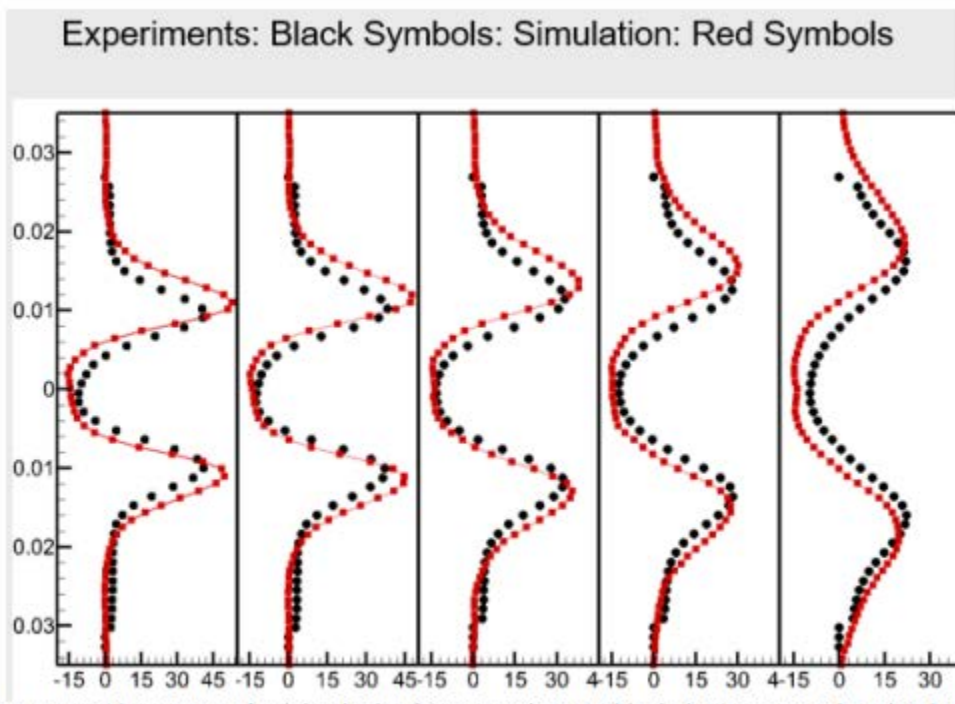


Figure 4. Time averaged contours of axial velocity from experiments (black dots) compared to simulations (red dots) at five axial stations showing the variation in radial directions for non-reacting conditions in the High Shear Rig

Validation of non-reacting spray boundary conditions and transport

Parametric study conducted for the spray initial conditions revealed that the spray evolution downstream and the flame location depends very strongly on the spray inlet boundary conditions such as the initial size distribution, position and velocity. Typically spray formation processes are not modeled in the reacting LES, due to the excessive modeling complexities and the computational cost required for simulating the atomization processes. Known empirical spray size distributions are prescribed as initial conditions (ignoring the primary break-up process). Log-normal and Rosin-Rammler are two popular spray size distributions that match experimentally measured spray size distributions for different injectors and flow conditions. But these correlations assume the same size distribution is valid across the entire fuel nozzle cross-section, which is known to be incorrect. Droplet velocity information is also not specified by these correlations and hence all droplets (regardless of their size) are assumed to be injected at the same velocity which can be another source of major error in the simulations. PDPA based measurement data can provide correlated spray size-position-velocity information, however, it is difficult to obtain such data very close to the injector and data is available only some distance downstream of the fuel injector. For this particular fuel injector and swirler configuration, UTRC conducted a testing campaign to obtain detailed PDPA data to simultaneously measure spray position, size and velocity for three different fuels at several flow conditions. Modeling team devised an approach to utilize the spray PDPA data measured downstream and specify boundary conditions close to the fuel injector. A snapshot image of the spray dispersing out of the fuel nozzle geometry is shown in Figure 5 below.

Our approach is based on geometric projection of the measured data, from the actual measurement plane to a plane close to the injector called the CFD injection plane. In the Figure 5, the dashed red line shows the location of the measurement plane. Because the measurement planes are reasonably close to the swirler exit, it was assumed here that no significant evaporation would have occurred and that the droplet size obtained in the measurement is the result of atomization only. Based on this, we defined annular concentric strips at an arbitrary injection plane close to the injector face, as shown by the image in the middle of the panel in Figure 5. The number of strips corresponds to the number of radial location at



which the PDPA data was obtained. In CFD, droplets are injected from a random location inside the strips. During the time of injection, drop size to be injected is determined by sampling the actual droplet CDF that was measured at the corresponding radial location (typical cumulative size distribution functions (CDF) are shown in the bottom right section of Figure 5. Measurements of volume flux is used to estimate the droplet number density at different location of the spray cone.

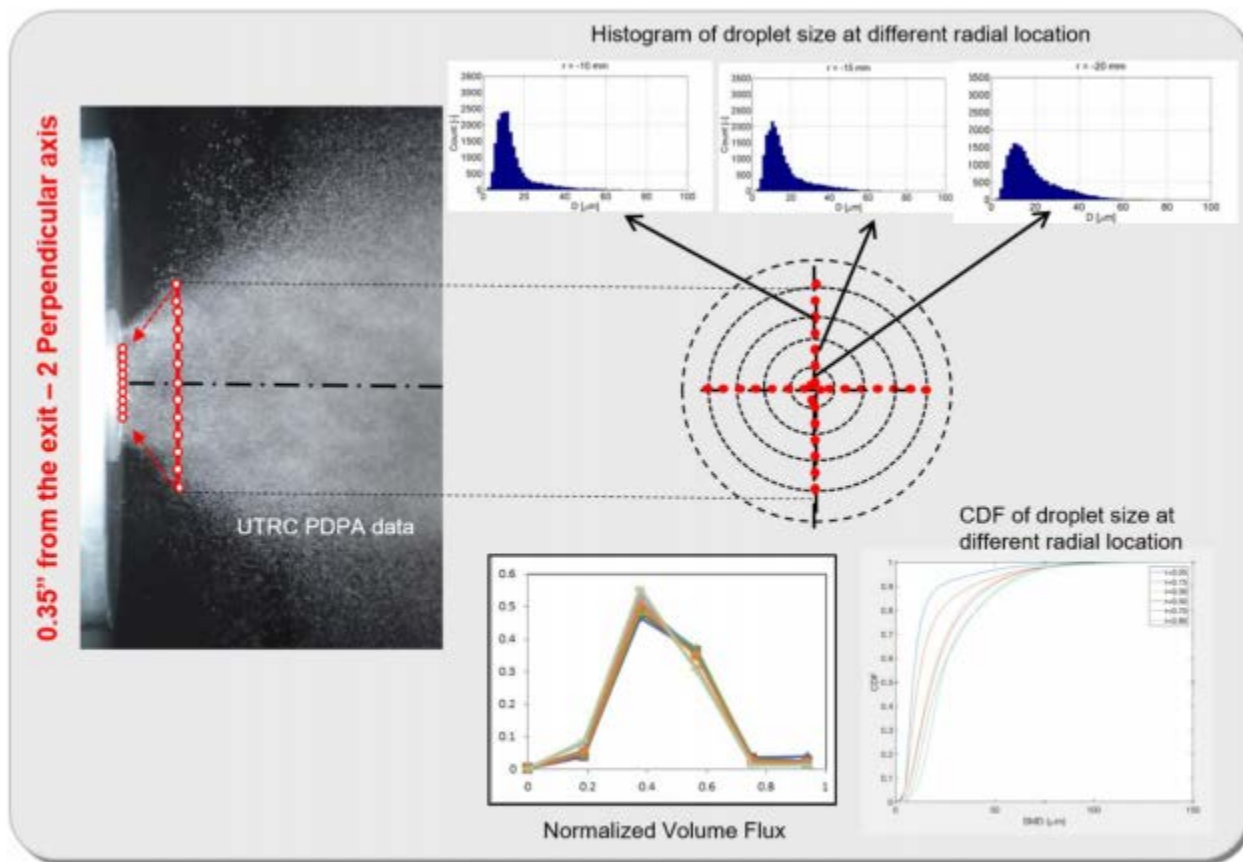


Figure 5. A snapshot of the spray injected out of the fuel nozzle and a conceptual image of the spray boundary conditions employed in the current work

Because PDPA gives correlated droplet size and velocity, one could also use the measured droplet size directly from the measurement as well. If all three components of the velocity are known from the measurement, then there is no need to specify spray cone angle. In the absence of a component data, one could use the spray cone angle to obtain an estimate of the velocity components that is not available from the measurements. The key advantage of this approach is that joint PDF of drop-size-velocity and position can be specified in CFD. Droplets at different location disperse to different positions based on their size and hence it is important to preserve the correlation between position, size and velocity to obtain the correct droplet dispersion. This would ensure that the correct size droplets disperse to the correct location which in turn would yield correct flame location and structure. Another major advantage of this approach comes from the use of measured data that is far enough from the injector face where secondary breakup and other atomization processes are nearly complete. By using such a data, one could avoid the need for secondary break-up models which further saves computational time. The major drawback of this approach is the implicit assumption that the droplet trajectories follow the geometrical projection from the injection plane to the measurement plane and that the evaporation between the CFD injection plane and the actual measurement plane is minimal. So validation of this approach is required to ensure that such approximations do not introduce unacceptable errors in the reacting flow simulation.

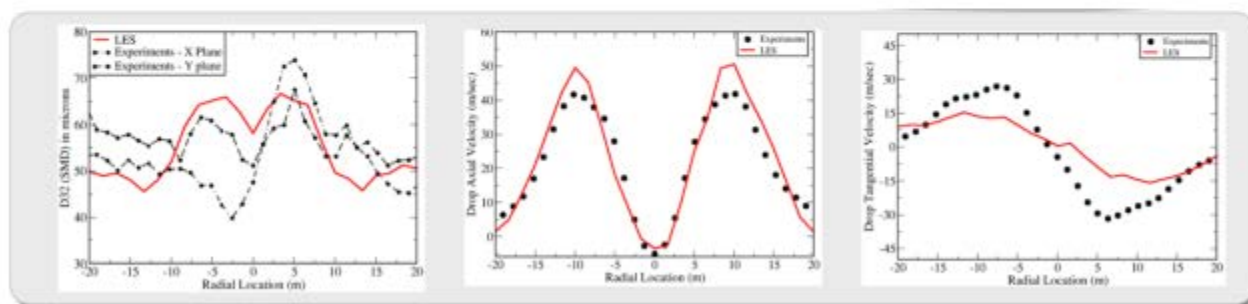
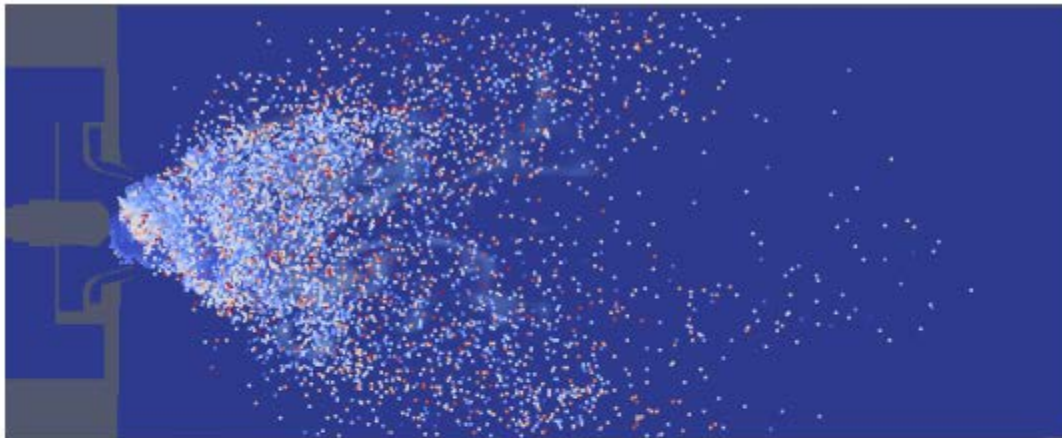


Figure 6. Top: Snapshot of spray dispersion in the high shear rig combustor (bottom) comparison of spray SMD, droplet axial and tangential velocity profiles between experiments (black dots) and simulations (red line).

Figure 6 (top image) shows the spray dispersion pattern from the spray boundary conditions described in this section. Experimental images and animations confirmed that the swirling air flow disperses the smaller sized drops in a swirling pattern and the simulated swirling spray pattern is in line with the expectation. In figure 6, (bottom image) compares the measured PDPA data with simulations. The image on the left-most side compares the Sauter mean diameter (D_{32}) and the comparison is reasonable with differences less than 5 microns. The image in the middle of the panel compares the drop axial velocity and the agreement is excellent validating the supposition that the spray parcels follow the flow as assumed in the injection boundary conditions model. The image on the right hand side of the panel compares the droplet tangential velocity with data. The differences seen here are attributed to the lack of specification of tangential velocity boundary conditions for the droplets. Even though it is possible to specify the tangential component of droplet velocity, it was not used here intentionally due to the supposition that the swirling carrier gas flow would impart the momentum to the droplets and enable the droplets to achieve the correct velocity. As it can be observed from the simulation data that the droplets have picked up a tangential component and this can be further improved by specifying the tangential component of droplet velocity. Overall, the agreement in spray size, velocity and position demonstrates the potential of the proposed boundary conditions and also serves as a validation of this relatively easier and affordable methodology.

Multi-component evaporation models

Jet fuels are multi-component in nature with 100s of species. Liquid fuel vaporization depends on many thermo-physical properties such as its density, heat capacity, latent heat of evaporation, vapor pressure etc. Since these properties are functions of local temperature, pressure and composition, a good evaporation model is important to capture the correct evaporation behavior and the correct spatial distribution of fuel-air mixture which in turn impacts flame-stabilization and



blowout. UTRC developed a multi-component evaporation model based on the distillation curve (under a different contract in NJFCP) and validated with partial data from the AFRL. This model provides all thermo-physical properties for the liquid fuel based on a surrogate representation of the liquid that matches the distillation curve constrained by liquid-vapor thermodynamic equilibrium. An ab initio equilibrium calculator (SuperTrapp) from NIST that uses the corresponding state theory (the cubic equations of state which take into account the molecular potential energy interaction between different hydrocarbons) was utilized to compute the equilibrium fluid properties of the mixture. The distillation curve calculator was derived from the equilibrium library of SuperTrapp to simulate the ASTM distillation process. This method is designed to track the changes in the composition in the liquid (and gas) during the evaporation process. The distillation curve computed for a given surrogate fuel is then compared with the experimentally obtained distillation curve, overall molecular weight, and density and other fuel properties, such as viscosity, surface tension etc. The surrogate model is adjusted until it provides a good match to available data and meeting other constraints such as the overall C to H ratio and average molecular weight. This process of adjustment is based on the properties of each component; for example, increasing the composition of a cyclic compound while decreasing an aliphatic compound of the same carbon number will change the density of the mixture while keeping all other properties constant. The surrogate model thus found was then utilized to predict all fuel properties during the evaporation process. This way, we are basically deriving fuel properties from first principles using a representative set of hydrocarbons found in a specific fuel sample with fuel physical properties that are valid for a wide range of temperature and pressure. This model assumes that as a droplet evaporates, it follows the distillation curve and hence the volume recovery fraction is a one-to-one function of temperature. This way one can construct a look-up table for all fluid properties using temperature as the independent variable. For temperatures below the starting temperature of the distillation curve, we evaluate the liquid properties along the curve defined by the loci of the bubble point.

Figure 7 shows the distillation curves and liquid density variation as a function of temperature predicted by the surrogate model of JetA, JP8 and JP5 fuel at 1Bar. The modeling results compared with experimental data (from AFRL) show very good agreement and is also in good agreement with Jet A distillation curve data found in the CRC handbook.

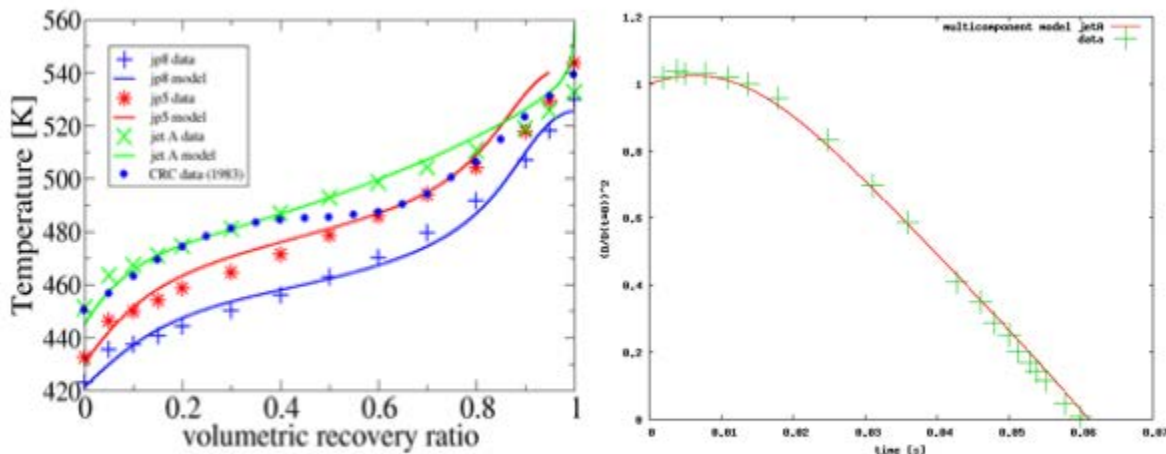


Figure 7: (left) Comparison of distillation curve predicted using data from AFRL and UTRC multicomponent evaporation model (right) comparison of single droplet evaporation time using the evaporation model

The properties needed for droplet evaporation simulation, computed using our surrogate models, are all tabulated and implemented into the reacting LES CFD code. Standard equations for droplet momentum, heat and mass transport equations are solved with classical correlations for drag and other inter-phase exchange terms. Another validation of the model was performed by simulating a single droplet evaporation. An isolated droplet of size 100 microns at an initial liquid fuel temperature of 300K embedded in ambient conditions of 1 bar and 800K was simulated for the Jet A fuel. Figure 7 (right) compares the D₂ variation with time for Jet A as a function of time at 1 bar pressure and compares with the results from Burger et al exhibiting a very good level of agreement. Figure 8 shows the fuel physical properties for a range of temperatures and for 3 different pressures. Data at 1 atm is used for comparison with the models and data at 2 atm and



3 atm are used for LES simulations of referee rig (which operates at 2 atm) and high shear combustor rig (which operates at 3 atm), respectively. Overall the model captures the physical property variation for a wide range of conditions.

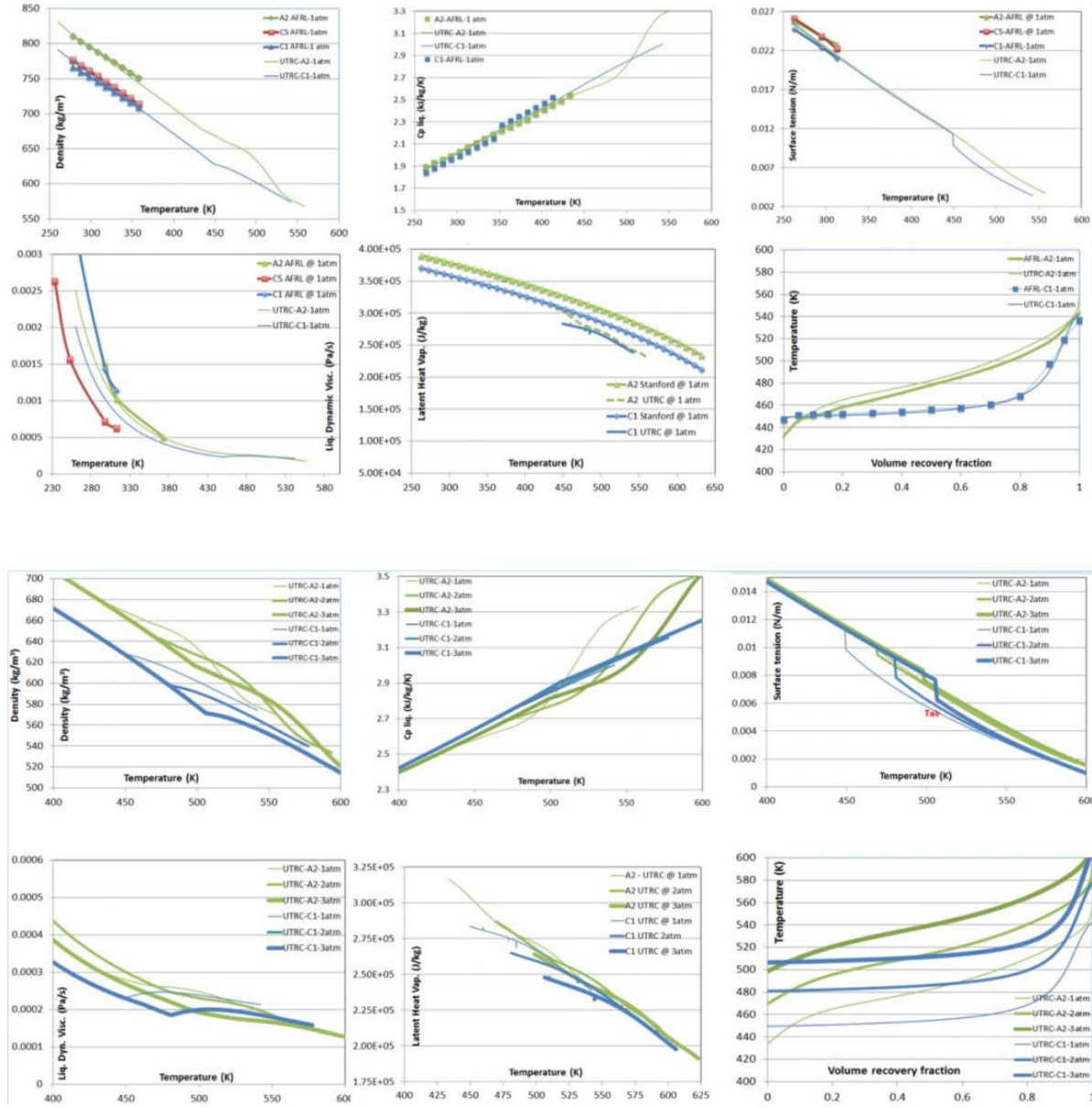
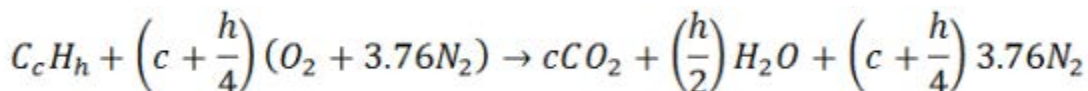


Figure 8: Prediction of fuel physical properties from the multi-component evaporation model. The top two rows (six figures) show comparison of density, specific heat surface tension, viscosity, vapor pressure and distillation curve at 1 atm and comparison to available data from AFRL. The bottom two rows of six figures shows the same properties at three different pressures.



Combustion Chemistry Mechanisms

As a part of the National Jet Fuels Combustion Program (NJFCP) teams from Stanford University developed a version of HyChem model for combustion chemistry or chemical kinetic mechanisms for A2, C1 and C5 fuels. The detailed chemical mechanism was calibrated and validated using species yields measured from flow reactor experiments. Research teams from the University of Connecticut developed skeletal and reduced mechanisms using Directed Graph Approach and verified these mechanisms by matching with combustion target properties like flame- speed, ignition delay, extinction strain rate, etc. These mechanisms consists of over 30 species and 100s of reaction steps and hence would be expensive to use in reacting LES of high shear rig combustor. As a compromise, we devised a single step chemistry with 5 species as shown below:



The reaction rate expression was chosen to mimic the Westbrook and Dryer single step chemistry and an empirical Pre-exponential factor (AFAC in the expression shown below) was introduced to account for the changes in the reaction rate as the local equivalence ratio varies in an evaporating spray combustion environment.

$$k = AFAC * 5.1e^{11} \exp\left(-\frac{15098}{T}\right) Fuel^{0.25} O_2^{1.5}$$

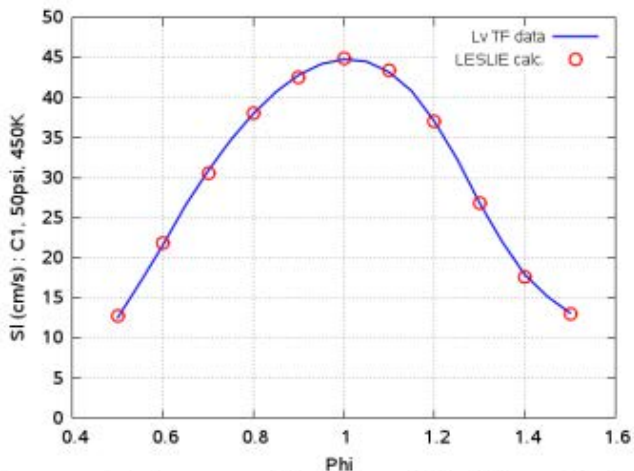
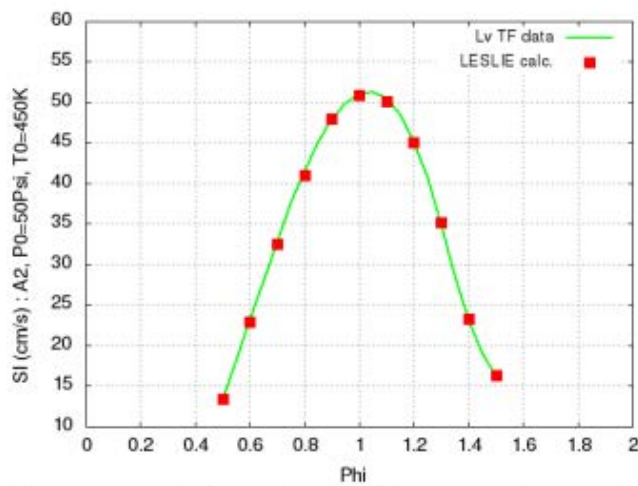


Figure 9: (left) Comparison of flame-speed for A2 fuel between single-step mechanism and detailed mechanism based on HyChem V2 chemistry model. (Right) Comparison of flame-speed for C1 fuel between current single-step mechanism and detailed mechanism based on HyChem V2 chemistry model

We simulated a one-dimensional freely-propagating premixed flame for different values of equivalence ratio (ϕ). For each value of ϕ , the AFAC term was changed until the mechanism yielded the correct flame-speed compared to the detailed mechanisms. By repeating this exercise for different values of ϕ , a correlation for AFAC as a function of ϕ was obtained that would be used in the reacting LES simulation of the high shear rig. Figure 9 shows the comparison of flame-speed obtained from the single-step mechanism for A2 and C1 fuels at inlet temperature and pressure corresponding to the high shear rig experiments. Overall an excellent agreement is obtained using this simple but empirical approach for deriving combustion chemistry models for complex LES simulations



Turbulent Combustion Models

The final sub-model that is needed for performing reacting LES is a turbulent combustion model. Even though different turbulent combustion models are available in the current CFD solver, a simple direct laminar closure model was used in this study. This model assumes that most of the turbulent mixing is resolved by the grid and hence the subgrid turbulent mixing can be ignored. As a result, the resolved species mass fractions, temperature, density and pressure can be used directly in the reaction rate expressions. The validity of the model is a function of how well the fine scale turbulent mixing is resolved by the underlying computational meshes used in this study.

In the next section, results from the simulations of high shear rig at near blow out but stable conditions will be presented for A2 and C1 fuels. Qualitative and quantitative comparisons of the contours and line plots will be presented to highlight any similarities and differences in the flow-field and flame structure for the two different fuels used here.

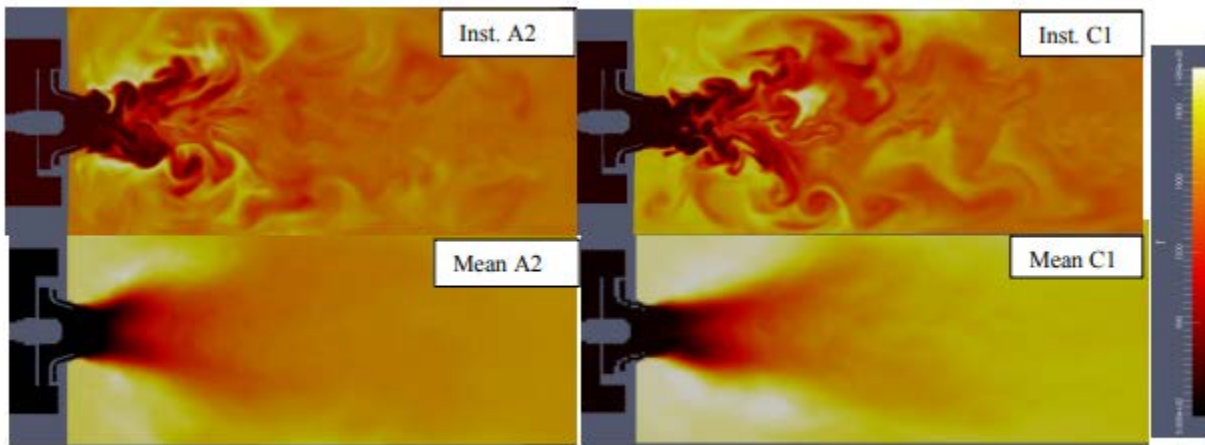


Figure 10: Contours of temperature from reacting LES of high shear rig combustor (top row) Instantaneous temperature contours (bottom row) mean or time-averaged temperature contours in central plane

Figure 10 shows the contours of temperature from the reacting simulations using the A2 and C1 fuels at near blowout (but stable) condition. The top row shows an instantaneous snapshot of the temperature contours at a particular instant and the bottom row shows time-averaged temperature contours for the same setup. Simulations were run for approximately 100 milli-seconds before averaging. To obtain mean or time-averaged data, simulation results were run for another 100 milli-seconds due to the lengthy combustor dimension. Darker regions near the swirler indicate colder air and it appears like a lifted flame is realized in this setup. The outer or corner recirculation zones bring in partially burnt hot products and mix them with the fresh air and evaporating fuel spray near the shear layers at the swirler exit. This creates a lifted flame that is stabilized between the shear layers and the central recirculation zones. It should be noted however that neither the instantaneous images nor time-averaged images show any visually significant differences for the two fuels simulated in this study.

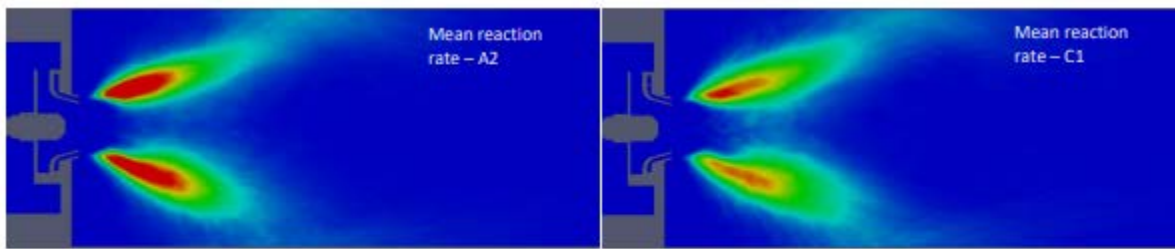


Figure 11: Contours of time-averaged fuel reaction rate obtained from reacting LES of high shear rig combustor (left) for A2 fuel (right) for C1 fuel



Figure 11 shows the contours of time-averaged fuel species reaction rate from the simulations of the stable conditions using A2 and C1 fuels. It can be observed that the flame structure, flame angle, anchoring locations are very similar for the two fuels. However, the magnitudes are noticeably different. A2 flame seems to have higher values of time-averaged reaction rates compared to C1 which is an indication that the A2 flames more robust and stable compared to the C1 flames, even though the C1 fuel has higher volatility compared to A2 fuels. This counterintuitive behavior is associated with the fact that all liquid fuel components in C1 fuel evaporate nearly at the same boiling temperature and hence in a very small region. Locally the mixture can be rich and has very little time for premixing. On the other hand the distillation curve for A2 fuel is gradual (see fig. 7) and different liquid fuel component evaporate at different boiling temperature. Hence, all the fuel vapor are not dumped in a small region but instead smoothly spread over a wide area which gives it time for premixing and combustion. This observation is consistent with the experimental observation under stable and lean blow out conditions.



Figure 12: Contours of temperature from reacting LES of high shear rig combustor (top row) Instantaneous temperature contours (bottom row) mean or time-averaged temperature contours in central plane

Figure 12 shows contours of time-averaged axial velocity fields obtained from the reacting simulations using A2 and C1 fuels in the high shear rig. Consistent with the temperature contours, very little differences can be observed in the velocity fields. However, notable differences can be seen in comparison to the non-reacting velocity fields (Figure. 3). The angle of the annular swirling jet that comes out of the swirler in the reacting flow is shallower than the non-reacting flow field. This is an indication of a reduction in swirling or tangential component of the velocity due to combustion related flow acceleration in the axial direction. The magnitude of the axial velocity was also higher than the non-reacting flow field. The combined effect of the reduction in angle and increase in velocity leads to a more coherent or lengthy annular jet which will have an impact on the flame stabilization.

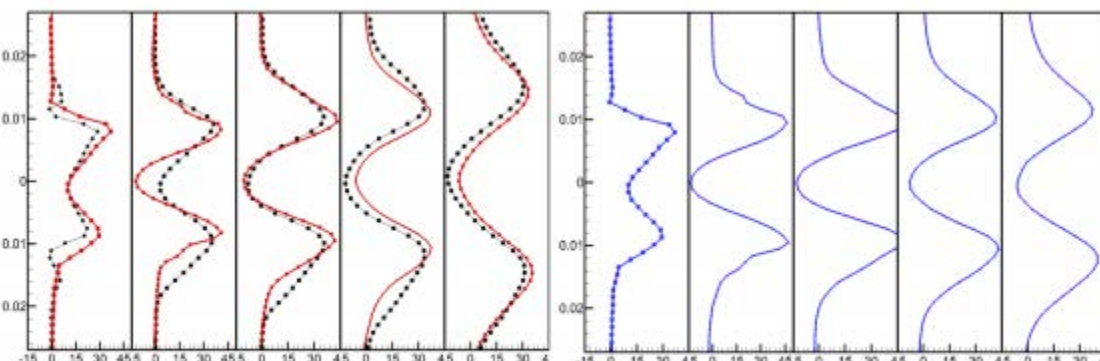


Figure 13: Radial profiles of axial velocity at five different axial stations for the A2 fuel (left) and for the C1 fuel (right). For the A2 fuel black dots represent the measurements and the red lines are from the simulation. For the C1 fuel measurements are not shown due to unavailability of the data at the time of comparison

Figure 13 shows the radial profiles of axial velocity at five different axial stations from the reacting simulations using A2 and C1 fuel. For the A2 fuel, comparison is also shown with measured data. For C1, fuel measurement data were not available for comparison with simulations. While some differences can be seen relative to the measurements, the agreement is still reasonable. As before, no significant differences can be observed between the two cases for these conditions. The lack of differences in the velocity fields between the two fuels indicate that the flames see/encounter



similar level of turbulence and mixing and any notable differences in the lean blow out behavior would be due to evaporation and or chemistry effects.

Lean Blow Out Simulations

Upon completion of the reacting LES for the two fuels at near blowout but stable condition, simulations were performed to understand the capability of the tools to predict observed lean blow out trends for the two fuels considered in this study. Starting from the near blowout simulations, fuel flow rate was reduced in steps of 6% and held constant for 100 milli seconds before reducing the fuel flow rate again. This was continued until the flame blow-out was observed. It was empirically determined based on the simulation that it takes approximately 100 milliseconds for the combustor to respond to the flow rate change and stabilize at the new condition. Based on the experiments, the near blowout fuel flow rate was set at 11.40 pph. Figure 14 shows the variation of liquid fuel evaporation rate as a function of time that was observed in the simulations for A2 and C1 fuels. It can be observed that for the A2 fuel, it takes approximately 100 milli-seconds (black line) to reach ~94% evaporation efficiency (defined as evaporation rate/injected fuel flow rate). It is hypothesized that the isothermal heat transfer boundary condition employed in this study does not accurately reflect the true heat transfer magnitudes and location from the experiments and therefore, could be over-predicting the heat loss, which in turn reduces the evaporation efficiency in the simulations. However, in the absence of accurate wall temperature measurements from the tests, this approximate boundary conditions is a compromise between the accuracy and simulation cost. It is also possible if the simulations were continued further, the evaporation efficiency may increase and reach 100%. However in the interest of getting to the lean blow out conditions, it was empirically assumed to be the steady state and the fuel flow rate was reduced at this point. At this stage, the fuel flow rate was reduced instantaneously to 10.72 pph (6% lower than the near blowout condition), and the simulation was continued for another 100 milli-seconds (red line). With the fuel flow rate reduction, a slight increase in evaporation rate was observed for a brief period before it begins to reduce and approach a mean steady value of ~10.3 pph. Again this is approximately 93-94% of the liquid fuel flow rate and similar to the previous flow rate complete evaporation was not achieved. At this state, the fuel flow rate was further reduced instantaneously to 10 pph (green line) and the simulations were continued for another 100 milliseconds. The evaporation rate further decreased and appears to reach a steady state for which ~95% evaporation efficiency was predicted. Figure 14 (right image) shows the evaporation rate for C1 fuel. At a flow rate of 11.40 pph (black line) an improved evaporation rate for C1 compared to A2 fuel. Approximately 98% of the fuel evaporates after 100 mil-seconds. This is in line with the expected better vaporization characteristics of the C1 fuel. As the fuel flow rate was further reduced to 10.72 pph, the evaporation rate decreased after a brief period and reaches a near stable state evaporating 98% of the injected fuel. As the flow rate was reduced to 10 pph, initially the evaporation rate decreased to ~88% and then it increases and reaches a near steady value of 96%. This is an indication of some unsteadiness as the fuel flow is approaches the lean blowout range (~9 pph) but not a conclusive evidence of the tool's ability to discriminate the effect of fuel property on the LBO behavior.

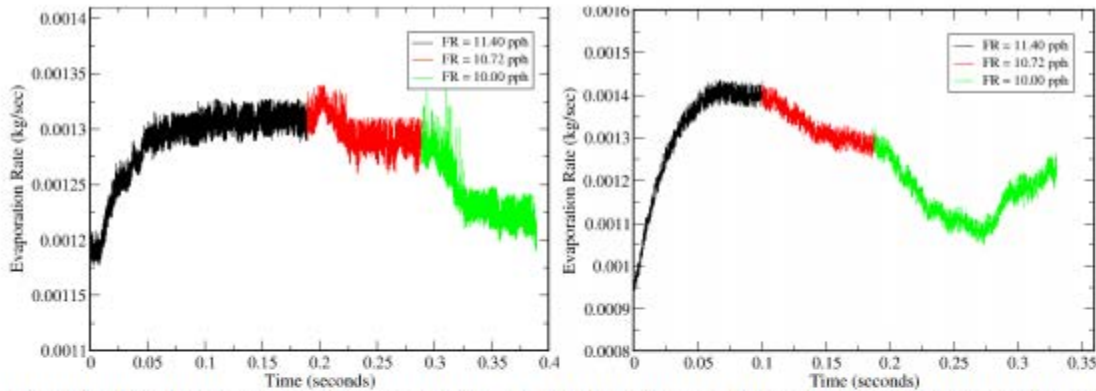


Figure 14: Profiles of evaporation rate evolution as a function of time (left) for A2 fuel and (right) for C1 fuel at three different flow rate conditions identified in the legend box

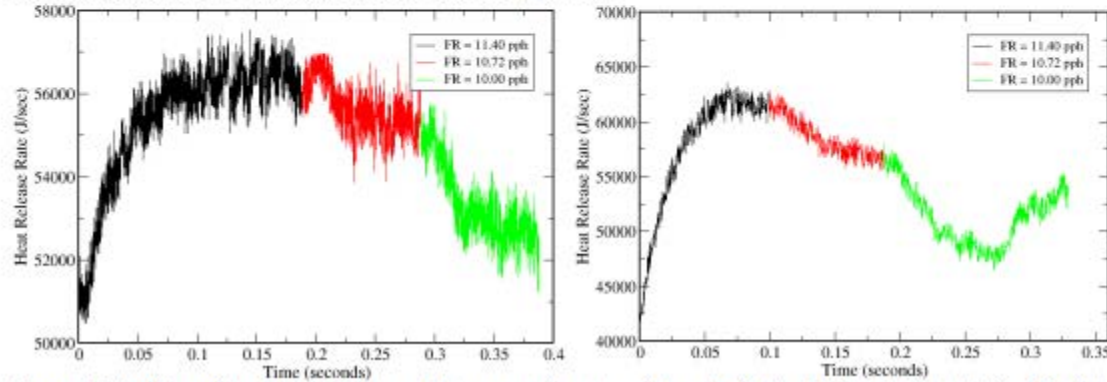


Figure 15: Profiles of heat release rate evolution as a function of time (left) for A2 fuel and (right) for C1 fuel at three different flow rate conditions identified in the legend box

Figure 15 shows corresponding profiles of heat release rate for the two fuels as the fuel flow rate was decreased systematically from the near blow out condition. Similar to the evaporation rate profiles, the heat release rate also decreases as the flow rate is reduced. In alignment with evaporation rate, heat release also shows relatively higher fluctuation levels for A2 fuel compared to C1 fuel. While the lower heating values of the two fuels are nearly the same (~43 MJ/kg) slightly lower levels of evaporation observed in the A2 fuel simulation leads to a slightly lower values of heat release rates predicted for A2 fuel. Overall, the two fuels show differences in evaporation rate and also commensurate differences in heat release rates. Both the simulations show reduction in heat release rate as the flow rate is reduced but C1 seems to be dropping faster relatively compared to A2. The experimental work indicates that the blowout for both the fuels was a sharper event unlike the referee rig combustor. Even though the current simulations show reduction in evaporation rate and heat-release rate, it is hard to infer the propensity of one fuel to blowout compared to the other unless the simulations were continued to fuel flow rates lower than the experimentally observed LBO flow rates. Unfortunately, these simulations take significantly long execution times due to small time-step, and long combustor length. For instance, each 100 mill-seconds of simulation requires 2.5 million steps of calculation and assuming discrete steps of fuel flow rate reduction, it requires 15 million time-step simulation for each fuel. The steady state at near blowout was run for significantly longer times. As a result of this long simulation times, we could only simulate three different flow rate reduction and use the results to extrapolate the model behavior.

Figures 16 and 17 shows the contours of temperature and fuel mass fraction contours for the simulations using A2 fuel at five different time instants during the simulation. Qualitative behavior of the flame can be inferred from such snap-shots and are usually helpful in providing insights about the driving mechanisms responsible for a particular physics. It can be observed from the temperature plots that the outer recirculation zones near the bulkhead are effective in mixing the hot products and the incoming fresh mixture of fuel vapor and air. Due to the increased residence time available in this area, the gas temperature in these locations are always hotter. Also, due to good turbulent mixing at shear layer, the flame



anchors in this location. As the flow moves downstream, the mixing and chemistry gets enough time for combustion and relatively higher temperatures can be observed. At lower fuel flow rates, with a globally lean mixture, the temperatures go down. Relatively cooler combustion products get pulled into the corner recirculation zones and the temperature in these locations begin to reduce as seen by darker contours of temperature. At the lowest flow rate simulated, much cooler temperatures were observed downstream to the exit of the combustors. Even though the global equivalence ratio reduces, the local equivalence ratio may not be as lean and hence in regions around the shear layers, robust flame structure can still be seen as one moves from one flow rate to the other. It is hypothesized here that the corner recirculation zone controls the lean blow out in this combustor. Reduction of fuel flow rate reduces the overall temperature of the hot products in the corner recirculation zone, which will be further reduced by the incoming cold air at the shear layers. If the resulting temperature is below the ignition temperature, then chemical reaction cannot be completed on time and it would be blown away. On occasion, local hot pocket from the corner recirculation zone may successfully burn a local fuel vapor-air mixture and hence re-ignition events may be possible in this combustor as observed in the experiments. A2 fuel having a wide distillation range, would be able to provide a spatially smoother fuel vapor distribution and hence has a better chance to reignite or sustain combustion for a longer time. Figure 17 shows the fuel vapor mass fraction contours at the corresponding time instants and it can be seen that higher values of fuel vapor (purple color) can be seen in the corner recirculation zone as the fuel flow rate is reduced due to the decrease in temperature and decrease in reaction rates which results in incomplete combustion of the reactants.

Figures 18 and 19 show the contours of temperature and fuel mass fraction contours for the simulations using C1 fuel at five different time instants during the simulation. Even though the same physics of shear layer mixing of reactants with hot products from the corner-recirculation zone applies in this scenario, evaporation rates are different for these two fuels. As a result increased values of fuel mass fraction is seen both near the injector and also inside the combustor. While increased vaporization rates are beneficial, it also leads to quick build of fuel vapor in a concentrated region and if the flow conditions in that region is not conducive in terms of residence time for completing the reaction, then it would result in even more accumulation of fuel vapor from the incomplete combustion. In the case of C1 fuel, this is hypothesized to be the mechanism for earlier flame blow out compared to the A2 fuel. While our simulations do not conclusively shows this, the qualitative trend seems to indicate that the models have the ability to discriminate between the different fuel physical properties and its impact on the lean blow out behavior.

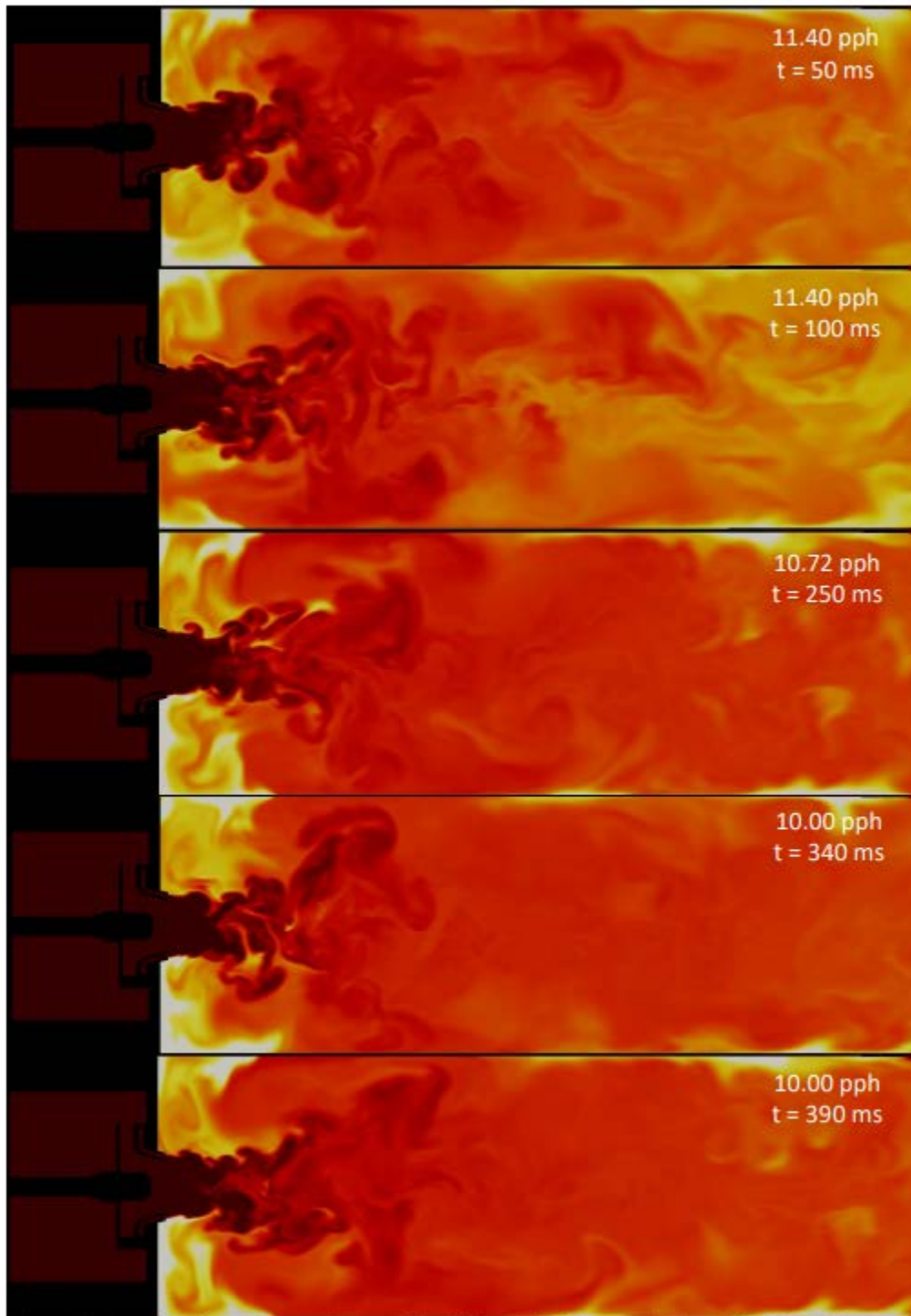


Figure 16: Contours of temperature shown at five different time instants for the A2 fuel simulation

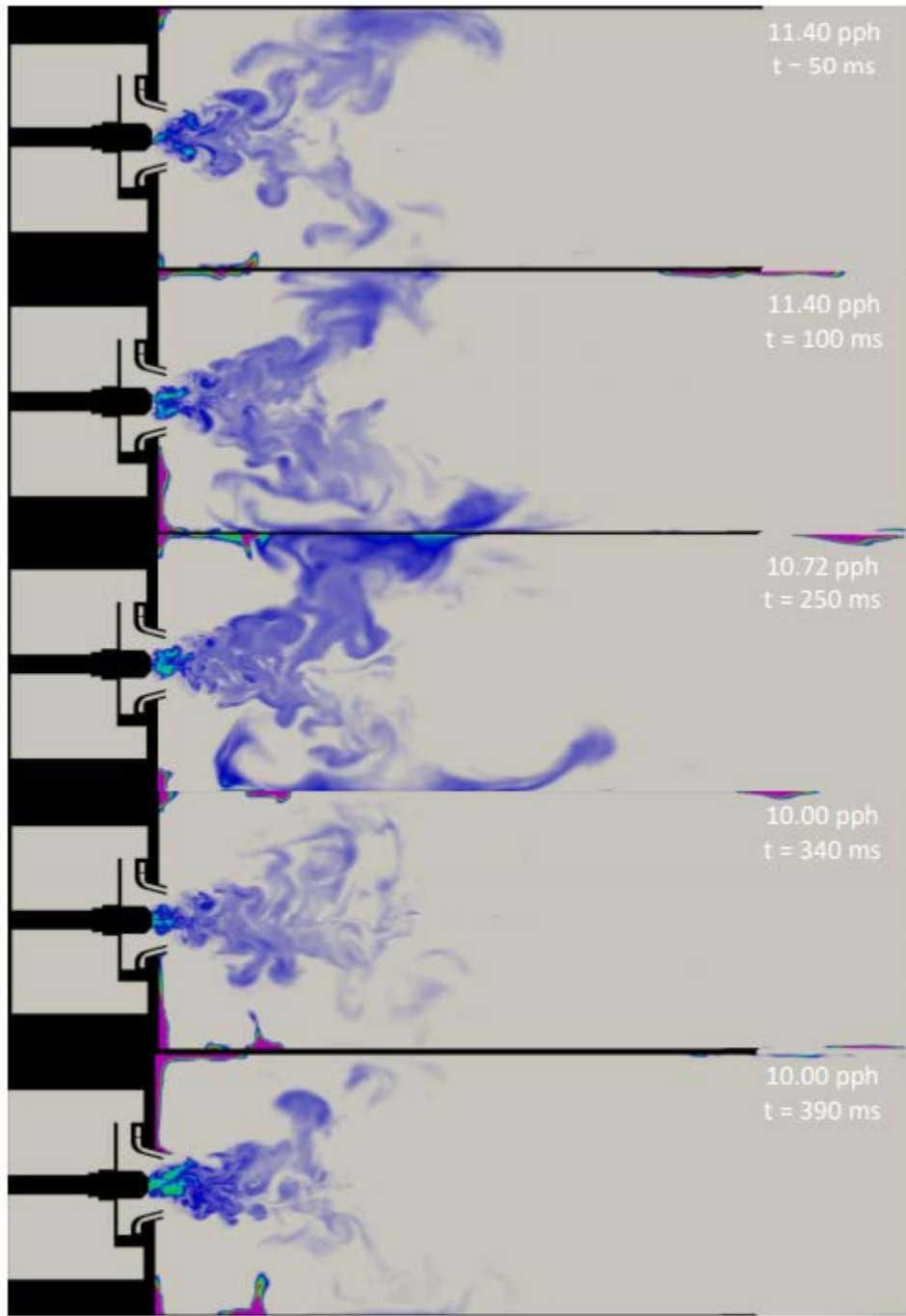


Figure 17: Contours of fuel mas fraction shown at five different time instants for the A2 fuel simulation

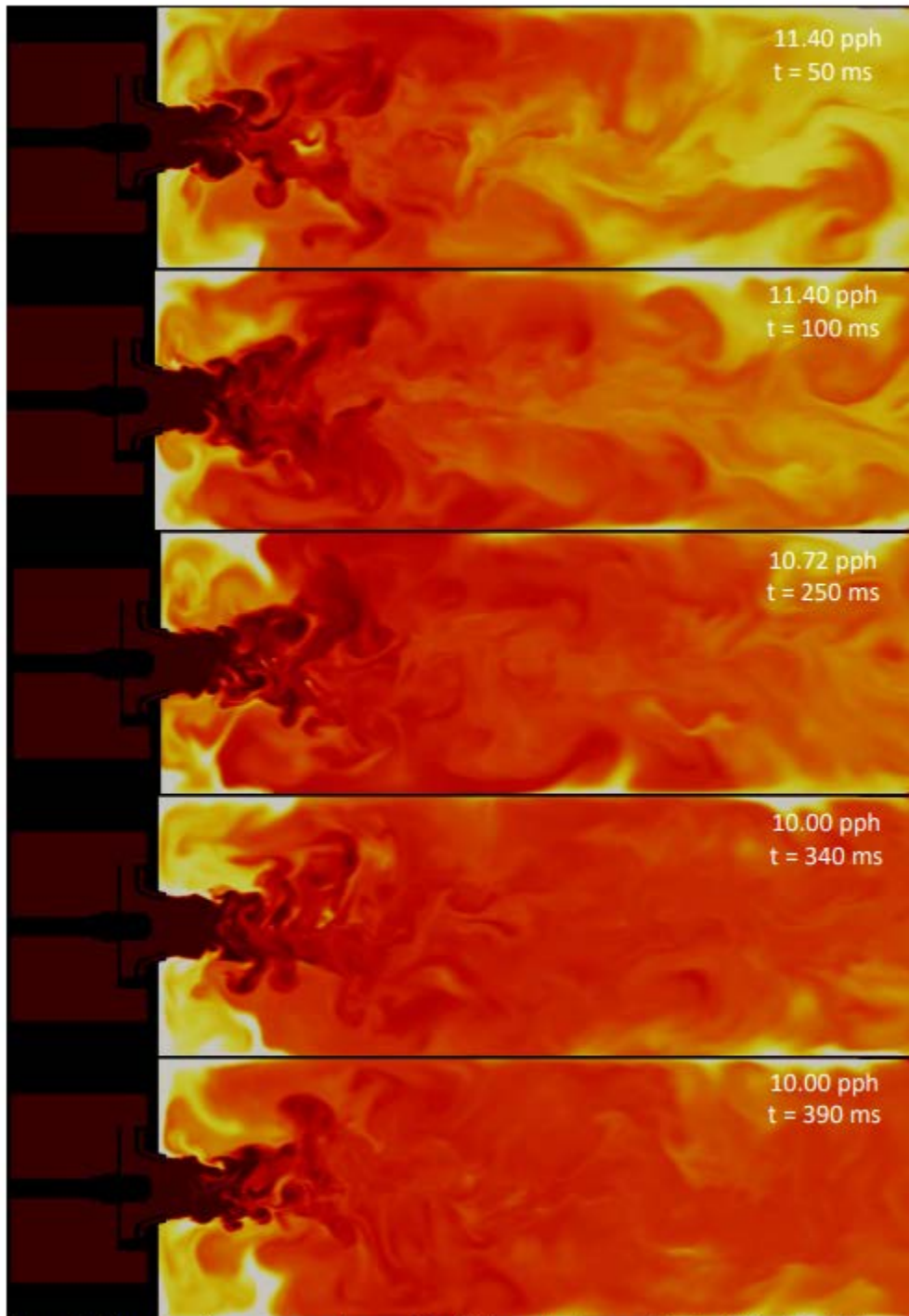


Figure 18: Contours of temperature shown at five different time instants for the C1 fuel simulation

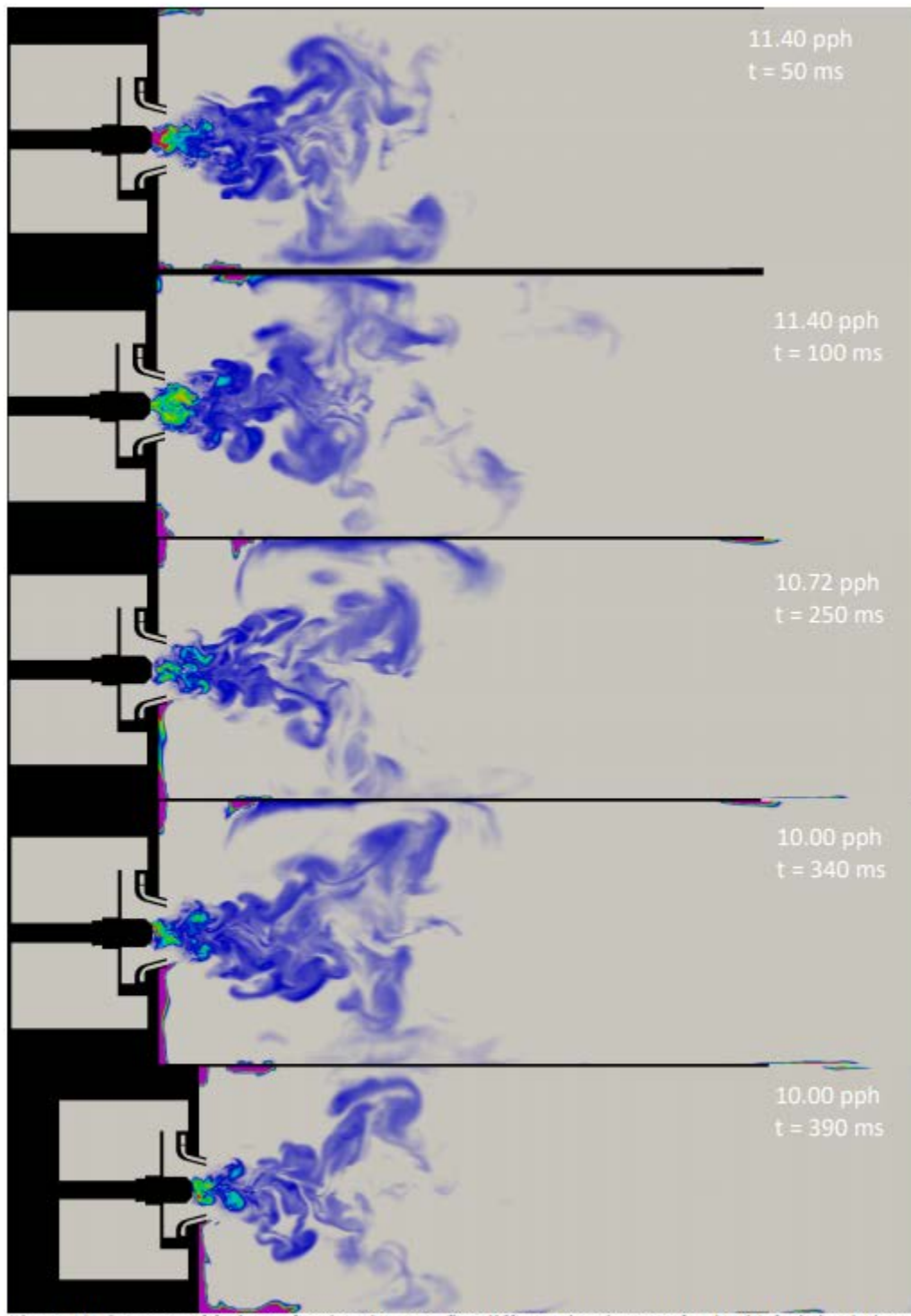


Figure 19: Contours of fuel mas fraction shown at five different time instants for the C1 fuel simulation



Conclusions

A Large Eddy Simulation-based analysis of the high shear rig combustor that was experimentally studied at Georgia Institute of Technology was performed in this study. The objective of this effort is to develop, enhance and apply computational fluid dynamics-based models to simulate stable combustion and lean blowout behavior in a high shear rig combustor. The goal is to understand if the models can predict the dependence of lean blowout phenomena on the physical and chemical properties of the alternative jet fuels. Several sub-models for unsteady flow simulation, spray injection boundary conditions, spray evaporation models, wall heat flux boundary conditions and turbulent combustion models are required to correctly simulate the physical processes. In this report we presented a description of different sub models, along with validation or verification where possible. Upon completion of the reacting LES for the two fuels at near blow out but stable condition, simulations of the lean blowout were performed by instantaneously reducing the fuel flow rate in steps of 6% for three different values of fuel-flow rates. Each flow rate was held constant for 100 mill-seconds for the combustor to respond to the flow rate change and stabilize at the new condition. Overall, the two fuels show differences in evaporation rate and also commensurate differences in heat release rates. Both the simulation show reduction in heat release rate as the flow rate is reduced but C1 seems to be dropping faster relatively compared to A2. C1 fuels also shows increase evaporation rates compared to A2, however this leads to quick build of fuel vapor in a concentrated region and if the flow conditions in that region is not conducive in terms of residence time to complete the reaction, it contributes to even more accumulation of fuel vapor from the incomplete combustion. In the case of C1 fuel, this is hypothesized to be the mechanism for earlier flame blow out compared to the A2 fuel. Long combustor dimension coupled with very small time steps to resolve the flame structure, leads to excessive computational time at each flow rate for the combustion to reach a quasi-steady state. As a result, it was not possible to reduce the flow-rate all the way to the lean blow out value to demonstrate the lean blow out behavior. However, the qualitative trend observed from the three simulate fuel flow rate conditions seems to indicate that the models employed in this study have the ability to discriminate between the different fuel physical properties and its impact on the lean blow out behavior.

Other Efforts

As a part of this contract UTRC also participated in working group meetings to provide and receive updates on the progress of different areas of research and also travelled to mid-year and yearly review meetings.

Milestone(s)

- Execution of sub-contract.
- Simulation of multiple fuels for the swirler and nozzle configuration at Georgia Tech.

Major Accomplishments

Completion of sub-contract period of performance.

Publications

None

Outreach Efforts

None

Awards

Joshua Heyne – SOCHE Faculty Excellence Award, 2016.

Student Involvement

None

Plans for Next Period

LBO simulations are being conducted to assess the impact of fuel on the LBO phenomena. UTRC to deliver final report on Area 3 spray simulations in Spring 2019.





Task 7- Ignition and LBO Testing of Conventional and Alternative Jet Fuels

University of Dayton Research Institute

Research Approach

A. Atmospheric Cold Start

A study of atmospheric cold start ignition was completed for nine NJFCP fuels in the Referee Combustor Rig. The conditions for the study near atmospheric pressure, in the combustor, and fuel and air temperatures ranging from 239K to 258K (-30 to +5 °F) with a pressure drop across the dome of 2 or 3.5%. For all of the experiments, the fuel temperature was controlled to match the air temperature.

The controlled cooling of the fuel and air temperatures was accomplished using a system designed around two recirculating fluid process chillers and five heat exchangers. A schematic and image of the cooling system are shown in Figure 1. The air is cooled in two stages, via four heat exchangers, with the heat transfer fluid supplied from two different chillers. To achieve air temperatures of -30°F, the air first passes through two parallel heat exchangers to cool the air down to -10°F. The air then flows through a second stage of heat exchangers, also arranged in parallel, cooled by the fluid circulated by a second chiller, to finish the cooling process and supply air at target temperature at the combustor. Control of the air temperature was accomplished by PID control of the temperature from both chillers and by controlling the fraction of coolant from the lower temperature chiller that was supplied to the air heat exchangers.

For all of the ignition experiments, the igniter current and voltage were measured and computed a delivered energy (to the igniter plug). The measurements of the spark energy provided a check on the consistency of the delivered energy for each spark as well as an early detector of excessive igniter plug erosion. The combustor pressure before ignition for the cold experiments was approximately 1 atm and the fuel and air were controlled to the same temperature ($T_{air} = T_{fuel} = -30°F$ or 5°F). For each combination of fuel type and flow conditions (ΔP , P_{cmb} , T_{air} , T_{fuel}) at least five volume flow rates were selected which resulted in between high and low ignition probabilities, at each fuel flow rate there were ten ignition attempts which consisted up to 40 sparks occurring at a frequency of ~3.5 Hz. After a successful ignition attempt was confirmed by video of the combustor, the spark sequence was stopped, and the fuel flow was stopped to end the ignition attempt. If ignition did not occur with 40 sparks the ignition attempt was halted for safety to avoid filling the downstream rig exhaust with large quantities of unlit fuel.

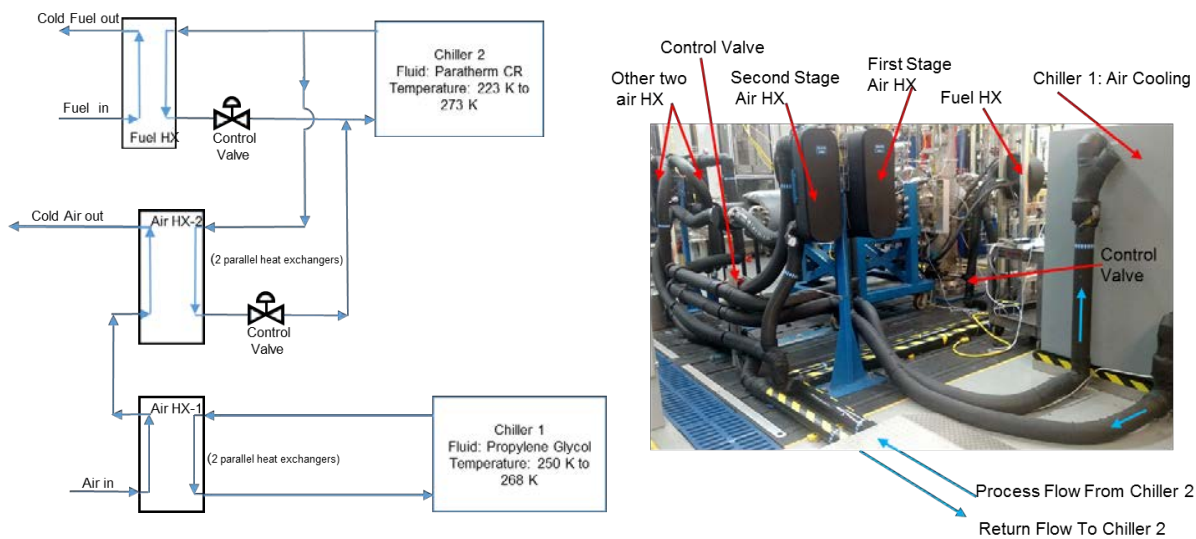


Figure 1. Schematic and Image of the Air and Fuel Cooling System

Each individual spark resulted in either a successful ignition, determined by spreading of the visible flame upstream of the spark ignitor and across the combustor, or an ignition failure. The successful ignition was determined from the



photodiode traces as a continuous elevated signal above the threshold extending in time past the next spark. Figure 2 shows a bar chart for each set of combustor conditions noting the number of successful and unsuccessful sparks for each fuel. A total of 23,548 sparks were attempted, resulting in 1438 successful ignitions.

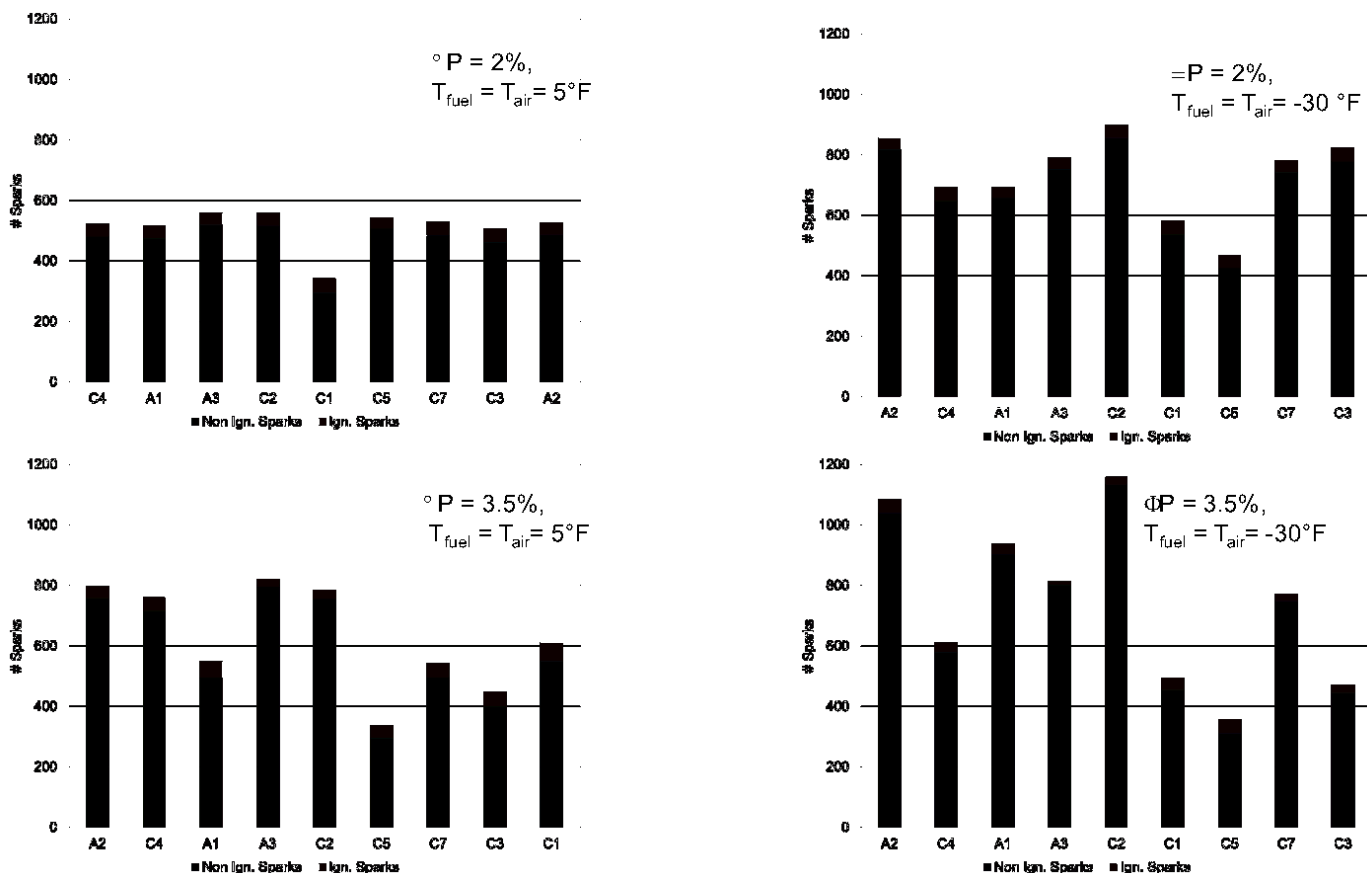


Figure 2. Summary of Sparks Resulting in Ignition and Non-Ignition for the Atmospheric Ignition Experiment.
23548 Sparks total, 1438 Successful Ignitions

The results from each spark were used to calculate ignition probabilities, with the sparks counted using the photodiode and characterized as either a 1 for ignition or a 0 for non-ignition. At low values of equivalence ratio the probability of ignition is essentially zero, whereas at higher equivalence ratios the probability approaches one. In between these two extremes there is a region where the successful and non-successful ignition results overlap. Binomial logistic regression was used with the logistic function to reduce the 0's and 1's into a probability curve vs the equivalence ratio.

Ignition probability curves are plotted in Figure 3 and Figure 4 for $3.5\% \Delta P$ cases. The data is shown as a regression line for each case and fuel plotted up to the maximum equivalence ratio ϕ tested. Each curve increases in ignition probability as ϕ increases. For all fuels and pressure drop conditions, raising the temperature increased the ignition probability at a given ϕ . The rankings of the ignition performance for all of the fuels remained consistent as the imposed external conditions (T_{fuel} , T_{air} and ΔP) changed, with the only exception being the performance of C1 and A1 relative to each other.

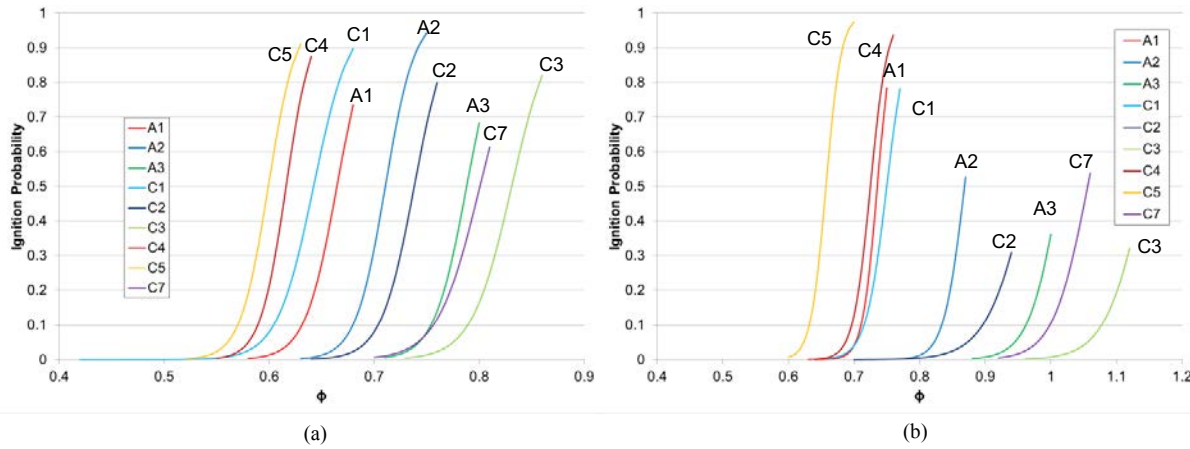


Figure 3. Ignition Probability vs ϕ for cases with $\Delta P = 2\%$, $P_{comb} = 1$ atm. (a) $T_{air} = T_{fuel} = 5^{\circ}F$, (b) $T_{air} = T_{fuel} = -30^{\circ}F$

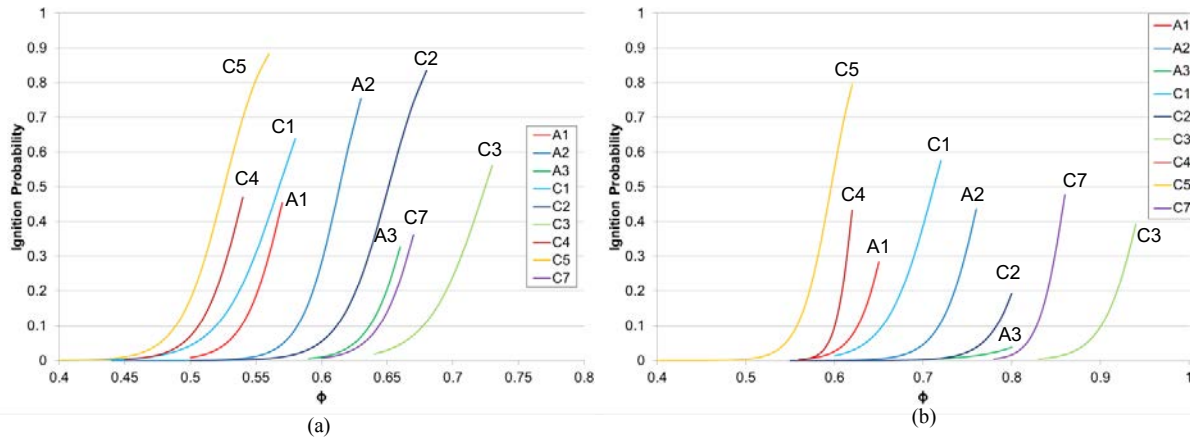
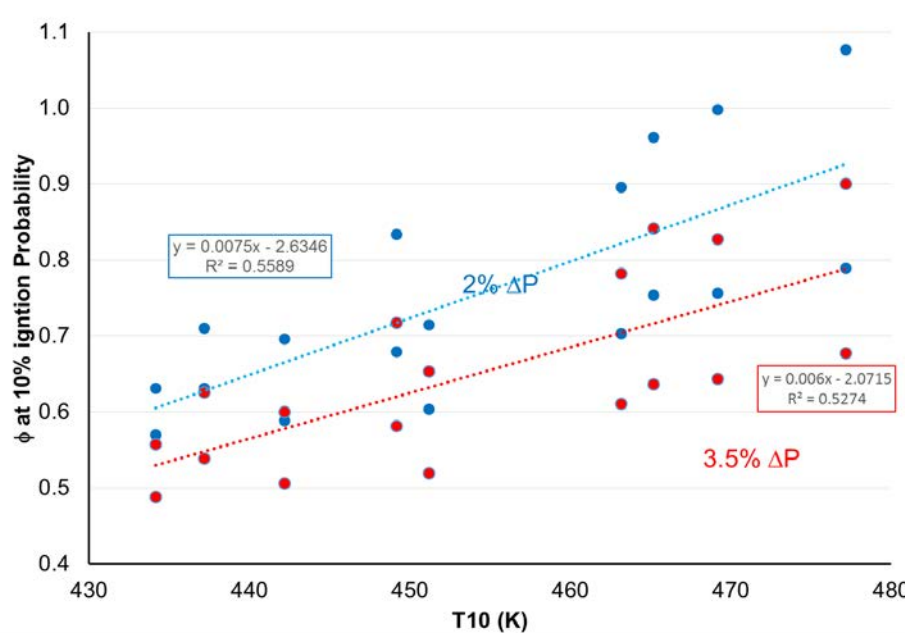
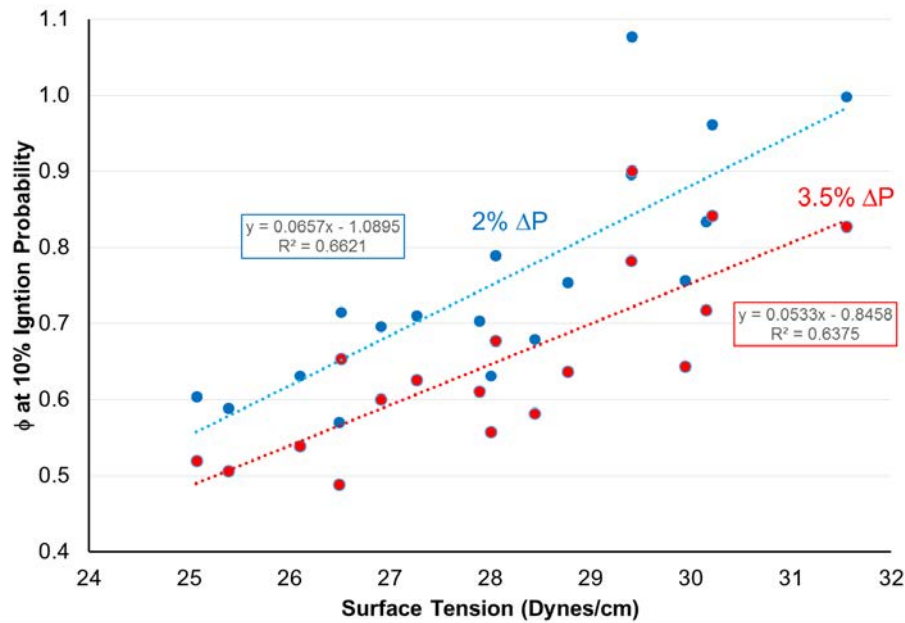


Figure 4. Ignition Probability vs ϕ for cases with $\Delta P = 3.5\%$, $P_{comb} = 1$ atm. (a) $T_{air} = T_{fuel} = 5^{\circ}F$, (b) $T_{air} = T_{fuel} = -30^{\circ}F$

The effect of the physical properties on the ignition performance of the fuels was considered and partial results are shown in Figure 5 - Figure 7. Strong correlations are shown with the atomization, surface tension, & viscosity, and distillation properties (T₁₀, and T₂₀). Further efforts are underway to better understand the relationship to of ignition to properties through advanced regression analysis. Further details from the cold start ignition experiments were presented at the AIAA SCITECH conference [1].



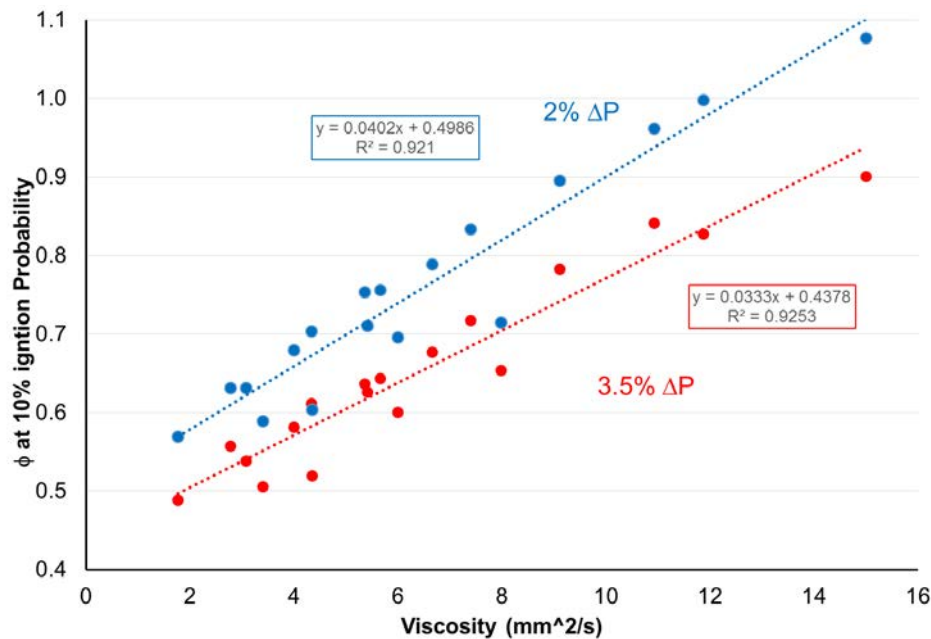


Figure 7. Equivalence Ratio at 10% probability vs Viscosity for Atmospheric Cold Start Tests

B. Cold Lean Blowout Experiments

Lean Blowout data was also obtained from form a subset of the tests cold start tests. The conditions represented during the LBO are not strictly conditions that show up in operation of the normal operation but represent a stressed, low pressure, low temperature condition. The motivation for this test came from the OEM committee involved with the project, with the rationale of “as long as we are lighting the combustor we may as well get data during blowout.”

Several practical testing issues made these tests challenging and time consuming. The normal LBO experiments, conducted previously at high temperatures and pressures, were conducted over a time period of ~5 minutes per LBO attempt, and the hardware downstream of the combustor was water-cooled. The cold flow experiments precluded the use of water cooling because of the difficulties of using water as a coolant at air temperatures 25 to 65 °F below the freezing temperature of the water. Therefore, the experimental method used was a quick LBO approach in which the ramp rate was greatly increased to allow LBO to occur within 20 seconds of light off, and rely on heat sink to cool the rig. This compromise approach worked, but required an additional 7-10 minutes, with the internal flow of cold air to cool the combustor back down to the baseline temperature, between ignition attempts.

Results for the cold LBO experiments taken at combustor pressures of ~1 atm are shown in Figure 8 along with previous results at 2 atm and $T_{air} = 250^{\circ}\text{F}$. It can be seen that the decrease in temperature decreases the magnitude of the phi at LBO. Previous results for LBO at high temperatures showed that the LBO results correlated strongly with Derived Cetane Number (DCN), and showed little correlation with atomization and evaporation parameters (Density, surface tension, viscosity) implying that the chemistry is important for LBO at normal conditions seen during LBO. For the cold LBO tests the opposite was observed. DCN showed little correlation to the LBO results and the LBO correlated best with viscosity and T50. Linear correlations of the LBO ϕ normalized by the LBO ϕ for A2 with viscosity and T50 are shown in Figure 9.

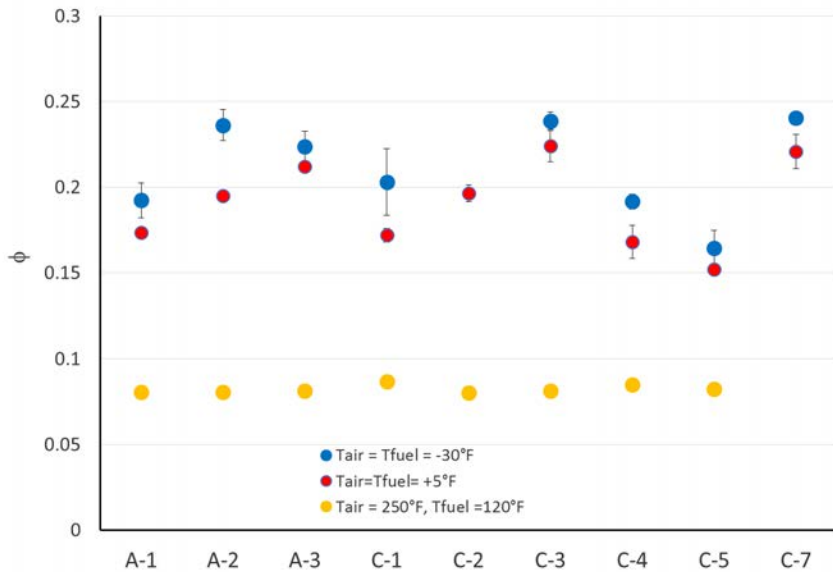


Figure 8. ϕ at LBO for Hot and Cold Experiments

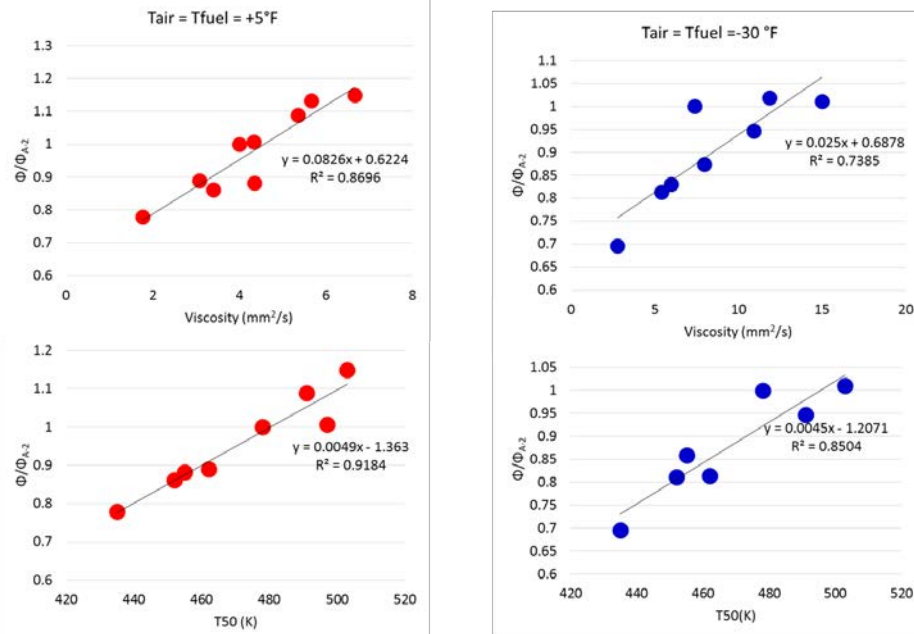


Figure 9. LBO Equivalence Ratio Relative to the Baseline A2 Fuel plotted vs T50 and Viscosity

C. Configuration for High Altitude Relight

The Referee Rig was modified in the past year to facilitate high altitude relight experiments. The ability to conduct altitude relight experiments at sub-atmospheric pressures was added to the facility by the addition of an air ejector and associated subsystems to the rig. The ejector was installed in the downstream side of the rig as shown in Figure 10. The control of the combustor back pressure for ignition experiment was set by maintaining a steady pressure at the ejector motive flow port. The pressure within the combustor was then controlled control valves to bleed room air at atmospheric pressure into



the duct upstream of the suction port of the ejector. The hazard of unburnt fuel downstream of the combustor was eliminated by sucking fuel through several ports on the exhaust stack, while the pressure on the exhaust was temporarily increased by stalling the ejector with air from additional ball valves.

In general, the altitude relight experiments required much more effort and time than the atmospheric cold start due to the low mass fuel mass flows which led to excessive heat gain between ignition attempts. Most of the sub-atmospheric experiments were conducted at a temperature of -30°F and a combustor pressure of 5.45 psia (0.37 atm) which corresponds to the pressure at 25,000 ft. Initial experiments attempted to use the same nozzle that was used for the atmospheric experiments, however it was not possible to ignite either A2 or C5 fuel at the desired conditions at equivalence ratios up to 1.3. It should be noted that the low air flow rates at high altitude resulted in low fuel flows which, in turn, resulted in low fuel pressures resulting in poor atomization. After the initial experiments with the larger flow number nozzle, a small flow number nozzle, was selected for the rest of the studies. With the low flow number (higher pressure drop) nozzle it was possible to ignite all of the fuels at the imposed temperatures and air flow rates.

Figure 11 shows a bar chart of the sub atmospheric ignition experiments over 5880 sparks leading to 456 successful ignitions. Figure 12 shows the regression curves reduced from all of the data points for the altitude relight experiments. The rankings of the fuels were similar to those at atmospheric pressure, shown in Figure 3a above, with the same fuel and air temperature (-30°F) with the exception of C5 and C1. At atmospheric pressures the C1 performed better than the A1 and A2, however, for the altitude case the C1 was shifted to the right (worse performance) of the A2 fuel. The C5 fuel which was the easiest to light under all conditions explored in the atmospheric cold start experiments exhibited odd ignition characteristics. At altitude C5 was the easiest to light at low ignition probabilities. However, the ignition probability curve for C5 crossed that for the other fuels leading to lower performance (higher ignition ϕ) at higher ignition probabilities. In addition, the confidence intervals for the C5 fuel were much wider than the other fuels. The reasons for these differences is under examination.

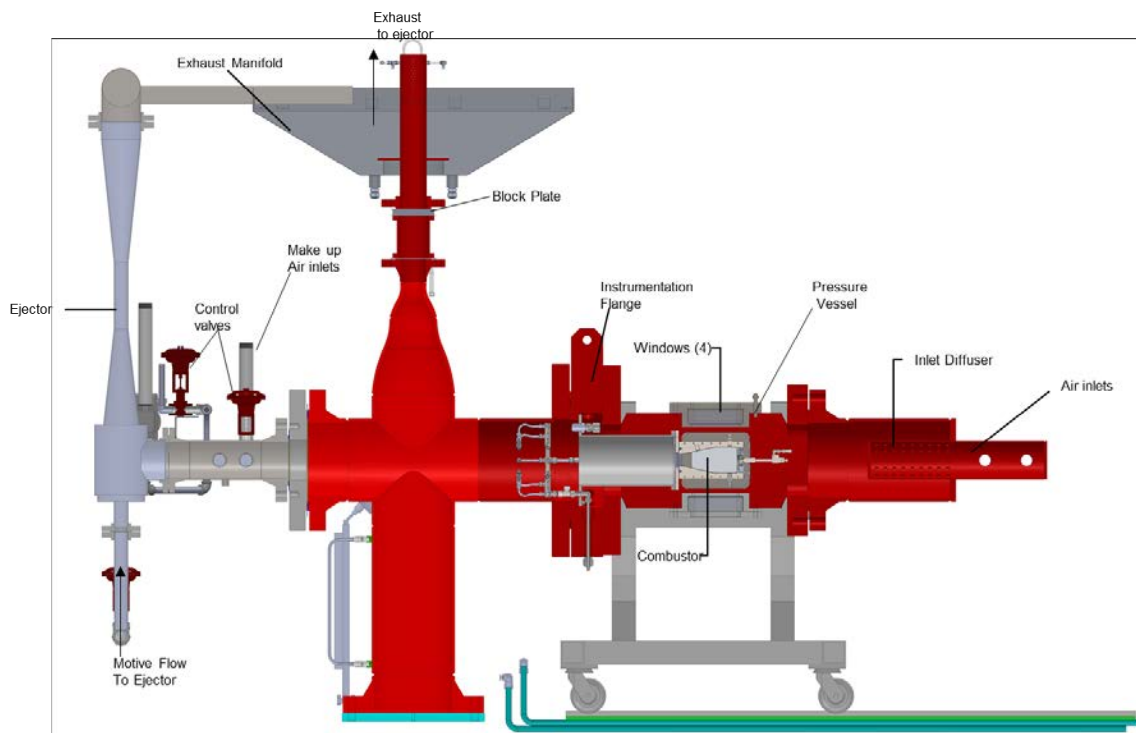


Figure 10. Referee Rig Configured for High Altitude Relight Studies

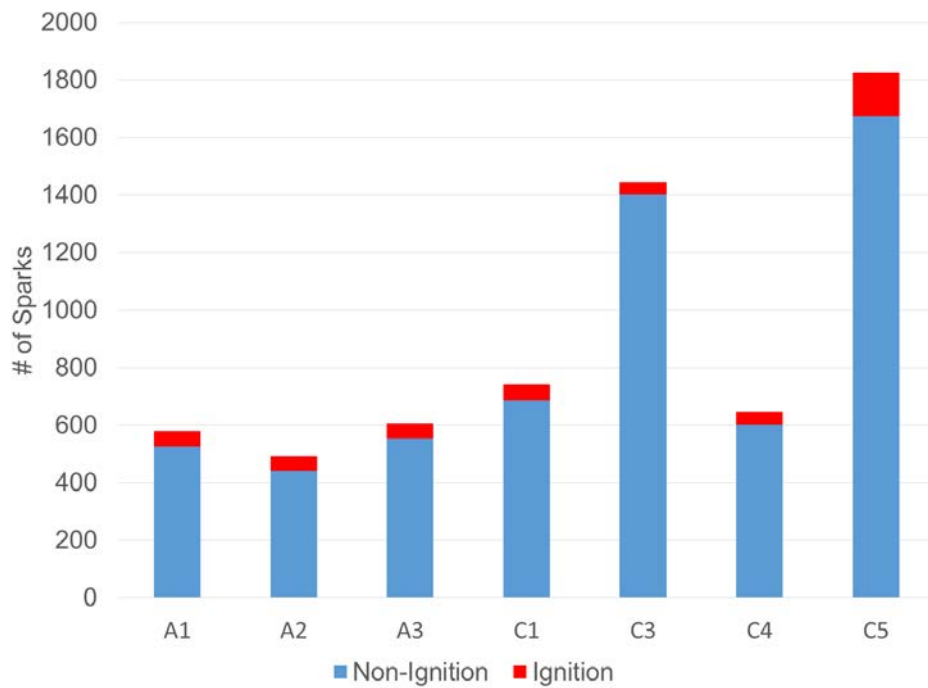


Figure 11. Summary of Sparks Resulting in Ignition and Non-Ignition for the High Altitude Ignition Experiment.
5881 Sparks total, 456 Successful Ignitions

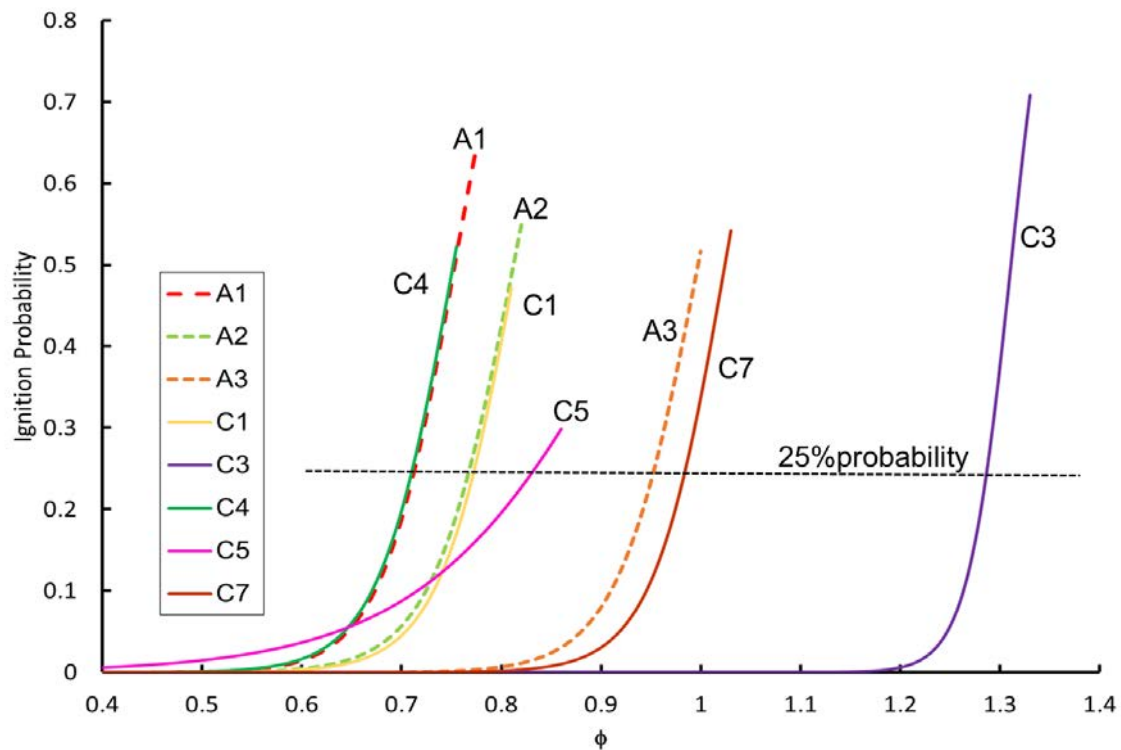


Figure 12. Ignition Probability Curves for $P_{cmb} = 5.45$ psi, $\Delta P = 2\%$, $T = -30^{\circ}\text{F}$.



The effect of the various physical properties vs the equivalence ratio at 25% ignition probability is examined in Figure 13 - Figure 14. The best correlations were found with the viscosity and the distillation properties. The ignition performance showed poor correlation with DCN and vapor pressure. It was noted that the C3 fuel, which had the lowest viscosity, showed high sensitivity to temperature change. Figure 15 shows the ignition probability at different fuel and air temperatures for C3 fuel. The viscosity curve for the C3 is also plotted. The results were obtained by 10 separate ignition attempts of up to 40 sparks at each temperature. The results show a large drop in ignition performance between -18 and -30 °F. This range is also the range in which the viscosity exceeds 12 cSt.

After noting that fuel viscosity seemed to be a major driver of ignition performance, an experiment was conducted to determine if three fuels of the same viscosity (created by heating the more viscous fuels to higher temperatures) would have the same ignition performance. Figure 16 shows the results for C1 at -30 °F, A3 at -16 °F and C3 at 4 °F. For reference, the 25% probability line is shown along with the crossing points marked by x's. It can be seen that increasing the temperature shifted the curves for the C3 and A3 to the left (improved performance) however, the effect was not enough to overlap the curves showing that the viscosity, while important, is not the only driver of ignition performance.

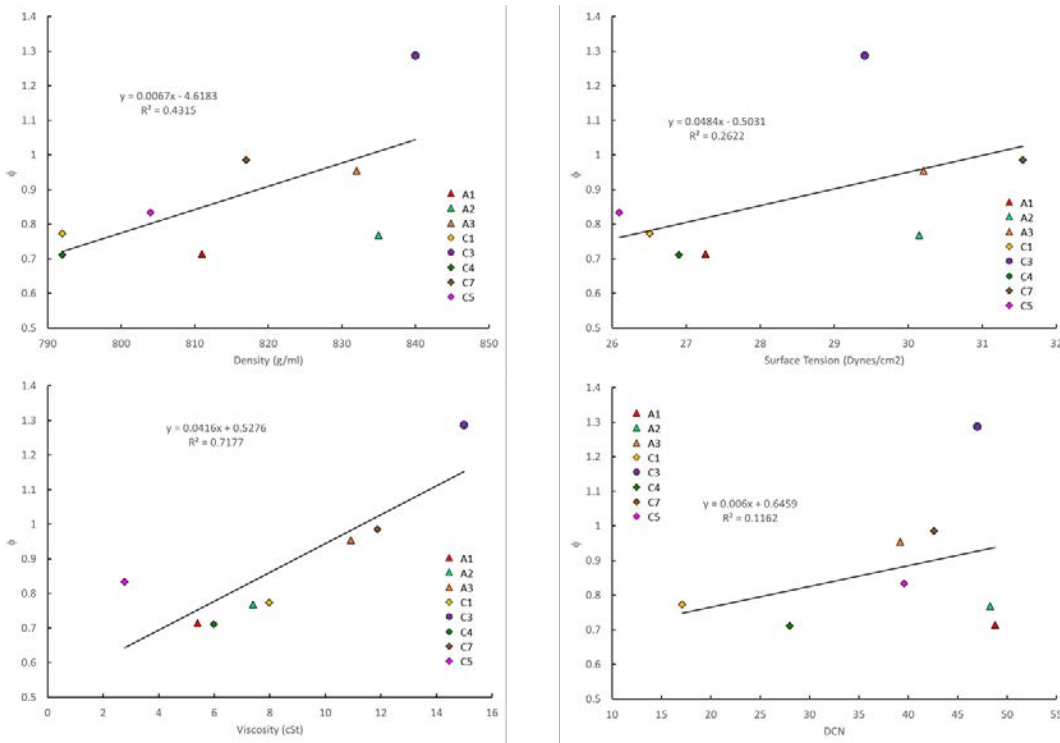


Figure 13. ϕ at 25% ignition Probability vs Atomization and Chemical Properties

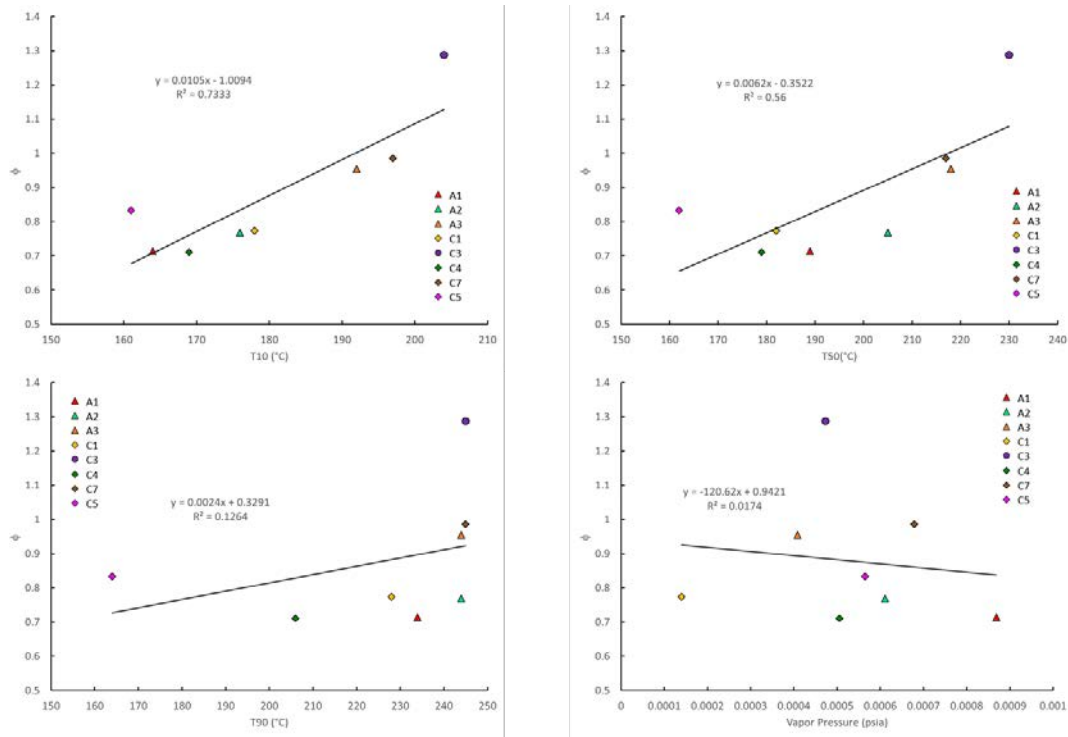


Figure 14. ϕ at 25% ignition Probability vs Atomization Properties

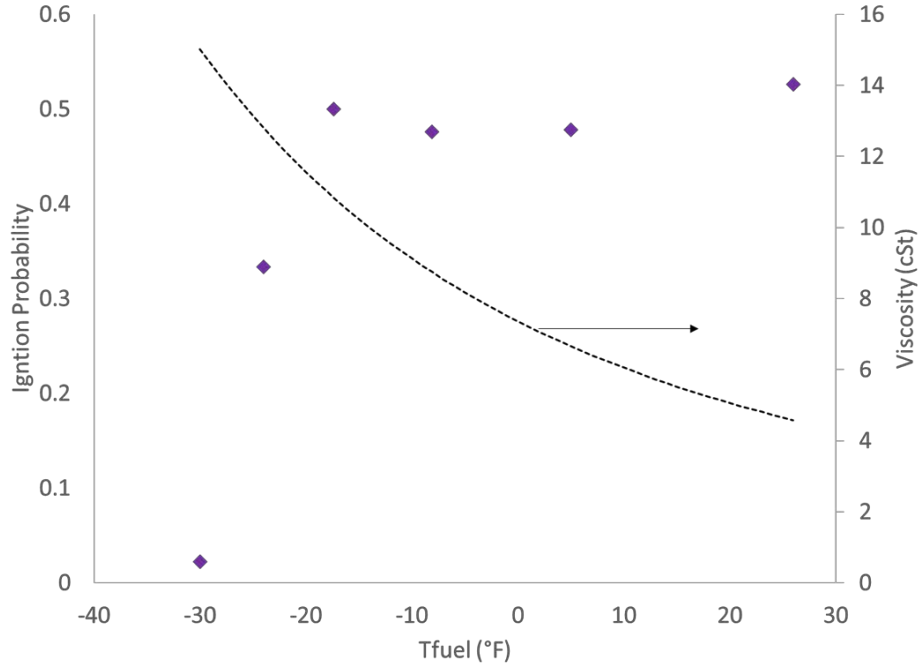


Figure 15. Ignition probability of C3 at Various Fuel and Air Temperatures $\Delta P = 2\%$, $P_{cmb} = 5.45$ psia.

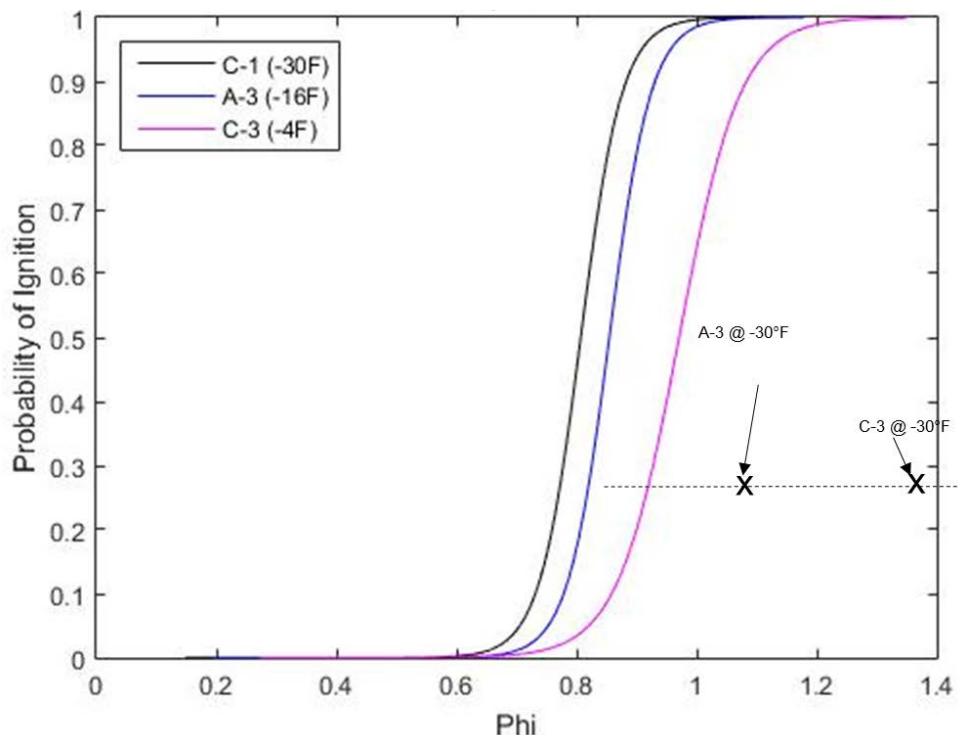


Figure 16. Ignition Probability Curves for Three Fuels at the Same Viscosity

The results from these experiments are under further analysis and will be presented at an upcoming AIAA meeting [2].

Near Term Activities

After completing experiments in cold conditions the focus for the experiments in the referee rig are being shifted to LBO at elevated pressures and temperatures. This requires several major hardware changes. The timeline for starting LBO experiments again is in November 2018. We are also working on further analysis of the data which will allow us to publish the results in archival journals. In addition, we are working with others to present the results in a coordinated way in an AIAA book on alternative fuels.

Milestone(s)

The generation of cumulative distribution functions for the various conventional and alternative jet fuels in the Referee Rig at cold conditions for ignition.

Major Accomplishments

Demonstrating significant fuel sensitivity in ignition probability for various fuels.

Publications

None

Outreach Efforts

Presentation and poster at ASCENT meetings in 2018.

Awards

None

Student Involvement

Jennifer Colborn, Undergraduate Research Assistant.



FAA CENTER OF EXCELLENCE FOR ALTERNATIVE JET FUELS & ENVIRONMENT



Plans for Next Period

1. Additional LBO measurements.
2. Testing of the Shell IH² fuel when it arrives.
3. Additional cold ignition tests once appropriate fuels are identified and LBO testing is over.
4. Writing up the results in a conference and journal publication.

References

- [1] T. H. Hendershott, S. Stouffer, J. R. Monfort, J. Diemer, K. Busby, E. Corporan, P. Wrzesinski and A. W. Caswell, "Ignition of Conventional and Alternative Fuel at Low Temperatures in a Single-Cup Swirl-Stabilized Combustor," in *2018 AIAA Aerospace Sciences Meeting*, 2018.
- [2] Stouffer, S.D., Hendershott, Colborn, J.T.H.,Monfort, J.R., Corporan, E., Wrzesinski, P., Caswell, A.W., "Altitude Relight Performance of Conventional and Alternative Fuels", paper under preparation to be presented at SCITECH 2019, Jan 2019.

